The Maule (Chile) Earthquake of February 27, 2010

Consequence Assessment and Case Studies

Amr S. Elnashai
Bora Gencturk
Oh-Sung Kwon
Imad L. Al-Qadi
Youssef Hashash
Jeffery R. Roesler
Sung Jig Kim
Seong-Hoon Jeong
Jazalyn Dukes
Angharad Valdivia

02-27-10
03:34 am
$M_w = 8.8$

Mid-America Earthquake Center

MAE Center Report No. 10-04

MAE CENTER TEAM REPORT CONTRIBUTIONS

Amr S. Elnashai, planning and initial management, lead on structural engineering field investigations, case study on Cathedral of Talca, executive summary and conclusions.

Bora Gencturk, logistical trip and team management, coordinator of data collection, coordinator of complete report, case study on Odontology building, overview, engineering seismology, structural engineering (effects on buildings and historical structures).

Oh-Sung Kwon, lead on structural engineering and case study analyses, case study on Paso Cladio Arrau, structural engineering (regional damage description and statistics, effects on bridges).

Imad L. Al-Qadi, lead on transportation networks, roads and embankments.

Youssef Hashash, lead on geotechnical engineering, engineering seismology.

Jefferey R. Roesler, planning and initial management, lead on communications with researchers from Chilean institutions, transportation networks, roads and embankments.

Sung-Jig Kim, strong ground motion, case study on Odontology building.

Seong-Hoon Jeong, case study on Las Mercedes Bridge.

Jazalyn Dukes, seismic fragility analysis of Las Mercedes Bridge, socio-economic features and impact on communications.

Angharad Valdivia, lead on communications during field mission, socio-economic features and impact on communications.

EXECUTIVE SUMMARY

On February 27, 2010 at 03:34 am local time, a powerful earthquake of magnitude 8.8 struck central Chile. The epicenter of the earthquake was approximately 8 km off the central region of the Chilean coast. With an inclined rupture area of more than 80,000 square km that extends onshore, the region of Maule was subjected to a direct hit, with intense shaking of duration of at least 100 seconds, and peak horizontal and vertical ground acceleration of over 0.6 g. According to the Ministry of Interior of Chile, the earthquake caused the death of 521 persons, with almost half of the fatalities caused by the consequential tsunami. Over 800,000 individuals were directly affected through death, injury and displacement. More than a third of a million buildings were damaged to varying degrees, including several cases of total collapse of major structures. The transportation system was dealt a crippling blow, with 830 failures registered with the Ministry of Public Works on roads in both the public and private transportation networks. Severe disruption of commerce as well as the rescue and response effort resulted from the damage to roads, embankments and bridges.

Only a few acceleration records were released to the engineering community as of December 2010; this withholding of such information of great importance to detailed studies that benefits society at-large is regrettable. The available records confirm the severe shaking that resulted from the earthquake and the long duration of the strong-motion part of the records. The dearth of available records led the MAE Center group to generate spectrum compatible signals, as described in the report, for back-analysis. Geotechnical effects were widespread and comprised massive landslides, buried tank heave, uplift of up to 3 m, and liquefaction. Buildings and bridges suffered damage because of both structural and foundation failure. The major harbor facilities at Coronel and Talcahuano suffered excessive damage and were closed for several weeks after the earthquake.

Failure to engineered buildings was due to the common causes of irregularity and limited ductility, with a few cases of damage due to a special provision in the Chilean code that allows structural walls with thin webs. On the whole, the performance of engineered structures was reasonable, taking into account the magnitude and proximity of the earthquake. The latter conclusion is supported by the observations from several back-analyses presented in this report. Damage to non-engineered construction is as expected in major earthquakes. Most reinforced concrete bridges behaved well; displacements were in general larger than the design displacements, as evidenced by the severe yielding of seismic restrainers and the demolition of shear keys in abutments. Fragility relationships for common types of overpasses in Chile have been derived in this report and are offered for use in assessment of the impact from future earthquakes.

The role of social networking tools in enabling the affected population to communicate was a most interesting feature in the response to this earthquake. Due to

the failure of the power grid, and the congestion of the cellphone network, the population resorted to short message service and web social media. Ham radio networks were activated to fill gaps due to the failure of the radio network in places.

The MAE Center field reconnaissance team members consider that Chilean engineering was proven to be robust and that seismic design provisions and construction practices are of high standard. The extensive damage from this M_w = 8.8 earthquake is expected and within the 'life safety' performance target of seismic design codes.

TABLE OF CONTENTS

LIST OF FIGURES

LIST OF TABLES

1 OVERVIEW

1.1. MACRO-SEISMIC DATA

On February 27, 2010 at 03:34 am local time, the fifth largest worldwide recorded earthquake with a magnitude of 8.8 struck central Chile. The earthquake nucleated in the subduction region between the oceanic Nazca plate and the continental South American plate. The epicenter of the earthquake was approximately 8 km off the Chilean coast (35.909° S, 72.733° W) and the hypocenter was located at a depth of 35 km. The epicenter of the earthquake was relatively far away from major cities (the closest city Chillán was 95 km from the epicenter), and the fault associated rupture covered a region of approximately 80,000 square kilometers, causing major disruption and losses. Taking into account the inclined fault rupture and the earthquake magnitude, most cities in the coastal region of central Chile were subjected to a direct hit with almost zero distance from the causative fault.

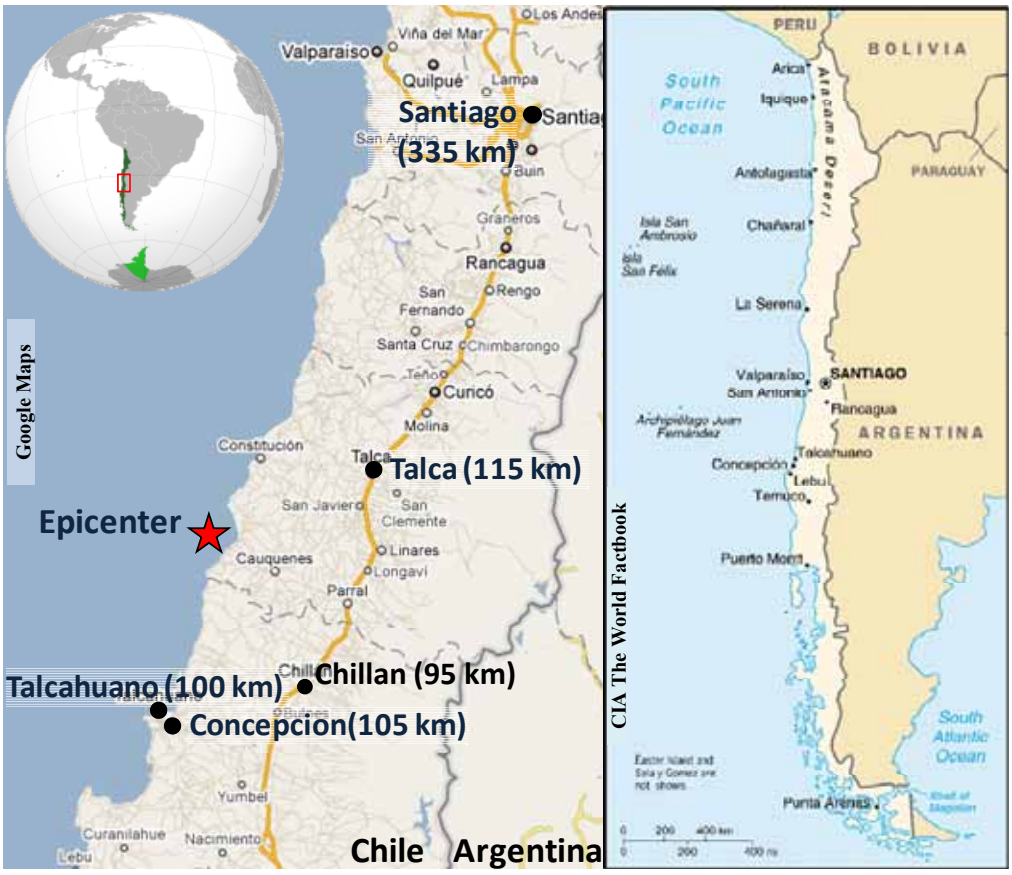

Figure 1.1 Left: epicenter of the February 27, 2010 Maule, Chile earthquake and closest major cities; Right: geographical location and bordering countries of Chile (note: epicentral distances mean very little in the case of great earthquakes of fault rupture regions of thousands of square kilometers)

Chile borders the South Pacific Ocean between Argentina and Peru (Figure 1.1). From north to south, Chile extends 4,270 km (with a coastline of 6,435 km) while the average east to west distance is only 177 km. The northern two-thirds of Chile is located on the Nazca Plate which moves towards the South American Plate and forms the Peru-Chile Trench. The strip shape of Chile that runs parallel to the Peru-Chile Trench makes the country prone to earthquakes. Chile has experienced several large earthquakes including the strongest ever recorded earthquake (1960 Valdivia earthquake) within the last century. The history of earthquakes forced Chile to develop strict regulations on seismic design of infrastructure.

1.2. STATISTICS ON DAMAGE, CASUALTIES, AND ECONOMIC LOSSES[1]

Over 12 million people were estimated to have experienced intensity VII or larger (on the Modified Mercalli scale), over 2 million people were affected to some level and there were 800,000 victims (injured, lost housing, died or missing) as a consequence of the earthquake. The impacts of the earthquake were observed in the following regions: Valparaíso, Metropolitan, O'Higgins, Maule, Bíobío and Araucania. Five large and 45 small cities in these regions with populations over 100,000 and 5,000, respectively, were impacted. The death toll as reported by the Ministry of Interior of Chile was 521. Fifty six people were reported to be missing. The fatalities were mainly in coastal areas, and where caused by the tsunami (more than 200 out of 521). Tsunami heights were calculated or observed to be as high as 12 m at some locations.

A total of 370,051 houses were damaged from earthquake and the consequential tsunami. The damage distribution is given in Table 1.1. The cost of damage to private houses is estimated as $3.7 billion. The adobe construction in Maule region suffered the most damage. In Curicó, 90 percent of adobe construction was destroyed. According to the Ministry of Health, 130 hospitals have experienced some damage accounting for the 71 percent of all public hospitals in Chile. The distribution of these hospitals in affected regions is provided in Table 1.2. Out of 130 hospitals, four became uninhabitable, 12 had greater than 75 percent loss of function, only eight were partially operational after the main shock, and 80 hospitals needed repairs. The estimated damage to hospitals is $3.6 billion. A total of 4,013 schools (representing nearly half of the schools in the affected areas) suffered significant damage. Repair and reconstruction needs are estimated as $3 billion. Four hundred and forty four churches, which account for the 47 percent of all churches in the country, were heavily damaged. The engineered buildings in general performed very well. According to the reconnaissance report prepared by Los

[1] The information in this section is compiled from reports issued by the government of Chile, Pan American Health Organization (PAHO), International Federation of Red Cross and Red Crescent Societies (IFRC), United Nations Office for the Coordination of Humanitarian Affairs (OCHA), and United Nations (UN) Country Team in Chile. Statistics from reconnaissance efforts of other agencies including: Technical Council on Lifeline Earthquake Engineering (TCLEE), Earthquake Engineering Research Institute (EERI), Los Angeles Tall Buildings Structural Design Council (LATBSDC), and Japan International Cooperation Agency (JICA).

Angeles Tall Buildings Structural Design Council, a study by Rene Lagos using the building permit statistics from National Institute of Statistics Chile indicated that out of 9,974 buildings constructed between 1985 to 2009, only four buildings collapsed and 50 buildings need to be demolished. Less than 2.5 percent of engineered structures in Chile suffered damage and out of all casualties, less than 20 died in engineered buildings.

Table 1.1 Housing damage distribution

	Destroyed	Major damage	Minor damage	TOTAL
Coastal	7,931	8,607	15,384	31,922
Urban Adobe	26,038	28,153	14,869	69,060
Rural Adobe	24,538	19,783	22,052	66,373
Government Housing Developments	5,489	15,015	50,955	71,459
Private Housing Developments	17,448	37,356	76,433	131,237
TOTAL	81,444	108,914	179,693	370,051

Table 1.2 Number of hospitals effected from the earthquake by region

Region	# of hospitals
Valparaiso	21
Metropolitan	31
O'Higgins	15
Maule	13
Bio-Bio	28
Araucania	22
TOTAL	130

According to the Ministry of Treasury, the economic losses are estimated to be $30 billion (loss of infrastructure: $20.9 billion, loss of production: $7.6 billion, other costs such as nutrition and debris removal: $1.1 billion) which is equivalent to 17 percent of the GDP of Chile. The Ministry of Agriculture estimated the agriculture sector losses to be $252 million from Valparaíso to Araucania. Seventy percent of the country's vineyards were located in the areas that were affected by the earthquake. According to Chilean Wine Corporation, an estimated 20 percent of the production was lost which amounts to $250 million. The Ministry of Public Works announced that the rehabilitation of damaged roads, airports, dams, canals, bridges and water towers will cost at least $1.2 billion. A major portion of the losses was to the transportation networks. According to the Ministry of Public Works, as of July 2010, the cost of the transportation infrastructure emergency repair is about $317 million while the reconstruction cost is estimated at $378 million for the public (non-private concessions) network only. According to the Ministry of Labor, a total of 8,417 people were made redundant from their jobs. The International Labour Organization reported this figure as 93,928.

The earthquake also caused a blackout that affected the 93 percent of the entire population and lasted for several days in some locations. Severe problems occurred in telecommunication systems due to power outage. Breaks or leaks to water and waste water pipes were observed and several elevated tanks collapsed, while buried tanks heaved out of the ground. Water canals also experienced some damage. The oil refinery in Santiago suffered minor damage and resumed operation 10 days after the earthquake. The other major refinery of the country located in Concepción (Bíobío region) experienced significant damage due to refractory in the heaters falling to the heater floor. Earthquake and the resulting tsunami damaged several ports (including the most important ports of the country: Valparaíso, Constitución, San Antonio, Talcahuano and Coronel), fish processing plants and wharfs. The damage to ports severely affected transnational trade. More than 26,000 small-scale fishermen lost their sustenance and the fishing capacity was reduced by 75 to 90 percent after the event. Out of the 59 ports considered by the National Confederation of Small-Scale Fisherman of Chile, 38 were found to have suffered significant damage. Santiago International Airport was out-of-operation for a week due to extensive nonstructural damage. This caused significant economic losses to airline companies and disruption to air traffic. Minor damage to Concepción Airport occurred. No commercial flights were allowed from and to Concepción airport for 10 days after the earthquake. Out of 12,000 highway bridges approximately 200 were damaged and about 20 of these bridges had collapsed spans.

1.3. FIELD MISSION ITINERARY AND GPS TRACKS

The MAE Center team traveled from Santiago (North) to Concepción (South) and back using ground transportation in three groups with focus on structural, transportation and geotechnical aspects of the reconnaissance mission. The team spent 6 days in Chile and visited several damage sites in Santiago, Talca, Concepción, Talcahuano and Coronel. The team also attended meetings with researchers from the Catholic University of Chile, University of Concepción, and University of Chile, the mayor of Talca, and officials from roadways concessions of Itata and Talca. Extensive follow-up work continued for several months, mainly undertaken by a member of the MAE Center who was on sabbatical at the Catholic University, Santiago. The field mission details, composition of the team and areas of expertise are provided in Table A.1. Figure 1.2 shows the travel route of the team as recorded by the GPS travel log. Detailed GPS travel logs in each city are provided in Appendix A.4. The subsequent chapters of this report provide more detailed information on the seismology and strong ground motion, performance of the built infrastructure, geotechnical observations, and social impacts of the earthquake.

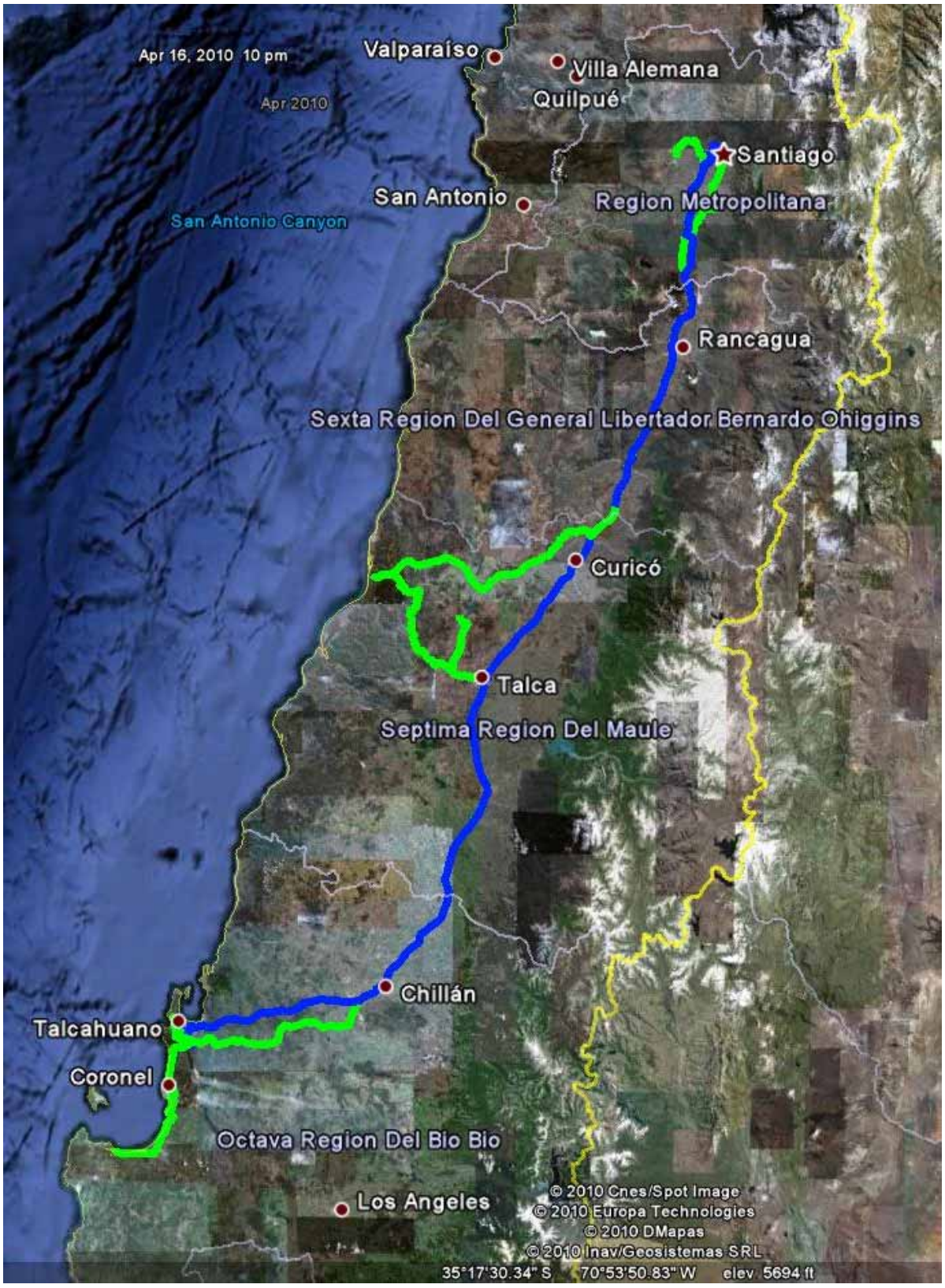

Figure 1.2 GPS travel log for the entire field mission (blue line: structures group, green line: geotechnical group)

1.4. ACKNOWLEDGEMENTS

The Department of Civil and Environmental Engineering at Illinois, and its Mid-America Earthquake Center wish to thank all colleagues from Chile who helped in so many ways, and without whose support the reconnaissance mission would have been much more challenging. Primary thanks go to Professor Rafael Riddell of the Catholic University of Chile in Santiago, and an Illini, for being the host and main contact, and for providing advice and practical support. Thanks are also due to Professor Guillermo Thenoux Z. and Mr. Marcelo González H. of the Catholic University and Center for Roadway Research and Engineering (CIIV) for establishing and leading the roadway damage visits along with Mrs. Carolina Cerda of CIIV for assisting in the trip logistics. A special thanks to Professor Carlos Videla of the Catholic University for his trip advice and presentation on building damage and Professor Mauricio López for accompanying the team on many of the site visits along with his valuable translation skills. Thanks to Professor Mauricio Pradena Miquel and colleagues of the University of Concepcion's Department of Civil Engineering for hosting our visit there and providing us with valuable earthquake and building damage data. The Earthquake team appreciates the site visit time and information provided by Juan Vargas (General Manager for the La Madera Concession), Luis Echeverria (Technical Manager for the La Madera Concession), Moisés Vargas Eyzaguirre (Technical Manager for the Itata Highway) and Mr. Fernando González (Senior Engineer) from the Cintra Talca-Chillán Concession. Finally, the Illinois team appreciates Professor Ramón Verdugo and colleagues at the University of Chile for their insightful earthquake damage presentations. Chapter 5 of this report was also contributed by Guillermo Thenoux, Marcelo González and Jonguen Baek.

2 ENGINEERING SEISMOLOGY

2.1. TECTONIC SETTING

The Maule Earthquake of 27 February 2010 nucleated on the subduction zone that runs along the entire ~5000 km length of the western coastline of South America, known as the Peru-Chile trench (http://earthquake.usgs.gov/). Earthquakes in this region are due to stress buildup resulting from the movement of the oceanic Nazca plate eastward and downward towards the South American plate, as shown in Figure 2.1, at a rate of approximately 70 mm per year (Schellart et al., 2007). This value can be compared to other subduction zones with slip rates of: ~70 mm/year for Java trench where the Indo-Australian plate subducts beneath the Sunda plate (Bilham et al., 2005), ~40 mm/year for the Cascadia subduction zone where Juan de Fuca plate subducts beneath the North American plate (DeMets et al., 1990), and ~20 mm/year for the Himalayan arc region where the Indian plate subducts beneath the Eurasian plate (Rao et al. 2003). As shown in Figure 2.2, the dense and heavy oceanic crust (Nazca plate) subducts beneath the lighter continental crust (South American plate). The formation of the Andes Mountain range is related to plate tectonics. It is believed that the thickening of the Andean crust is mostly due to tectonic shortening of the South American plate (Kley and Monaldi, 1998, Schellart et al., 2007).

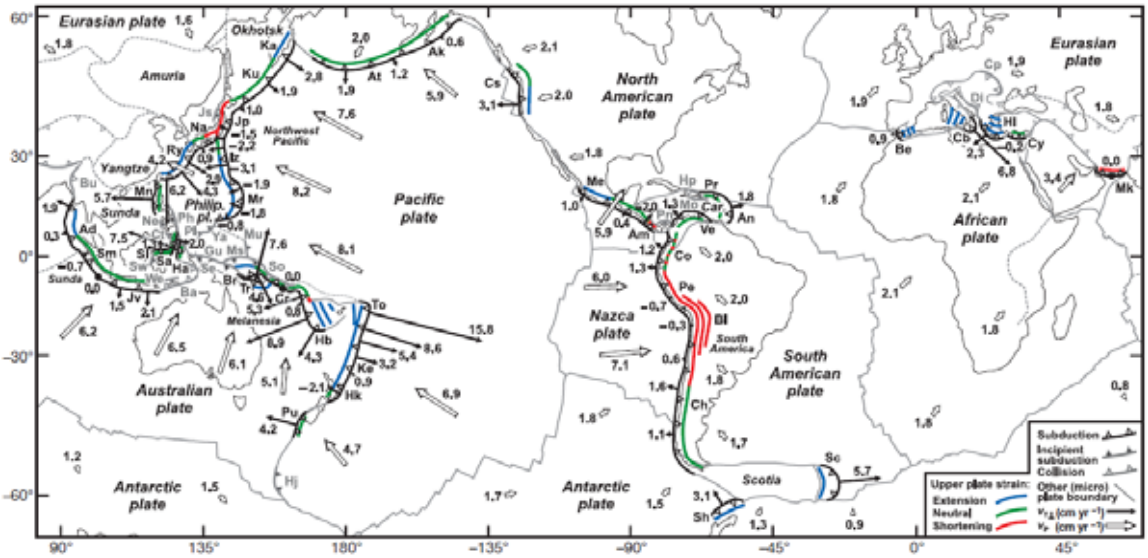

Figure 2.1 Subduction zone between the Nazca and South American plates (Schellart et al., 2007)

The Pacific rim that runs along the coast of Chile includes the following features: (1) an oceanic trench (as a topographic deep from latitude 4° N to 40° S, and a negative gravity belt from 40° S to 56° S), (2) a sub-parallel discontinuous chain of active and dormant volcanoes, (3) a zone of active seismicity (where the lower limit of earthquake

hypocenters deepening from beneath the trench to beneath the volcanic chain and the continent), and (4) progressive thickening of the crust away from the ocean basin from 11 km up to 55-70 km (Plafker and Savage, 1970). According to Barazangi and Isacks (1976) the Peru-Chile trench can be separated into five segments where each of the segments has a relatively uniform dip. The two segments along the shoreline of northern and central Peru (2° S to 15° S) and along central Chile (27° S to 33° S) have a dip angle of about 10° to the east. In contrast, the three segments near southern Ecuador (0° to 2° S), southern Peru and northern Chile (15° to 27° S), and southern Chile (33° S to 45° S) have steeper dip angles from 25° to 30°. It is interpreted that the individual segments are bounded by tears in the subducting slab. However, later studies (Bevis, 1986; Bevis and Isacks, 1984) interpreted the segment boundaries as a smooth contortion rather than a tear (Cahill and Isacks, 1992). An earlier study by Swift and Carr (1974) divides the northern and central Chilean seismic zone into seven segments. The northern Chile (from 19.5° S to 29° S) is characterized by four segments where the dip angle varies from 30° at the north to 15° at the south, while the central Chile is divided into three segments. It is observed that the earthquakes of magnitude greater than 8.2 occur within individual segments while the earthquakes with magnitude less than 8 occur on or near the segment boundaries.

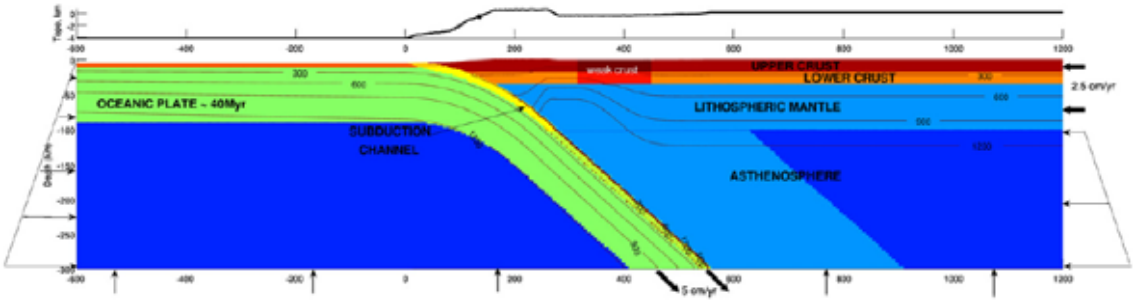

Figure 2.2 Cross-section of the subduction zone (Gerbault et al., 2009)

2.2. HISTORICAL SEISMICITY IN THE REGION

Due to the close proximity to the Nazca-South America subduction zone, Chile has long been subjected to earthquakes of large magnitude. On average, a magnitude 8.0 earthquake occurs every decade and a magnitude 8.7 earthquake or greater is observed within a century. Table 2.1 lists the earthquakes of magnitude 8.0 or greater that affected Chile since the records started in this region. Amongst these earthquakes, the most notable ones are the 1868 Valdivia and 1939 Chillán earthquakes that claimed more than 50,000 lives; the 1960 Valdivia earthquake which is the largest earthquake ever recorded by seismological instruments; and the 1730 Valparaíso and 1751 Concepción earthquakes which occurred in the vicinity of the 2010 earthquake and produced tsunamis of considerable size in the Pacific Ocean.

Before the 2010 Maule Earthquake, Ruegg et al. (2009) studied the seismic gap between Constitución and Concepción using GPS measurements and concluded that

more than 10 m of displacement accumulated since the last large interplate event (1835 earthquake) and the region has the potential to produce an earthquake of magnitude 8-8.5.

Table 2.1 Historical earthquakes in Chile with magnitude 8.0 or greater, from 1570 to 1953 from Lomnitz (1970), 1953 to present from U.S. Geological Survey (USGS) (http://earthquake.usgs.gov/earthquakes/world/historical_country.php#chile)

Year	Epicentral Region	Magnitude
1570	Concepción	8.5
1575	Valdivia	8.5
1604	Arica	8.5
1647	Santiago	8.5
1657	Concepción	8
1730	Valparaíso	8.75
1737	Valdivia	8
1751	Concepción	8.5
1796	Copiapó	8
1819	Copiapó	8.5
1822	Valparaíso	8.5
1835	Concepción	8.25
1837	Valdivia	8
1868	Arica	8.5
1877	Pisagua	8.5
1880	Illapel	8
1906	Valparaíso	8.6
1922	Huasco	8.4
1928	Talca	8.4
1939	Chillán	8.3
1943	Illapel	8.3
1960	Valdivia	9.5
1985	Santiago	8.0
1995	Antofagasta	8.0
2010	Maule	8.8

The map in Figure 2.3 shows recent major earthquakes in Chile alongside seismic gaps. The white circles indicate the rupture for individual events, the red circles show the epicenters and the yellow dots are the aftershocks. From north to south, the Peru-Chile trench has ruptured in several incidents except for three locations that are shown with red lines. The segment of the subduction zone, Concepción gap in Figure 2.3, between the 1985 Valparaíso and the 1960 Valdivia earthquakes, which last produced an earthquake in 1835, is the zone that ruptured during the 2010 earthquake. Another segment, the Arica gap has been relatively inactive since 1877 and has the potential to produce an earthquake of magnitude 8.0 to 8.5. There has been energy release with the

Valparaíso (1906 and 1985), La Serena (1943) and Vallenar (1922) earthquakes in the La Serena seismic gap but it is uncertain if all of the energy accumulated in this region has been released with these events.

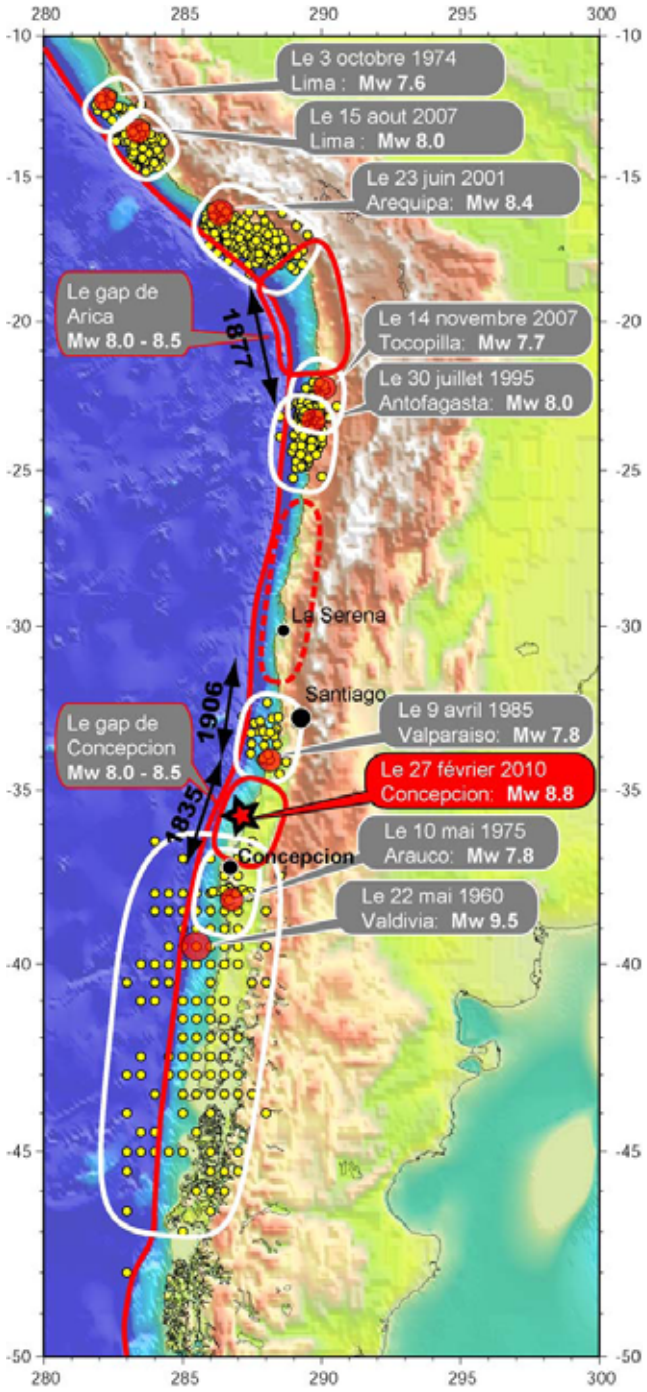

Figure 2.3 Recent major earthquakes in Chile and seismic gaps (Laboratoire de Géologie, Ecole Normale Supérieure (ENS), CNRS, Paris, France, http://www.geologie.ens.fr/~vigny/chili-f.html)

2.3. THE 27 FEBRUARY 2010 EARTHQUAKE

The Maule earthquake struck Chile on 27 February 2010 at 03:34 a.m. local time. The magnitude of the earthquake is estimated as Mw 8.8. The epicenter was located offshore at 35.909° S, 72.733° W with the following distances to major cities: Chillán 95 km, Concepción 105 km, Talca 115 km, and Santiago 335 km. The hypocenter was 35 km deep (http://earthquake.usgs.gov/earthquakes/eqinthenews/2010/us2010tfan/). The average slip over the approximately 81,500 km^2 rupture area was 5 m, with slip concentrations down-dip, up-dip and southwest, and up-dip and north of the hypocenter. Relatively little slip was observed up-dip/offshore of the hypocenter. The average rupture velocity was estimated to be in the range of 2.0-2.5 km/sec. The Global Centroid Moment Tensor (GCMT) solution yielded a seismic moment of 1.84 x 10^{22} Nm, a centroid location of 35.95° S, 73.15° W, and a best double couple fault plane geometry with strike and dip angles of 18°, and a rake angle of 112° (Lay, et al., 2010).

The simulation of the fault rupture based on the study by Lay et al. (2010) is provided in Figure 2.4. It is seen from the inset in Figure 2.4 that shows the normalized power as a function of time that the duration of the earthquake exceeded 3 min. However, the significant energy was released within the first the 2 min. It is also concluded by studying the propagation of rupture that the fault was bilateral, spreading away from the epicenter in both the north and south directions.

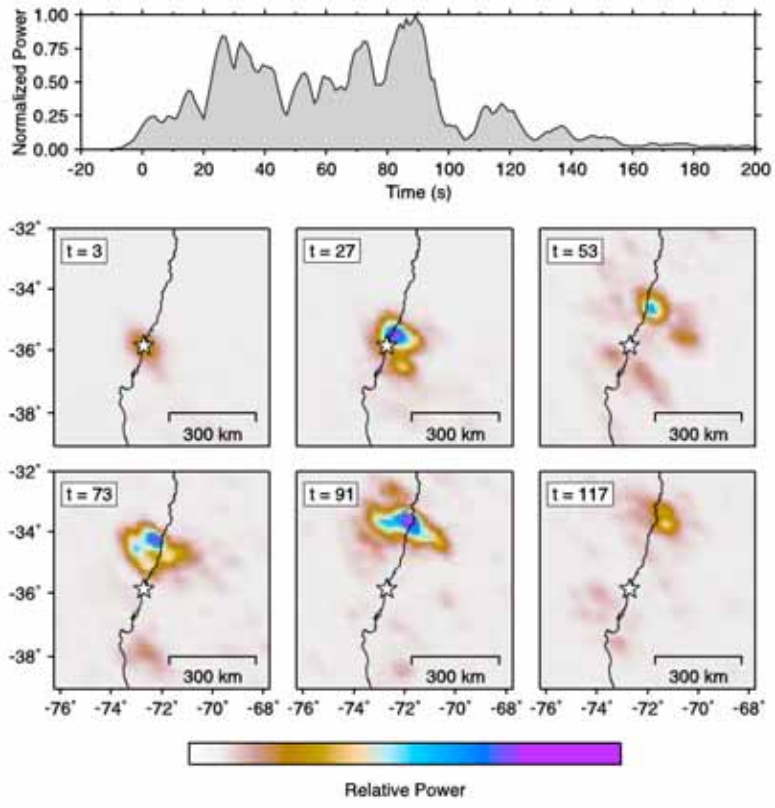

Figure 2.4 Frames from the simulation of the fault rupture (Lay et al., 2010)

The size of the fault zone varies depending on the calculation method. According to method proposed by the National Earthquake Information Center (NEIC), the size of the fault zone is 189 x 530 km. This method is also used for the strong ground motion derivations given in Section 2.4 of this report. The fault zone by NEIC is shown in Figure 2.5. The prediction from California Institute of Technology yields a fault size of 170 x 560 km, as shown in Figure 2.6. The colors on the fault zone indicate the amplitude of slip, relative movement of one fault plane with respect to the other. The slip amplitude reached 9 m at peak location. As a comparison, the maximum value of slip during the Chile event is only about 2 times that of the recent Haiti earthquake (maximum slip is about 5 m). However, the amount of energy release is approximately 500 times larger. This is due to much larger rupture zone in the Chile earthquake as compared to the case of Haiti. The slip distribution on the fault cross-section is shown in Figure 2.7.

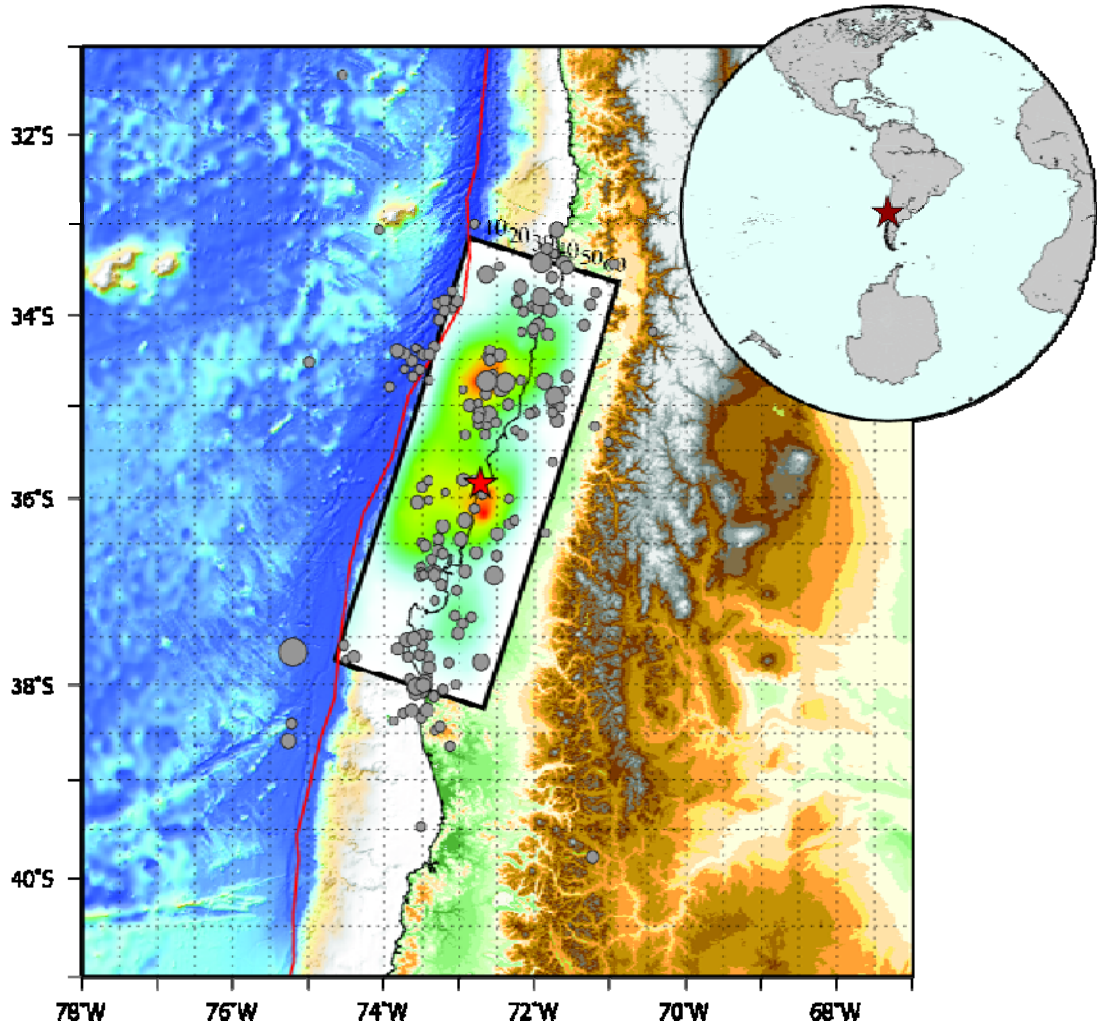

Figure 2.5 Fault zone and surface prediction of the slip distribution, NEIC, USGS (http://earthquake.usgs.gov/earthquakes/eqinthenews/2010/us2010tfan/finite_fault.php)

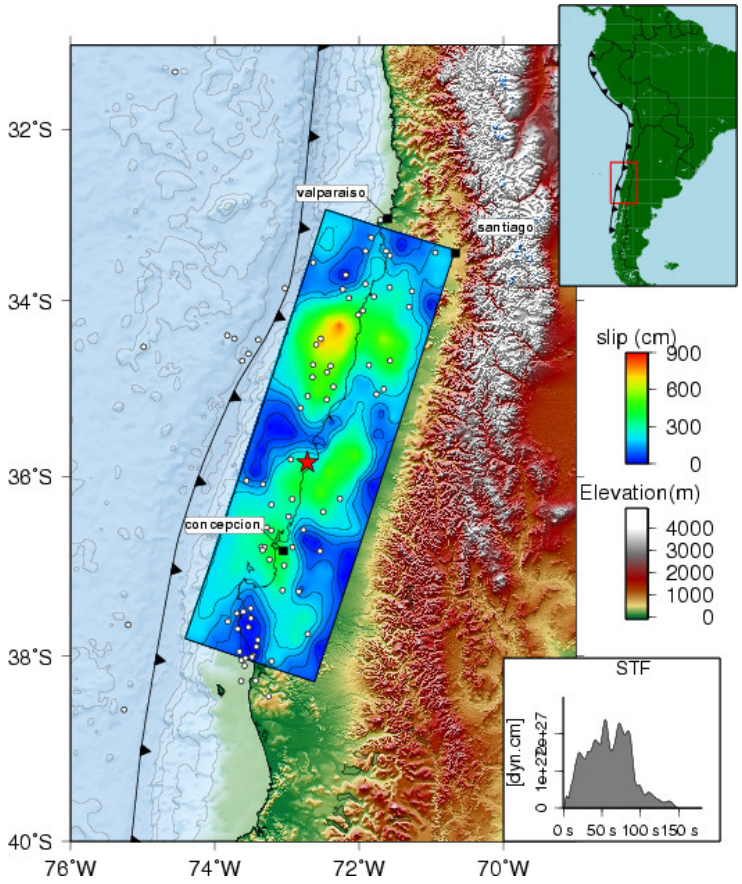

Figure 2.6 Fault zone and surface prediction of the slip distribution, California Institute of Technology (http://www.tectonics.caltech.edu/slip_history/2010_chile/)

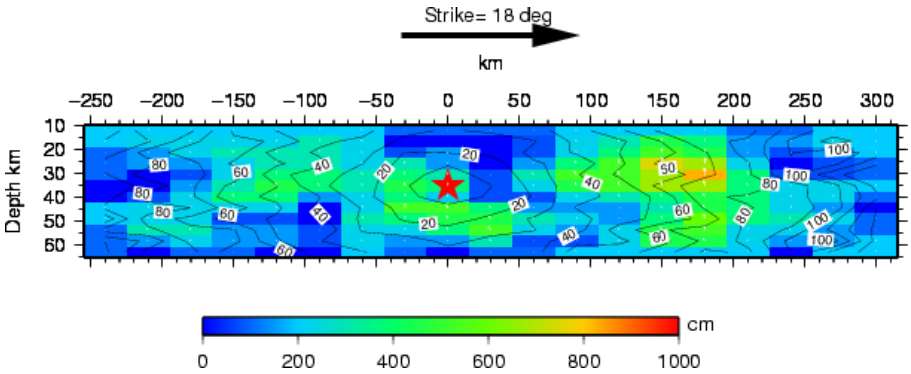

Figure 2.7 Slip distribution on fault cross-section according, California Institute of Technology (http://www.tectonics.caltech.edu/slip_history/2010_chile/)

The vertical movement of the ground is shown in Figure 2.8. The uplift reached as high as 2 m and settlements of 0.4 m were observed. The coast of Chile moved west, into the ocean as much as 6 m at some locations.

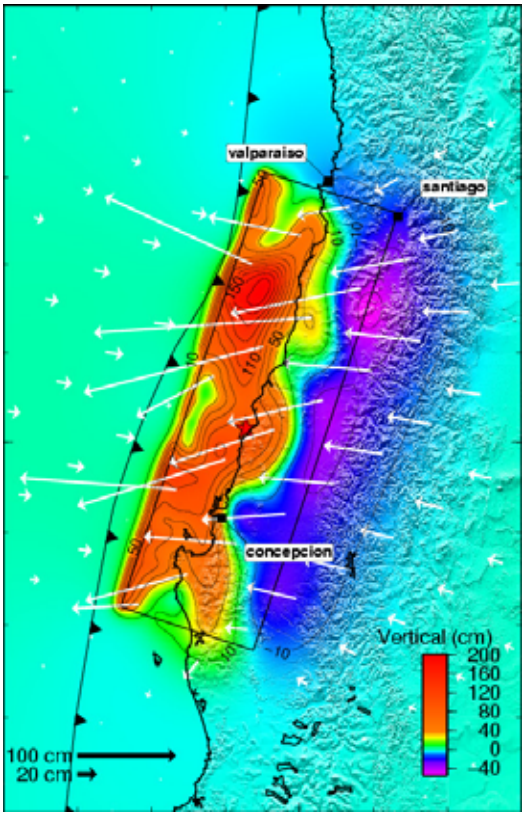

Figure 2.8 Predicted surface deformation. The vertical component is shown with color scale and the horizontal component is indicated with arrows (http://www.tectonics.caltech.edu/slip_history/2010_chile/)

The instrumental intensity map for the main event is shown in Figure 2.9. As seen in the figure, the earthquake was strongly felt in a large area, and the instrumental intensity reached as high as IX at some locations. Several aftershocks followed the main event. According to U.S. Geological Survey (USGS), by 6 March 2010 more than 130 aftershock were recorded, thirteen with magnitudes greater than 6.0, by 26 April 2010, 304 aftershocks of magnitude 5.0 or greater were registered. Out of these earthquakes 21 had magnitudes greater than or equal to 6.0. The distribution of aftershocks within the period from the main event until 24 March 2010 scaled by magnitude is shown in Figure 2.10. The aftershock distribution color-coded by depth is shown in Figure 2.11.

The earthquake was the 5th strongest earthquake recorded worldwide (after the 1960 Chile, 1964 Alaska, 2004 Sumatra and 1952 Kamchatka earthquakes). It was felt as far as Southern Peru, Bolivia, Argentina and Brazil. The initial event was strong enough to even cause seiches in Lake Pontchartrain near New Orleans, Louisiana (The Weather Channel, www.weather.com). According to a joint study between several institutions including the Ohio State University and University of Memphis, GPS measurements indicated that the South American plate moved westward: Concepción and Santiago moved 3 m and 27.7 cm to the west, respectively and even Buenos Aires

(Argentina) moved 4 cm (http://researchnews.osu.edu/archive/chilequakemap.htm). The displacements of the South American plate based on the GPS measurements are shown in Figure 2.12.

When compared to other events that occurred on the same trench, the 2010 earthquake created relatively small tsunami. It is hypothesized that the earthquake had its largest stress release in shallower waters compared to previous events. Hence, the height of the displaced water column is much less. The earthquake generated large waves and caused more dramatic effects locally but did not have enough energy to travel the Pacific Ocean and cause significant damage in other parts of the world (Faculty of Geo-Information Science and Earth Observation, University of Twente, http://www.itc.nl/27February2010-Earthquake-in-Chile).

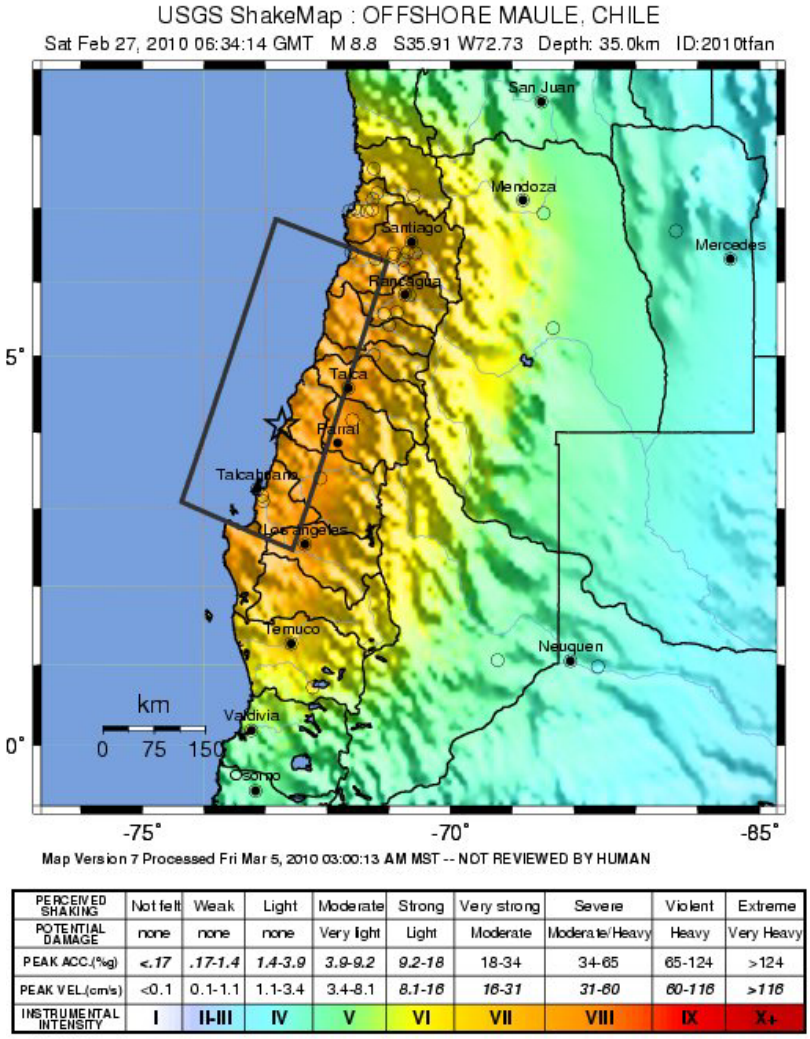

Figure 2.9 Instrumental intensity map for the main shock (http://earthquake.usgs.gov/earthquakes/shakemap/global/shake/2010tfan/)

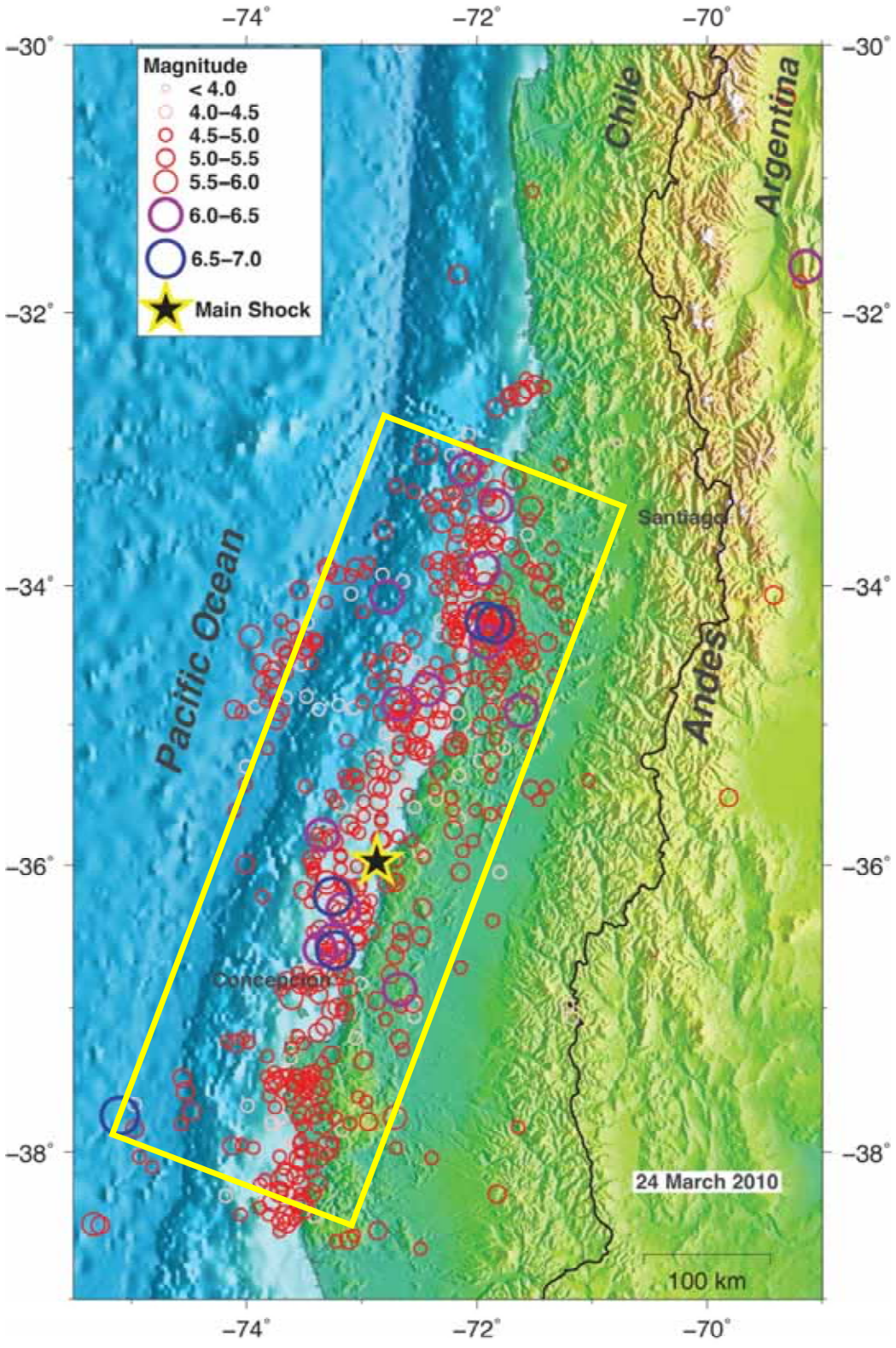

Figure 2.10 Aftershocks by magnitude, 2/27/10 to 3/24/10, the superimposed rectangle has dimensions 200 km x 600 km (http://www.iris.edu/hq/chile/maps)

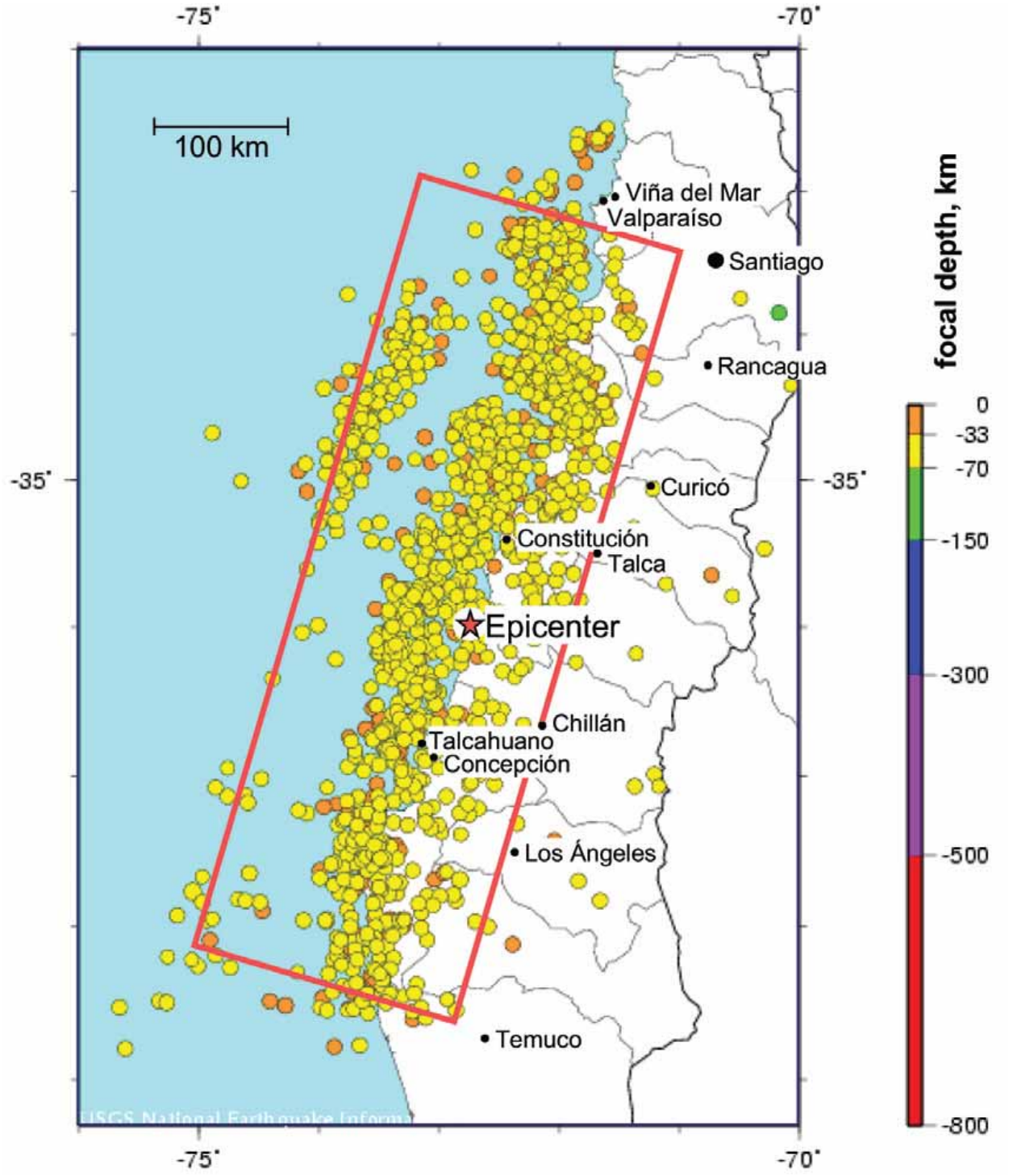

Figure 2.11 Aftershocks by depth, 2/27/10 to 3/27/10, the superimposed rectangle has dimensions 200 km x 600 km (http://earthquake.usgs.gov/earthquakes/eqinthenews/2010/us2010tfan/)

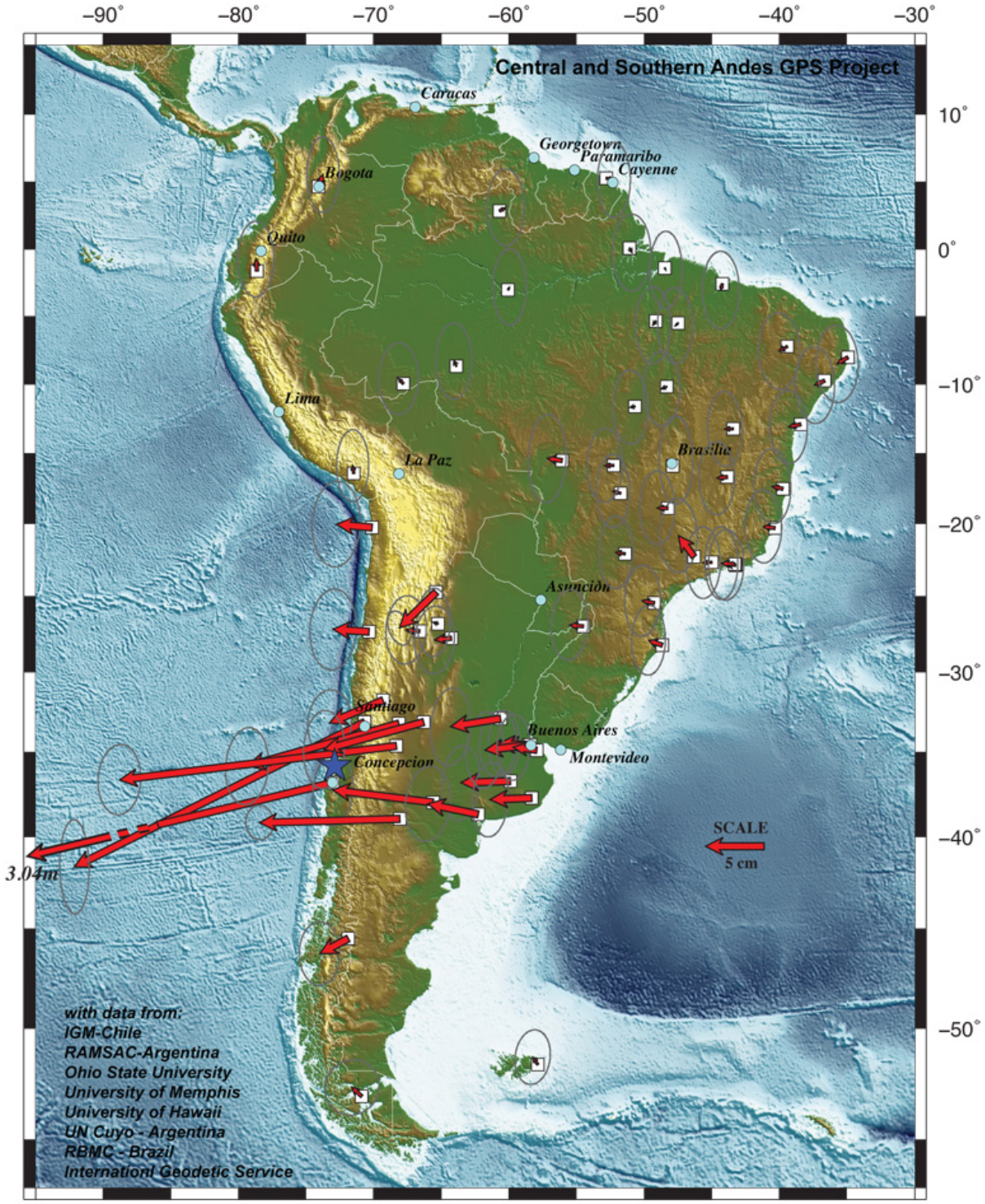

Figure 2.12 Displacement of the South American Plate as a result of the 2010 Maule earthquake (http://researchnews.osu.edu/archive/ chilequakemap.htm)

2.4. STRONG GROUND MOTION

2.4.1. Available Measurements

Ground motions were recorded by two departments at the University of Chile. At the time of writing this report, recordings at 10 stations were available from the Seismological Service at the department of Geophysics and recordings at 9 stations were available from Red National de Acelerografos Departamento de Ingenieria Civil (RENADIC). These stations are listed in Table 2.2, along with peak ground acceleration of each component and distances to fault based on different measures. RENADIC did not provide digital records. However, plots of acceleration time-histories and response spectra were made available. No information is available regarding the site classifications for any of the strong motion stations. The finite fault model by Hayes (2010) shown in Figure 2.5 is used to calculate the closest distance to the rupture plane. Figure 2.13 shows the surface projection of fault and location of the stations along with seismic zones defined by the Chilean seismic code, NCh 433 (1996).

Table 2.2 Information on stations and the recorded strong ground motions

Station		PGA (g)			Distance (km)*			
ID	Name	NS	EW	Vert	d_e	d_h	d_{sp}	d_{rup}
Seismological Service								
CCSP	Colegio San Pedro, Concepción	0.65	0.61	0.58	109.1	114.6	0.0	36.4
CSCH	Casablanca	0.29	0.33	0.23	311.7	313.6	20.9	48.5
MELP	Melipilla	0.57	0.78	0.39	283.0	285.1	0.0	52.5
ANTU	Campus Antumapu, Santiago	0.23	0.27	0.17	323.0	324.9	25.3	66.1
STL	Cerro Santa Lucia	0.24	0.34	0.24	334.2	336.0	32.5	69.2
LACH	Colegio Las Americas	0.31	0.23	0.16	339.1	340.9	39.8	72.9
CLCH	Cerro Calán, Satiago	0.21	0.23	0.11	343.8	345.6	43.1	74.8
OLMU	Olimue	0.35	0.25	0.15	353.7	355.4	62.2	78.6
SJCH	San José de Maipo	0.47	0.48	0.24	332.5	334.4	49.8	78.8
ROC1	Cerro El Roble	0.19	0.13	0.11	361.6	363.3	67.9	85.4
RENADIC								
MMVM	Viña del Mar (Marga Marga)	0.35	0.34	0.26	336.7	338.5	47.0	60.8
CEVM	Viña del Mar (Centro)	0.22	0.33	0.19	337.8	339.6	48.5	61.0
MAIP	CRS MAIPU RM	0.56	0.48	0.24	321.3	323.2	19.1	64.0
CURI	Hosp. Curicó	0.47	0.41	0.20	170.4	174.0	13.0	65.1
SRSA	Hosp. Sotero de Río RM	0.27	0.26	0.13	325.2	327.1	29.7	68.0
UCSA	Universidad de Chile Depto Ing. Civil (Interior Edificio) Satiago	0.17	0.16	0.14	331.6	333.5	30.0	68.0
MMSA	Estación Metro Mirador Satiago	0.24	0.17	0.13	329.5	331.3	30.3	68.2
LTSA	Hosp. Luis Tisne RM	0.30	0.29	0.28	332.3	334.2	33.4	69.6
VALD	Hosp. Valdivia	0.09	0.14	0.05	437.8	439.2	182.8	192.7

*d_e: epicentral distance, d_h: Hypocentral distance, d_{sp}: distance to surface projection of the fault, and d_{rup}: distance to rupture plane.

Figure 2.13 Rupture zone, seismic zone from the Chilean seismic code and locations of stations; green circle – RENADIC, yellow circle – Seismological Service

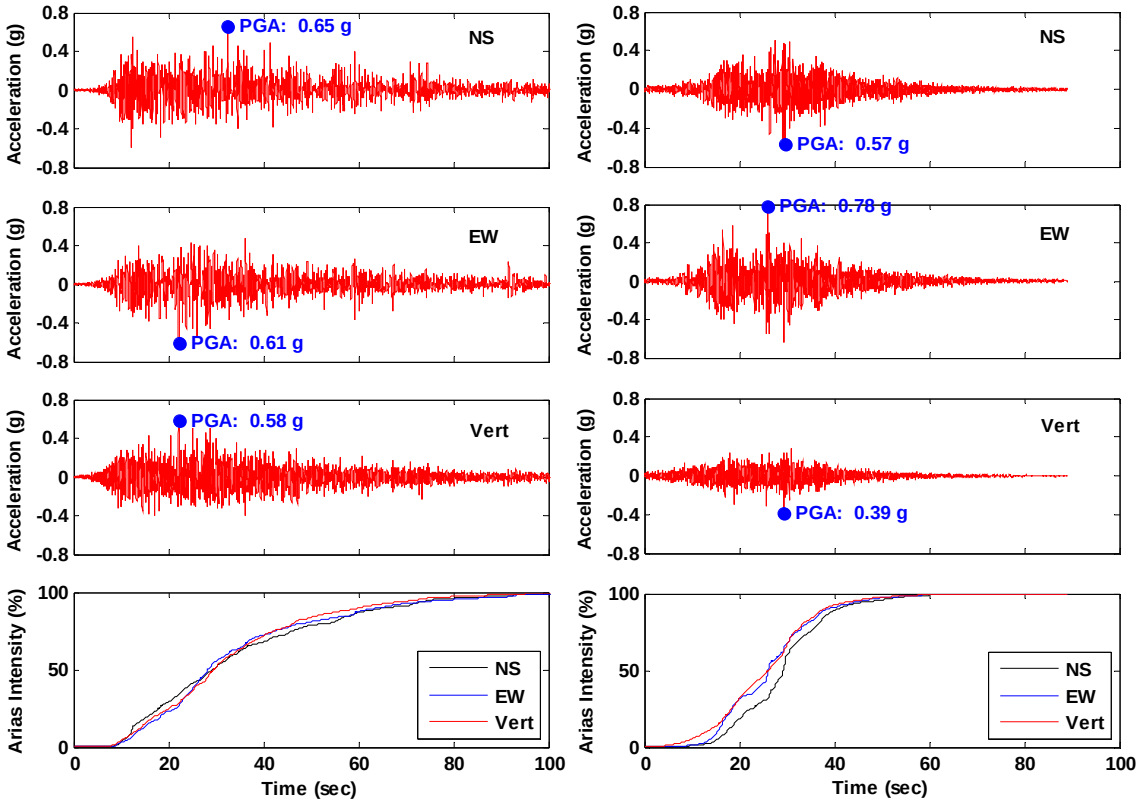

Figure 2.14 Accelerations and Arias Intensity, *Left:* station CCSP; *Right:* station MELP

Figure 2.14 shows the two records, provided by the Seismological Service, that have the highest peak ground acceleration (PGA), alongside their Arias Intensity. PGA of horizontal component from CCSP and MELP are 0.65 g and 0.78 g, respectively. The 5 percent damped elastic spectra for the recorded ground motions are shown in Figure 2.15. Figure 2.16 shows the spectra separated based on the seismic zone specified in the Chilean seismic code along with the recommended design spectra for soil types I to IV (from rock to saturated cohesive soil). In general the design spectra from Chilean seismic code match relatively well with the spectra from recorded ground motions. However, for soil I and II, the spectra of records exceed the design spectra for the intermediate period range. Additionally, as shown in Figure 2.16 (c and d), the spectra of the records at stations MAIP, CURI, CCSP and MELP, exceed significantly the design spectra for periods shorter than 1 sec. Moreover, the amplifications for these records are 4.26, 4.06, 3.39, and 3.67, respectively, which is an indication of the severity of these records, particularly when compared with the value of 2.70, which is the 84 percentile amplification factor given by Newmark and Hall (1982), and used widely. The amplifications of these records are also noteworthy when compared with the amplification factors from the Chilean seismic code, which vary from 2.76 to 3.09 depending on the soil class. Such a feature could result in relatively high demand imposed on short period structures that are designed to conform to code requirements.

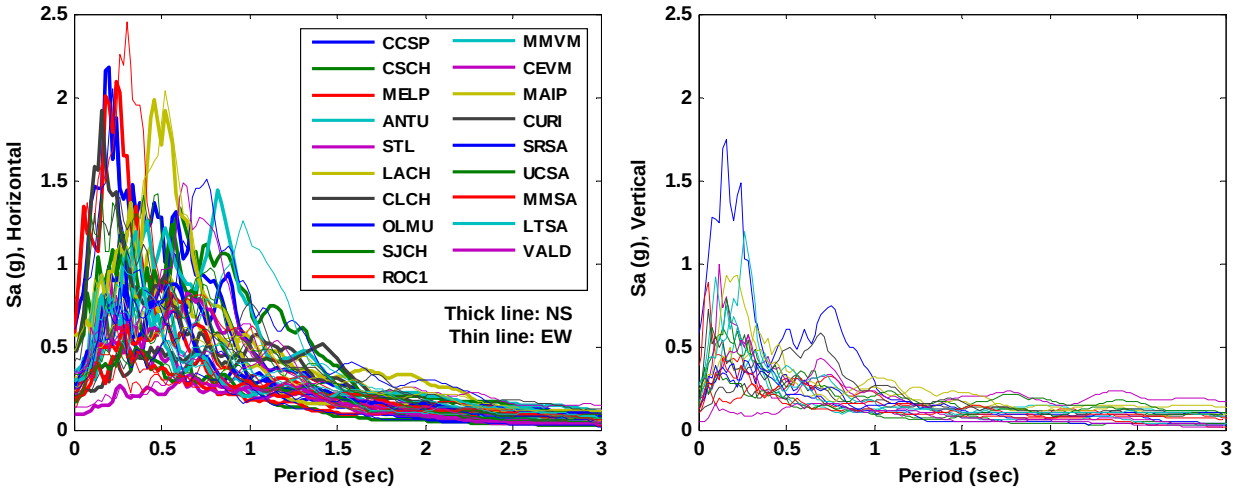

Figure 2.15 *Left:* horizontal spectra; *Right:* vertical spectra

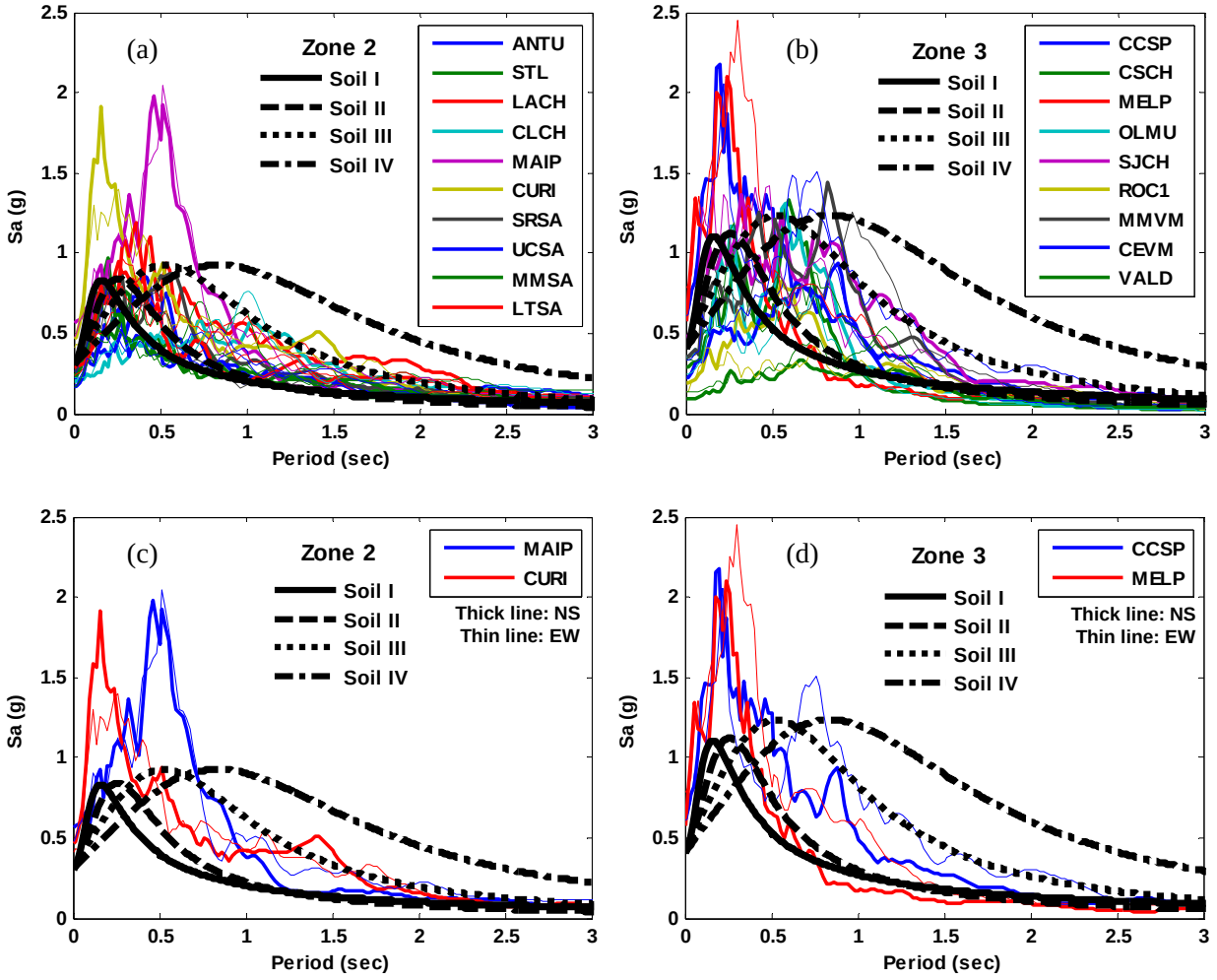

Figure 2.16 Comparison of measured spectra (5 percent damping) with design spectra from the Chilean seismic code

Table 2.3 shows the durations of the records based on the bracketed (with a threshold = 0.05 g) and significant duration definitions. The duration of shaking is directly related to the inelastic deformation and energy dissipation demands on the structure. If a structure is deformed beyond its elastic limit, the amount of permanent deformation will depend on how long the shaking is sustained. Therefore, the duration of earthquake shaking is a very important measure of the damage potential of the ground motion. The duration of strong ground motion can vary depending on the magnitude, source distance, and local site conditions. The duration of strong ground motion increases with increasing earthquake magnitude (Chang and Krinitszky, 1977). The existing attenuation relationships for strong motion duration (Kamiyama, 1984, Papazachos et al., 1992) show that the bracketed duration decreases with increasing distance from the source, while the significant duration increases. This is because the bracketed duration uses the absolute threshold of the amplitude, which decreases with increasing distance from the fault. On the other hand, the significant duration utilizes the relative threshold and thus, is related to the geometry of the accelerogram, regardless of its absolute amplitude. The existing attenuation relationships for a large earthquake like the Chile earthquake are sparse. Therefore, to compare the severity of the durations from the Chile earthquake records, horizontal components of large earthquake records are selected from the Pacific Earthquake Engineering Research (PEER), Next Generation Attenuation (NGA) project database (http://peer.berkeley.edu/nga). The selected records are from relatively large earthquakes ($M_w \geq 6.9$) with a peak ground acceleration of 0.1 g or more and source distances of less than 100 km. Figure 2.17 shows the comparison of the bracketed durations (with a 0.05 g threshold value). This figure indicates that the records from the Chile earthquake exhibit longer duration when compared with records from other earthquakes. Therefore, this feature of the records from the Chile earthquake could have increased the amount of damage.

Table 2.3 Bracketed and significant durations of ground motions (in seconds)

Station ID	NS		EW		Vert	
	D_b*	D_s**	D_b	D_s	D_b	D_s
CCSP	113.14	64.23	110.91	67.62	98.87	61.80
CSCH	45.17	32.18	50.26	30.07	41.49	32.08
MELP	60.23	31.94	58.83	31.78	49.59	33.79
ANTU	44.50	37.52	45.88	37.68	45.02	47.56
STL	58.93	41.20	50.96	37.37	59.80	40.86
LACH	49.33	36.73	54.87	37.54	52.04	46.95
CLCH	47.06	42.42	49.30	38.32	44.00	50.38
OLMU	47.06	27.56	48.86	32.08	28.76	34.02
SJCH	71.21	37.93	68.36	38.56	70.71	53.98
ROC1	34.89	31.88	34.20	35.48	22.95	36.63

* D_b: bracketed duration with a threshold of 0.05g
** D_s: significant duration (5 – 95 % of Arias Intensity)

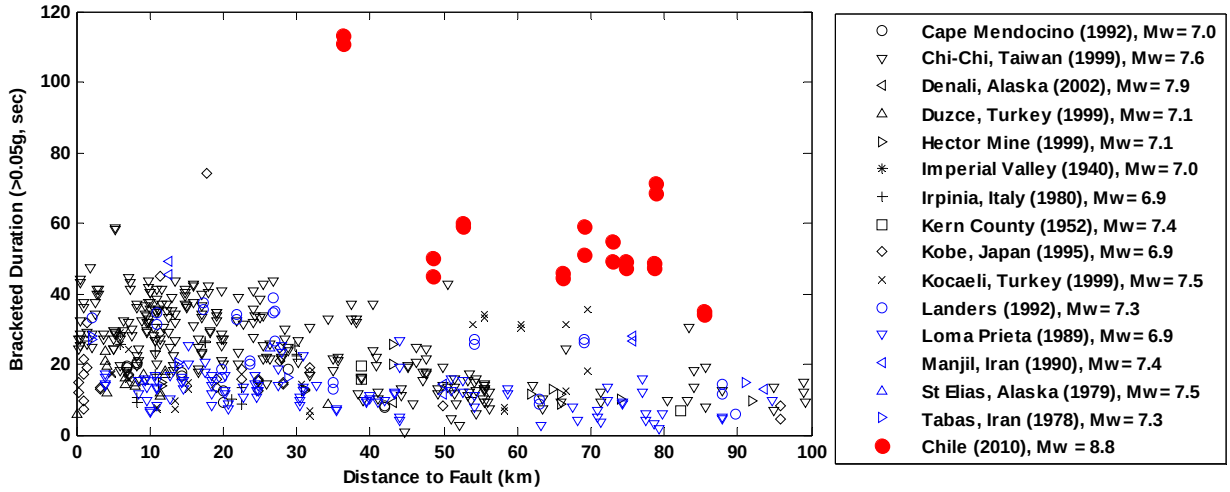

Figure 2.17 Comparison with the durations of horizontal components of earthquake records selected from the NGA database

2.4.2. Attenuation of Ground Acceleration

The available data from the 19 stations in Chile are used to select appropriate attenuation relationships for horizontal ground motions. Attenuation relationships that are developed for subduction zones with thrust mechanisms and large magnitude events, and that utilize a large and uniformly processed data base are selected here. The five candidate attenuation relationships are

- Zhao et al. (2006)
- Atkinson and Boore (2003)
- Campbell and Bozorgnia (2003)
- Gregor et al. (2002)
- Youngs et al. (1997)

Note that most of the existing attenuation relationships are not developed to account for large magnitude earthquakes such as the 2010 Chile earthquake. Due to lack of soil type information for the ground motion records, comparison of the selected attenuation relationships is made for rock site as shown in Figure 2.18. The predictions of the candidate attenuation relationships for the various soil classifications are provided in Appendix B. As shown in Figure 2.18, the PGA and spectral acceleration values predicted by the attenuation relationship by Zhao et al. (2006) and Campbell and Bozorgnia (2003) are in good agreement with the measured data. Therefore, these attenuation relationships are selected to generate hazard maps and the ground motions required for back-analysis.

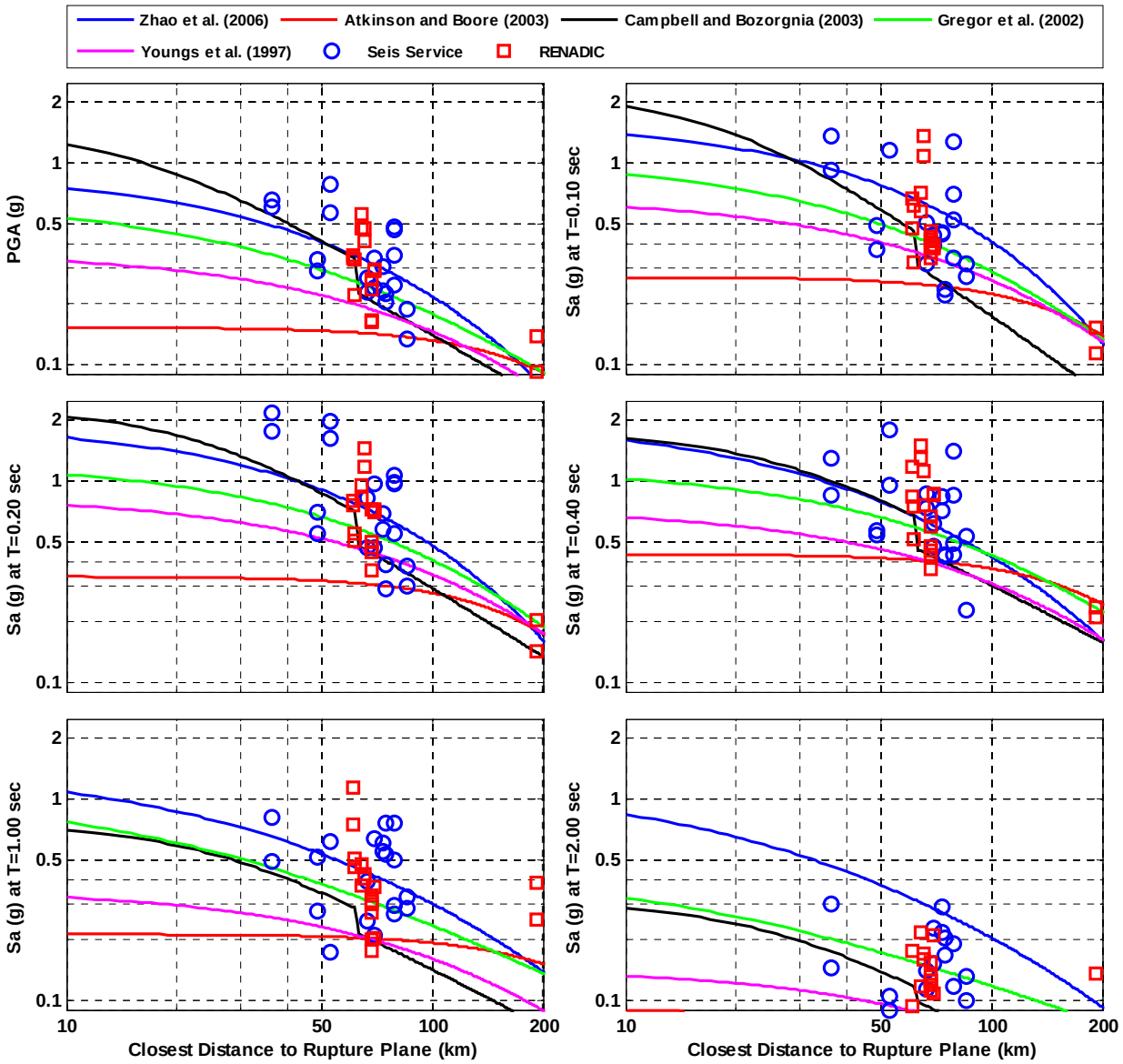

Figure 2.18 PGA and response spectra attenuation relationships for rock

2.4.3. Selection of Records for Back-Analysis of the Case Studies

The records for back-analysis of the case studies reported in Chapter 4 are selected amongst the digital recordings available through the Seismological Service at the University of Chile. Most of the stations provided by RENADIC are located north of the rupture plane and none of the stations are within 100 km from case study structures. Additionally, no digital records from RENADIC are available. Therefore, records from the Seismological Service are considered as seed signals to generate records for back-analysis. Figure 2.19 shows locations of structures for case studies and the locations of the stations.

Figure 2.19 Yellow dots: location of stations (that are maintained by the Seismological Service) and red dots: structures considered as case studies

To generate a suite of records representative of the hazard at the location of the structures where no recordings exist, distance from the fault, attenuation relationship for PGA, and acceleration response spectra are considered. Particularly, the selected attenuation relationships are combined accounting for their standard deviation as follows:

$$RSA = RSA_z(m_z \pm \alpha\sigma_z)\cdot W_1 + RSA_c(m_c \pm \alpha\sigma_c)\cdot W_2 \quad (2.1)$$

where RSA_z is the attenuation relationship by Zhao et al. (2006), RSA_c is the attenuation relationship by Campbell and Bozorgnia et al. (2003), m is the mean value, α is the weight on standard deviation, here selected as 0, ± 0.5, ± 1.0 and ± 1.5, σ is the standard deviation, and W is the weight on the spectral acceleration attenuation relationship.

Figure 2.20 shows the comparison between the combined attenuation relationship and PGA or spectral values of the recorded ground motions. The attenuation relationship is plotted along with its standard deviation of $\pm 0.5\sigma$, $\pm 1.0\sigma$ and $\pm 1.5\sigma$. The combined attenuation relationship is used to generate the target spectra. The target spectra for each site are shown in Figure 2.21. The mean spectra and spectra generated with $\pm 0.5\sigma$ are selected to be used in spectrum matching of the case study records as this range is considered to capture the variation in the strong ground motions from the Chile earthquake.

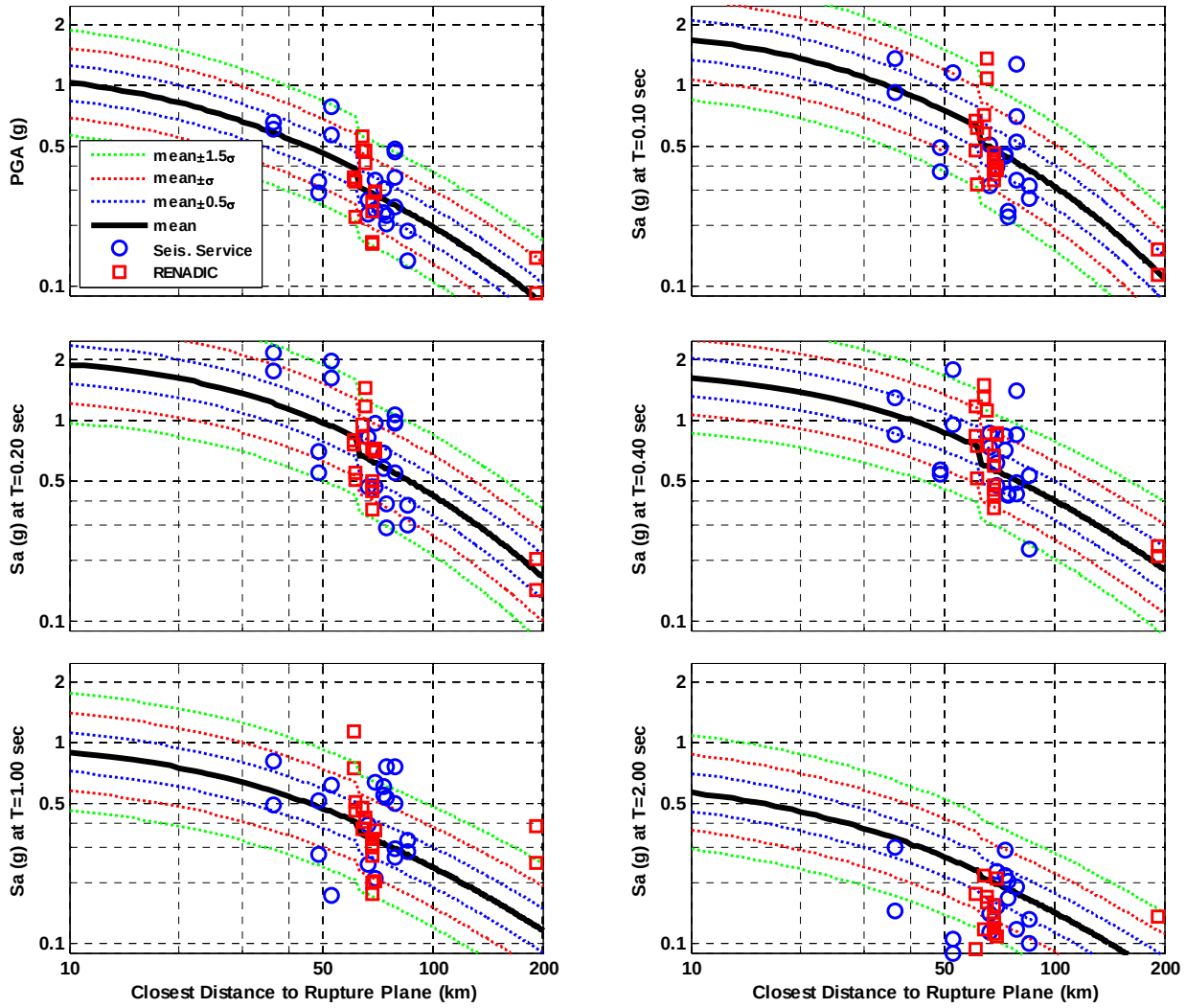

Figure 2.20 Combined attenuation relationship for rock site for PGA and spectral acceleration at different periods

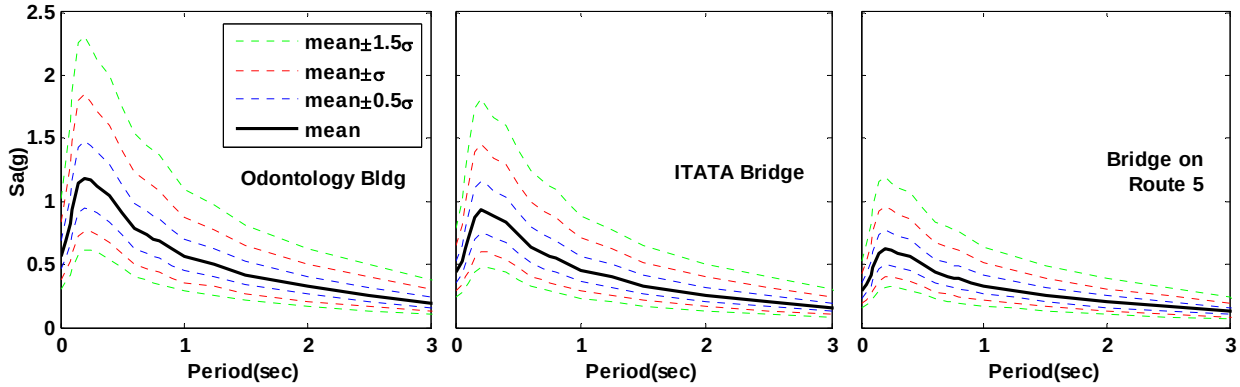

Figure 2.21 Target spectra for back-analysis of the case studies

The spectrum-matched records are generated by using WavGen (Mukherjee and Gupta, 2002) program. WavGen modifies a given seed record to render it compatible with a given spectrum. The seed records are selected from the ground motions recorded by the Seismology Service at the University of Chile. Table 2.4 lists the synthetic records for each site and Figure 2.22 shows example acceleration time histories for the generated records and the ensuing response spectra.

Table 2.4 Generated synthetic records for back-analysis of the case studies

Site	Fault Distance (km)	Seed Records
Odontology Building	37.9	CCSP-NS, MELP-NS
ITATA Bridge	53.4	MELP-NS, STL-EW
Bridge on Route (Ruta) 5	68.9	LACH-NS, STL-EW

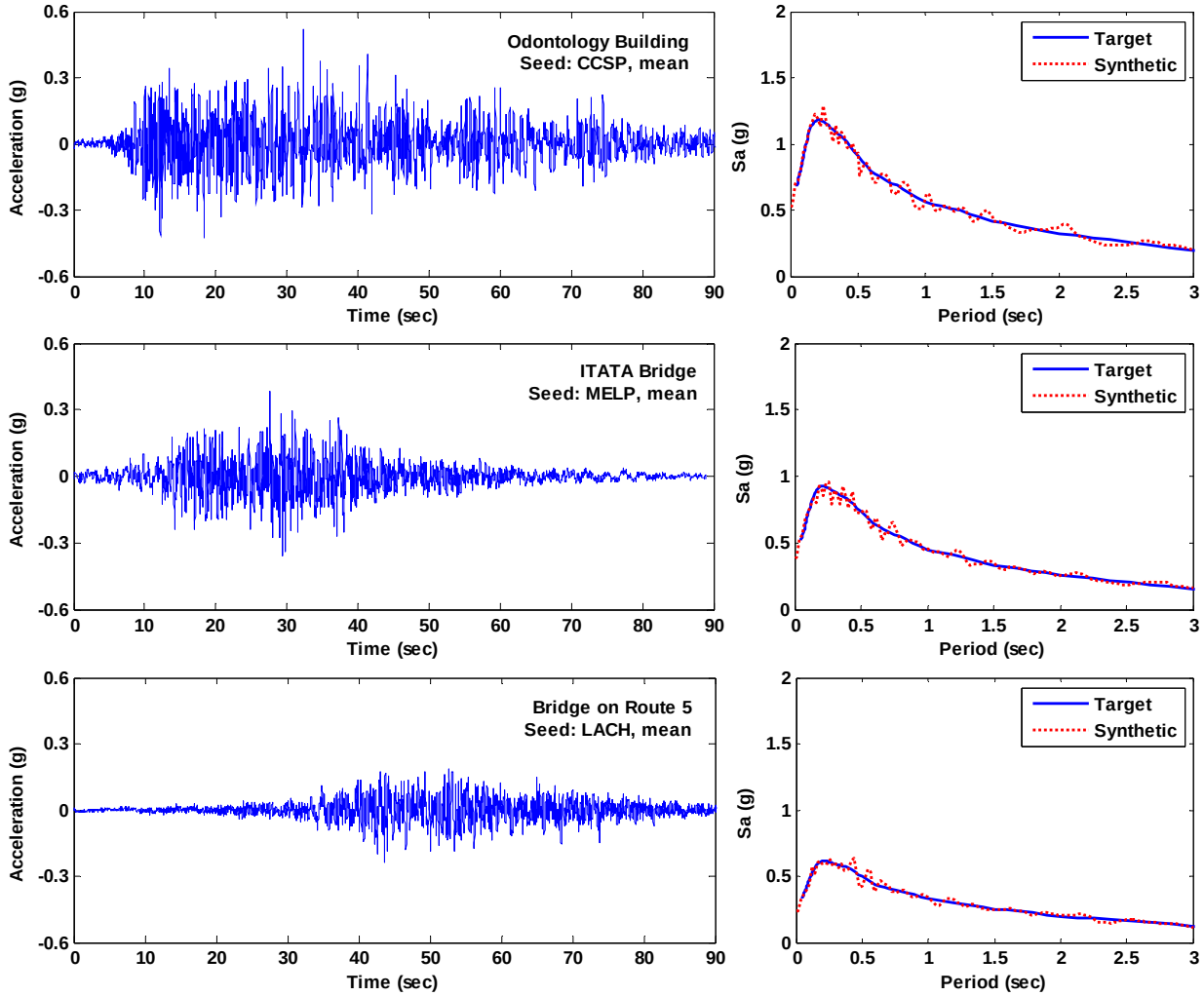

Figure 2.22 Spectrum matched records for back-analysis of the case studies

2.5. REFERENCES

Atkinson, G.M. and Boore, D.M. (2003), "Empirical ground-motion relations for subduction-zone earthquakes and their application to Cascadia and other regions." Bulletin of the Seismological Society of America, 93(4), 1703-1729.

Barazangi, M. and Isacks, B. L. (1976), “Spatial distributio of earthquakes and subduction of the Nazca plate beneath South America,”, Geology, 4, 686-692.

Bevis, M. (1986), “The curvature of Wadati-Benioff zones and the torsional rigidity of subducting plates,” Nature, 323, 52-53.

Bevis, M. and Isacks B. L. (1984), “Hypocentral trend surface analysis: Probing the geometry of Benioff Zones”, Journal of Geophysical Research, 89, 6153-6170.

Bilham, R., Engdahl, E. R., Feldl, N., and Satyabala, S. P. (2005), "Partial and Complete Rupture of the Indo-Andaman Plate Boundary 1847-2004" Seismological Research Letters, Vol 76, 299-311.

Cahill, T. and Isacks, B. L. (1992), “Seismicity and shape of the subducted Nazca plate,” Journal of Geophysical Research, Vol 97, No. B12, 503-529.

Campbell, K.W., and Bozorgnia, Y. (2003), "Updated near-source ground-motion (attenuation) relations for the horizontal and vertical components of peak ground acceleration and acceleration response spectra." Bulletin of the Seismological Society of America, 93(1), 314-331.

Chang, F.K., and Krinitzsky, E.L. (1977), “State-of-the-art for assessing earthquake hazards in the United States; Report 8, Duration, spectral content, and predominant period of strong motion earthquake records from western United States”, Miscellaneous Paper S-73-1, U.S. Army Engineers Waterways Experiment Station, Vicksburg, Mississippi.

DeMets, C., Gordon, R. G., Argus, D. F. and Stein, S. (1990), Current plate motions, Geophysical Journal International, 101:425-478.

Gerbault, M., Cembrano, J., Mpodozis, C., Farias, M. and Pardo, M. (2009), “Continental margin deformation along the Andean subduction zone: Thermo-mechanical models,” Physics of the Earth and Planetary Interiors, 177, 180-205.

Gregor, Nicholas J., Silva, Walter J., Wong, Ivan G., Youngs, Robert R. (2002), “Ground-Motion Attenuation Relationships for Cascadia Subduction Zone Megathrust Earthquakes Based on a Stochastic Finite-Fault Model”, Bulletin of the Seismological Society of America, 92: 1923-1932

Kamiyama, M. (1984), “Effects of subsoils conditions and other factors on the duration of earthquake ground shakings," Proc. Eighth World Conference on Earthquake Engineering, Vol. 2, San Francisco, pp. 793-800.

Kley, J. and Monaldi, C. R. (1998), “Tectonic shortening and crustal thickness in the Central Andes: How good is the correlation?”, Geology, 26, 723-726.

Lay, T., Ammon, C. J., Kanamori, H., Koper, K. D., Sufri, O. and Hutko, A. R. (2010), “Teleseismic inversion for rupture process of the 27 February 2010 Chile (Mw 8.8) earthquake,” Geophysical Research Letters, Vol. 37, L1331.

Lomnitz, C. (1970), “Major earthquakes and tsunamis in Chile during the period 1535 to 1955,” International Journal of Earth Sciences, 59(3), 938-960.

Moreno, M., Rosenau, M. and Oncken, O. (2010), 2010 Maule earthquake slip correlates with pre-seismic locking of Andean subduction zone, Nature, 467, 198-202, doi:10.1038/ nature09349

NCh 433 (1996), Seismic design of buildings and industrial facilities – Official Chilean Standard, NCh 433.Of96, Diseño sísmico de edificios e instalaciones industriales, Instituto Nacional de Normalización (in Spanish).

Newmark, N. M., and Hall, W.J. (1982), “Earthquake spectra and design”, Earthquake Engineering Research Institute, Berkeley, California, 103 pp.

Papazachos, B.C., Papaiannou, C.A., Margaris, V.N., and Theodulidis, N.P. (1992), “Seismic hazard assessment in Greece based on strong motion duration”, Proc. Tenth World Conference on Earthquake Engineering, Vol. 2, Madrid, pp. 425-430.

Plafker, G. and Savage, J. C. (1970), “Mechanism of the Chilean Earthquake of May 21 and 22, 1960,” Geological Society of America Bulletin, 81, 1001-1030.

Rao, N. P., Kumar, M. R. and Tsukuda T. (2003), “Current deformation of the Himalaya–Tibet–Burma seismic belt: inferences from seismic activity and strain rate analysis,” Journal of Geodynamics, 36, 485-496.

Ruegg, J. C., Rudloff, A., Vigny, C., Madariaga, R., Chabalier, J. B., Campos, J., Kausel, E., Barrientos, S. and Dimitro, D. (2009), “Interseismic strain accumulation measured by GPS in the seismic gap between Constitución and Concepción in Chile,” Physics of the Earth and Planetary Interiors, 175, 78-85.

Schellart, W. P., Freeman, J., Stegman, D. R., Moresi, L. and May, D. (2007), “Evolution and diversity of subduction zones controlled by slab width,” Nature, 446, 308-311.

Swift, S. A. and Carr M. (1974), “The segmented nature of the Chilean seismic zone,” Physics of the Earth and Planetary Interiors, 9, 183-191.

Youngs, R.R., Chiou, S.J., Silva, W.J., and Humphrey, J.R. (1997), “Strong ground motion attenuation relationships for subduction zone earthquakes,” Seismological Research Letters, 68(1), 58-73.

Zhao, J.X., Zhang, J., Asano, A., Ohno, Y., Oouchi, T., Takahashi, T., Ogawa, H., Irikura, K., Thio, H.K., Somerville, P.G., Fukushima, Y., and Fukushima, Y. (2006), "Attenuation relations of strong ground motion in Japan using site classification based on predominant period", Bulletin of the Seismological Society of America, 96(3), 898-913.

3 GEOTECHNICAL ENGINEERING

Chapter 3 provides the observations of the geotechnical group of the MAE Center team. The MAE Center geotechnical team was also the GEER (http://www.geerassociation.org/) Team D, the reconnaissance was a joint activity and the observations are also reported in GEER (2010). For a detailed and extensive set of observations of geotechnical damage during this earthquake the reader is referred to the GEER report.

The visited sites are categorized under (i) landslides, (ii) ports, (iii) roadway embankments, (iv) bridges, (v) bridge embankments, (vi) underground structures, (vii) retaining structures, and (viii) building foundations. Further observations related to bridge structures that have geotechnical implications are given in Chapter 4, Section 4.3.

3.1. LANDSLIDES AND POTENTIAL TECTONIC MOVEMENTS

The team visited a series of landslides along road P22 south of Arauco as illustrated in Figure 3.1 through Figure 3.4. The series of landslides formed a linear feature nearly parallel to the coastline as illustrated in Figure 3.2. All along the road vertical offsets were observed in the pavement as illustrated in Figure 3.4 indicative of deeper movement. This was the case even when the road was further away from the landslide. It appeared that this was more than a classical “surficial” landslide feature with potentially larger tectonic movement. In our discussions with faculty at the University of Chile they indicated that this linear feature was related to tectonic movement. Additional investigations of this feature would be worthwhile.

Figure 3.1 Arauco landslides/coastal bluff features view 1, (-37.246292°,-73.324251°) to (-37.242213°,-73.421207°)

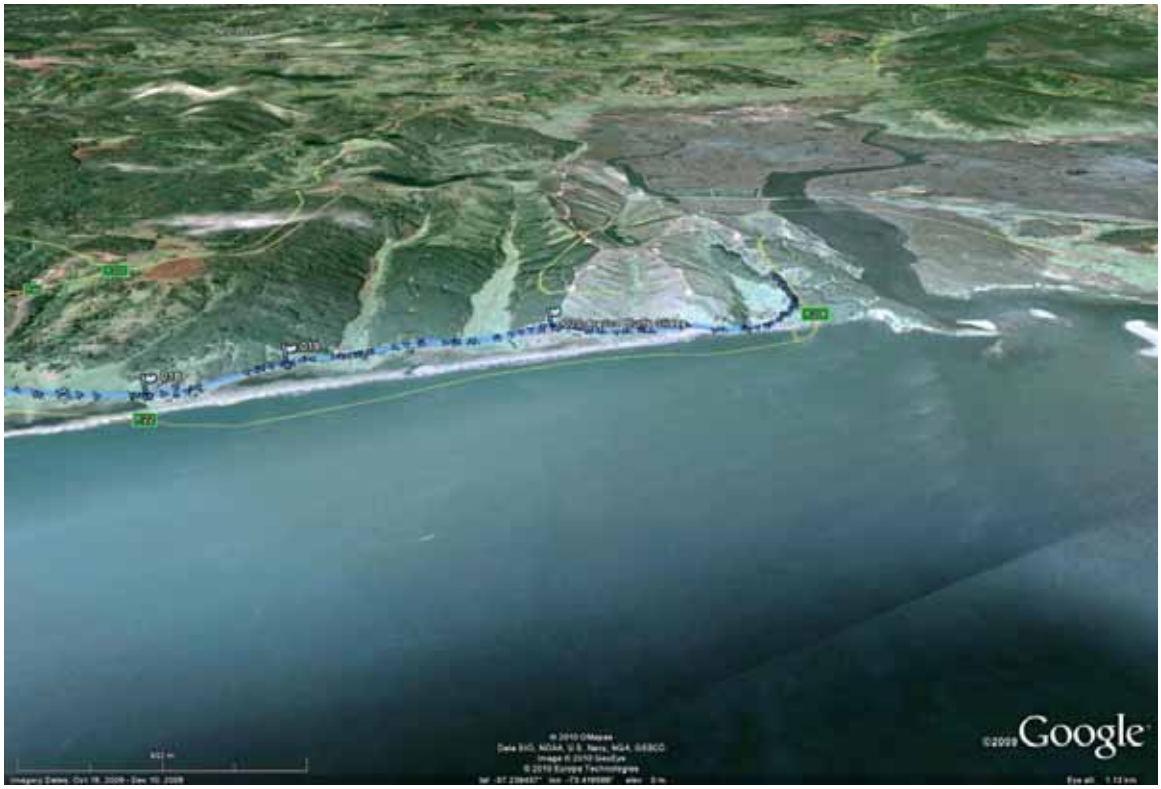

Figure 3.2 Arauco landslides/coastal bluff features view 2, (-37.246292°,-73.324251°) to (-37.242213°,-73.421207°)

Figure 3.3 Arauco landslides/coastal bluff features, April 14, 2010

Figure 3.4 Arauco landslides/coastal bluff features, note linear feature in the road showing a vertical offset, April 14, 2010

3.2. PORTS

The port structures that were visited by the MAE Center team are listed in Table 3.1. The locations are marked on maps in Appendix A.4 with the icons that are designated in Table 3.1.

Table 3.1 Locations of the port structures visited by the MAE Center team

Icon	Name	Latitude	Longitude	Figures in the report
P2	Port of Talcahuano	36°42'52.21"S	73° 6'30.22"W	Figure 3.5, Figure 3.6, Figure 3.7, Figure 4.8, Figure 4.9, Figure 4.24
P3	Port of Coronel	37° 1'43.95"S	73° 8'59.16"W	Figure 3.8, Figure 3.9, Figure 3.10, Figure 3.11, Figure 3.12, Figure 3.13
P4	Port Lota	37° 5'50.26"S	73° 9'33.59"W	Figure 3.14, Figure 3.15, Figure 3.16
P5	Port St. Vicente	36°43'31.86"S	73° 7'56.60"W	Figure 3.17, Figure 3.18, Figure 3.19, Figure 3.20

3.2.1. Port of Talcahuano

The port of Talcahuano and the surrounding area were inundated by a tsunami caused by the main earthquake shock (Figures 1-3). The tsunami reached about 0.5 km inland and caused significant damage to the port facilities. Numerous ships were carried inland or were toppled. The sea walls and port dock were also damaged. The damage appeared to be a result of lateral spreading and liquefaction. However, it was difficult to determine whether this liquefaction was a result of ground shaking or due to the sudden

rise in pore water pressure due to dynamic loading resulting from the tsunami induced waves. Most likely, this was a result of a combination of both factors.

Figure 3.5 Port of Talcahuano, arerial view (-36.71109°, -73.113898°)

Figure 3.6 Tsunami displaced ship, Port of Talcahuano, April 15, 2010 (-36.71109°, -73.113898°)

Figure 3.7 Damaged sea wall and dock, Port of Talcahuano, April 15, 2010 (-36.71109°, -73.113898°)

3.2.2. Port of Coronel

The port of Coronel is a major commercial port parts of which experienced damaged due to liquefaction and lateral spreading. A laydown area for container storage, consisted of fill supported by a shallow sheet pile experienced extensive damage. Figure 3.8 through Figure 3.13 show the corresponding photos of the visited areas. The sheet pile wall is embedded about 4-6 m below the ground surface and protrudes about 15-20 m above the ground surface. At waypoint 11 (see Figure 3.8) an outward movement of about 110 cm was measured, while the port officials reported their survey gives about 150 cm. The measurements extended all the way back to the warehouses. At waypoint 12 lateral displacements of about 40 cm was measured, and at waypoint 13, an outward movement of 10 cm was measured. It did not appear that the underlying sands were treated during construction to minimize liquefaction potential.

Figure 3.8 Port of Coronel, area marked by GPS tracks along the coast experienced lateral spreading (-37.028874°,-73.149768°)

Figure 3.9 Lateral spreading looking north view 1, Port of Coronel, April 14, 2010 (-37.028874°, -73.149768°)

Figure 3.10 Lateral spreading looking north view 2, Port of Coronel, April 14, 2010 (-37.028874°, -73.149768°)

Figure 3.11 Lateral spreading looking south, Port of Coronel, April 14, 2010 (-37.028874°,-73.149768°)

Figure 3.12 Sand eject, lateral spreading, Port of Coronel, April 14, 2010 (-37.028874°,-73.149768°)

Figure 3.13 Seaside view of the sheet pile wall that experienced lateral spreading, Port of Coronel, April 14, 2010 (-37.028874°, -73.149768°)

3.2.3. Port Lota

The team visited a pier used by fishing boats at Port Lota. The pier appeared undulating likely due to pile settlements. Numerous battered piles with broken connections were observed.

Figure 3.14 Port Lota (-37.097295°,-73.159331°)

Figure 3.15 View of undulating fishing pier, Port Lota, April 14, 2010 (-37.097295°,-73.159331°)

Figure 3.16 Typical broken pile connections, Port Lota, April 14, 2010 (-37.097295°,-73.159331°)

3.2.4. Port St. Vicente

The team also visited a wharf at Port St. Vicente (Figure 3.17) that experienced lateral spreading and failure of a gravity wall resulting in complete loss of section of the wharf or significant lateral movement as shown in Figure 3.18 through Figure 3.20. The lateral displacement of the wall was measured to be about 167 cm close to the section of the wall that failed and about 63 cm further away. Nearby there were fish processing plants that experienced significant damage due to lateral spreading of the foundations.

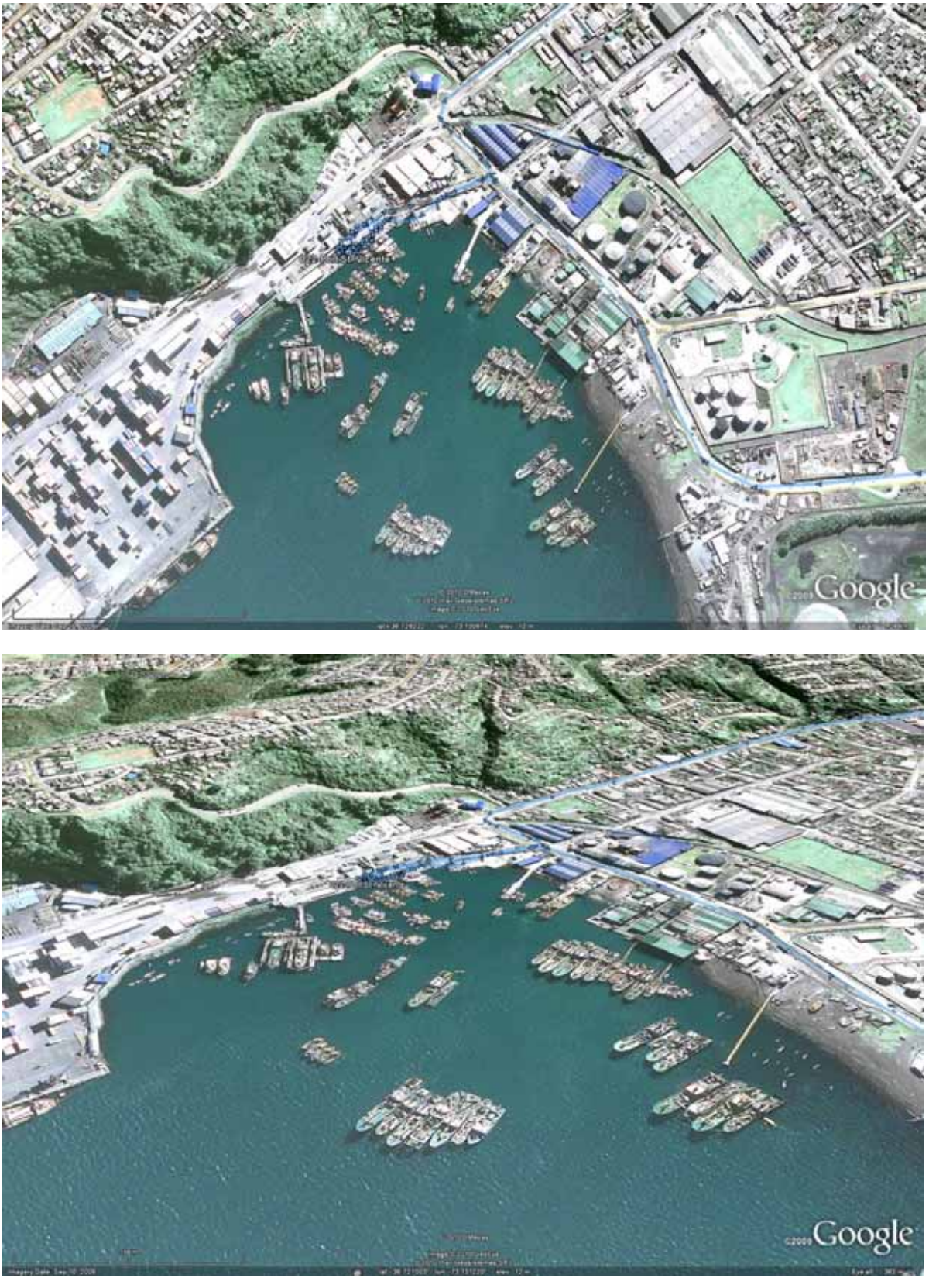

Figure 3.17 Port St. Vicente, observation along fishing wharf

Figure 3.18 Lateral spreading and damage to quay wall, blue fish processing plants in the background damaged by lateral spreading, Port St. Vicente, April 15, 2010 (-36.725517°, -73.132390°)

Figure 3.19 Failed section of the quay wall, Port St. Vicente, April 15, 2010 (-36.725517°, -73.132390°)

Figure 3.20 Measurement of displacement of the wall due to lateral spreading, Port St. Vicente, April 15, 2010 (-36.725517°,-73.132390°)

3.3. ROADWAY EMBANKMENTS

More detailed information regarding the performance of roadway embankments during the earthquake is given in Chapter 5. The observations in the sections below have apparent geotechnical features, therefore included here.

3.3.1. Roadway Embankment ~5km south of Parral

Numerous roadway embankments failed throughout the earthquake-affected zone. This includes a number of embankments along the main north-south highway, Route (Ruta) 5. The failures were due to either failure of the underlying soils or the embankments themselves. Figure 3.21 and Figure 3.22 show a repaired embankment along Route 5. The failed section was bounded by two streams (Figure 3.21) and it is likely that the failure of the embankment was due to loss of strength in the underlying soils (liquefaction) during shaking.

Figure 3.21 Roadway embankment ~5km south of Parral, north is up, Route 5 South (-36.185671°,-71.825415°)

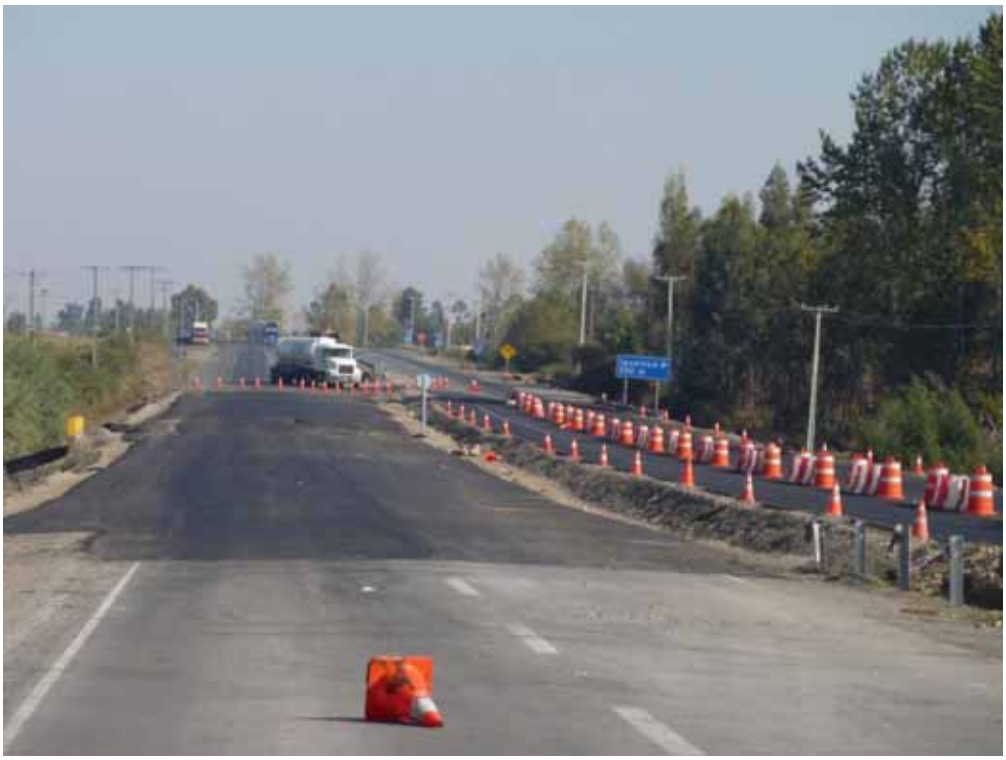

Figure 3.22 Northbound lane looking south, Repaired Roadway Embankment ~5km south of Parral, Route 5 South, April 15, 2010 (-36.185671°, -71.825415°)

3.3.2. Route 5 South Overpass Embankment, to Retiro at Tucapel Mill Overpass

The team visited a damaged overpass embankment on the right side of the northbound lane of Route 5 South. The damage of the embankment appeared to be due to shaking of the embankment material. The underlying soil appears to be intact with no evidence of loss of strength. The embankment bulged laterally and settled. The overpass embankment to the left of the northbound lane did not show signs of damage.

Figure 3.23 Route 5 South overpass embankment, looking north, to Retiro at Tucapel Mill (-36.051209°,-71.768005°)

Figure 3.24 Damage to overpass embankment, Route 5 South overpass embankment, to Retiro at Tucapel Mill, April 15, 2010 (-36.051209°,-71.768005°)

Figure 3.25 Route 5 South overpass embankment, to Retiro at Tucapel Mill, April 15, 2010 (-36.051209°,-71.768005°)

3.4. BRIDGES

The observations provided in Section 3.4 are specifically on the geotechnical failures at the Mataquito Bridge. The overall behavior of bridges during the M_w 8.8 Maule earthquake is described in detail in Section 4.3.

3.4.1. Puente Mataquito

This bridge crosses the Mataquito River close to the Pacific Ocean. Extensive liquefaction and lateral spreading occurred at the north and south abutments and in the adjacent fields. Figure 3.26 though Figure 3.34 show photos of the bridge and the damage.

The lateral spreading at the south abutment appeared to be more confined due to the topography of the area. However, at the north side, due to existence of large fields around the bridge, extensive lateral spreading was observed (extending ~270 m from the river edge). The lateral spreading from the edge of the abutment wall to the first row of piers was ~54 cm and the total lateral spreading from the edge of the abutment wall to the river's edge was ~180 cm (over a distance of ~65 m). The approach embankment was ~7.6 m high, and settled ~70 cm relative to the bridge deck. The approach embankment experienced outward transverse movement of ~60 cm from the centerline as manifested by cracking of the asphalt along a distance of ~200 m. This appeared due to liquefaction and failure of the underlying soil and was evidenced by compression ridged in the field at the toe of the embankments.

Figure 3.26 Puente Mataquito, looking north, April 16, 2010 (-35.050712°,-72.162258°)

Figure 3.27 Lateral spreading on the south end of the bridge, Puente Mataquito, April 16, 2010 (-35.050712°,-72.162258°)

Figure 3.28 Lateral spreading on the north end of the bridge, Puente Mataquito, April 16, 2010 (-35.050712°,-72.162258°)

Figure 3.29 Settlement of the north abutment of the bridge, 70 cm offset at the bridge deck, Puente Mataquito, April 16, 2010 (-35.050712°,-72.162258°)

Figure 3.30 Cracking and transverse movement (60 cm on each side) of embankment due to liquefaction of underlying soil, north abutment of the bridge, Puente Mataquito, April 16, 2010 (-35.050712°,-72.162258°)

Figure 3.31 Compression ridges at toe of embankment, due to liquefaction of underlying soil and settlement of embankment, north abutment of the bridge, Puente Mataquito, April 16, 2010 (-35.050712°,-72.162258°)

Figure 3.32 Lateral Spreading towards the river, north abutment of the bridge, Puente Mataquito, April 16, 2010 (-35.050712°,-72.162258°)

Figure 3.33 North abutment shoved into bridge deck due to lateral spreading, Puente Mataquito, April 16, 2010 (-35.050712°,-72.162258°)

Figure 3.34 Shearing of bridge girder, north abutment of bridge, Puente Mataquito, April 16, 2010 (-35.050712°,-72.162258°)

3.5. BRIDGE EMBANKMENTS

Not many embankment failures were observed at the bridge sites that the structures team investigated in the field (Sections 4.3 of Chapter 4). A few bridge embankments suffered minor damage due to strong shaking as shown in Figure 3.35 and Figure 3.36. The approach road that the embankment supports did not show cracks that may have caused by the minor damage. It is expected that the cracking of the embankment may have affected the dynamic properties of the embankment during the strong shaking, but it is not clear how this would have affected the seismic response of the bridge.

Figure 3.35 Surface cracks at the embankment of Las Mercedes Bridge

Figure 3.36 Cracks at the embankment of Perquilauquén Bridge

3.6. UNDERGROUND STRUCTURES

All underground structures encountered by the team appeared to be undamaged by the earthquake shaking. The following types of underground structures were encountered:

a. Wide highway box structures (Figure 3.37): these were cut and cover high way box structures with 3 lanes of traffic in one direction. These are constructed in the relatively stiff gravels. The portal of these structures consisting of U-shaped wall sections appeared undamaged. These structures were encountered at two locations and each of them was more than 1 km long.

b. Santiago Metro underground structures (Figure 3.38): no damage was observed in the tunnels and underground stations of the Santiago Metro.

c. Highway Tunnels (Figure 3.39): highway tunnels encountered by the team appeared to be intact. A highway tunnel failure (not observed by the team) was reported on the northbound lane of Route 5, north of Santiago. It is known as “La Calavera” tunnel near Calera. The tunnel is old and had problems before the earthquake. It was in rock with rock bolts providing support. After the earthquake, rock block was dislodged.

It appeared that well engineered underground structures performed very well even under strong shaking. This is consistent with observations during other earthquakes elsewhere.

Figure 3.37 Highway box structures in Santiago, *Top:* inside highway box structures, April 12, 2010 (-33.424750°,-70.622422°); *Bottom:* approach to box tunnels, April 16, 2010 (-33.541472°,-33.541472°)

Figure 3.38 Santiago Metro, Baquedano Station, April 12, 2010

Figure 3.39 Highway tunnel, Route 5 South, April 12, 2010
(-33.912867°,-70.725533°)

3.7. RETAINING STRUCTURES

The team did not observe damage to modern retaining wall structures. The mechanically stabilized earth walls forming the approach embankment for the two ring road bridges, which have failed, have remained intact as illustrated in Figure 3.40 and Figure 3.41.

Figure 3.40 Mechanically stabilized earth wall, bridge ring 3, Lo Echevers Bridge, Santiago, April 13, 2010 (-33.376159°,-70.747742°)

Figure 3.41 Mechanically stabilized earth, bridge ring 2, Miraflores Bridge, Santiago, April 13, 2010 (-33.394269°,-70.769402°)

3.8. BUILDING FOUNDATION

A building in Talcahuano, that was tilted, which appeared to be due to failure in the foundation soil, was encountered. This was in an area very close to Port of Talcahuano that was hit by a tsunami. Unfortunately the team was unable to further verify this as the building was demolished shortly afterwards.

Figure 3.42 Green Building, Talcahuano (-36.714268°,-73.116368°)

Figure 3.43 Tilting of the Green Building due to bearing soil failure, Talcahuano, April 15, 2010 (-36.714268°,-73.116368°)

3.9. REFERENCES

GEER (2010), “Geo-engineering Reconnaissance of the 2010 Maule, Chile Earthquake,” report of NSF Sponsored GEER Association Team, J. Bray & D. Frost, eds., http://www.geerassociation.org/

4 STRUCTURAL ENGINEERING

The MAE Center field reconnaissance team visited several cities affected by the earthquake. The visited cities are Santiago, Concepción, Talcahuano, and Talca. Several meetings were held with researchers and city officials in Chile to gain a better and more wide-ranging understanding of structural response in the earthquake. In the following, an overview of the regional damage where the MAE Center team visited is presented followed by detailed discussion on damage of specific buildings and bridges from the affected region. In addition, inelastic response history analyses of one building and two bridges are presented to clearly understand the damage observed from the field investigation and the interaction between the strong shaking and structural response. Fragility curves for a common bridge type are also derived.

4.1. REGIONAL DAMAGE DESCRIPTION AND STATISTICS

4.1.1. Santiago Region

Santiago Region is one of the Chile's 15 administrative divisions. Santiago in the Santiago Region is the capital of Chile with a population of around 5.2 million. Although the epicentral distance to Santiago is 335 km, the city is close to the rupture area due to the large size of the fault as shown in Figure 4.1. There were six seismic stations operating in the city during the earthquake event. The PGAs of the recorded accelerations were in the range of 0.17 g to 0.56 g for horizontal components and 0.11 g to 0.28 g for vertical components. Figure 4.2 compares the response spectra of the recorded ground motions with the design response spectrum for Santiago. The figure clearly shows that the recorded acceleration is significantly higher than the design spectrum for the station CRS MAIPU RM. The seismic intensity (MMI) of the city was VII based on 922 responses in "Did You Feel It?" community survey system in USGS (accessed on Nov. 1, 2010). The intensity of VII corresponds to very strong shaking and moderate structural damage.

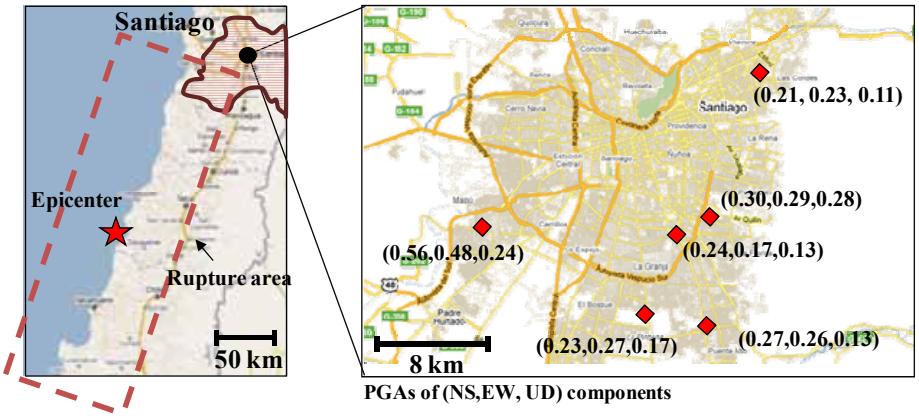

Figure 4.1 Location of Santiago Region and recorded PGAs in Santiago

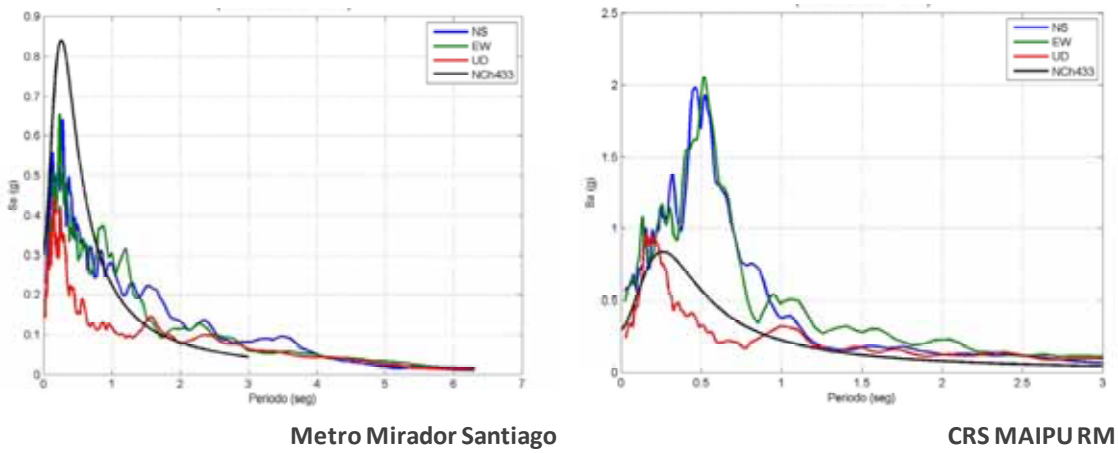

Figure 4.2 Location of Santiago Region and recorded PGAs in Santiago, compared to the code design spectrum (black line)

The majority of the RC building structures performed well, suffering only minor damage or even no damage at all. A limited number of RC buildings suffered significant damage due to structural deficiencies such as soft stories, horizontal and vertical irregularities, and short-column effects. Several other buildings were damaged due to the failure of RC walls since proper confinement in walls were not required until recently in the Chilean Building Code. The followings are some of the observed damage in Santiago.

The building shown in Figure 4.3 and Figure 4.4 was used as a hotel. It consists of a tall tower and a low-rise commercial building. The damage shown in the figures are at the juncture of the two structures. As it can be observed in Figure 4.3, the beams connecting the tall tower and the low-rise building were fractured at different locations. It is speculated that the beams were damaged as the tall building vibrated out-of-phase from the low-rise building, which could develop large force demand at the connection between the two buildings. The beams connecting the two buildings may not have been designed to resist the force demand from the vertical irregularity. Figure 4.4 shows that the longitudinal reinforcement bars of the beam in the in-plane direction have relatively smaller diameter than the longitudinal bars of the beam connected in the transverse direction. It is speculated that the beam running in transverse direction was designed to support gravity loads from above while the in-plane beam shown in the figure was designed only to support its self-weight.

The building in Figure 4.5 was constructed with load bearing walls covered with masonry cladding. The surface of the bearing walls was chipped such that the cement mortar can develop bond strength between the walls and masonry cladding. During the earthquake, a large portion of the cladding collapsed possibly causing injuries or even death should people have been around the building at the time of the earthquake. The building also incurred damage on a beam between two vertically slender windows, which separate the two large walls. The beam apparently acted as a link (or coupling)

beam between the two large walls, and did not have enough shear strength to resist the force demand imposed on it. Figure 4.6 presents the failure of a beam-column connection where heavy longitudinal reinforcement bars were used without sufficient shear stirrups within the beam-column connection.

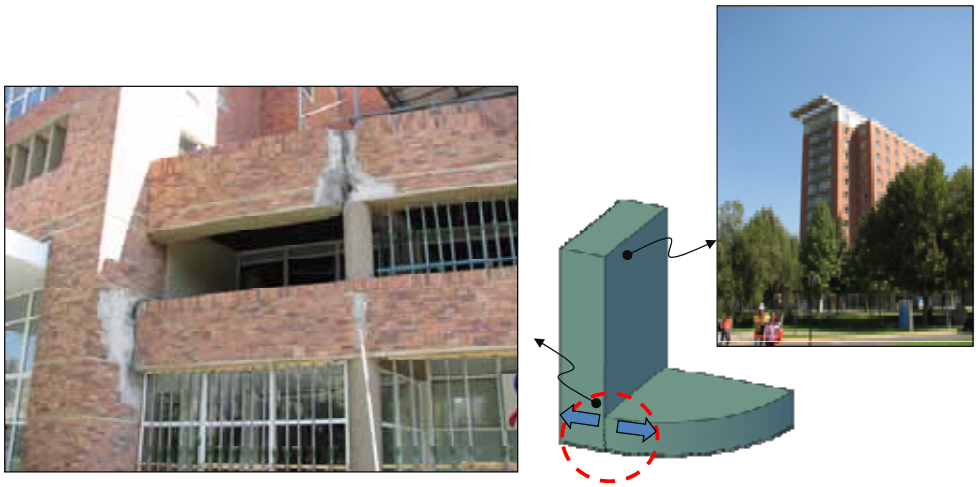

Figure 4.3 Failure due to vertical irregularity

Figure 4.4 Close-up view of the damaged structure

The observed damage summarized above is limited to the buildings that the MAE Center team visited. Other teams from around the world reported damage to several different structures (e.g. EERI, 2010). For instance, several buildings with reinforced concrete walls were damaged due to insufficient confinement in the bearing walls. Until recently, the Chilean design code did not require confinement in the wall due to the satisfactory performance of buildings during the past earthquakes. Latest design code, however, requires walls to be designed as special structural walls. In conclusion, overall

the building structures in Santiago performed very well except only a few heavily damaged buildings.

Figure 4.5 Collapsed masonry cladding wall and a damaged beam

Figure 4.6 Failure of beam-column connection

4.1.2. Bíobío Region

The Bíobío region is located at the south half of the rupture area as shown in Figure 4.7. The coseismic slip displacement of Talcahuano and Concepción areas was approximately 300 cm as shown in Figure 2.12. Main damage to the region was in the coastal towns of Arauco Province, Talcahuano city, and Dichato town. These coastal towns were severely damaged due to the tsunami that followed the earthquake. The area in Talcahuano Bay that was inundated with the tsunami is approximately 11 km^2 as shown in Figure 4.8, and more than 30,000 people were directly affected by the tsunami (INE, 2010).

In Concepción, several buildings collapsed and several 15 to 20 story buildings were severely damaged and will have to be demolished. Due to the damage in multi-story buildings, streets in downtown Concepción were closed.

In terms of transportation networks, most of the highways and streets suffered only minor damage but a few bridges were damaged or suffered collapse. In the Bíobío region, two bridges with 2 km length collapsed and one bridge of 2 km length was severely damaged. While the number of failed bridges is small, they constituted critical links in the regional transportation network. The failed bridges connect the industrial areas to the ports. In addition, many people living in San Pedro City used to commute to Concepción through these bridges. After the failure of the bridges, there was one to two hours of delay in crossing the Bíobío River. In addition, some people who used to live in San Pedro and commute to Concepción had to relocate to Concepción due to the delay in commuting. Even though the number of bridge failures was small, the failure of the critical bridges led to significant impact on the area. At the time of the field investigation around one and half months after the earthquake, only 30 percent of industries were operating in the region due to the damage to structures, lack of power, or difficulty in accessing the facility. There were failures in critical lifeline networks, such as gas, electricity, water, and wastewater. Based on information obtained from researchers in the University of Concepción, the electricity network was restored before other utility networks. The gas network was not restored to many areas in the region even after several weeks. As some parts of the network were very old, the vulnerability was high leading to irreparable damage in some instances.

In general, the central valley area of the Bíobío region, shown in Figure 4.7, was not largely affected by the earthquake except for damage to a few highway bridges and slopes. The area, however, suffered failures in water irrigation systems.

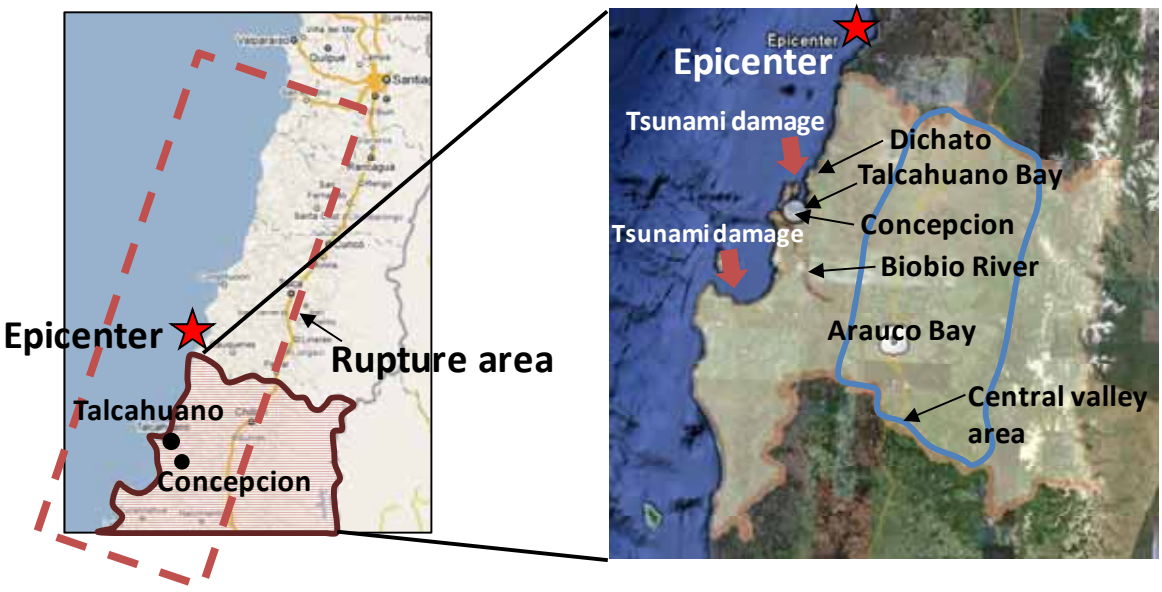

Figure 4.7 Damage to Bíobío Region

Figure 4.8 Talcahuano Bay area affected by tsunami

Figure 4.9 shows the effects of tsunami on structures in Talcahuano Bay. In Figure 4.9 (Left), the roof of the building nearly collapsed and tanks were toppled due to the tsunami. Many ships were found inland and some of the ships hit to building structures damaging the buildings as shown in Figure 4.9 (Right).

Figure 4.9 Effects of the tsunami on Talcahuano Bay. Top: toppled tank and collapsed building due to tsunami; Bottom: a dislocated ship, which damaged a storage building

4.1.3. Maule Region

The epicenter of the earthquake was located offshore Maule Region as shown in Figure 4.10. Talca is the capital of the Maule region with a population of 230,000 and a building stock of 75,000 houses. The city suffered the heaviest damage from the earthquake due to its proximity to the rupture area. In addition, there was a large number of adobe houses in Talca built without seismic provisions, thus compounding the damage. Out of 75,000 houses in Talca, around 15,000 houses were damaged among which around 4,000 either collapsed or need to be demolished. Many of these buildings were built 100 to 200 years ago. Especially in the old downtown area, where the majority of buildings were made of adobe, approximately 80 percent of buildings were damaged and half of the damaged buildings are intended for demolition.

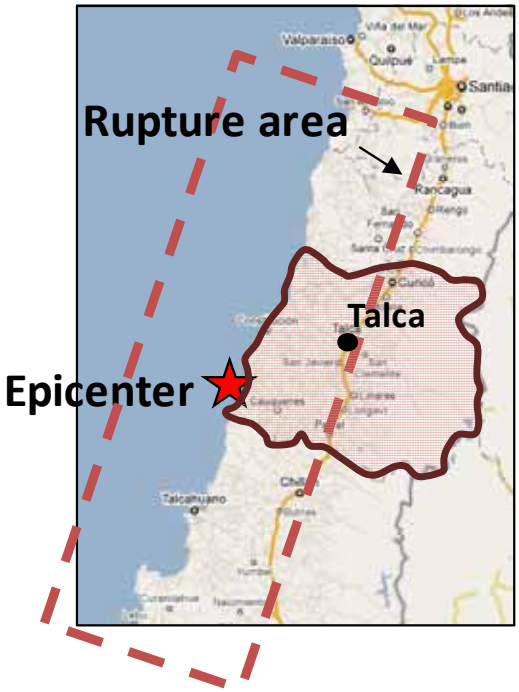

Figure 4.10 Location of the Maule Region and the rupture plane

In addition to the adobe construction, there are many new reinforced concrete or masonry structures built according to the modern design code. The newly constructed buildings rarely suffered damage except for a couple of buildings which suffered architectural damage rather than major structural damage. Structures constructed in timber with adobe infill performed relatively well. When interviewed by the field reconnaissance team, the mayor of the city expressed concern that people in the city may rebuild their houses with adobe due to its low construction cost. At the time of the visit, the city did not have modern design guidelines for adobe construction.

The failure of adobe buildings is expected to cause a secondary problem. The area has a rainy winter season between May and August. The debris from adobe buildings

can easily turn to mud and may block the sewer system causing flooding hazard. After the earthquake, the city suffered damage of critical lifeline network including gas, water, and electricity. All lifeline networks were recovered in seven-to-ten days. Downtown areas took longer to recover from damage as networks were relatively dense and therefore difficult to repair. While the networks were recovered in a relatively short time, the city suffered from interdependency of networks operation. For instance, the water system was repaired earlier than electricity. Due to the lack of electricity, however, water could not be pumped to higher grounds.

Figure 4.11 shows modern RC buildings in Talca. The building on the left did not suffer noticeable damage. The building on the right suffered damage to an architectural feature. Though this is not a structural failure, it is life threatening. The buildings on the left in Figure 4.12 are typical adobe structure and the one on the right is a masonry historic structure in downtown Talca. The majority of the damaged buildings in Talca were similar to those shown in Figure 4.12.

Figure 4.11 Modern RC buildings in Talca

Figure 4.12 Adobe buildings and historic structures

4.2. EFFECTS ON BUILDINGS

Section 4.2 focuses on the effect of the earthquake on building structures. Damage observed in specific structures that were visited by the MAE Center team is described qualitatively. The information regarding the visited buildings is provided in Table 4.1. The location of each building and the related figure(s) in the report are also provided in the table. The column “icon” indicates the label of the buildings as shown in the figures in Appendix A.4. Additionally, a case study building is modeled and numerical analysis is performed. The analytical results are compared with the field observations.

Table 4.1 List of buildings visited by the MAE Center team

Icon	Name/Description	Latitude	Longitude	Figure
B1	Ciudad Empresarial Hotel	33°23'23.20"S	70°37'8.93"W	Figure 4.5 Figure 4.6
B2	University of Concepción - Chemistry Building	36°49'46.25"S	73° 2'13.42"W	Figure 4.13
B3	University of Concepción - Gymnasium	36°49'35.47"S	73° 2'12.10"W	Figure 4.14
B4	Case Study 1: University of Concepción - Odontology Building	36°49'32.78"S	73° 2'11.35"W	Figure 4.15 Figure 4.16
B5	Damaged Highrise in Concepción	36°49'45.02"S	73° 2'43.00"W	Figure 4.17
B6	O'Higgins Tower in Concepción	36°49'44.35"S	73° 3'16.70"W	Figure 4.18
B7	Alto Río Condominium in Concepción	36°49'41.82"S	73° 3'42.07"W	Figure 4.19
B8	Building close to Talcahuano Port	36°43'9.76"S	73° 6'29.63"W	Figure 4.22
B9	Building at the Talcahuano shorefront	36°43'6.13"S	73° 6'29.94"W	Figure 4.23
B10	Building at the Talcahuano Port	36°42'58.19"S	73° 6'28.06"W	Figure 4.24
B11	Typical adobe failures in Talca	35°25'32.82"S	71°39'2.74"W	Figure 4.12
B12	Edificio Aranjuez	35°25'40.75"S	71°39'57.46"W	Figure 4.25
B13	Tribunales de Justicia de Talca	35°25'16.65"S	71°40'3.83"W	Figure 4.11 (Right)
B14	Building at the Ciudad Empresarial Business Complex	33°23'16.99"S	70°37'2.57"W	Figure 4.3 Figure 4.4

4.2.1. Observed Building Damage

A number of buildings of the University of Concepción experienced damage to different extents. Fire started immediately after the earthquake in the Chemistry Building, Figure 4.13. It is postulated that no significant structural damage occurred. However, the steel framed structure was completely burned and had to be demolished.

The columns carrying the steel roof of the University Gymnasium suffered cover spalling, most probably, due to slight buckling of longitudinal reinforcement (Figure 4.14). It was observed that no transverse reinforcement existed and smooth bars were used as longitudinal reinforcement, typical of pre-1960 construction in Chile. Deep cracks, which are expected to result from the out-of-plane movement of the walls, were also observed on the sidewalls at the discontinuity region (where the tiered seats end).

Figure 4.13 Fire in the Chemistry Building after the earthquake and the demolishing process

Figure 4.14 Gymnasium, University of Concepción, buckling of longitudinal reinforcement and cover spalling, out-of-plane failure of sidewalls at the wall discontinuity

The most severe structural damage to University of Concepción buildings was observed in the Odontology building, Figure 4.15. The damage was concentrated at the first story due to high demands and relatively small dimensions of the columns. Combined axial and shear failures were observed at the top portions of the first story columns. Non-uniform spacing of stirrups, as seen in Figure 4.15, due to construction errors is expected to have caused the decrease in shear capacity. Shear failure of columns due to short column effect was also observed in addition to diagonal cracks

around openings in masonry infill walls. As shown in Figure 4.16, the Odontology building was being retrofitted at the time of the MAE Center team's visit. The retrofitting efforts included the jacketing of first and service story (a half height story used for accessing the building utility lines) columns.

Figure 4.15 Odontology Building, University of Concepción, combined shear-compression failure at the top of first story columns, short column effect, and diagonal cracks in masonry infill walls around openings

Figure 4.16 Retrofitting of the Odontology Building, University of Concepción

Several engineered buildings in Concepción have suffered significant damage. It is speculated that this is mainly attributed to soil conditions in the city, which is sedimentary valley with sand deposits having depths of approximately 80 m. The soft

soil conditions might have resulted in relatively high accelerations at long periods. Other high-rise RC buildings in the city (some of them are mentioned below) also suffered significant damage supporting the effect of soil conditions. The reinforced concrete condominium high-rise building shown in Figure 4.17 suffered severe damage to bearing walls and was left uninhabitable.

Figure 4.17 Severely damaged condominium high-rise building in Concepción

The O'Higgins tower in Concepción attracted considerable attention of structural engineers due to its mode of failure. The building was constructed in 2008 with 21 stories above ground level and 2 stories underground. The building experienced collapse of a story at the framing setbacks, Figure 4.18. The severe damage to coupling beams was also clearly visible at the façade of the building.

The 15-story Alto Río condominium in Concepción, Figure 4.19, collapsed in a spectacular manner. It is postulated that the walls on one side of the building, as-designed, were not continued to the ground level which caused the building to overturn, leading to tensile failure of RC walls and toppling of the entire structure. The discontinued walls that caused the irregularity in plan and elevation, hence twisting of the structure, are shown in plan and elevation view sketches of the building in Figure 4.20 and Figure 4.21, respectively. At the time of the earthquake 87 people were inside the building among whom eight people died and 79 survived (52 escaped on their own efforts, 27 were rescued).

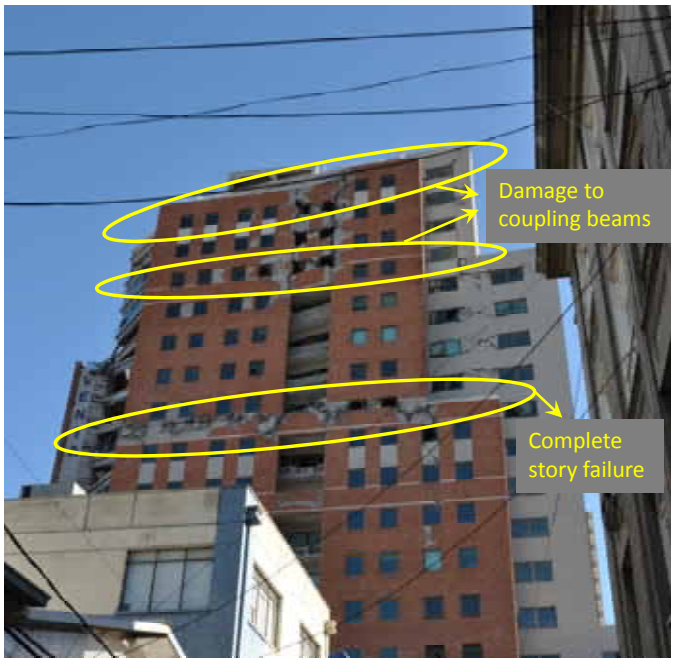

Figure 4.18 O'Higgins tower in Concepción suffered partial story collapses

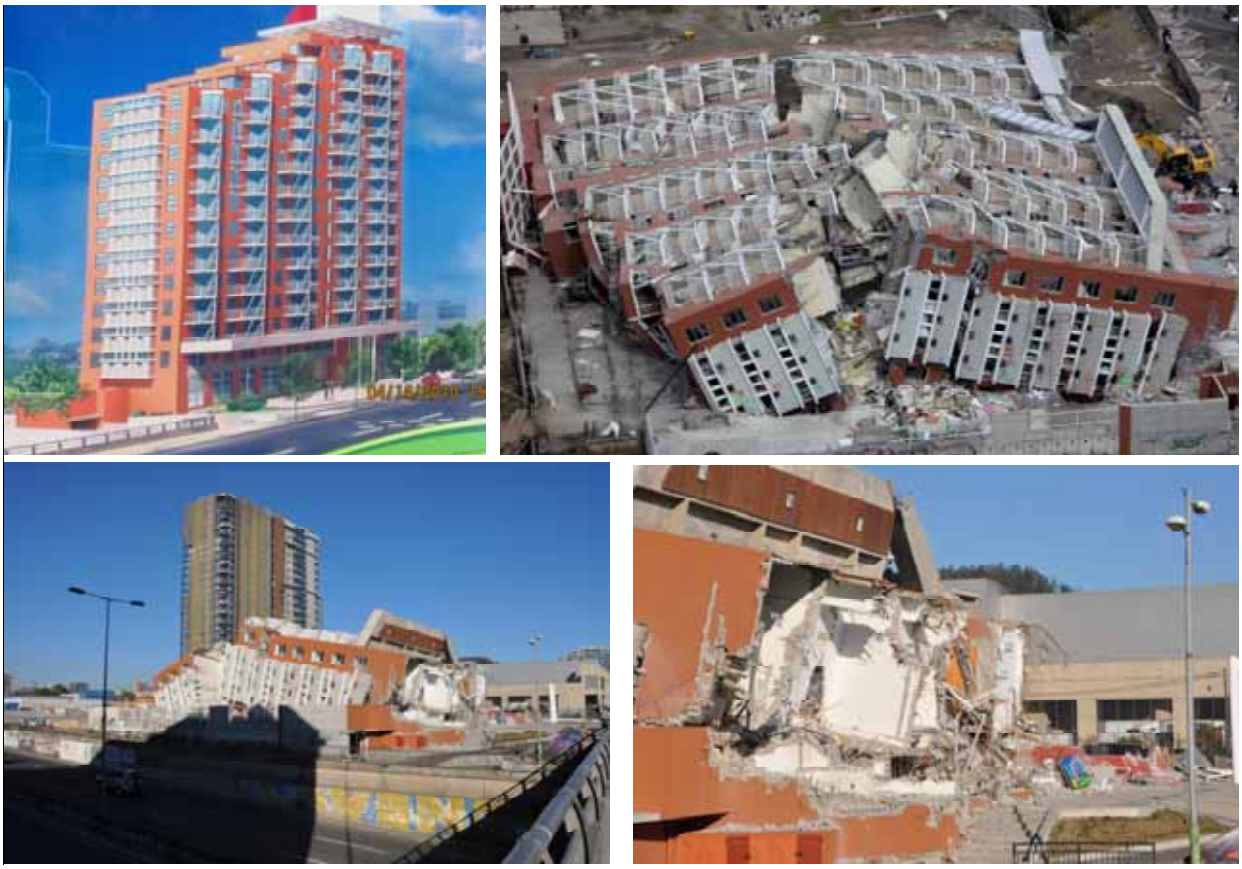

Figure 4.19 Alto Río condominium in Concepción, structure toppled on one side, and failure of bearing walls

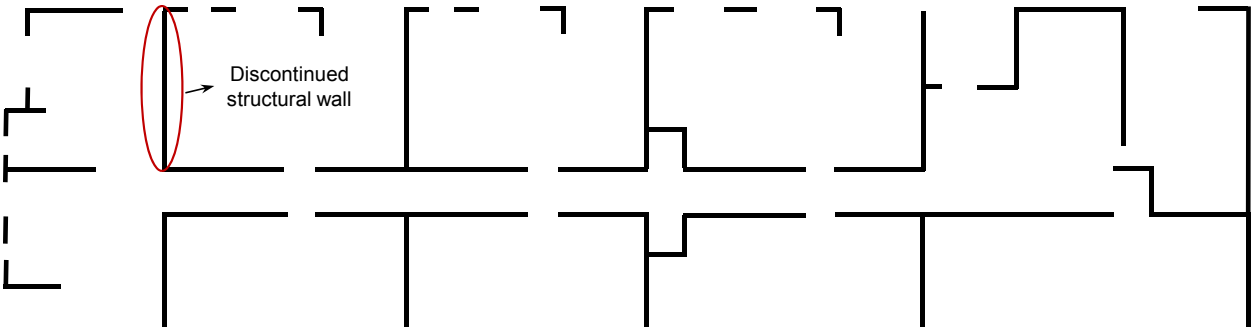

Figure 4.20. Sketch of plan view for Alto Río condominium (the sketch is based on the information provided in the reconnaissance report by the Los Angeles Tall Building Structural Design Council)

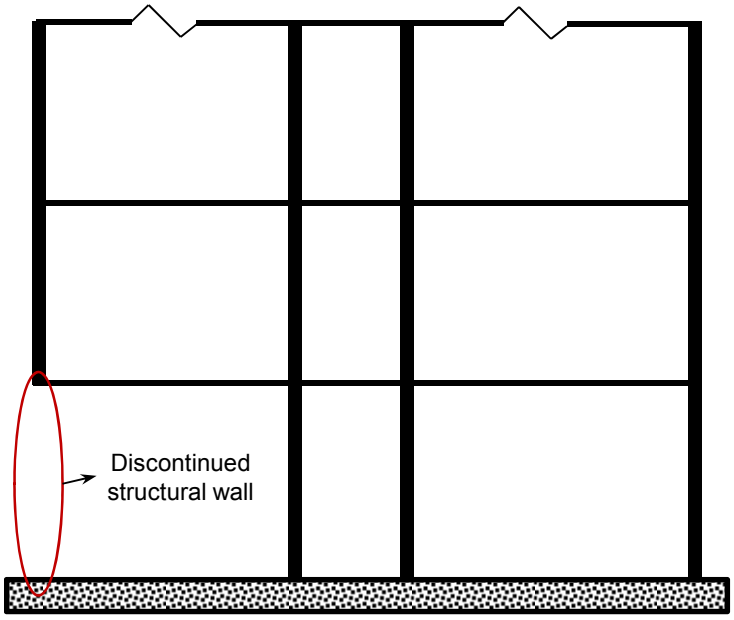

Figure 4.21. Sketch of elevation view for Alto Río condominium

Talcahuano region near Concepción was also seriously affected from the combined effects of strong ground motion and tsunami. The RC building, Figure 4.22, beside the shoreline near the port of Talcahuano was damaged beyond repair. Figure 4.23 shows a number of several buildings at the shorefront damaged due to hydrodynamic loading of the waves carrying debris. The buildings of the Talcahuano port, which were mostly steel frame, were also damaged and rendered nonfunctional, as shown in Figure 4.24.

The MAE Center team also visited Talca. The 6-story RC office building shown in Figure 4.25 suffered from non-structural damage. The decorative features constructed from lightweight concrete on the façade of the building fell down during the earthquake. This building exemplified several cases where the non-structural damage rendered buildings nonfunctional and caused interruption of various extents after the earthquake.

Figure 4.22 RC building near the port of Talcahuano damaged beyond repair

Figure 4.23 Buildings at the shorefront in Talcahuano damaged due to hydrodynamic loading

Figure 4.24 Damaged buildings of the Talcahuano port

Figure 4.25 Edificio Aranjuez (6-story office building) was rendered nonfunctional due to nonstructural damage after the earthquake

In addition to adobe buildings, unreinforced masonry construction was also abundant in Talca. The team visited the three story unreinforced masonry government building in Talca (Edificio Intendencia Maule, Figure 4.26) which was heavily damaged during the earthquake and was nonfunctional at the time of visit. Another unreinforced masonry building that was severely damaged in Talca is the Liceo de Niñas Marta Donoso, Figure 4.27. Failure of masonry walls due to diagonal shear cracks is shown in the figure.

Figure 4.26 Edificio Intendencia Maule in Talca

Figure 4.27 Liceo de Niñas Marta Donoso in Talca

4.2.2. Case Study: Odontology Building of the University of Concepción

4.2.2.a. Introduction and building configuration

This case study aims to explain the observed damage in the Odontology building of the University of Concepción. A brief description of the damage observed by the MAE Center team is provided in Section 4.2.1. The Odontology building is located at the southern east part of Concepción as shown in Figure 4.28. The structure was used as the school of dentistry, which also included rooms for examination and medical treatment of patients. Due to the requirements of the building occupancy, the reinforced concrete structure has a particular configuration. As shown in Figure 4.29, the structure has three regular stories and three, approximately half height, service stories that serve to utility lines.

A typical floor plan of the structure is shown in Figure 4.30. The building has a rectangular shape with seven bays in x-direction and five bays in y-direction. Structural core-walls are provided at center of the building to resist the majority of the lateral loads. Except for minor differences in column dimensions of the exterior frames with five bays, the structure is symmetrical with respect to both x- and y-axes.

Figure 4.28 Location of the Odontology building of the University of Concepción and the ground motion recording station labeled CCSP

Figure 4.29 The Odontology building of the University of Concepción

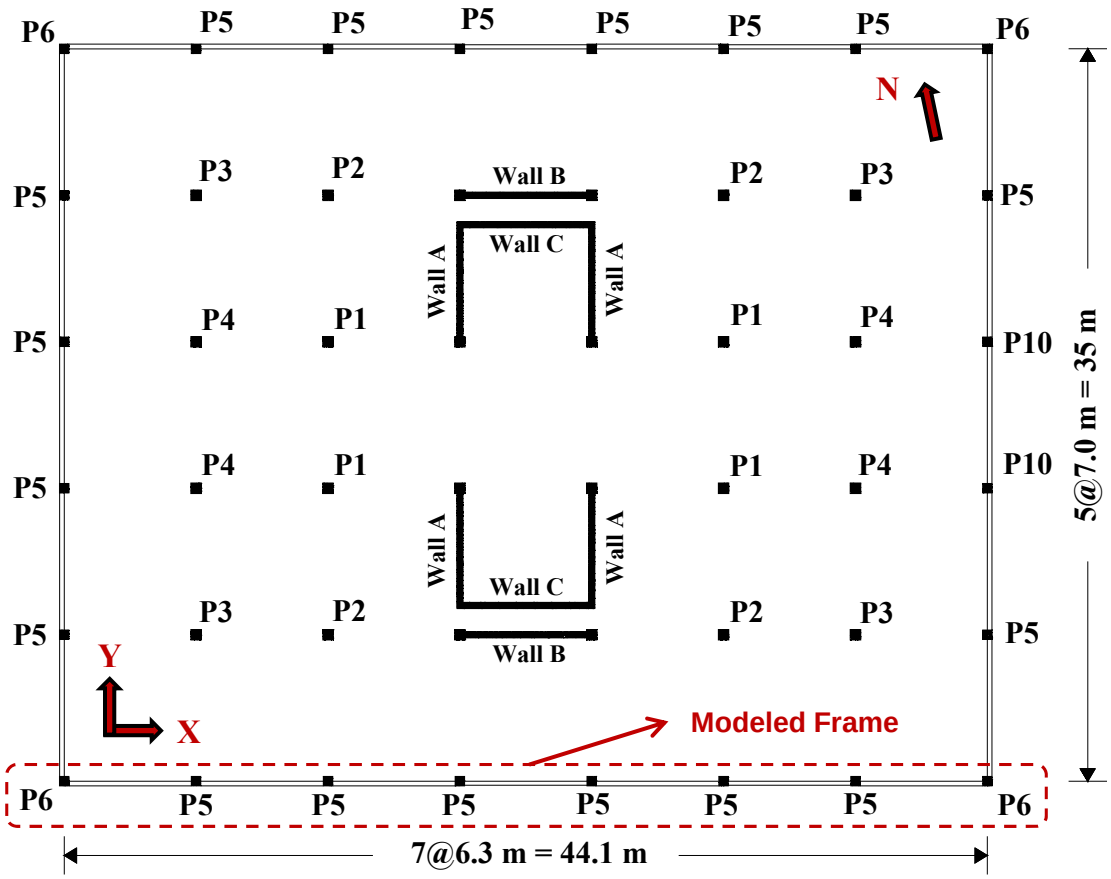

Figure 4.30 Typical plan view sketch of the Odontology building

As shown in Figure 4.31, three floors of the building are designed as flat slabs. Flat slab floors have shallow (slab-depth) beams between the columns and the slab spans the entire floor in both directions. Flat slab design, without the column capitals (or drop panels) is commonly used around the world for light loads. Flat slab construction is preferred in that it provides more clear space, easier formwork (hence shorter construction time), less building height, and architectural flexibility. For the Odontology building of the University of Concepción the flat slab design is used for the service floors which carry considerably lighter loads compared to the regular floors.

As seen in Figure 4.29 (also shown in the elevation sketch, Figure 4.31), another feature of the building is that masonry infill walls are used at the first floors of the exterior frames. Based on the information that the MAE Center team has, it is not certain whether the lateral resistance provided by these infill walls were included in design calculations. It is postulated that these walls were considered to be non-structural. The height of the first story is 3.1 m and the height of the masonry infill walls was measured to be approximately 2.1 m.

4.2.2.b. Observed damage

The earthquake caused interesting damage patterns to the Odontology building of the University of Concepción. The structural damage was confined to columns of exterior frames. The rest of the observed damage was non-structural; cracking of the partition walls (inside the building) and the diagonal cracks of the masonry infill walls at the exterior frames.

As previously discussed in Section 4.2.1, field observations indicated that the combined axial-shear failure at the top portions of the columns were due to commonly observed short-column effect that results from increased shear demands on a specific portion of the vertical members due to a decrease in the effective length. Proper seismic design of vertical members targets at formation of plastic hinges at the member ends (under the extreme seismic demand). This type of failure can dissipate large amounts of energy without a significant reduction in the load carrying capacity. However, the unexpected decrease in the member lengths (which resulted from the existence of masonry infill walls in the case of the Odontology building) leads to shear failure in the members that were designed for flexure. Several of the first-story columns of the Odontology building that failed due to short-column are shown in Figure 4.44.

In the light of the above described observations, it was decided to model the 7-bay exterior frame of the building, as indicated in Figure 4.30. The modeling approach, earthquake input and the results are described in the following sections.

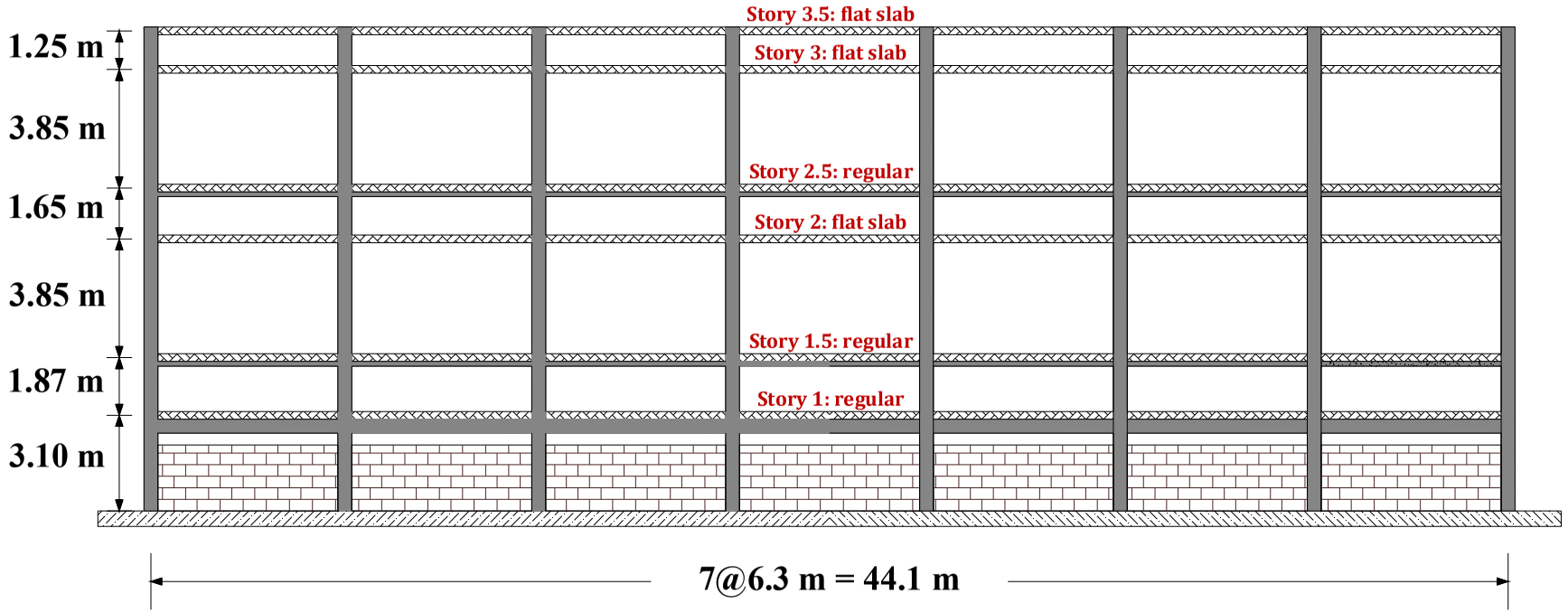

Figure 4.31 Elevation view sketch of the Odontology building

Figure 4.32 Short-column effect observed at the Odontology building

4.2.2.c. Modeling approach

The fiber-based finite element analysis software ZEUS NL (Elnashai et al., 2010) is used to model the frame shown in Figure 4.30. Modeling approaches for four different types of members of the frame: columns, T-beams, flat slabs, and masonry infill walls are described below.

Typical column, beam and slab sections of the frame are shown in Figure 4.33. All members except for the masonry infill walls are represented with 3-D elasto-plastic beam-column elements described by a cubic shape function (Izzuddin and Elnashai, 1993). The columns and slabs are modeled using rectangular sections. The fiber-based finite element modeling approach allows for modeling of the cross-section and placement of the reinforcing bars at their exact locations. The effective flange width (for regular floors where a T-beam exists) is calculated according to ACI 318-08 (ACI, 2008). For the flat-slab floors, the portion of the slab that contributes to the frame analysis is determined by using the following formulation proposed by Luo and Durani (1995a, 1995b).

$$\alpha_i = \chi \frac{R_{12}\left(\frac{c_2}{l_2}\right)}{0.05 + 0.002\left(\frac{l_1}{l_2}\right)^4 - 2\left(\frac{c_1}{l_1}\right)^3 - 2.8\left(\frac{c_1}{l_1}\right)^2 + 1.1\left(\frac{c_1}{l_1}\right)} \tag{4.1}$$

where:

$$R_{12} = -0.0221\left(\frac{c_1}{c_2}\right)^4 + 0.0281\left(\frac{c_1}{c_2}\right)^3 + 0.1535\left(\frac{c_1}{c_2}\right)^2 + 0.773\left(\frac{c_1}{c_2}\right) + 0.0845 \tag{4.2}$$

$$\chi = \left(1 - 0.4\frac{V_g}{4A_c\sqrt{f_c'}}\right) \tag{4.3}$$

Parameter χ is the reduction factor accounting for gravity loads. c_1 and c_2 are the column dimensions in the bending directions and normal to bending direction, respectively. l_1 and l_2 are the span length in bending direction and in transverse direction, respectively, both measured from center to center of the columns. In Eqn. (4.3), V_g is the direct shear force due to gravity load only, A_c is the area of slab critical section, and f_c' is the concrete compressive strength. These formulations were developed based on the results of several tests conducted on slab-column connections and reported in literature.

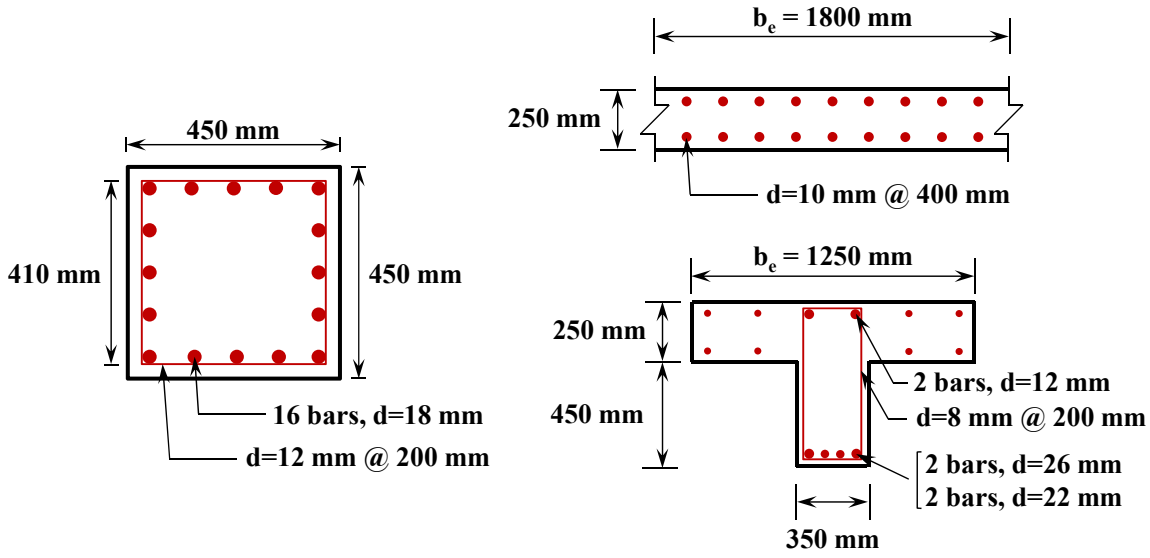

Figure 4.33 Typical column, beam and slab sections

The concrete material is modeled using the constant confinement constitutive relationship developed by Martinez-Rueda and Elnashai (1997) based on the formulations by Mander et al. (1988). Steel is modeled with a bilinear elasto-plastic

model with kinematic strain hardening. Based on the information on the design drawings, the following material properties are used: a concrete compressive strength of 29.4 MPa, steel yield and ultimate strengths of 411.6 MPa and 617.5 MPa, respectively.

In modeling the masonry infill walls the following assumptions are made: infill walls do not carry any vertical loads and they can be represented with diagonal struts that have horizontal resistance only. The first assumption is justified due to the fact that the infill walls have openings for windows which do not transfer the gravity loads. The second assumption is related to the modeling approach as described below.

Masonry walls are modeled with two diagonal compressions struts. The strengths of the struts are determined based the following possible failure modes: compression failure of diagonal strut, sliding shear failure of masonry along horizontal mortar, and diagonal tensile cracking (Paulay and Priestley, 2002). Amongst these failure modes, the first and the second one are the most commonly observed for infill walls. Here, the shear strengths of each infill wall corresponding to the compression failure of diagonal strut and sliding shear failure are calculated and the minimum of the two is used as the ultimate strength.

The modeling of masonry infill walls follow the approach proposed by Mostafaei and Kabeyasawa (2004) as adopted by Kwon and Kim (2010). The procedure is described in the following. The compressive strength of the masonry prism is an important parameter in the modeling approach. According the Paulay and Priestley (2002), the compressive strength of the masonry prism, f_m' is estimated as

$$f_m' = f_y = \frac{f_{cb}'\left(f_{tb}' + \alpha f_j'\right)}{U_u\left(f_{tb}' + \alpha f_{cb}'\right)} \tag{4.4}$$

where h is the height of the masonry unit, $\alpha = j/4.1h$, j is the thickness of mortar, U_u is the stress nonuniformity coefficient and equal to 1.5, f_{cb}' is the compressive strength of brick, f_{tb}' is the tensile strength of brick and equal to $0.1f_{cb}'$, and f_j' is the mortar compressive strength.

The use of Eqn. (4.4) requires mechanical properties of the brick and the mortar. This information is not available, however, NCh 2123 (2003) specifies the minimum compressive strength for clay brick units in the range from 4 MPa (hand-made bricks) to 11 MPa (machine-made bricks). Additionally, Moroni et al. (2004) provides that the typical strength of masonry bricks in Chile is 6-12 MPa. Based on this information, 11 MPa is selected as the masonry strength (f_{cb}') in this study. The minimum compressive strength for masonry cement mortar (f_j') is specified as 10 MPa in NCh 2123 (2003) which is also adopted here.

Compression failure of infill walls occurs as a result of the compression failure of the equivalent diagonal strut. The horizontal component of the diagonal strut capacity is calculated as

$$V_c = z t_w f'_m \cos\theta \tag{4.5}$$

where z is the equivalent strut width calculated based on FEMA 306 (1999), t_w is the thickness of the infill panel, and θ is the angle defined by the infill height and length. z and θ are illustrated in Figure 4.34. The following information is obtained from field investigation of the building: mortar thickness is 30 mm, height of masonry units is 75 mm, and the wall thickness including mortar is 200 mm.

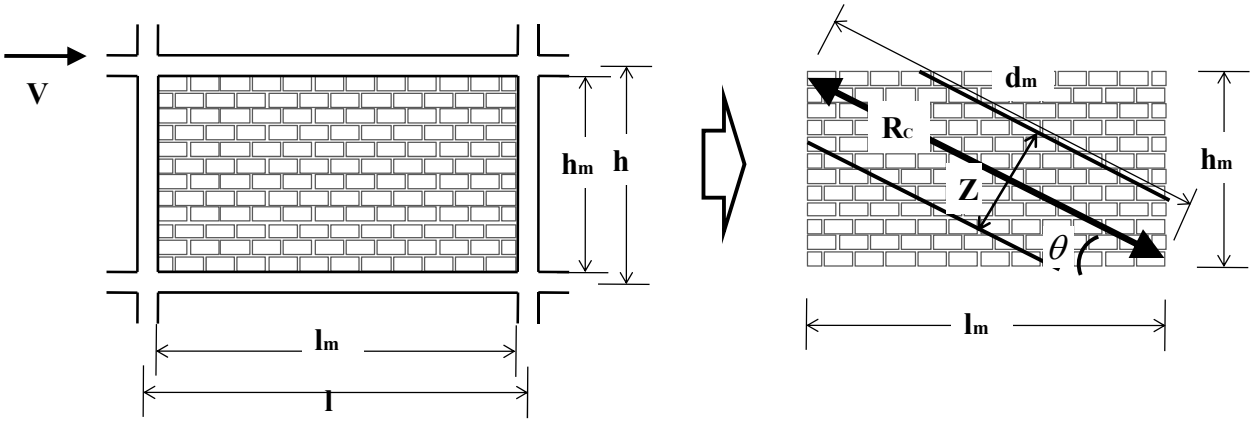

Figure 4.34 Masonry infill walls and the equivalent diagonal strut (Kwon and Kim, 2010)

The sliding shear strength of masonry infill walls is calculated based on the Mohr-Coulomb criteria as follows

$$\tau_f = \tau_0 + \mu\sigma_N \tag{4.6}$$

where τ_0 is the cohesive capacity of the mortar beds, μ is the sliding friction coefficient along the bed joint, and σ_N is the vertical compression stress in the infill wall. The shear strength in terms of force can be written as

$$V_f = \tau_0 t_w l_m + \mu N \tag{4.7}$$

where l_m is the length of infill panel (as shown in Figure 4.34) and N is the vertical load on the infill wall. The infill walls of the Odontology building do not carry vertical loads, therefore, N is approximated as the vertical component of the diagonal compression force, i.e. $R_c sin\theta$, where R_c is the diagonal compression force (shown in Figure 4.34) which is given as

$$R_c = V_f = \frac{\tau_0 t_w l_m}{1 - \mu\tan\theta} \tag{4.8}$$

As per Kwon and Kim (2010), the typical ranges for τ_0 and μ are $0.1 \leq \tau_0 \leq 1.5\ MPa$ and $0.3 \leq \mu \leq 1.2$. It is assumed here that $\tau_0 = 0.04 f_m'$. The friction coefficient μ is calculated based on the work by Chen (2003) as

$$\mu = 0.654 + 0.00525 f_j' \tag{4.9}$$

The shear strength calculated based on the diagonal compression failure and the sliding shear failure cannot exceed 0.83 MPa according to ACI 530-05/ASCE 5-05 (2005) which imposes the following condition

$$\frac{V_{\max}}{t_w l_m} = 0.83\,MPa \tag{4.10}$$

The two diagonal struts of infill walls provide resistance against lateral load. Here, it is assumed that the force-displacement relationship of each diagonal strut follows a tri-linear curve in terms of compression and the strut has zero tensile strength as shown in Figure 4.35. The hysteretic behavior of diagonal struts is modeled with lumped springs at the end of the strut and the strut is modeled with rigid truss element. The tri-linear displacement-force relationship consists of yield shear force (V_y), maximum shear force (V_m), yield displacement (U_y) and maximum displacement at peak force (U_m). The maximum displacement at maximum lateral force is calculated based on the following equation by Madan et al. (1997)

$$U_m = \frac{\varepsilon_m' d_m}{\cos\theta} \tag{4.11}$$

where ε_m' is the masonry compressive strain at maximum compressive stress and assumed to be 0.0018 and d_m is the diagonal strut length. The maximum drift limitation of 0.8 percent is applied as suggested by Kwon and Kim (2010). The initial stiffness K_0 is determined as (Madan et al., 1997)

$$K_0 = \frac{2V_m}{U_m} \tag{4.12}$$

where V_m is the maximum strength taken as the lower of those obtained based on the above defined two failure criteria, the stiffness ratio (α) is assumed to be 0.2, and U_y and V_y are estimated based on V_m, K_0 and α.

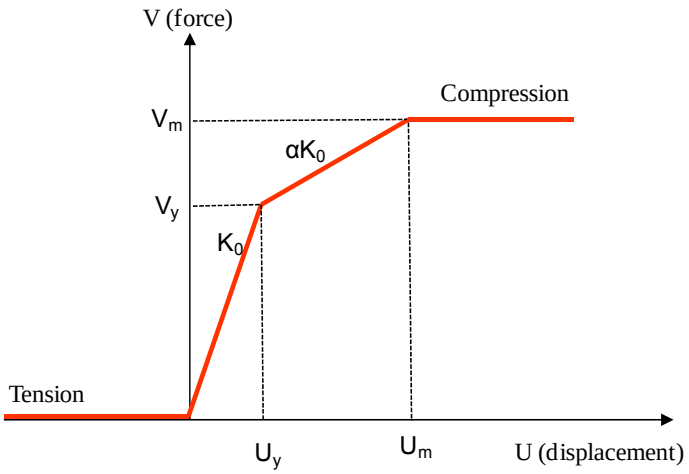

Figure 4.35 Hysteretic behavior of diagonal strut elements (Kwon and Kim, 2010)

The analytical model for the considered frame of the Odontology building is shown in Figure 4.36.

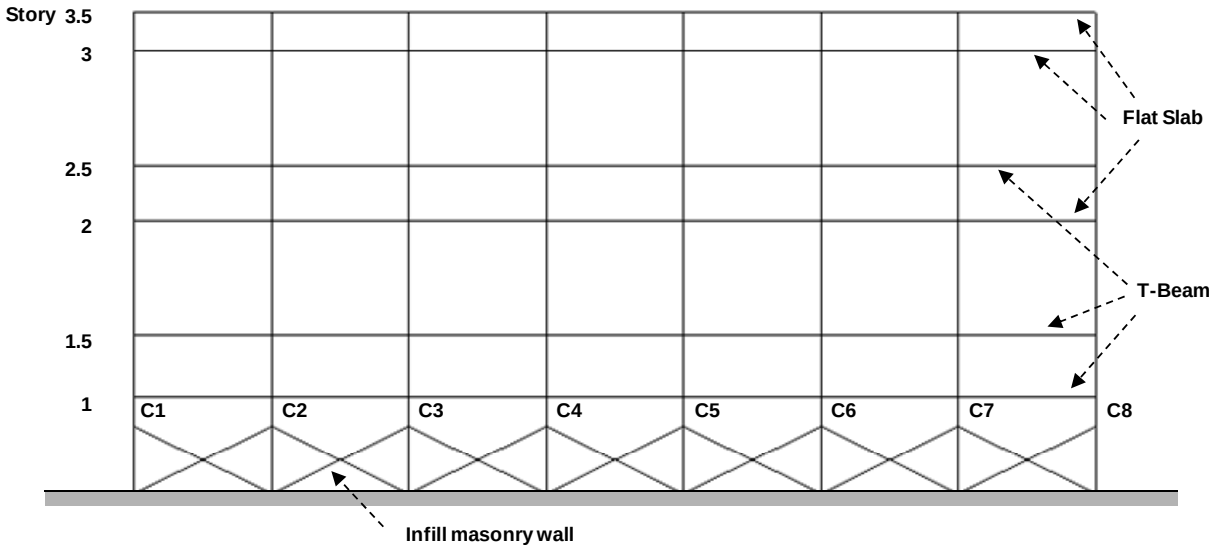

Figure 4.36 Analytical model for the exterior frame of the Odontology building

4.2.2.d. Analysis results

Since the objective of the analysis conducted here is to investigate the effect of masonry infill walls on the response of the structure and observed damage, two building configurations are considered: with and without infill walls. An eigenvalue analysis of the structure is conducted. The mode shapes for the first three modes (for the configuration with infill walls) are shown in Figure 4.37 and the periods for both configurations are summarized in Table 4.2.

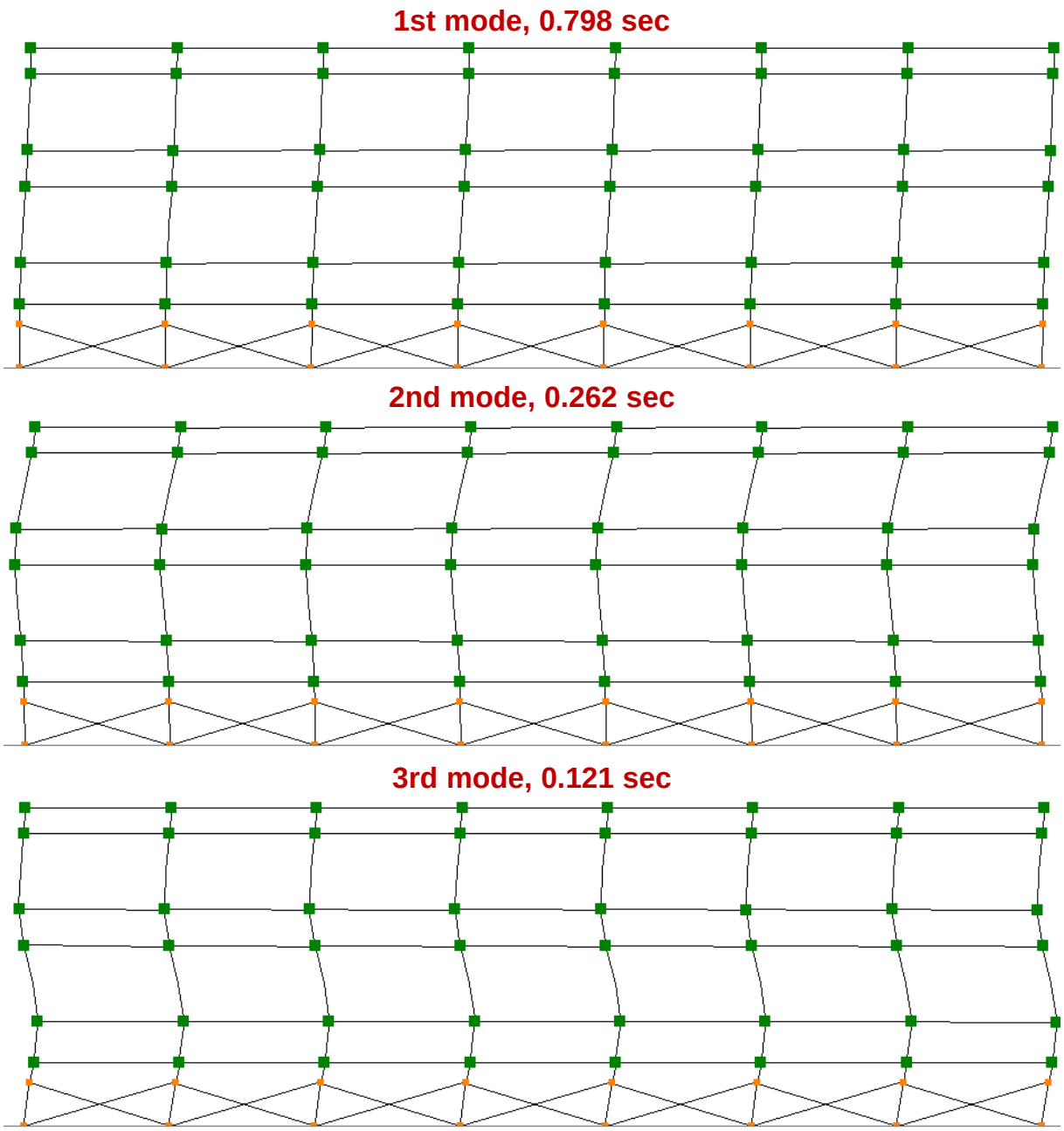

Figure 4.37 Mode shapes for the first three modes (frame with infill walls)

Table 4.2 Periods of the building with and without infill walls

	Periods (sec)	
	w/ infills	w/o infills
1st mode	0.798	0.829
2nd mode	0.262	0.273
3rd mode	0.121	0.164

A total of eight ground motion records are used for inelastic dynamic time history analysis of the building. As it is described in detail in Section 2.4.3, for the sites of case study buildings a mean acceleration spectrum is developed using the source characteristics and a set of suitable attenuation relationships. Two additional spectra (+0.5σ and -0.5σ) are also developed. Two seed records are selected (stations CCSP and MELP for the case of Odontology building) and spectrum matching is used to obtain the spectrum compatible records. For the back-analysis conducted here, the original (without spectrum matching) record from the CCSP station (both horizontal components) is also used due to close proximity of the station to the building site (6.7 km as illustrated in Figure 4.28).

The interstory drift ratio profiles for all eight records and the two configurations (with and without infill walls are provided in Figure 4.38.

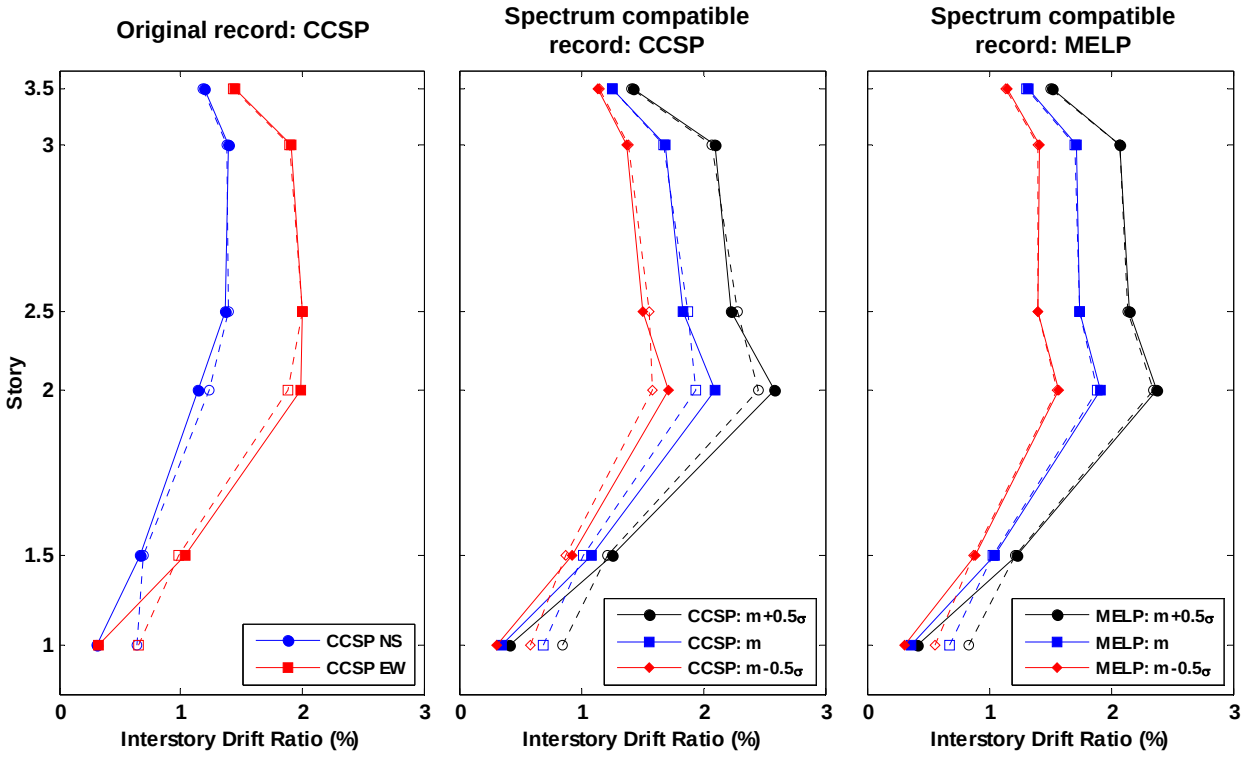

Figure 4.38 Maximum interstory drift ratio: dotted lines show frame without infill wall, solid lines show frame with infill wall

The interstory drift ratio for all ground motions are compared for the two configurations (with and without infill walls) in Table 4.3. Based on the information that is provided in Figure 4.38 and Table 4.3, it is concluded that there is a significant reduction in the interstory drift ratio of the first floor, reaching as high as 51 percent, when the effect of maonry infill walls are considered.

Table 4.3 The effect of infill walls on the interstory drift ratio, ID (ID values are in %)

Ground motion		Structure type	Story 1	1.5	2	2.5	3	3.5
Raw Record at station, CCSP								
	NS	F*	0.64	0.70	1.24	1.39	1.38	1.18
		FW**	0.32	0.67	1.15	1.36	1.40	1.19
		EIW***	-50.42	-3.38	-7.06	-1.92	1.15	0.88
	EW	F	0.65	0.99	1.88	2.00	1.90	1.43
		FW	0.33	1.03	1.98	2.00	1.90	1.44
		EIW	-49.73	4.61	5.39	-0.24	0.36	0.99
Synthetic record								
CCSP	Mean + 0.5σ	F	0.84	1.22	2.45	2.28	2.07	1.42
		FW	0.41	1.26	2.59	2.24	2.09	1.43
		EIW	-51.26	3.02	5.50	-1.81	1.18	1.02
	Mean	F	0.69	1.02	1.94	1.88	1.68	1.26
		FW	0.35	1.08	2.09	1.83	1.69	1.26
		EIW	-49.31	5.95	7.78	-2.51	0.54	-0.13
	Mean - 0.5σ	F	0.59	0.88	1.58	1.56	1.39	1.15
		FW	0.31	0.93	1.72	1.51	1.37	1.14
		EIW	-46.58	6.51	8.84	-3.26	-0.93	-0.81
MELP	Mean + 0.5σ	F	0.83	1.22	2.35	2.14	2.07	1.51
		FW	0.42	1.23	2.38	2.16	2.08	1.52
		EIW	-49.66	0.81	1.02	0.68	0.61	0.85
	Mean	F	0.68	1.03	1.89	1.74	1.71	1.31
		FW	0.36	1.04	1.91	1.74	1.71	1.32
		EIW	-47.34	1.46	1.32	0.32	0.40	0.56
	Mean - 0.5σ	F	0.57	0.88	1.56	1.40	1.41	1.14
		FW	0.31	0.89	1.58	1.40	1.41	1.15
		EIW	-44.43	1.24	1.30	-0.04	0.42	0.75

** ID for frame without infill wall, ID_F*
*** ID for frame with infill wall, ID_{FW}*
**** Effect of infill wall on ID (in %), $EIW(\%) = (ID_{FW} - ID_F)/ID_F \times 100$*

In order to explore causes of the shear failure of columns due to the previously described short-column effect, it is required to compute the shear capacity of the columns and compare it against the shear demand imposed during the earthquake. The shear strength of the RC column is calculated according to ACI 318-08 (2008). The nominal shear strength (V_n) is the summation of the contribution of concrete (V_c) and the contribution of steel (V_s)

$$V_n = V_c + V_s \tag{4.13}$$

where

$$V_s = \frac{A_v f_y d}{s} \tag{4.14}$$

$$V_c(t) = 0.17\lambda\left[1+\frac{N_u(t)}{14A_g}\right]\sqrt{f_c'}b_w d \qquad \text{(axial compression)} \tag{4.15}$$

$$V_c(t) = 0.17\lambda\left[1+0.29\frac{N_u(t)}{14A_g}\right]\sqrt{f_c'}b_w d \qquad \text{(axial tension)} \tag{4.16}$$

and A_v is the area of shear reinforcement within a spacing distance of s, f_y is the yield strength of steel, d is the effective depth of the section. The contribution of the concrete in shear resistance is calculated using Eqn. (4.15) if the member is subjected to a compressive force, on the other hand if the member is subjected to axial tension the modified equation given in Eqn. (4.16) is used. In Eqns. (4.15) and (4.16): A_g is the gross sectional area in mm^2, N_u is the axial force in N with compression being positive, f_c' is the compressive strength of concrete in MPa, b_w is the width of the section web in mm. The variable λ is taken as 1.0 and 0.75 for normal and light weight concrete, respectively.

Since the shear capacity of the member is a function of the axial force acting on it, the capacity is evaluated for each time step of the dynamic analysis. The shear demand is directly obtained from the finite element simulation. As an example, the shear capacity and the shear demand on column 8 (the column numbering is shown in Figure 4.36) are compared in Figure 4.39. It is observed that the presence of masonry infill walls significantly increase the shear demand on the columns and the shear capacity is exceeded at certain times throughout the analysis. The shear demand to shear capacity ratio for the first story columns are provided for both frames (with and without the infill walls) and all ground motion records in Table 4.4. For illustration purposes, these ratios are shown using bar plots in Figure 4.40 through Figure 4.42 for different ground motion records. It is concluded that the shear demand exceeds the shear capacity of the columns for various considered cases. The existence of masonry infill walls significantly increases the likelihood of exceeding the shear capacity. For the building without the infill walls, the shear demand is exceeded for none of the considered cases under the original CCSP record, which can be thought as a more realistic description of the earthquake demand. It is known that spectrum compatible records contain a range of frequencies that usually do not exist in natural records.

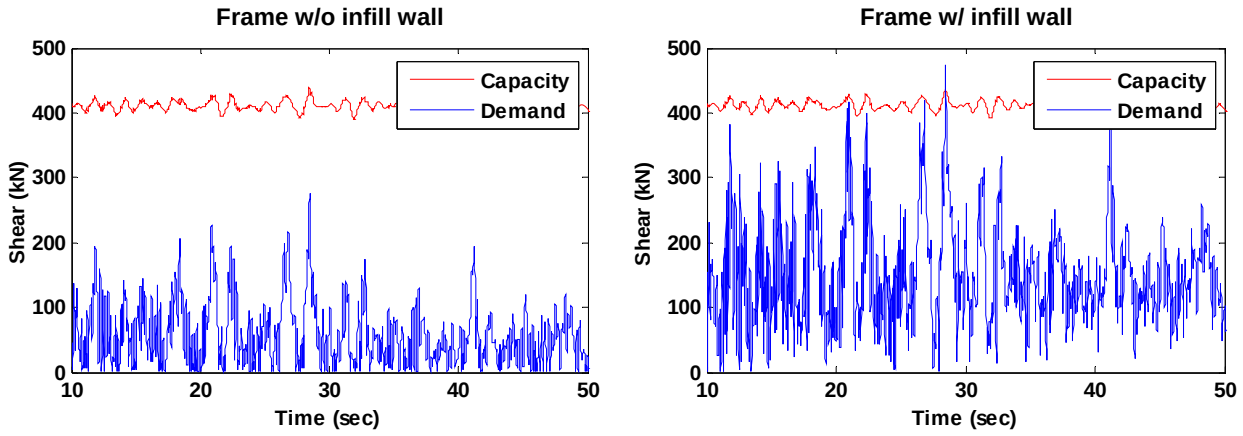

Figure 4.39 Comparison of shear capacity and demand for column 8, spectrum compatible mean record with seed CCSP

Table 4.4 Shear demand-to-capacity ratio of columns for the first story

Ground motion			Max. Shear Demand/Capacity							
			C1	C2	C3	C4	C5	C6	C7	C8
Raw Record at station, CCSP										
	NS	F	0.57	0.89	0.77	0.70	0.65	0.68	0.79	0.54
		FW	***1.01***	***1.03***	0.89	0.83	0.82	0.88	0.96	0.93
	EW	F	0.55	0.84	0.74	0.66	0.72	0.82	0.97	0.62
		FW	***1.06***	***1.07***	0.88	0.81	0.91	***1.01***	***1.19***	***1.18***
Synthetic record										
CCSP	Mean + 0.5σ	F	0.64	***1.05***	0.93	0.85	0.88	0.99	***1.16***	0.68
		FW	***1.19***	***1.17***	0.98	0.87	0.88	***1.01***	1.23	1.26
	Mean	F	0.56	0.86	0.77	0.69	0.74	0.84	0.99	0.63
		FW	***1.03***	0.96	0.81	0.72	0.73	0.85	***1.04***	***1.09***
	Mean - 0.5σ	F	0.49	0.71	0.63	0.57	0.62	0.70	0.83	0.56
		FW	0.89	0.80	0.65	0.58	0.58	0.70	0.87	0.95
MELP	Mean + 0.5σ	F	0.69	***1.16***	***1.01***	0.92	0.85	0.88	***1.04***	0.64
		FW	***1.22***	***1.22***	***1.02***	0.89	0.81	0.89	***1.09***	***1.15***
	Mean	F	0.59	0.92	0.80	0.73	0.68	0.71	0.85	0.56
		FW	***1.06***	1.03	0.83	0.74	0.67	0.73	0.93	***1.02***
	Mean - 0.5σ	F	0.51	0.75	0.64	0.59	0.55	0.57	0.69	0.48
		FW	0.91	0.87	0.69	0.61	0.54	0.60	0.79	0.90

** Bold italic font indicates that the shear demand exceeds the shear capacity*

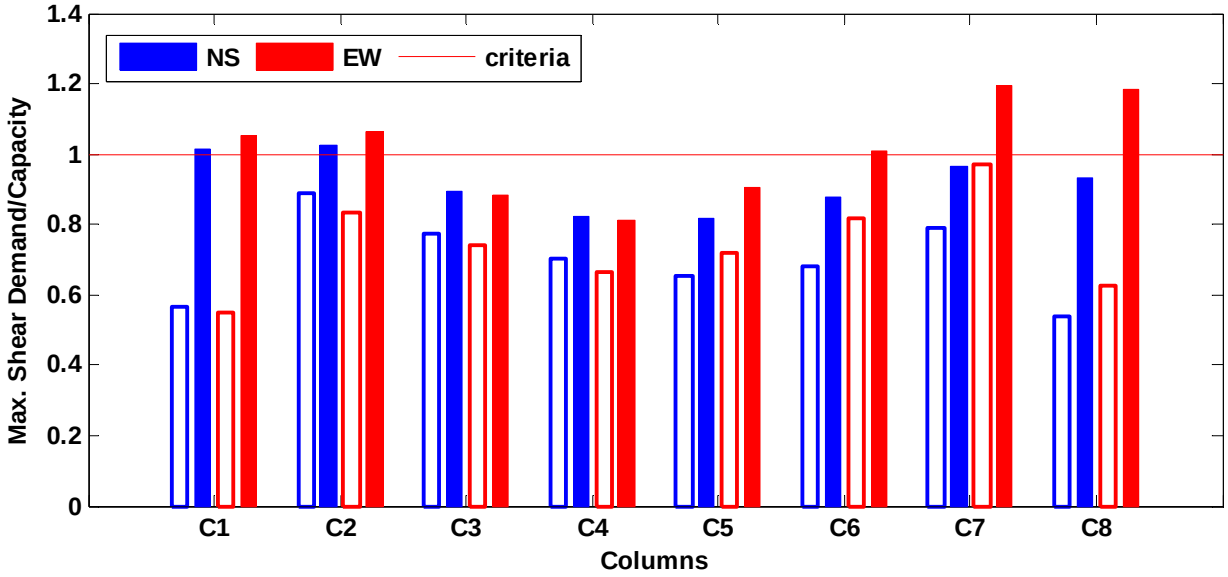

Figure 4.40 Maximum shear demand to capacity ratio, CCSP record (unmodified): empty bars indicate frame without infill walls, solid bars indicate frame with infill walls

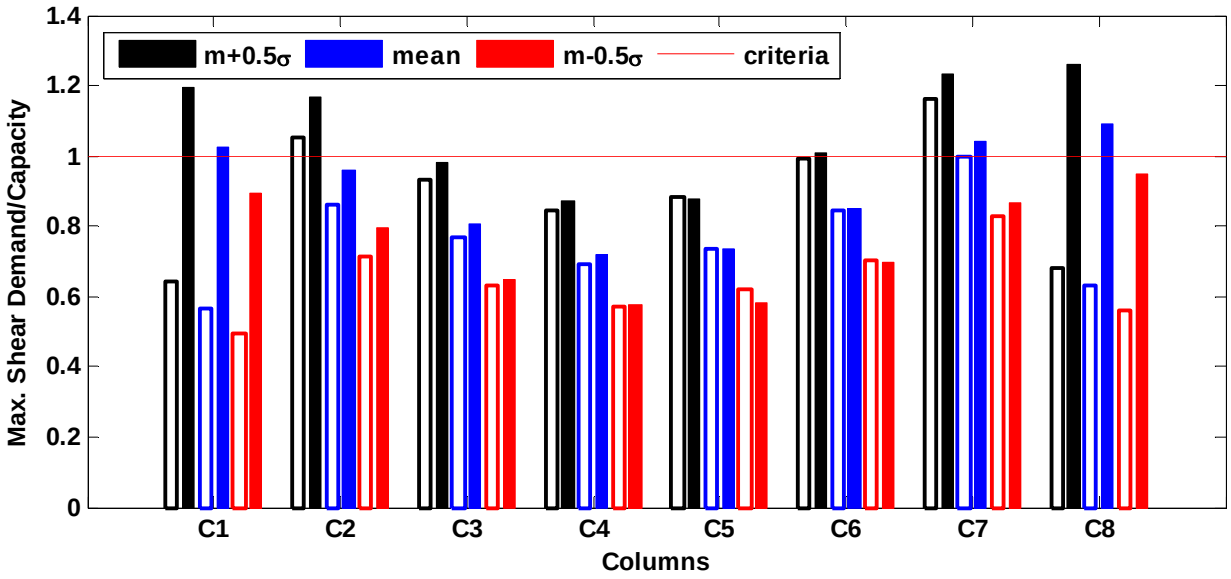

Figure 4.41 Maximum shear demand to capacity ratio, spectrum compatible record CCSP: empty bars indicate frame without infill walls, solid bars indicates frame with infill walls

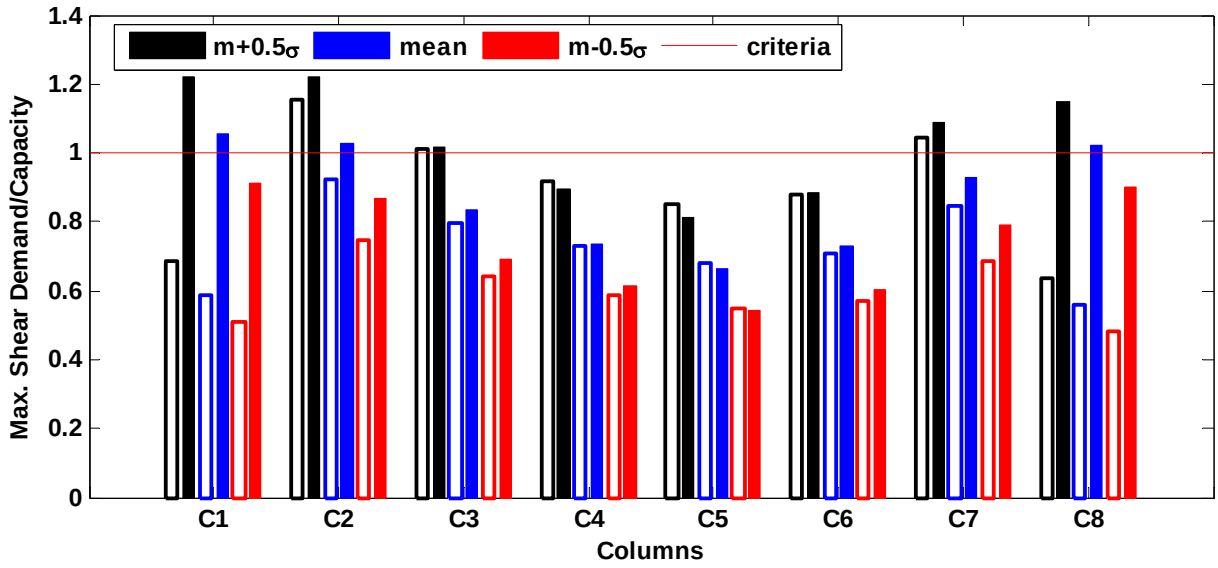

Figure 4.42 Maximum shear demand to capacity ratio, spectrum compatible record MELP: empty bars indicate frame without infill walls, solid bars indicate frame with infill walls

4.2.2.e. Conclusions

In Section 4.2.2, back-analysis of the Odontology building of the University of Concepción is conducted. Field inspection of the building indicated that shear failure of the columns on the exterior frames may be due to short-column effect. Rigorous modeling of the building is conducted using fiber-based finite element analysis software. Two models are constructed, with and without masonry infill walls, in order to study the effect of masonry walls on the observed damage. It is concluded that the interstory drift ratio at the first story is significantly reduced when the infill walls are present. Furthermore, many columns of the first story are expected to fail due to increased shear demand as a result of the masonry infill walls. Particularly, for the exterior columns of the considered frame the shear demand exceeded the shear capacity considerably which indicated severe damage. The analytical results are in agreement with the observed damage in the field.

4.3. EFFECTS ON BRIDGES

4.3.1. Observed Bridge Damage

Considering the large earthquake magnitude and rupture area, the damage to bridge structures was less than could have been expected. The major highways in Chile are constructed and maintained by private companies. The highway network is approximately 2,200 km in length and has around 2,000 bridges with span length longer than 10 m. Among these structures, only one percent (8 highway and 12 pedestrian

bridges) collapsed due to the earthquake. Approximately 100 bridges (50 highway and 50 pedestrian bridges) were damaged to a level requiring repair.

The MAE Center field investigation team visited several damaged bridges to study failure modes. There had been several teams from other organizations, such as Earthquake Engineering Research Institute (EERI) and Japan Society of Civil Engineers (JSCE), which focused on bridge performance. Table 4.5 presents a compiled list of damaged bridges, their locations, and failure modes based on the data collected from the field investigation and reports available in the public domain (Kawashima et al. 2010; Yashinsky et al., 2010).

The most commonly observed bridge damage was due to unseating or displacement of superstructure, especially for skewed bridges. Even if the centers of mass and stiffness coincide, skewed bridges tend to develop rotation, which results in unseating of the bridge girder or failure of shear keys. Bridges designed according to relatively recent design practice apparently suffered more damage than bridges constructed in the past. In the old construction practice, the integrity of bridge superstructure was high due to diaphragms connecting the girders. On the other hand, bridges constructed in recent years often did not have diaphragms. As a result of the lack of in-plane stiffness and connectivity, bridge girders were damaged due to the pounding of the superstructure onto the shear keys. In the report from another field investigation team (Yashinsky et al. 2010), it is stated that the seat-width on bridge bent was not large enough to prevent unseating. In addition, in many bridges, shear keys were not strong enough to resist the lateral forces from the pounding superstructure.

Only a few bridges reportedly had damage of their substructure. It is speculated that as there are not many bridges with integral superstructure-substructure connection, the large inertial force from superstructure was not transferred to the substructure. The inertial force caused the unseating or large movement of the superstructure, or the failure of shear keys.

In the following, detailed description of bridge failure modes are presented, which is followed by numerical case studies in Section 4.3.2.

Table 4.5 List of damaged and/or collapsed bridges

Bridge name | Roadway carried by the bridge | Location	Damage / failure modes and other remarks
Miraflores Bridge | Vespucio Norte Express | Independencia, Santiago	North bridge had diaphragm between girders and concrete shear keys preventing the movement of the superstructure. Damage on concrete shear keys. South bridge had steel shear keys for each girder. Most of shear keys were damaged.
Lo Echevers Bridge | Vespucio Norte Express | Lo Echevers, Santiago	Skewed bridge. Unseating of superstructure due to large transverse displacement.
Quilicura Bridge | n/a | n/a	Skewed steel girder bridge. Unseating of deck. Failure of shear keys. Shear keys at only one side was damaged. The bridge was maintained by ministry of public work.
Las Mercedes Bridge* | Route 5 South | 34° 4.3235′ S 70° 45.753′ W	Skewed pre-stressed girder bridge. Unseating of deck. No diaphragms joining pre-stressed girders.
Costanera Norte | n/a | n/a	Skewed bridge. Shear key failure. Large displacement of superstructure at abutment.
Pasarela Peatonal | Route 5, Norte | n/a	Pedestrian bridge. Bridge deck was bolted to the bent of the bridge. The bolts were sheared and the superstructure unseated. The bridge bent was undamaged.
Perquilauquén Bridge* | Route 5 | 36° 15.208'S 71° 48.8257'W	Consists of two bridges, one built in mid-1990s and the other one recently built. The older bridges suffered less damage than the new one. The damage on the new bridge was large transverse displacement of superstructure. The shear key of the new bridge was very weak and failed.
Juan Pablo II Bridge | n/a | Concepción, 36° 49.401'S 73° 5.477'W	Shear failure on bridge column due to lateral spreading of soil toward river.
Llacolén Bridge | n/a | Concepción, 36° 50.039′ S 73° 4.623'W	Indication of lateral spreading toward river. Unseating of several ramps.
Bíobío Bridge | n/a | Concepción, 36° 50.442' S 73° 4.115' W	Built in 1930s. Closed before the earthquake for maintenance. Steel stringer bridge. Unseating of bridge decks. Total collapse.
Las Ballenas Bridge | n/a | Suburb of Concepción	Rupture of elastomeric bearings.
Río Claro Bridge | n/a | n/a	Unreinforced masonry bridge built in 1870. Collapsed during the earthquake.
Tubul Bridge | n/a | Arauco	South most location of complete bridge collapse. Steel girder bridge. All eight steel girders were unseated. In JSCE slide, it was reported that performance of foundation was insufficient.
Paso Cladio Arrau* | n/a | 36° 39.536' S 72° 19.545' W	Minor transverse translation of the superstructure. The bridge was serviceable after the earthquake.
Route 5 overpass near Chillán* | Route 5 (overpass) | Chillán 36° 35.083' S 72° 6.534' W	Skewed bridge. Large translation and close to unseating of superstructure. Shear key at the abutment was not long enough to provide resistance to superstructure.

Notes: Detailed discussion on bridge damage are presented in the following for the bridges with asterisks (*).

4.3.1.a. Las Mercedes Bridge

The bridge shown in Figure 4.43 is an overpass on Route 5 located at 34°4'19.44"S, 70°45'45.18"W based on GPS coordinate. The bridge is a two-lane two-span bridge with three pre-stressed concrete girders and reinforced concrete deck. The structure has a skew angle of approximately 10 degree. The superstructure is supported on elastomeric bearings and restrained to the substructure with seismic restrainers with a diameter of 23.6 mm, which corresponds to #7 or #8 bars in the U.S.

Major damage to the bridge was caused by the rotation of the superstructure, which resulted in the failure of shear keys and unseating of a girder. Ideally, if a bridge's centers of mass and center of stiffness coincide, the superstructure should not develop rotational seismic demands even if there is a skew angle. Due to the nonlinearity of bridge components, such as gaps between superstructure and abutment, the skewed bridges can relatively easily be subjected to large rotational demand. For instance, Figure 4.44 (a) shows an illustration of an intact skewed bridge. When there is seismic demand in longitudinal or transverse direction that is large enough to close the gap between the superstructure and the abutment, the center of stiffness is shifted toward the abutment where the gap is closed. Once the centers of stiffness and mass become different, the translational seismic demand develops rotational seismic demand as shown in Figure 4.44 (b), which eventually causes rotation of the superstructure. The rotational seismic demand can cause torsional failure of bridge bents in the monolithic bent-deck construction. As superstructure was supported on elastomeric bearings for the investigated bridge, the superstructure rotated, which resulted in the failure of shear keys and unseating of a girder.

Figure 4.45 shows deformation of bridge superstructure. The west end of the superstructure was shifted toward the south by approximately 1.5 m as shown in Figure 4.45 (a). The gap between the superstructure and east abutment was closed and the gap between west abutment and superstructure was about 0.5 m. Bent remained nearly intact except for the cracks on the shear keys. Figure 4.46 shows the seismic restrainers connecting the superstructure and substructure. The seismic restrainers seemed to have been installed to prevent uplift of the superstructure. The effectiveness of the restrainers on actual seismic performance of the bridge superstructure could not be clearly explained based on the information obtained during the field investigation. It appeared, however, that the restrainers did not provide lateral resistance. The shear keys in the abutments and the bent were damaged as shown in Figure 4.47. Shear keys appeared to be flexible and did not have enough strength to resist the force from the superstructure.

Figure 4.43 Rancagua Bypass

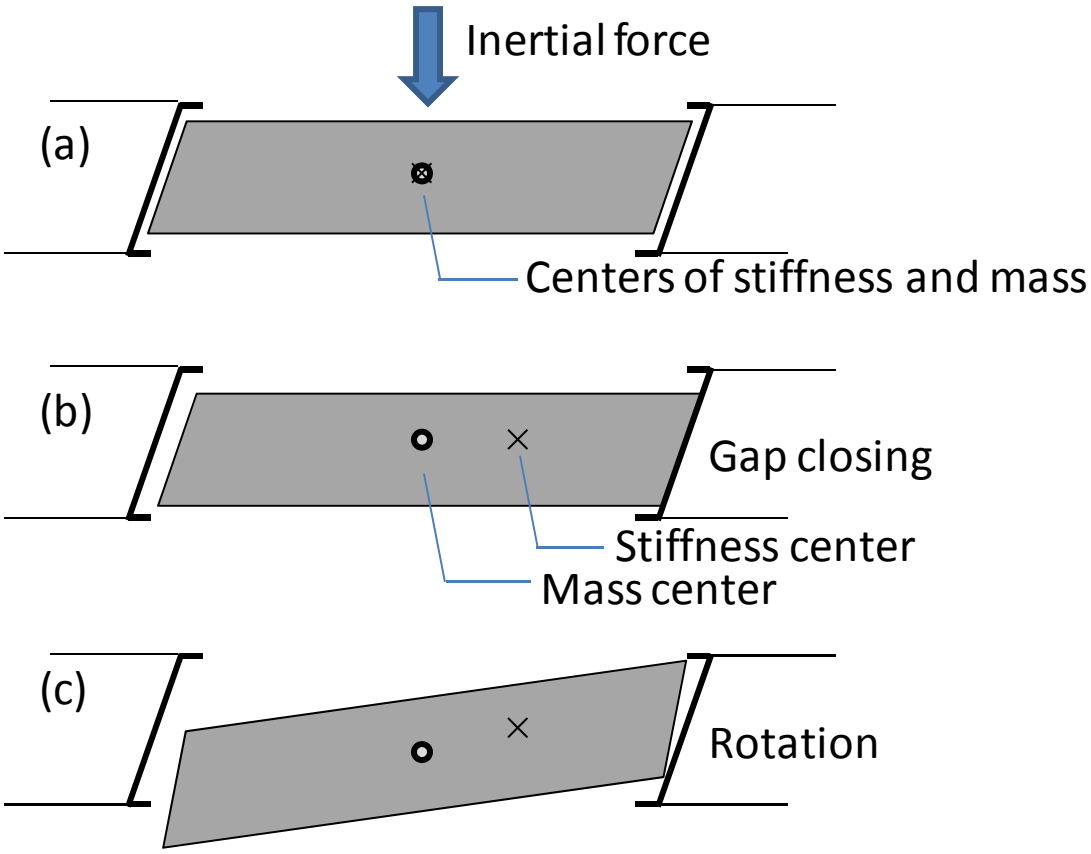

Figure 4.44 Effect of skew angle on seismic demand

Figure 4.45 Translation of bridge superstructure

Figure 4.46 Seismic restrainers connecting superstructure to abutment

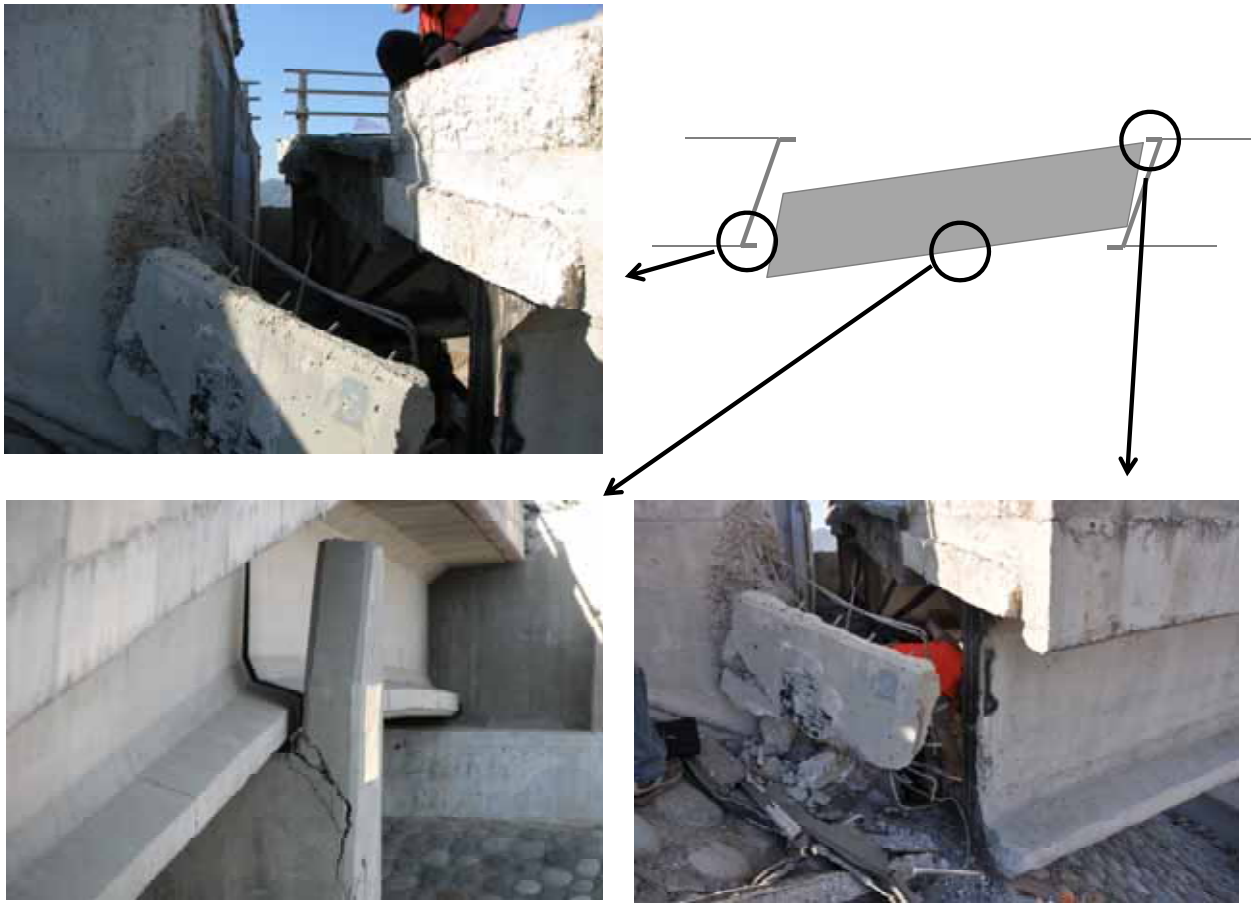

Figure 4.47 Failure of bridge shear keys

4.3.1.b. Perquilauquén Bridge

The Perquilauquén Bridge is also located on Route 5. The bridge carrying the northbound traffic was built recently and the bridge carrying the southbound traffic was built in the mid-1990s. The recently constructed bridge adopted pre-stressed girders for superstructure and circular piers for substructure. The bridge constructed in 1990s consisted of box girder for superstructure and wall pier as shown in Figure 4.48. As the two bridges were constructed with different structural systems, the comparison of damage in both bridges provided an insight into how different structural systems perform differently when subjected to similar earthquake demand.

Both bridges did not collapse due to the earthquake event. The bridge carrying the northbound traffic, which was constructed recently, however, showed much more damage than the older bridge. The major damage to the bridge was due to approximately 0.4 m displacement of bridge superstructure in the transverse direction. The shear keys of the bridge failed. The shear keys did not have enough strength to resist the force from the pounding superstructure. Due to the slenderness of the shear key, it is speculated that the shear key on the east side of the bridge was damaged from the inertial forces of the superstructure as shown in Figure 4.50. The superstructure was very close to unseating as shown in Figure 4.51. The other bridge, however, did not show clear evidence of translation. The shear keys of the bridge appeared to have higher strength and stiffness than those of the bridge carrying the northbound traffic.

Figure 4.48 Perquilauquén Bridge

Figure 4.49 Displaced bridge superstructure and damage on shear keys

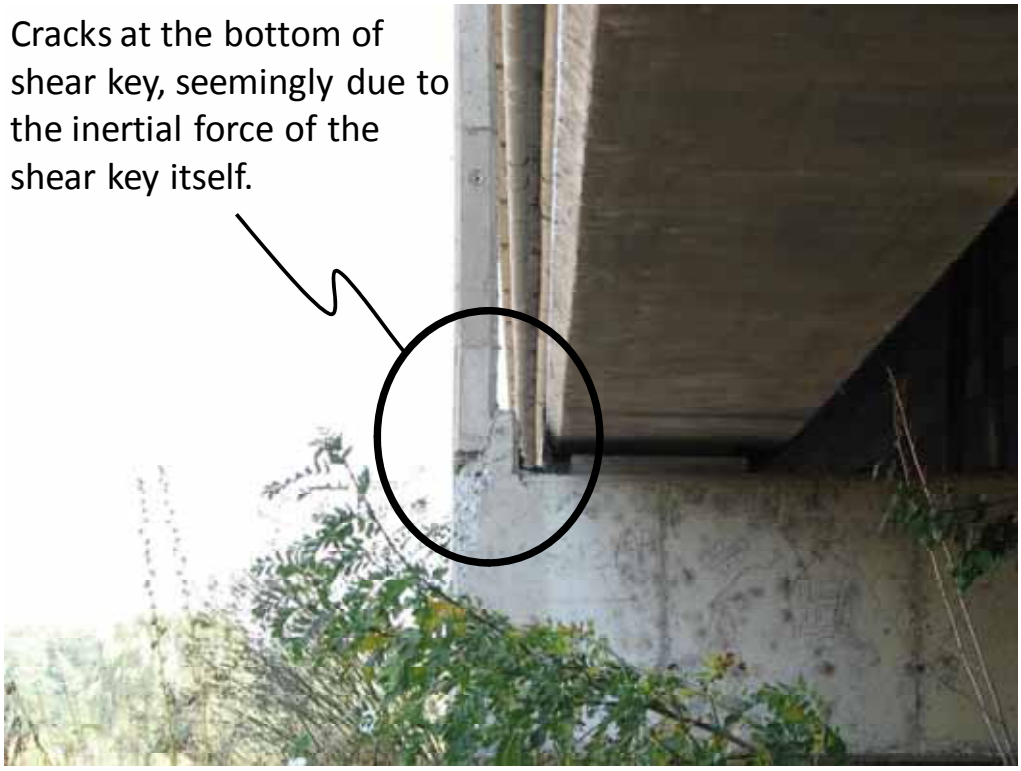

Figure 4.50 Damage at the bottom of a slender shear key

Figure 4.51 Bridge girder close to unseating

4.3.1.c. Paso Cladio Arrau

This bridge is located at 65 km (36°39'32.16" S, 72°19'32.7" W) from Concepción. The roadway was constructed and had been maintained by Autopista Del Itata. Based on discussions with representatives from the company, the roadway did not suffer significant damage from the earthquake. The bridge, Paso Cladio Arrau, consists of four spans as shown in Figure 4.52 and each span consists of ten pre-stressed concrete girders, which are integrated with diaphragms at the both ends and in the middle of each span. Each bent consists of ten reinforced concrete piers. The bridge suffered minor damage due to movement of the superstructure in the transverse direction. As a result of the movement of the superstructure, shear keys at the abutment were cracked (Figure 4.53) and seismic restrainers connecting the superstructure to the abutment yielded (Figure 4.54). The seismic restrainers were protected from corrosion with steel pipes. The end of the steel pipes yielded in both direction indicating that the superstructure developed large translation in both directions and moved back to original configuration, possibly due to the elasticity of the elastomeric bearings.

While the damage to the bridge structure is minimal, the bridge maintenance company was concerned that moving the superstructure to its original position and pre-stressing the seismic restrainers would require significant time and effort.

Figure 4.52 Paso Cladio Arrau

Figure 4.53 Damaged shear key at abutment

Figure 4.54 Yielded seismic restrainer and steel tube protecting the restrainer from the weather

4.3.1.d. Route 5 overpass near Chillán

The bridge shown in Figure 4.55 was a two-span bridge, which consisted of pre-stressed concrete girders. The bridge was very typical highway overpass commonly found along Route 5. The superstructure of the bridge was highly skewed.

The major damage to the bridge was due to a displacement of more than 0.3 m of the superstructure in transverse direction as shown in Figure 4.56. Large gaps were formed between the superstructure and both abutments as shown in Figure 4.57. The total gap at both ends was about 0.65 m, which is much larger than gaps normally planned for thermal expansion. In addition, the east embankment showed cracks on the embankment soil, possibly from the passive pressure of the abutment toward the embankment Figure 4.57 (a). Based on these observations, it is speculated that the inertial force from the superstructure applied large passive pressure on both abutment developing permanent deformation of the embankment.

Figure 4.55 Route 5 overpass near Chillán

Figure 4.56 Displacement of the superstructure

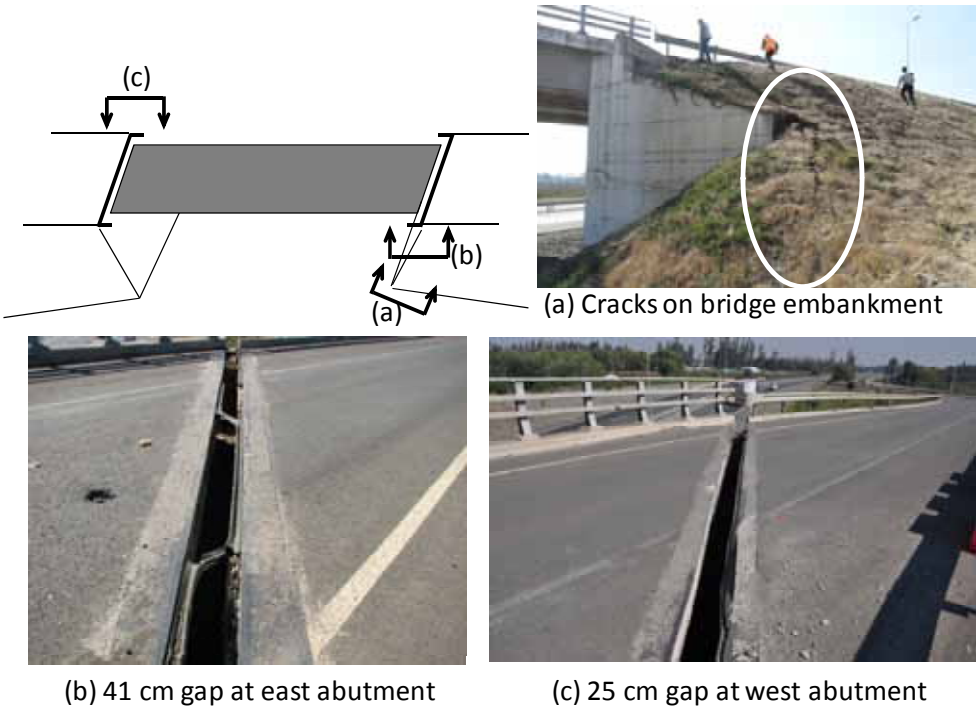

Figure 4.57 Gap between superstructure and abutments

4.3.2. Case Study 1: Paso Cladio Arrau

4.3.2.a. Configuration of the reference bridge

The reference bridge for this case study is a 4-span 77.5-m long bridge (Paso Cladio Arrau) which was introduced in Section 4.3.1.c. The bridge has three bents each of which consists of 10 piers as shown in Figure 4.58. As observed in most other bridges in Chile, the bridge was installed with seismic restrainers, which connect bridge deck to bent caps. Girders are supported on elastomeric bearings made of neoprene. The bridge has a skew angle of approximately 50 degrees.

The bridge suffered minor damage from the earthquake. The superstructure displaced in the transverse direction, seismic restrainers yielded and elongated, and the shear keys were damaged. The superstructure was not unseated. While the damage to the bridge was minor, it is chosen for this case study to investigate the effect of skew angle and seismic restrainers on the response of a bridge system.

The schematic drawing of the bridge and configuration of bents and piers is shown in Figure 4.58. For modeling the bridge, ZEUS NL (Elnashai et al., 2010) is used. Each structural member is assembled using cubic elements capable of representing the spread of inelasticity within the member cross section and along the member length by using fiber sections (Izzuddin and Elnashai, 1933). To model the bearings and gaps, lumped spring elements are used. The observed damage and numerical modeling of elements are introduced in the following sections.

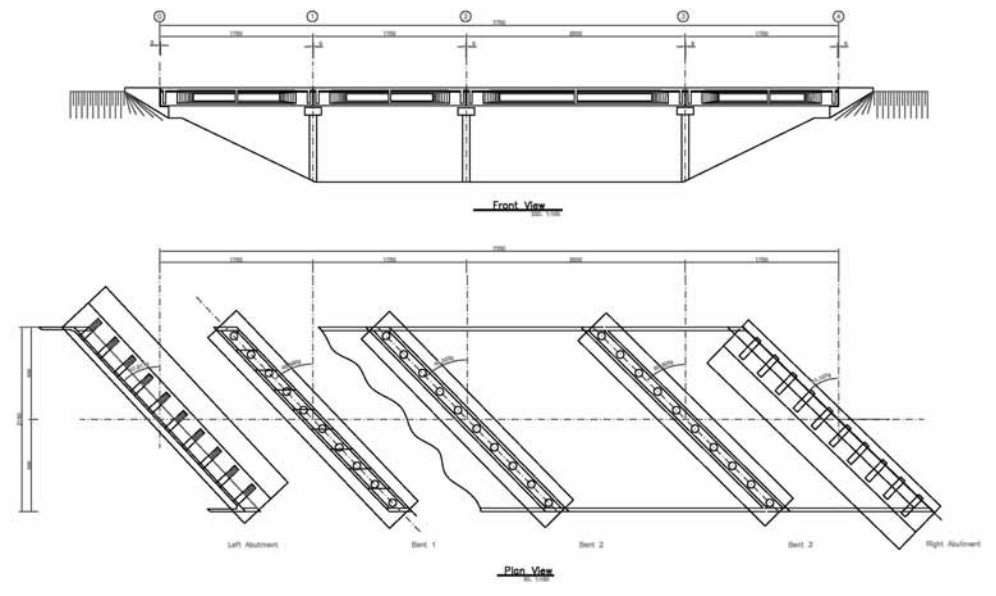

Figure 4.58 Configuration of bridge bents and abutments

4.3.2.b. Observed damage

Figure 4.59 shows a cracked shear key of the reference bridge due to the translation of the bridge superstructure. Even though the shear key was damaged, it may have prevented the unseating of the bridge superstructure. In addition to the shear key, it is speculated that the seismic restrainers may have played a role in reducing damage to the bridge structure. The seismic restrainer shown in Figure 4.60 yielded due to large displacement of the superstructure. Considering the large mass of the superstructure, the seismic restrainers themselves do not have enough strength to prevent the superstructure from lateral displacement. The post-tensioning force in the restrainers, however, could have increased the friction force in elastomeric bearings, which increases the energy dissipation capacity of the bearings.

Figure 4.59 Failure of the shear keys

Figure 4.60 Yielded seismic restrainers

4.3.2.c. Numerical modeling of the bridge elements

The 3D model of this bridge is created in ZEUS NL using the simplified model shown in Figure 4.61. This model consists of different elements, which represent an idealized characteristic of each component of the actual bridge. The stiffness of abutments and hysteretic behavior of bearings are modeled using the joint elements in ZEUS NL. Piers, seismic restrainers, and rigid elements are modeled using cubic beam-column elements. The deck is considered as a single rectangular beam with the similar section properties as the section of the girders and bridge deck. The configuration of numerical model is shown in Figure 4.62.

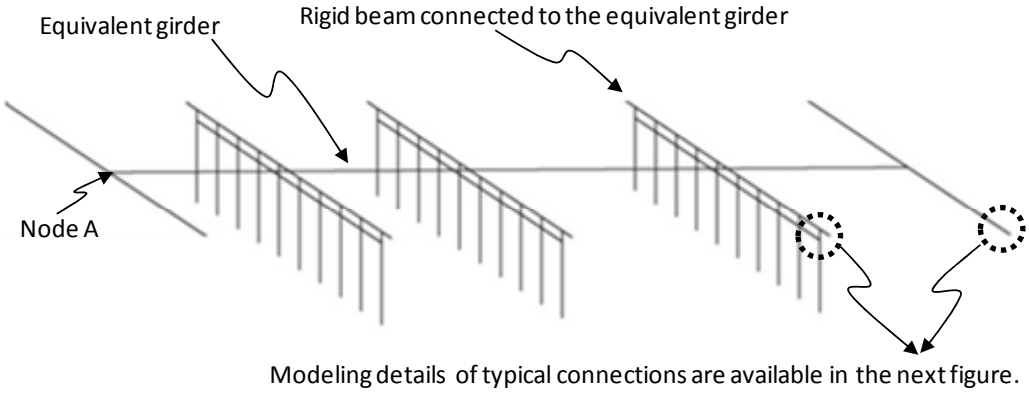

Figure 4.61 Simplified stick model of bridge used for modeling

In the reference bridge, there are gaps between the end span and the abutment, which allows for the thermal expansion of the bridge. In the drawing details, spacing between the abutment and deck, and deck and the shear keys are 6 cm. The abutment is modeled in ZEUS NL using joint elements. The stiffness of the abutment is calculated by the simplified procedure in CALTRANS Bridge Design Aids (1989), which only depends on the width of the bridge.

Elastomeric bearings were modeled with joint elements considering the weight of the deck and the initial tension force developed by the post-tensioned seismic restrainers. Seismic restrainers are modeled by cubic beam-column elements. Bilinear steel model and a hysteretic concrete model are used to idealize the pier reinforcements and concrete material. Strain hardening of the steel material is ignored in the analysis. According to the drawing details of the bridge, bearings are made of neoprene material whose hysteretic behavior is simplified as bilinear. Figure 4.62 illustrates how the connections between the superstructure, abutment, and the substructure are modeled using rigid and joint elements.

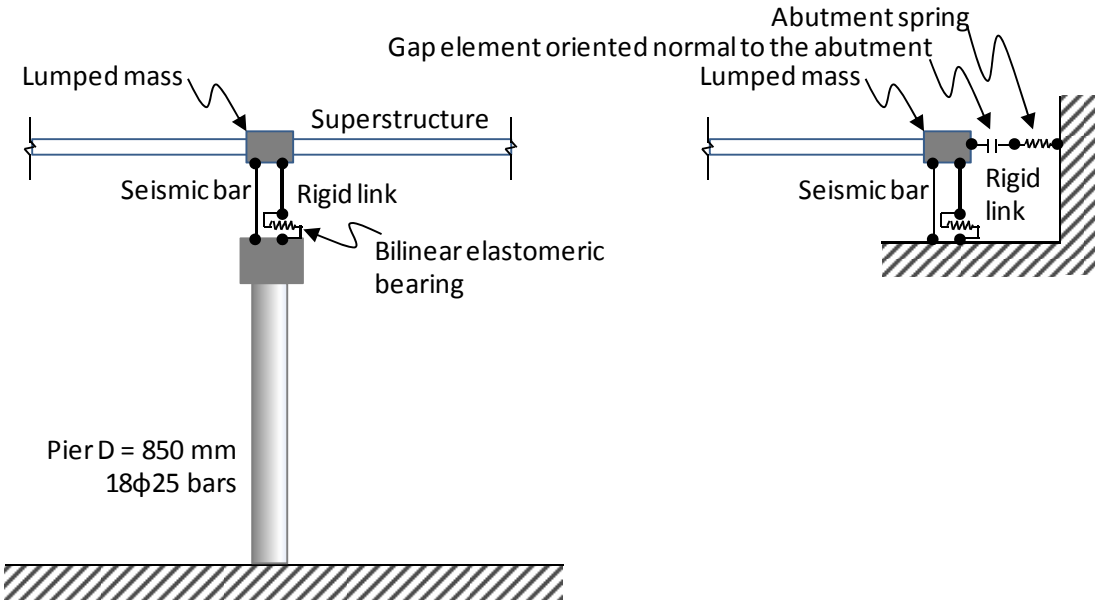

Figure 4.62 Configuration of lumped springs for bearings and gaps

4.3.2.d. Input ground motions and analysis cases

The spectrum compatible ground motions introduced in Section 2.4 are used for nonlinear response history analyses. A total of 18 horizontal components of ground motions records are applied in transverse direction. Maximum deformation of the superstructure from each analysis is monitored. To understand the relative effect of skewness and seismic restrainers on the response of the bridge, the following analysis cases are considered.

Table 4.6 Analysis cases for bridge analysis

	Skew angle: as built condition	Skew angle: 0 deg
With seismic bar	Case 1-#	Case 2-#
Without seismic bar	Case 3-#	Case 4-#

Note: '#' indicates ground motion number

4.3.2.e. Sample analysis results

To verify the response of structural components of the bridge, the hysteretic responses of the representative components are presented hereafter. Figure 4.63 compares the force-displacement relationship of a connection between superstructure and substructure assemblage for the cases without skew angle (Cases 2 and 4). It is noticed that when the seismic restrainers are included in the model (Case 2), the yielding force of elastomeric bearing is higher than the case without seismic restrainers (Case 4) as the post-tensioning of the seismic restrainer increases the normal force on the elastomeric bearings. The overall lateral displacement is smaller than the case without seismic restrainers due to higher energy dissipation capacity.

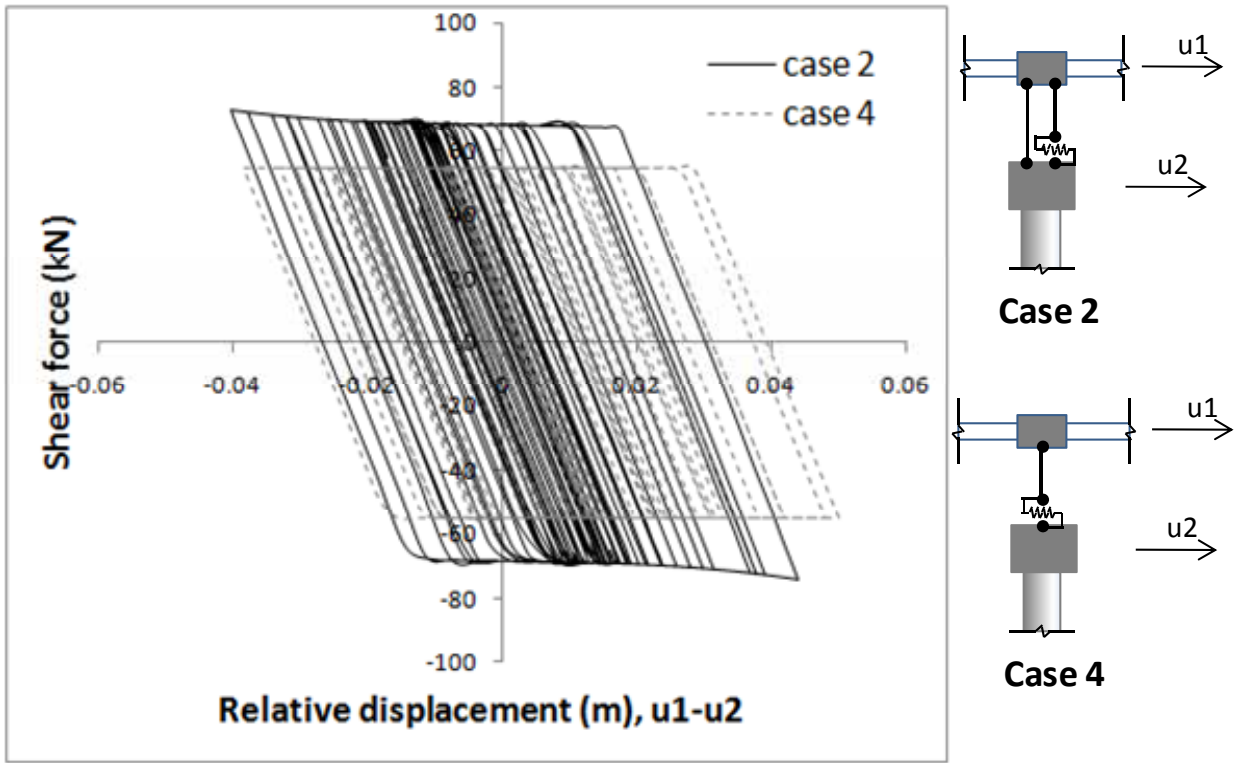

Figure 4.63 Effect of seismic restrainer on hysteretic response of bearings

Figure 4.64 shows the trajectory of the movement of node A in Figure 4.61. The bridge has a gap of 6 cm normal to the abutment. As the superstructure can move ±6 cm, it has a total 12 cm displacement range. The figure shows that the implemented gap model and its orientation properly limit the movement of the node.

Figure 4.65 illustrates the maximum displacement of the superstructure for Cases 1 and 2. As the shear keys of the bridge are not modeled, the superstructure can move in the transverse direction without restriction. The movement of the superstructure of Case 1 in transverse direction is limited by the closing of gaps between superstructure and

abutments. Due to the change in center of stiffness when the gap closes, the superstructure rotates, thus increasing torsional demand on the bridge bent.

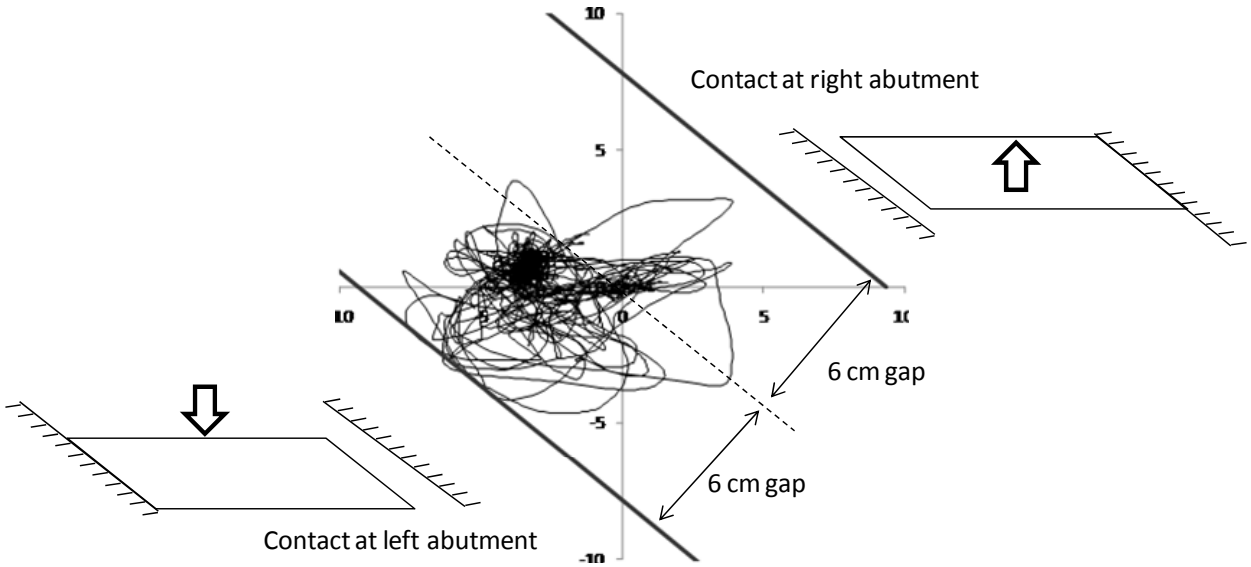

Figure 4.64 Trajectory of end of bridge span for Case 3-01

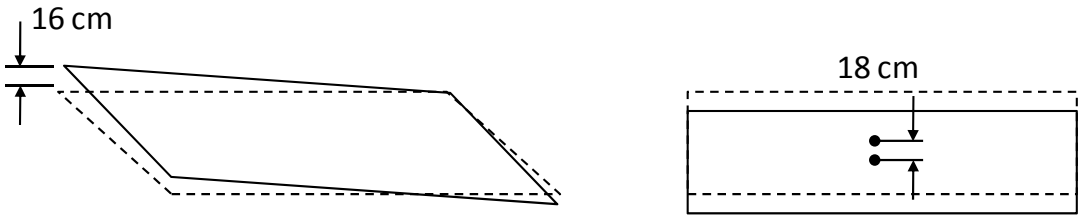

Figure 4.65 Trajectory of end of bridge span for Case 1-18 and Case 2-18

4.3.2.f. Comparison of results from four analysis cases

The results from the four analysis cases are compared in terms of maximum translational displacement of node A in Figure 4.61. The maximum displacements are compared in three plots to study the effect of skew angle and seismic restrainers. Figure 4.66 (Top) compares Cases 1 and 3. The difference between the two cases is seismic restrainers, which connect the superstructure and the substructure. Bridges in both cases have skewed superstructure. As observed from the figure, the Case 1 (with seismic restrainers) has relatively smaller seismic demand than the Case 3 (without seismic restrainers). The difference becomes larger as the shaking intensity increases. As the bearings in Case 1 have higher frictional force due to post-tensioning of seismic restrainers, it can dissipate more energy than Case 3. The resistance of seismic restrainer due to bending and/or pulling action is not significant. A similar trend is observed in Figure 4.66 (Middle) in which Case 2 and 4 are compared.

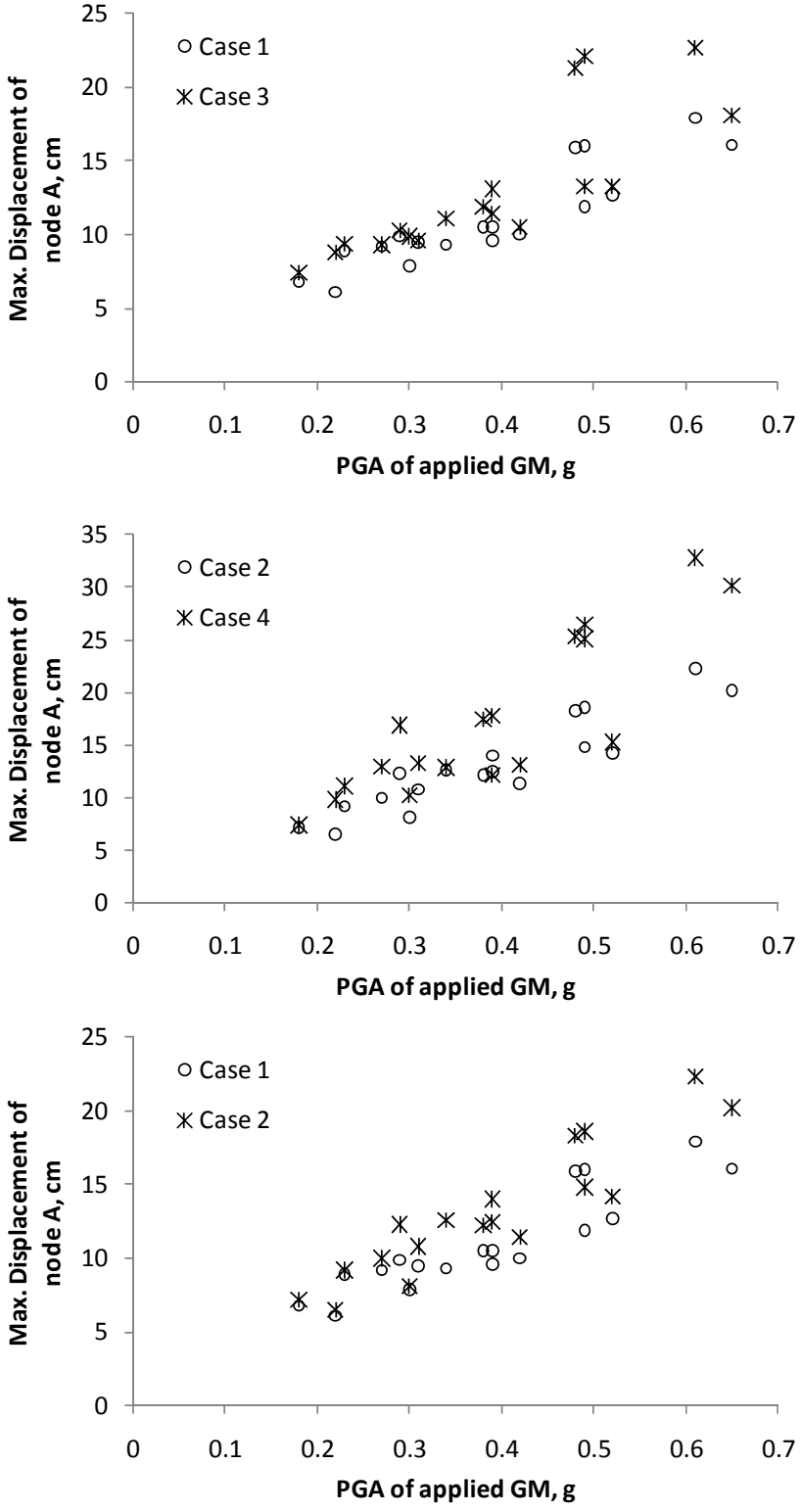

Figure 4.66 Maximum displacement of node A, *Top:* comparison of Cases 1 and 3, *Middle: c*omparison of Cases 2 and 4; and *Bottom: c*omparison of Case 1 and 2

Figure 4.66 (Bottom) compares Cases 1 and 2 to evaluate the effect of skew angle on superstructure response. The figure shows that at low intensity level (the first three ground motions), the two bridges' responses are very close. As the ground motion intensity increases, the Case 2 (without skew angle) tends to have larger displacement demand on node A. Before the analysis, it was expected that increase in rotational demand due to skew angle would increase the displacement demand. Based on the analysis results, however, it is found that at least for this reference bridge, the skew angle does not necessarily increase the displacement demand on the superstructure. It is probably due to the increase in transverse stiffness due to closing of the gap, which might have larger influence than the development of rotational demand. To generalize this conclusion, though, further study on the effect of skew angle (considering wide range of skew angles, span length/width ratios, and number of spans) is necessary.

4.3.3. Case Study 2: Las Mercedes Bridge

4.3.3.a. Configuration of the reference bridge

The bridge has a two-span continuous deck with a span length of 28.5 m. The superstructure of the bridge is a reinforced concrete slab-girder deck and each span has three pre-stressed concrete girders and a cast-in-place concrete slab. The bridge is supported by a two-column bent at the center and retaining walls at both ends as shown in Figure 4.67. The longitudinal direction of the bridge is skewed by an angle of 11 degrees from the perpendicular direction to Route 5, which it passes over. The axes of the column bent and retaining walls are parallel to the highway under the bridge. Superstructure is supported on elastomeric bearings and restrained to the substructure with seismic restrainers having a diameter of 22 mm. Overview of the reference bridge is given in Figure 4.68.

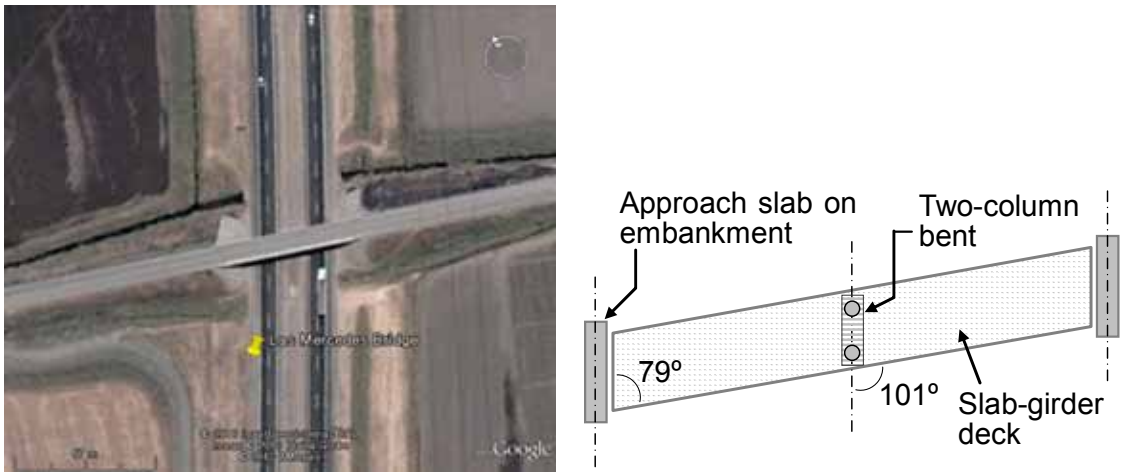

Figure 4.67 Configuration of Las Mercedes bridge, L*eft:* Satellite photo of the bridge and Route 5, *Right:* Skew angle

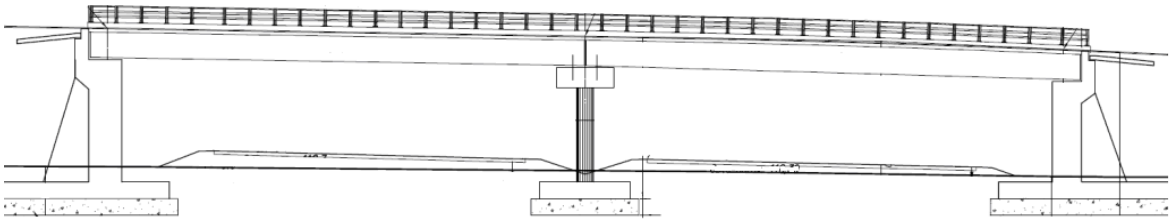

Figure 4.68 Overview of the bridge

4.3.3.b. Numerical model

A three-dimensional numerical model is generated to investigate the seismic response of the bridge. The analytical model is idealized to have a symmetric elevation along its longitudinal direction as shown in Figure 4.69 (Middle). The finite element analysis program ZEUS NL (Elnashai et al., 2010) is utilized to perform the necessary analyses for the assessment of the bridge such as nonlinear static pushover analyses, eigenvalue analyses, and nonlinear dynamic response history analyses. The superstructure, which consists of pre-stressed girders and cast-in-place reinforced concrete slabs, is assumed to be a rigid diaphragm in the analytical model. Based on the design drawings of a typical bridge on Route5 and Schmidt hammer tests at the field, compressive strength of concrete is assumed to be 50 MPa for girders and 35 MPa for other parts of the bridge including columns. Yield stress of reinforcement is assumed as 400 MPa. Overview of the numerical model is provided in Figure 4.69.

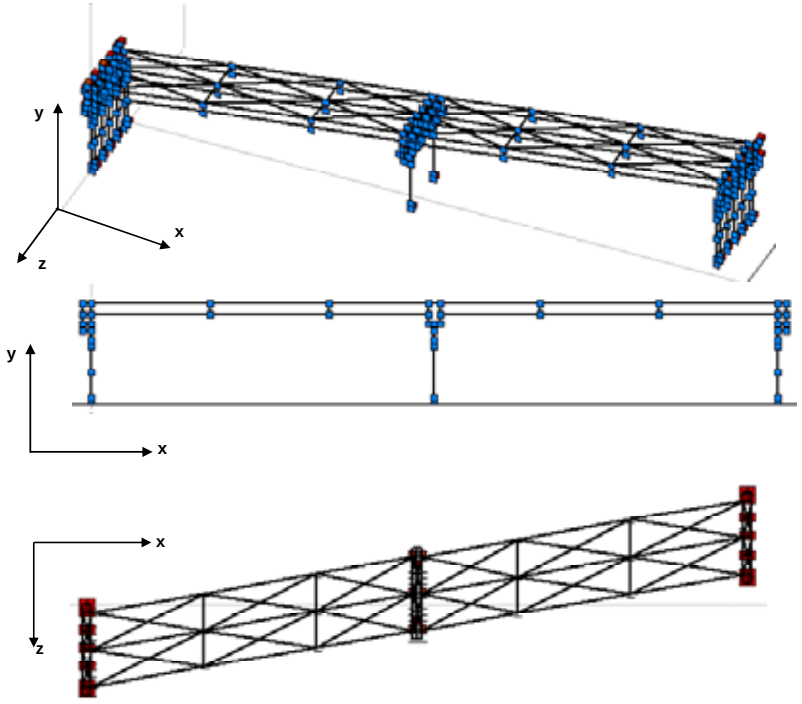

Figure 4.69 Numerical model of Las Mercedes Bridge, *Top:* overview, *Middle:* elevation, and *Bottom:* plan

A total of twelve bearings are used at both ends of each girder and their locations are given in Figure 4.70. The elastomeric bearing is assumed to be made of plain neoprene pad with hardness of 50 durometer. Details on the material properties of bearings and test methods are given elsewhere (AASHTO, 2006). The friction coefficient between the surfaces of the bearing and the girder is assumed to be 0.21 which is the friction coefficient between neoprene rubber and concrete. The thickness of elastomeric bearing pads on the column bent is 37 mm, while the thickness of those on retaining walls is 60 mm. Shear modulus (G) of the neoprene bearing (50 durometer) is 0.69 MPa and shear area (A) is 140000 mm^2 (400mm x 350mm). The lateral stiffness of an elastomeric bearing can be calculated as K = GA/h, where h is bearing height. Lateral force (F_b=63000N) at friction slip is obtained by multiplying the vertical force at each bearing (F_v=300000N) by friction coefficient (0.21). For the tall (60mm) bearing, the maximum displacement (Δ_b) at which the friction slip begin can be calculated as follows: $\Delta_b = F_b/K = 63000/(0.69\times 140000/60) \approx 40mm$. Similarly, the maximum friction displacement of the short (37mm) bearing is assumed to be 25 mm. The force-displacement relationship of the bearing used in the analytical model is shown in Figure 4.71.

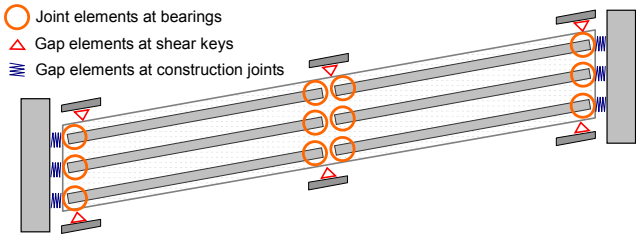

Figure 4.70 Locations of joint and gap elements in the numerical model (plan view)

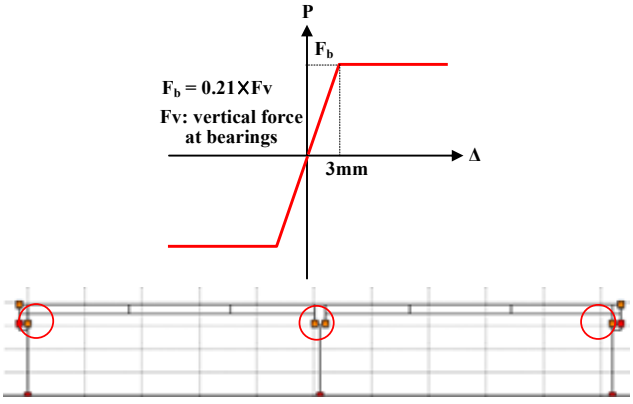

Figure 4.71 Locations and force-displacement relationship of a joint element for the elastomeric bearing

There are a total of 16 seismic restrainers located between bearing supports as shown in Figure 4.72. The diameter of restrainers is 22 mm and their yield stress is assumed to be 400 MPa. The details of the seismic restrainers in the design drawing

(Figure 4.73) shows that the top anchor of a seismic restrainer is not sufficiently strong to carry pre-stressing forces. The role of seismic restrainers is to stabilize the superstructure by preventing it from bouncing under earthquake excitations rather than giving extra friction resistance by pre-stressing loads. Therefore, pre-stressing force at seismic restrainers is not assumed in the analytical modeling.

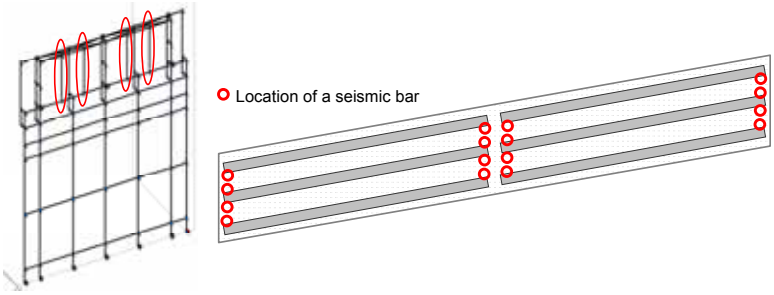

Figure 4.72 Analytical model and locations of seismic restrainers, Left: numerical modeling of substructure with seismic restrainers at the left end of the deck, Right: locations of the seismic restrainers (plan view)

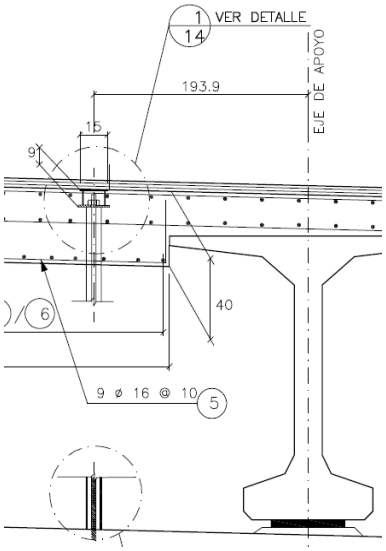

Figure 4.73 Details of the top anchorage of a seismic restrainer

Movements of the superstructure in the longitudinal direction are restrained by the abutments at both ends of the deck and governed by properties of elastomeric bearings. The construction joint at the latter abutment has unidirectional resistance. Gap elements are used to represent the delayed contact at the construction joints between the bridge deck and approach slabs on the abutments. Based on the design drawings, the clearance of the construction joint is assumed to be 60 mm. A unidirectional spring element is used to represent the conditional force transfer at the construction joint; only compressive forces are transferred when the gap is closed. The locations of the gap elements and the force-displacement relationships are represented in Figure 4.74.

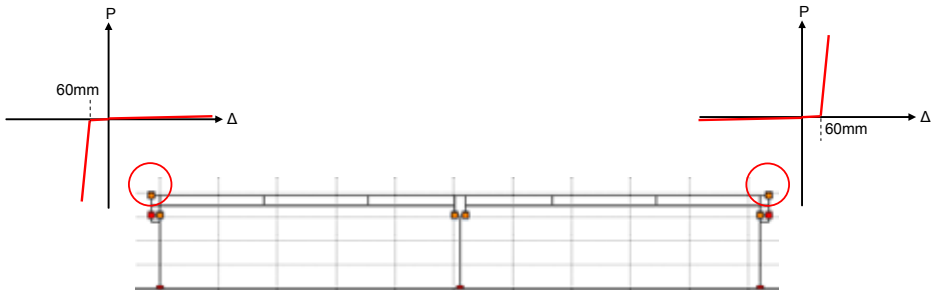

Figure 4.74 Numerical model of bent cap, elastomeric bearing, and seismic restrainer

4.3.3.c. Analysis cases and results

Under earthquake excitations, the simple bridge behaves like a rigid diaphragm on a relatively stiff substructure. Therefore, it is assumed that the seismic response of the superstructure is mainly affected by slip at the girder-bearing interface and the mode shape is determined by lateral stiffness and location of elastomeric bearings and spring properties representing construction joints. The fundamental period of the bridge is evaluated as 0.80 seconds and the latter mode is induced by the deformation of the elastomeric bearing before the friction slip. The first mode shape is determined by the movement of the superstructure in the transverse direction without torsional responses because the bridge is symmetric along the x direction (see Figure 4.69). Torsion is in the second mode as shown in Figure 4.75 (b and d) and the corresponding period is 0.77 seconds.

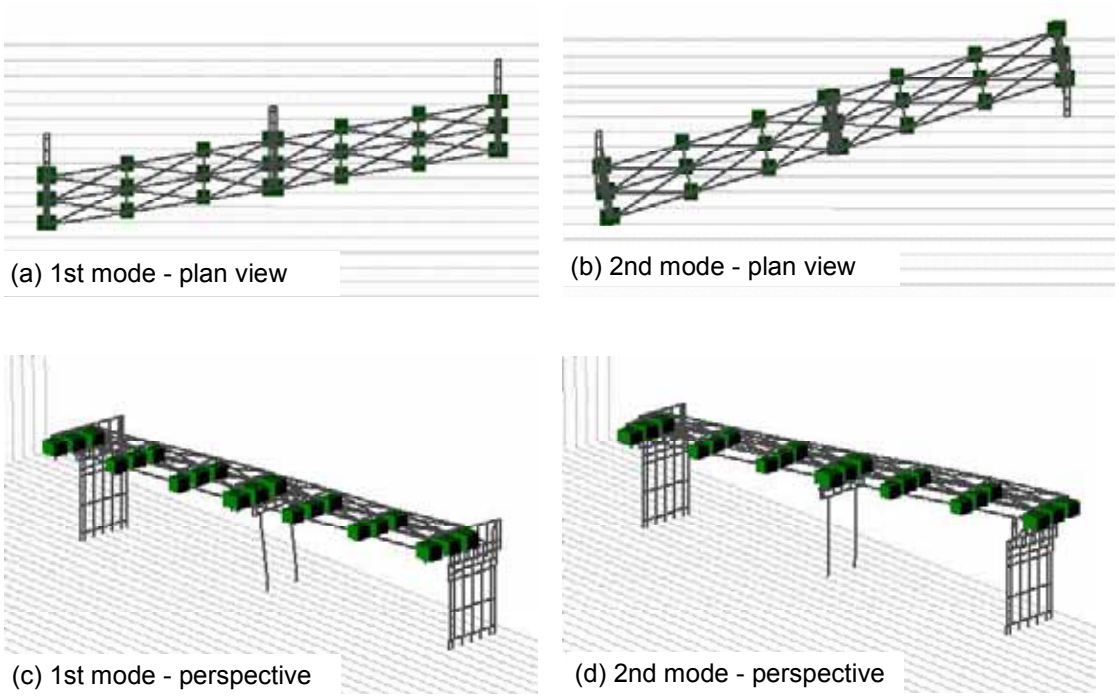

Figure 4.75 Mode shapes of the bridge

In the static pushover analysis, lateral forces are applied in the direction of the highway, which is parallel to the axes of the column bent and retaining walls (z direction in Figure 4.69). The locations of shear keys and direction of lateral forces are shown in Figure 4.69. . From the analysis results, it was observed that Shear key #1 reaches its ultimate shear capacity earlier than others, followed by severe damage on Shear key # 2. Uneven lateral force distribution on shear keys and unbalanced force redistribution can magnify torsion in highly inelastic response range of the bridge. The capacity curve of the reference bridge is shown in Figure 4.77. The status of the bridge on the capacity curve is explained as follows.

1. The superstructure is displaced due to deformation of elastomeric bearings,
2. The lower part of a girder hits a shear key,
3. Shear key #1 has reached its ultimate shear strength,
4. Force redistribution among shear keys,
5. Shear key #3 has reached its ultimate shear strength.

Figure 4.78 (a) shows an outer girder on a deformed elastomeric bearing. The maximum allowable deformation of the bearing pad is 40 mm, which is larger than the gap of 30 mm between the girder and the shear key. Therefore, the superstructure can safely move on the bearing pad without friction slip as long as the shear key is sufficiently strong. The shear key plays an important role in preventing the superstructure from experiencing excessive displacement. The stiffness and strength increase between response points ② and ③ in Figure 4.77 is the contribution of shear keys. In the analytical study, it is observed that the lateral force on shear key # 1 is transferred to shear key #2 and #3 after shear key #1 has reached its ultimate capacity. However, the latter force redistribution is not possible in the real structure. After the peak response point ③ in Figure 4.77, the loss of lateral strength of shear key #1 is abrupt and complete as shown in Figure 4.78 (b). Therefore, there is no possibility for force redistribution among shear keys. Additionally, as soon as the shear key has failed the girder and elastomeric bearing will slip off from the bearing support as shown in Figure 4.78 (c). Once the latter slip-off has occurred, the girder cannot move back to the opposite direction and thus its displacement will be accumulated unidirectionally. At the same time, the other end of the superstructure moves to the opposite direction, which causes cumulative torsion of the superstructure.

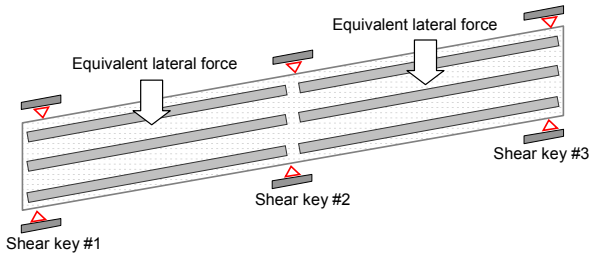

Figure 4.76 Direction of equivalent lateral forces and location of shear keys

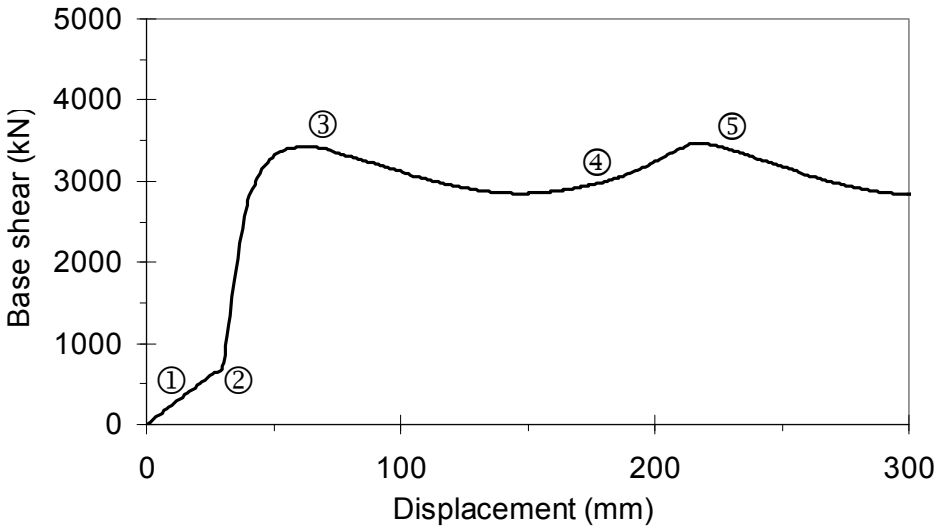

Figure 4.77 Results of a static pushover analysis

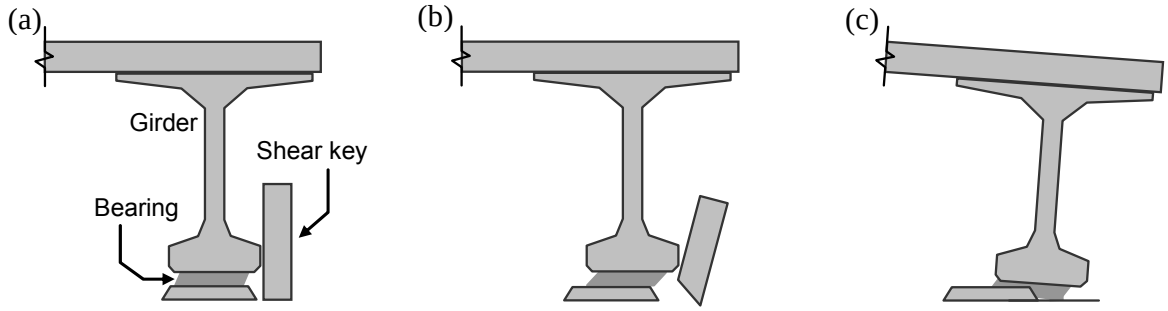

Figure 4.78 Girder slip on elastomeric bearing and bearing support

A sample plot of dynamic response history analysis, under the spectrum compatible record that is matched to +0.5σ spectrum using the original ground motion from the station STL (EW component) as the seed record (presented in Section 2.4), is shown in Figure 4.79. The earthquake loading is applied in the transverse direction of the bridge deck. Shear keys are omitted in the analytical model for dynamic response history analyses in order to investigate causes of torsion other than the uneven resistance of shear keys. While the maximum displacement is 90 mm, which is larger than the allowable deformation of the elastomeric bearing, the torsion is only about 0.0012 degree. This negligible amount of torsion implies that the large amount of torsion observed at the field (Figure 4.45) is not caused by dynamic characteristics of the structure.

It has been reported that torsion of skewed bridges is generally caused by pounding of a superstructure with embankments. However, the skew angle of this reference bridge is too small for the torsion observed at the field to be caused by the pounding response. Eccentricity between the centers of mass of the deck and the resultant

pounding forces at the embankment is too small to make sufficient couple forces. While substructures such as piers and embankment walls had negligible effects on the movements of the deck, properties of bearings and shear keys significantly affect responses of the superstructure. Premature failure of a shear key causes uneven and excessive displacement at the end of the superstructure. Then the girder ends slip off from the bearing support and this would initiate the torsion accumulated unidirectionally (Figure 4.78). This explains the large amount of torsion observed at the field (Figure 4.45 and Figure 4.47).

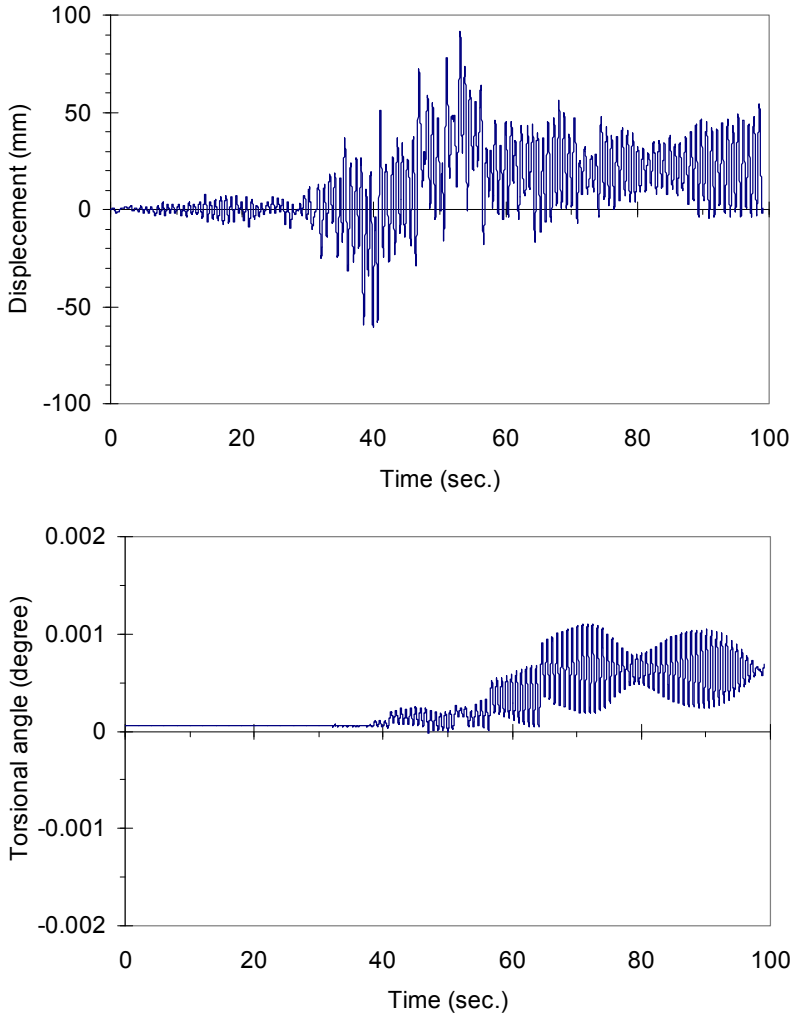

Figure 4.79 Selected dynamic response history results (response history by record: STL, EW component, mean $+0.5\sigma$)

4.3.4. Seismic Fragility of the Las Mercedes Bridge in Case Study 2

4.3.4.a. Fragility framework

Bridge seismic fragility curves are statistical functions that give probabilities of reaching or exceeding a certain damage level or state as a function of a ground motion intensity measure. The function can be written as $P[DS_i|PGA = y]$, where PGA is an example of a ground motion intensity measure, and DS_i is the damage state in question. Applications of fragility curves include aiding in emergency response optimization, design support for performance-based engineering, planning support for seismic events, and policy support. The current damage states used in most fragility curves refer to the state or condition of a bridge following an earthquake event. States such as “Moderate” or “Complete” damage are an indication of the capacity that may be left in the bridge or bridge component.

A fragility framework is described in this section for the deterministic bridge model subjected to several ground motions taken from or simulated for the region in question. The responses of several bridge components were recorded: the elastomeric bearings in the longitudinal and transverse directions, the abutment movement, and the column response.

The limit states chosen for this analysis are based on the HAZUS limit states developed by FEMA (2003). Table 4.7 shows qualitative descriptions for the limit states that inspection engineers can identify. For fragility analysis, these qualitative states need to be expressed quantitatively, in order to fit the response of the system to appropriate limit states. There are two ways of developing values, prescriptive and descriptive (Nielson, 2005). In this example, a prescriptive approach will be used, in which the values that are shown to be relevant to the physics of the structure and that can be confirmed in the field, are used.

Table 4.7 Qualitative description of bridge damage limit states

Damage States	**Description**
(N) – No Damage	No damage to a Bridge
(S) – Slight Damage	Minor cracking/spalling to abutment, cracks at hinges, minor spalling at column, or minor cracking to the deck
(M) – Moderate Damage	Moderate cracking and spalling at column, moderate settlement of approach, cracked shear keys or bent bolts at connection
(E) – Extensive Damage	Degraded column without collapse, some lost bearing support in connection, major settlement of approach
(C) - Complete Damage	Collapsed column, all bearing support lost in a connection, imminent deck collapse

4.3.4.b. Method of fragility curve development

Based on the origins of the damage data used in the generation of the curve, there are four main types of fragility curves in use. The methods include empirical, judgmental, analytical, and hybrid fragility curves, which combine data from different sources to create damage states. For this case study, a typical overpass bridge is modeled deterministically and analyzed to develop fragility curves using the analytical method. The ground motions used for this study are actual recordings from the earthquake (taken from different locations, 10 stations, 20 horizontal components), spectrum matched records developed using attenuation relationships (18 components, see details in Section 2.4), and scaled records to have data points at high PGA values (five records). In total 43 ground motion records are used to develop the fragility curves. The distribution of the PGA of the records used in fragility analysis is provided in Figure 4.80.

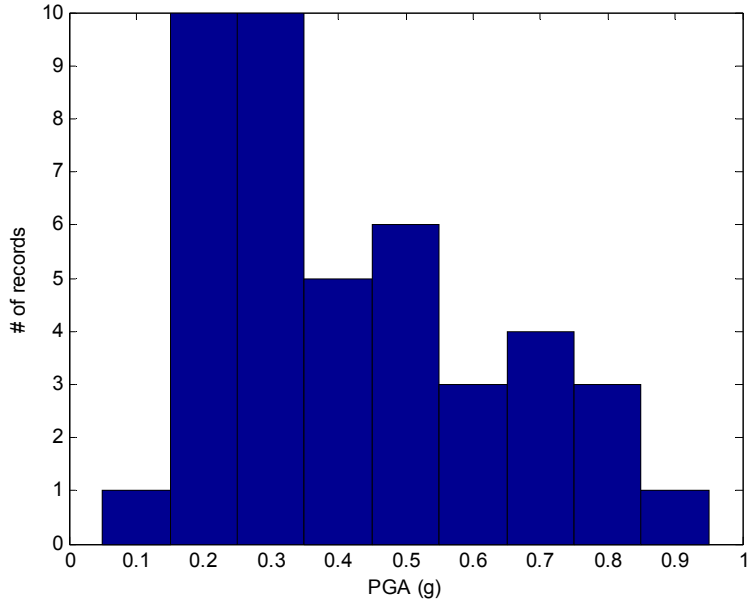

Figure 4.80 Distribution of the PGA of all records used in fragility analysis

4.3.4.c. Component demand

Many fragility curves focus on the response of one component, such as the drift of a column, to indicate the state of a bridge after an earthquake event. However, the responses of other major bridge components are emerging as significant elements in determining the fragility of the entire bridge (Nielson and DesRoches, 2007; Padgett and DesRoches, 2007). For this study, the responses of the column, abutment, and bearings in multiple directions are recorded. The responses that are monitored are the column curvature ductility and maximum drift ratio, fixed and expansion bearings longitudinal and transverse movements, and the abutment displacement in the

longitudinal and transverse direction. From these, responses, component fragilities are created. The aim is to find the fragility of the entire bridge system, so a joint probabilistic seismic demand model (PSDM) is developed from individual components' PSDMs.

To find the yield displacement and yield curvature of the columns, an approximate relationship given in Priestley et al. (1996) is used. To calculate the curvature of the columns, the maximum moment at the column base is used to determine the maximum curvature if the member is elastic, the plastic curvature is added to the elastic curvature if yielding has occurred. The plastic curvature is based on the failure mechanism of the column (Buckle et. al, 2006). It is assumed that low cycle fatigue failure of the longitudinal bars is likely (Buckle et. al, 2006). The drift ratio is the ratio of the maximum displacement at the top of the column to the column height. The curvature ductility is the ratio between the maximum and the yield curvature.

4.3.4.d. Limit states (capacity)

The capacities of the bridge components and subsequent limit states were adopted from the work of Nielson and DesRoches (2007), and Ramanathan, et al (2010). The capacities presented in their work were determined through experimental studies and results presented in previous publications. The capacities are converted into limit states by interpreting the data to represent some physical meaning. For example, for slight damage to a column, one might consider some small cracks. In an experiment, small cracks could be observed around some particular curvature ductility. Thus, this value would represent the slight damage state for a column. In those previous studies, multiple tests for each component were performed to determine a median value for each limit state and the dispersion parameter of the data. These values are used in the probabilistic seismic demand models of the components. Below is a table of the monitored bridge components and the median and dispersion values for each of the four limit states considered, as given in the work of Nielson and DesRoches (2007), and Ramanathan et al. (2010). The columns for this bridge were assumed to be seismically designed because of the close spacing of the transverse reinforcement. The column drift ratio limit states were adopted from the work of Mackie et al (2007).

Table 4.8 Bridge damage limit states

Component	Slight		Moderate		Extensive		Complete	
	Med	Disp	Med	Disp	Med	Disp	Med	Disp
Column Ductility (Seismic)	4.90	0.70	9.14	0.53	12.46	0.59	13.1	0.60
Column Residual Drift Ratio	0.50	0.30	1.25	0.40	2.00	0.40	6.72	0.35
Elasto Brg – Fixed – Longitud (mm)	28.9	0.60	104	0.55	136.1	0.59	187	0.65
Elasto Brg – Fixed – Transv (mm)	28.8	0.79	90.9	0.68	142.2	0.73	195	0.66
Elasto Brg – Expan – Transv (mm)	28.9	0.60	104	0.55	136.1	0.59	187	0.65
Elasto Brg – Expan – Longitud (mm)	28.8	0.79	90.9	0.68	142.2	0.73	195	0.66
Abutment – Longitudinal (mm)	37	0.46	146	0.46	1000	0	1000	0
Abutment – Transverse (mm)	9.75	0.70	37.9	0.90	77.2	0.85	1000	0

4.3.4.e. Probabilistic seismic demand models

If the fragility of the bridge were based on the response of one component, then the resulting fragility function could be given in a closed form solution, like the one shown below (Nielson 2007).

$$P[D > C \mid IM] = \Phi\left[\frac{\ln\left(S_d / S_c\right)}{\sqrt{\beta_{d|IM}^2 + \beta_c^2}}\right] \tag{4.17}$$

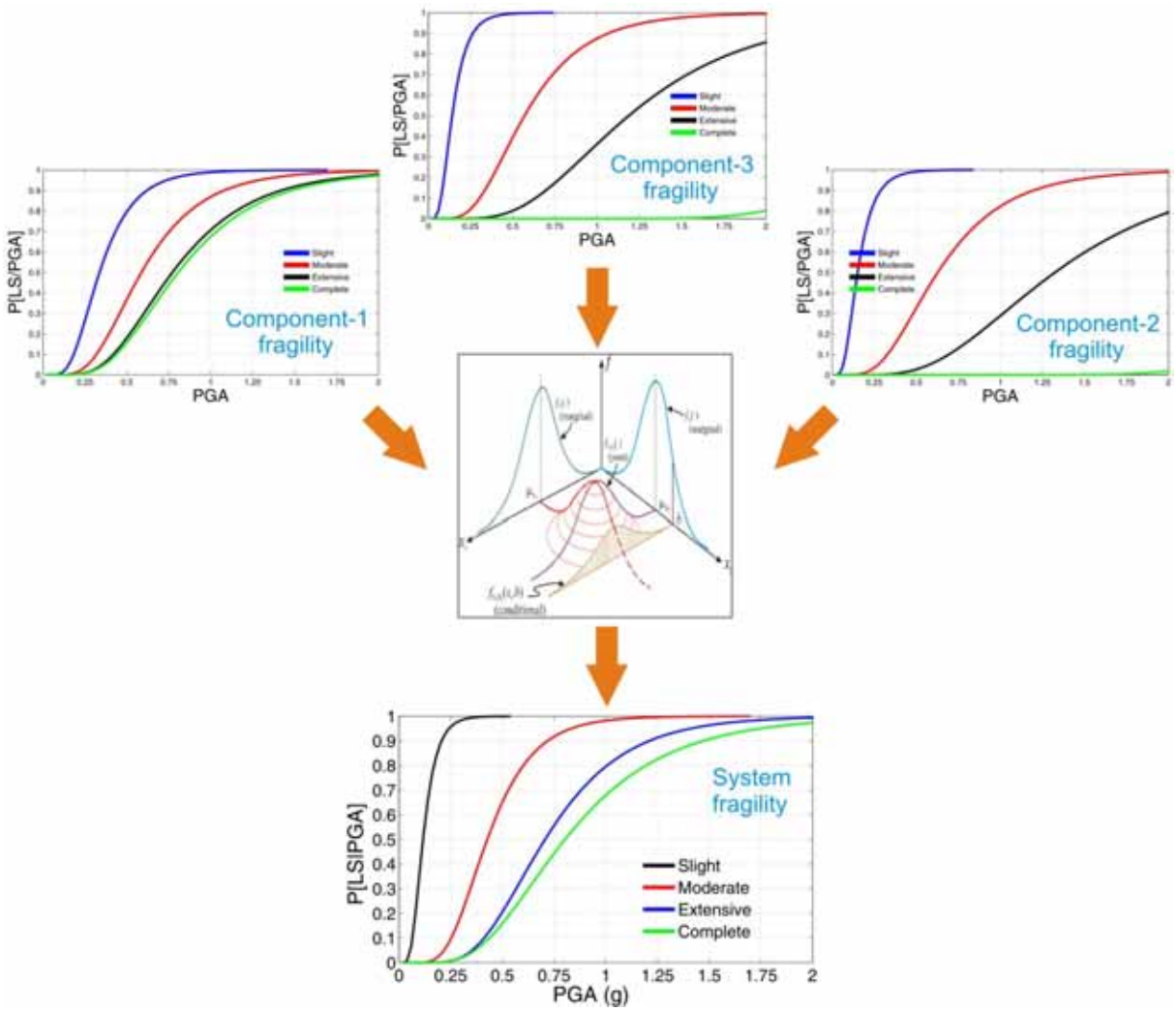

Figure 4.81 Illustration of combining component fragility to obtain system fragility

However, since the responses of several components are incorporated here, a joint probabilistic seismic demand model is needed. Following the procedure proposed by Nielson (2005), each bridge component and the responses are assembled into individual probabilistic seismic demand models using lognormal linear regression to find the model parameters.

$$S_d = aIM^b \tag{4.18}$$

$$\beta_{D|IM} = \sqrt{\frac{\sum_{i=1}^{N} (\ln(d_i) - \ln(aIM^b))^2}{N-2}} \tag{4.19}$$

From these models, the correlation between all of the components is calculated, and a joint PSDM (JPSDM) is found for the system. From this joint model, the system fragility is evaluated by performing a Monte Carlo simulation of the JPSDM and comparing the resulting demand values with the component capacities to determine the system failure at each damage level (Nielson and DesRoches, 2007). This procedure is illustrated in Figure 4.81, showing that the individual component fragilities are combined to give an overall system fragility curve through the use of the JPSDMs.

4.3.4.f. Uncertainties in modeling and resistance

The risk due to uncertainty must be mitigated and kept within acceptable levels, since it is impossible to eliminate all uncertainties. For a structural system analyzed under earthquake loads, uncertainty arises from the demand and capacity (Ji et al., 2007b). The uncertainties from the demand on a system derives from the ground excitation, which includes the soil conditions, load path of the motions, and the random motions generated from the source of the quake. The uncertainty from the capacity of the system is due to the material and geometric uncertainties, where the properties of the designed structure and materials are considered random.

Researchers have found ways to account for these uncertainties and mitigate the effects in their results (Wen et al, 2003). For the uncertainty in ground motions, it has been found that it is best to include many records of ground motions to cover as many frequencies and seismic energy levels as possible (Ji et al., 2007b). To account for this uncertainty, the bridge structure is analyzed with a suite of 43 ground motions that characterizes the specified region, and also provides a range of intensities. Some of the ground motions are actual records taken in Chile during the Mw 8.8 earthquake. Other records are those developed and described in Section 2.4 of this report using carefully selected attenuation relationships. Finally, the rest of the records are scaled from the actual time histories to give a broader range of frequencies for the analysis. Only 5 out of 43 records are derived using scaling and the records are chosen such that the scaling factors are between 1 and 1.5 in order not to distort the characteristics of the ground motions. These ground motions are unidirectional and applied only in one horizontal direction during the analysis.

From the capacity of the system, uncertainty can stem from the material properties used and the geometry of the structure. However, the variability of the response of the system is much more susceptible to the ground motion variability than the material uncertainties (Kwon and Elnashai, 2006). Therefore, for this analysis, the

bridge geometry and material properties are modeled deterministically, and only the ground motions chosen contribute to the variability in the response.

4.3.4.g. Bridge analysis and fragility

The case study bridge used for this analysis is a typical highway bridge crossing over Route 5, as described in Section 4.3.3. These 2-span concrete girder bridges were commonly observed along the north-south route in Chile. Another feature that is typical of these bridges is the vertical seismic restrainers connecting the deck to the bent cap or abutment. Several of the bridges had similar damage modes, which was transverse displacement of the bearings at the abutments. A picture of the bridge under consideration is shown in Figure 4.82, which had the most severe damage that was observed during the MAE Center reconnaissance mission.

Figure 4.82 Case study overpass bridge crossing Route 5

Fragility analysis was performed on this case study using the results of the preceding steps. The products of this analysis are fragility curves that describe the probability of meeting or exceeding a certain damage level at a particular intensity measure. The graphs in Figure 4.83 show two fragility curves for the case study bridge based on the PGA, one curve using column curvature ductility as the engineering demand parameter for columns, and the other using the maximum column drift ratio. Both of these parameters have been used in past research for predicting bridge fragility. As shown, these two parameters give different estimates of the fragility of this bridge, especially in the higher damage states. For example, for a PGA level of 0.5 g, the fragility curve based on curvature ductility predicts around 50 percent chance of slight

damage, while the drift ratio based curve predicts approximately 20 percent probability of slight damage. This difference could be due to the fact that the limit states come from different sources. These curves show that the bridge has a low vulnerability to damage for the more severe limit states.

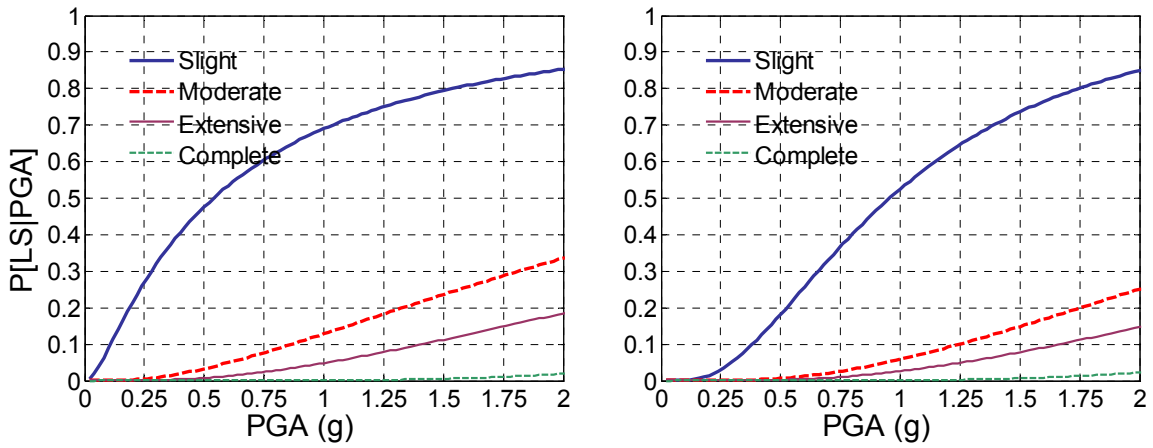

Figure 4.83 Seismic fragility curves in terms of different demand parameters (DP), *Left:* DP is curvature ductility; *Right:* DP is max drift ratio.

In addition to system fragility curves, the component fragility curves may be investigated to determine the most vulnerable component at each limit state. As shown in Figure 4.84, for the slight limit state from the drift-ratio based fragility curves, the response of the expansion bearings in the longitudinal direction contributes the most to the fragility of the system, followed by the response of the abutment in the transverse direction. For the moderate damage state, the response of the abutment in the transverse direction controls the fragility. As demonstrated in this case study, if the response of components of the bridge other than the columns were ignored, the fragility of the system would be miscalculated.

As a comparison, fragility curves of similar bridge types modeled for moderate seismic zones, such as the central and southeastern United States, are presented in Figure 4.85 to compare the relative vulnerability of the case study bridge to high seismic demand with a similar bridge subjected to moderate seismic demand. The fragility curves for the U.S. (Nielson, 2005) included separate curves for several bridge classes, including multi-span simply supported (MSSS) concrete girder bridges, like the bridge in this case study. One difference between the case study bridge and the bridge class in the quoted study is that U.S. bridges were not assumed to be seismically designed. The implication is that the limit state values for the column demand parameter are lower than the ones used in this study. Comparing the fragility curve below with that developed for the current case study based on curvature ductility, it is observed that the case study bridge is more robust and more likely to withstand greater ground motion shaking than the bridge modeled in a moderate seismic zone in the U.S.

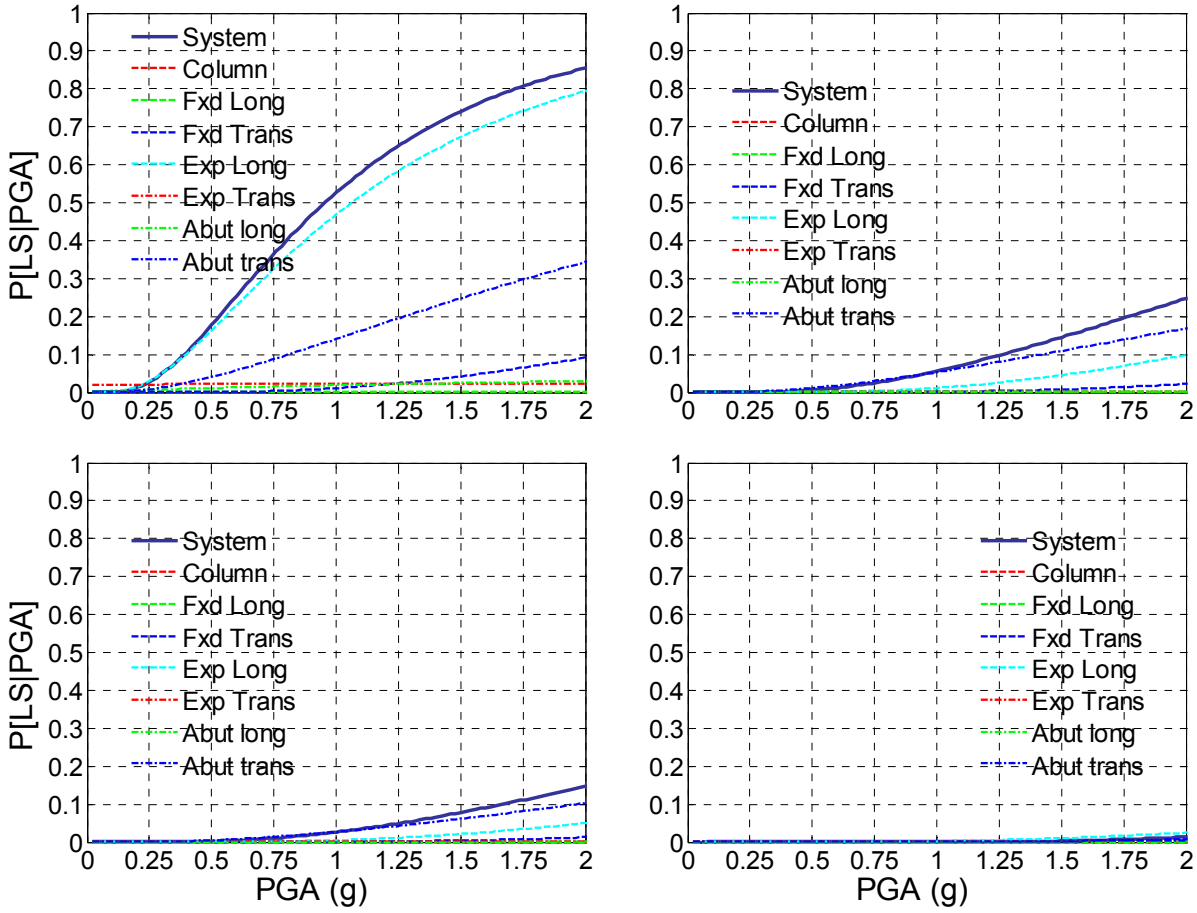

Figure 4.84 Seismic fragility curves of different structural components, *Top-Left:* Slight damage; *Top-Right:* Moderate damage; *Bottom-Left:* Extensive damage; *Bottom-Right:* Complete damage

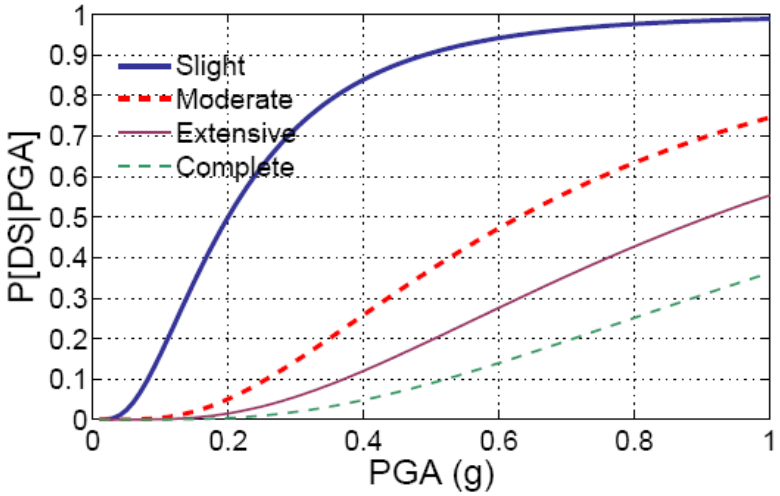

Figure 4.85 MSSS concrete girder bridge fragility curve for moderate seismic zones (Nielson, 2005)

4.4. EFFECTS ON HISTORICAL STRUCTURES

The 27 February earthquake damaged several historical structures in Chile. According to the preliminary report by the EERI team 444 churches were heavily damaged which accounts for 47 percent of all churches in the country (EERI, 2010). The AONBenfield event recap report indicates that over 90 percent of the historical center was destroyed in Curicó and dozens of homes in the historical center of Concepción collapsed (AONBENFIELD, 2010). Several historical structures were damaged in Talca (those that were visited by the team are shown in the next section) including the government building of Intendance (see Section 4.2.1). The damaged historical structures visited by the MAE Center team were limited to those in Talca as summarized in the next section.

4.4.1. Observed Damage

The MAE Center team visited the following historical structures in Talca; Iglesia Los Salesianos, which suffered severe damage, Figure 4.86; Cathedral of Talca, studied in more detail in Section 4.4.2, Figure 4.87; Edificio Intendencia Maule, Figure 4.88; and Liceo de Niñas Marta Donoso, Figure 4.89. All these structures were unreinforced masonry construction except for the Cathedral of Talca, which is an RC structure with masonry infills. The severe damage observed emphasized the vulnerability of historical structures in Chile to earthquakes. The list of visited historical structures is provided in Table 4.1. The location of each structure and the related figure(s) in the report are also provided in the table. The column “icon” indicates the label of the buildings as shown in the figures in 0.

Table 4.9 List of historical structures visited by the MAE Center team

Icon	Name/Description	Latitude	Longitude	Figure in report
H1	Edificio Intendencia Maule in Talca	35°25'34.79"S	71°39'55.43"W	Figure 4.26 Figure 4.88
H2	Liceo de Niñas Marta Donoso	35°25'22.76"S	71°39'28.55"W	Figure 4.27 Figure 4.89
H3	Iglesia Los Salesianos	35°25'43.68"S	71°39'36.64"W	Figure 4.86
H4	Cathedral of Talca	35°25'33.25"S	71°40'0.93"W	Figure 4.87

Figure 4.86 Iglesia Los Salesianos

Figure 4.87 Cathedral of Talca

Figure 4.88 Edificio Intendencia Maule

Figure 4.89 Liceo de Niñas Marta Donoso

4.4.2. Case Study: The Cathedral of Talca

4.4.2.a. Preamble

The City of Talca is about 240 km south of Santiago. It has a population of about 200,000. Talca is located on the projection of the fault plane from the Maule earthquake fault. It is a significant economic, agricultural and educational city, with two universities.

Because of the national significance of Talca to Chilean history and the importance of the Talca diocese within the archdiocese of Santiago, the Cathedral of Talca holds a revered place in Chilean Roman Catholicism. The Talca Cathedral has had a number of noted Bishops, as below:

- Miguel León Prado (apostolic administrator) - 12 June 1913 - 18 October 1925 appointed, auxiliary bishop of Santiago de Chile
- Carlos Silva Cotapos - 14 December 1925 - 21 January 1939 resigned
- Manuel Larraín Errázuriz - 21 January 1939 succeeded - 22 June 1966 died
- Carlos González Cruchaga - 4 January 1967 - 12 December 1996 retired
- Horacio del Carmen Valenzuela Abarca - appointed 12 December 1996 – current Bishop

The current Cathedral is at least the second (probably the third, since it is likely that the 1742 earthquake would have destroyed a place of worship on the same site) to be built in this location. The previous Cathedral of Talca was demolished in the 1928 earthquake (magnitude 8.4). The images in Figure 4.90 are possibly pictures of the Cathedral before (left) and after (right) the 1928 earthquake.

Figure 4.90 Cathedral of Talca before and after the earthquake in 1928

4.4.2.b. The New Cathedral

The Cathedral was started with a cornerstone ceremony in 1939, and construction started in 1941. It was opened to the public in 1951, and dedicated on Thursday 30 September 1954. The project architect was Ramon Venegas, and the engineer was Jose Mascayano (the design documents mention engineers Alberto Covarrubbias and Carlos Infante). The interior decorations were by Alejandro Rubio. The sitting Bishop of the time was Monsignor Manuel Larraín Errázuriz (1900-1966), who was Bishop from 1941 to 1966. Bishop Errázuriz was the driving force behind the new Cathedral during his term at Bishop-curate which was from 1938 to 1941.

The structure was designed for a seismic coefficient of 1/10 g, presumably meaning 10 percent of the weight, not a peak ground acceleration of 0.1 g, but this is not certain. A translation of the overview design sheet is given in Appendix C. The design live load on both floors and stairs was taken as 500 kg/sq. m, and the foundation design bearing pressure was 1.5 kg/sq. m. The Cathedral was raft foundation. All design aspects conformed to the Chilean code of 1933. The structural system of the Cathedral is reinforced concrete frame with massive brick masonry walls of considerable thickness.

The plan of the Cathedral is quite simple, with a main hall and one tower, as seen in Figure 4.91. It has a central nave and two isles, one on either side. The isles are lower than the nave, as indicated in Figure 4.91 and Figure 4.93, which is one of the causes of damage to the columns supporting the arches of the nave. The overall plan dimensions of the Cathedral are 56.75 m by 40.85 m. The isles are approximately 4 m wide and 9.85 m high, as compared to the total height of the nave, which is 19.65 m.

Figure 4.91 External view (side elevation) of the Cathedral before the earthquake

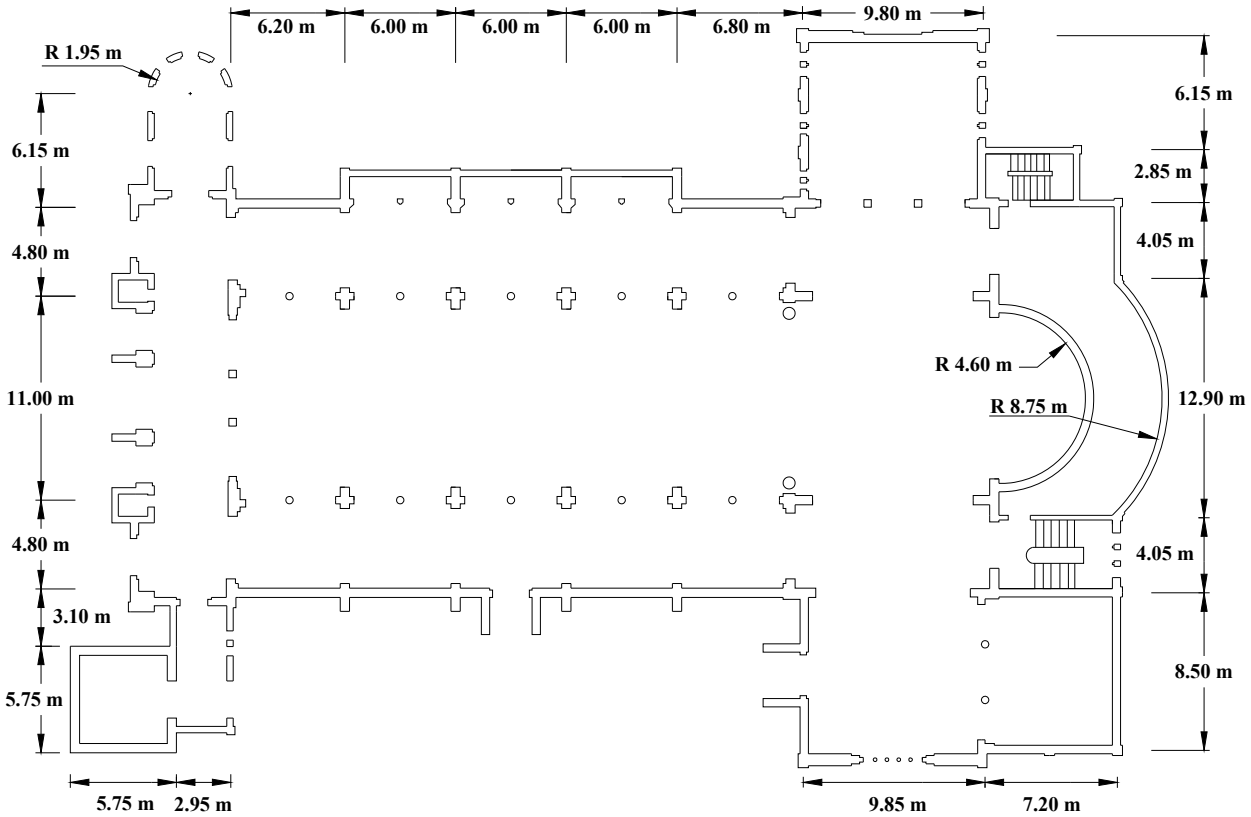

Figure 4.92 Plan view (recreated from design drawings)

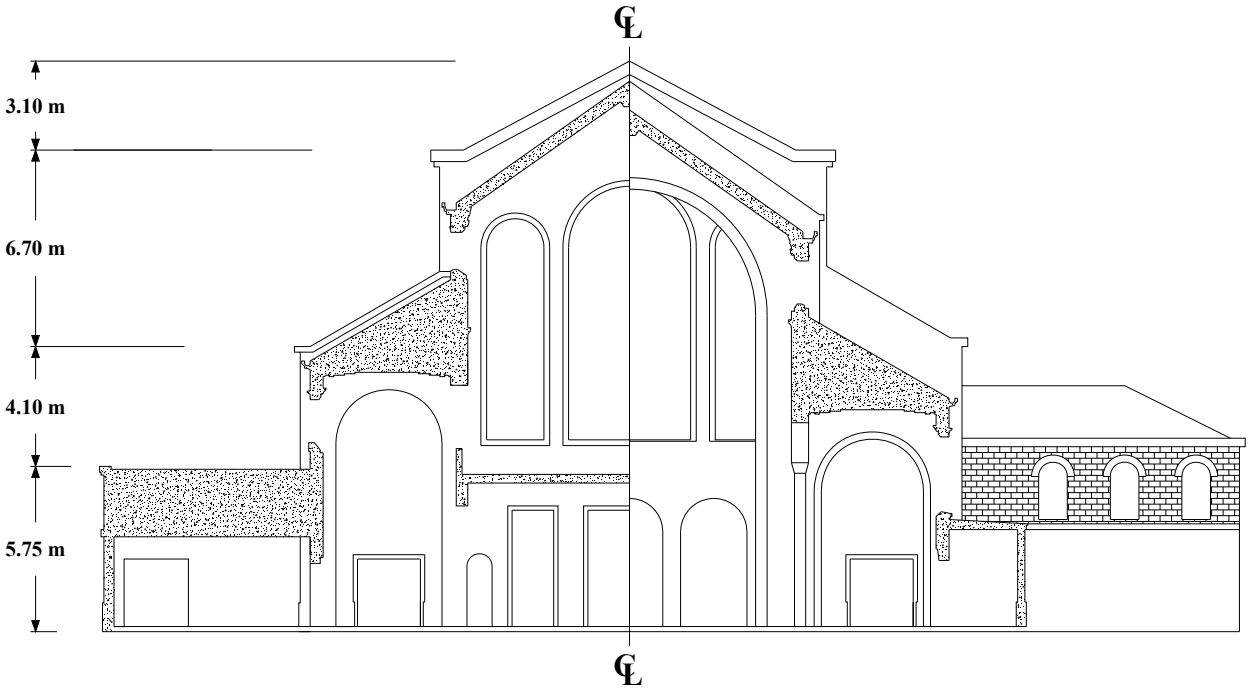

Figure 4.93 Front Elevation (recreated from design drawings)

4.4.2.c. Description of Observed Damage

Figure 4.94 shows one of the few exterior shear cracks at the corner of a window opening. The RC column is intact. It was also observed that damage was concentrated at corners of openings but all other structural elements are intact. There is no shedding of brick masonry walls due to their thickness, unlike the case of infills in buildings; this is shown in Figure 4.95.

Whereas there was no apparent damage to RC structural members, compression failure on the exterior of a heavily loaded corner column was observed (Figure 4.96). The smooth bars are very nearly buckled. The cover must have had considerable cracks leading to rusting of the longitudinal reinforcement.

With regard to the damage indicated in Figure 4.97, the masonry did not fail but rather the plaster peeled off. Some minor shear cracking was seen at the corner of the opening where stress concentrations occur.

Figure 4.98 confirmed that the concrete quality is high-to-very high. Smooth steel bars are used throughout. Reasonable spacing of ties but not all longitudinal bars are tied. Only spalling damage to RC was observed.

With reference to Figure 4.99, the masonry panel above the RC arch and cross beam is large and hence cracked in shear, with some horizontal cracking due to sliding that causes change in the direction of principle stresses. Spalling damage to the RC arch is observed. The arches in the background were not damaged possibly because

they were less loaded (there is a slab connecting them and thus distributing the load from above).

Finally, the side frames (or outriggers) have provided the circular columns with a degree of protection, which the slender arches that extend above the side frames did not have. This resulted in hinging at the end of the arch as shown in Figure 4.100. The arch in the background is much stiffer than those in the foreground. It has not suffered any damage. This pattern of damage, shown in Figure 4.100, was repeated in several locations.

Figure 4.94 Exterior damage to masonry walls

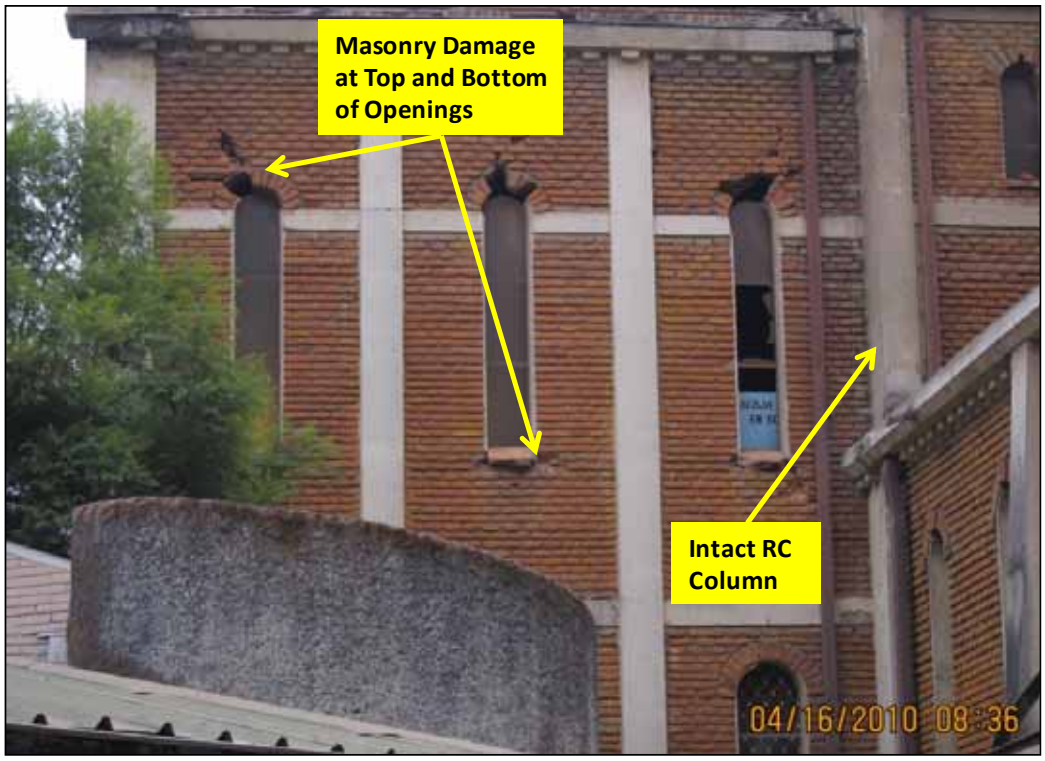

Figure 4.95 Exterior damage to masonry at corners of windows

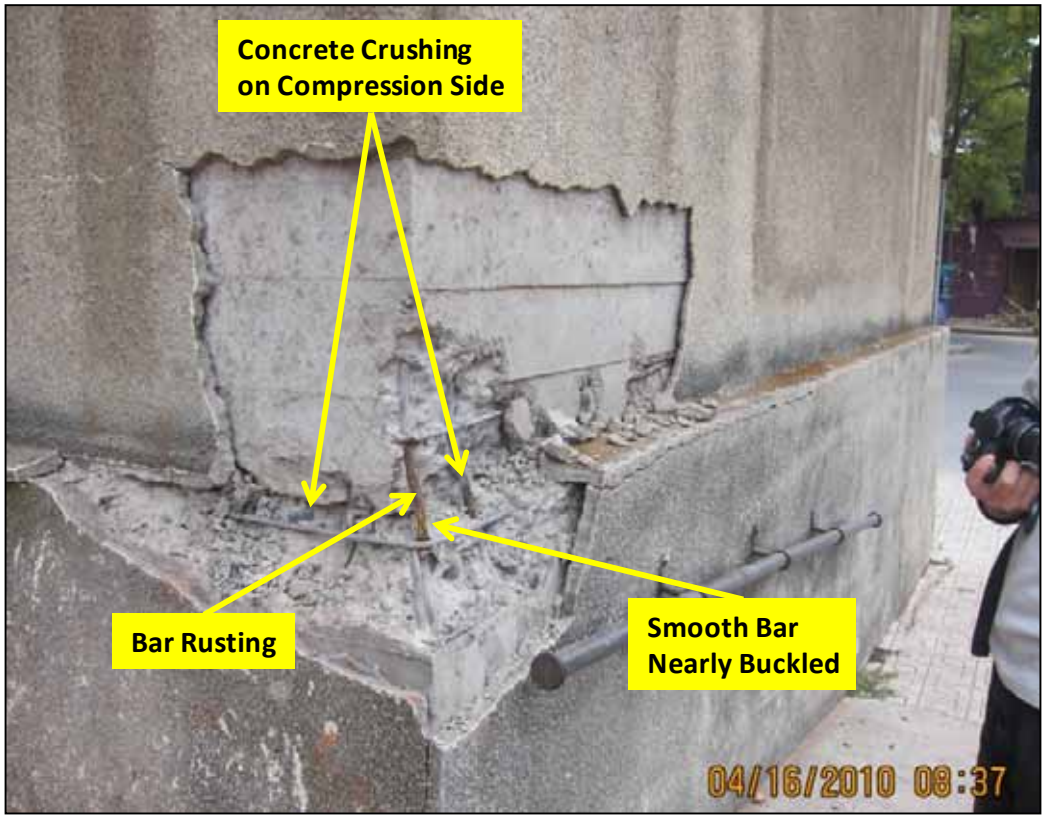

Figure 4.96 Compression-induced damage to exterior RC column

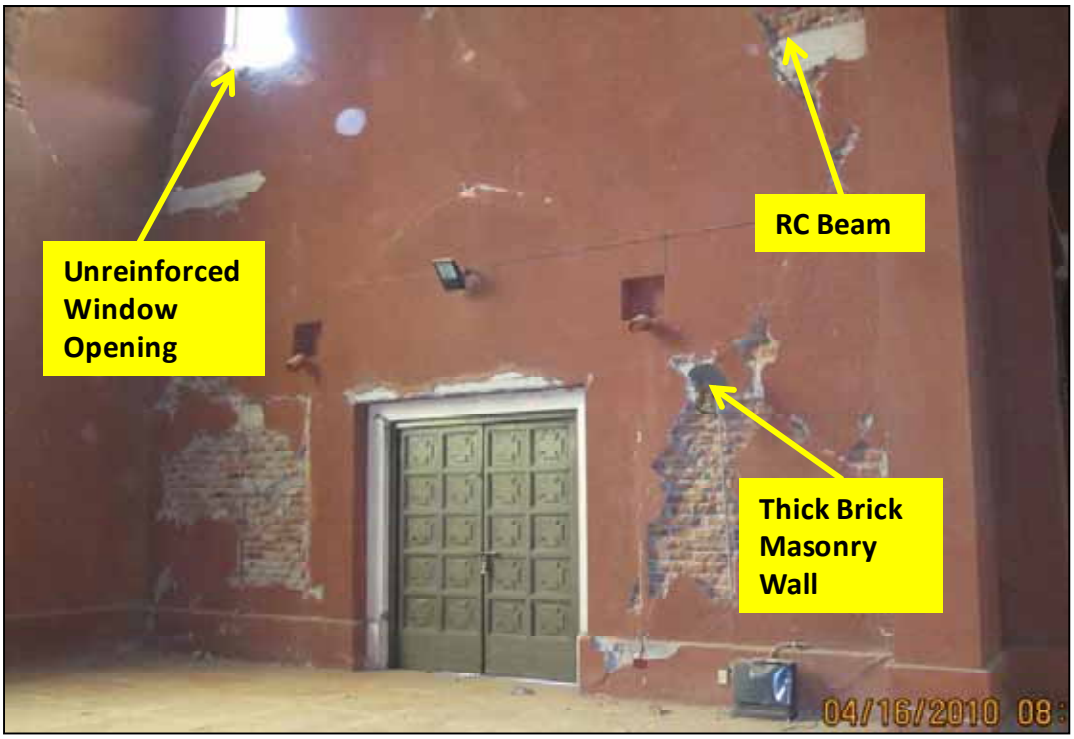

Figure 4.97 *Left:* Interior damage to masonry walls

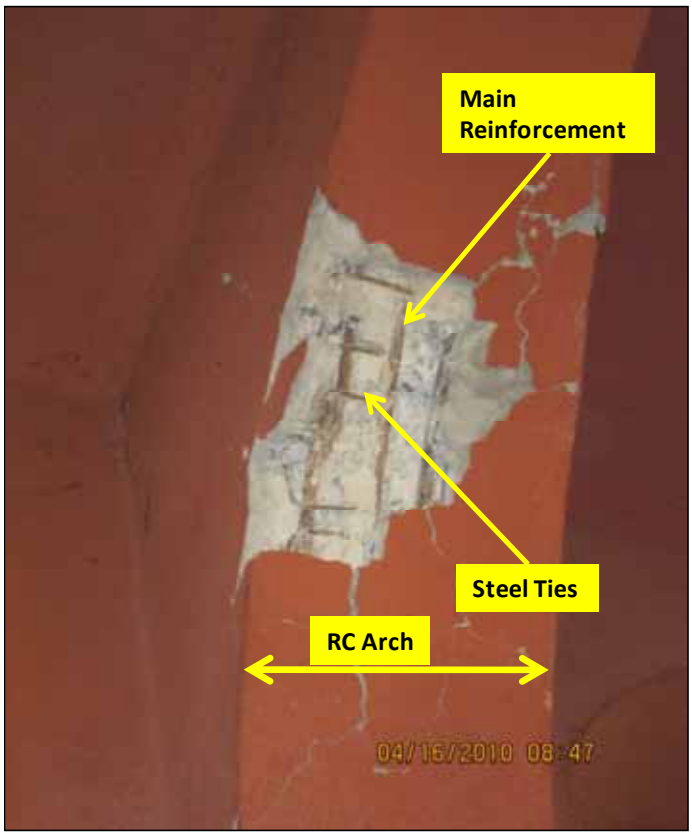

Figure 4.98 Interior spalling of RC cover – showing construction details

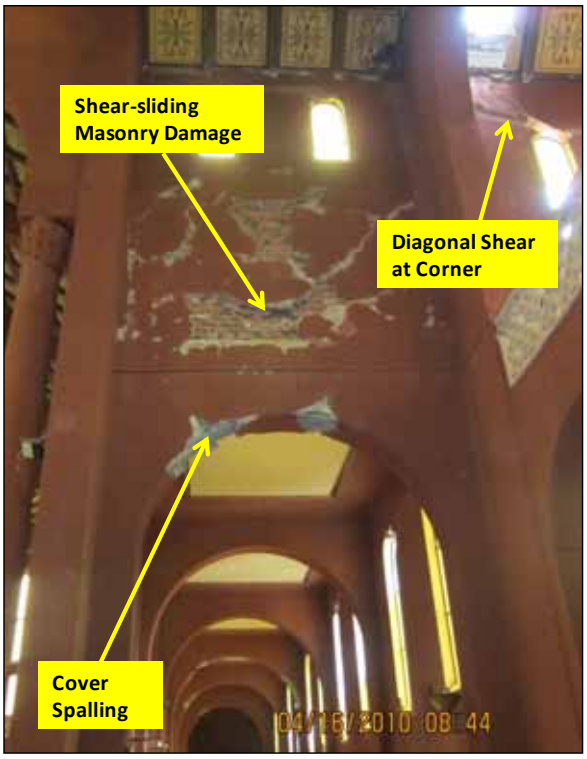

Figure 4.99 Side isles damage to RC arch and masonry wall

Figure 4.100 Interior damage to high columns at junction with side isles

4.4.2.d. Conclusions

The Cathedral behaved on the whole very well. Minor structural damage was observed constituting no threat of life. It is worth commenting on the design and construction. With regard to design versus performance, as indicated above it is not clear if the design acceleration was 0.1 g or the design base shear was 10 percent of the weight. If it were the former, then the design base shear with no response modification factors would be 25 percent of the weight. Taking into account minimum response modification based on overstrength, the design base shear (for a peak ground acceleration - PGA - of 0.1 g) would be about 9 percent of the weight, assuming a force reduction of 3. If the actual design base shear was 10 percent of the weight of the structure, then there is an implicit assumption that the ground acceleration used for design is about 0.3 g. The USGS hazard map shown in Chapter 2 of this report (Figure 2.9) gives a value of PGA of about 0.3 g - 0.4 g. Therefore, the Cathedral was subjected to at least the design ground acceleration, if not 30 percent higher. This argument confirms that the response of the Cathedral is considered as intended in the design. Regarding construction, it is the opinion of the MAE Center field mission team that the construction quality, both in terms of materials and placement, was of very high quality. Admittedly, the Cathedral is not in use. However, taking into account that no one lost their lives when the structure was subjected to one of the largest earthquakes ever measured, at a distance of about 100 km to the epicenter, with aftershocks that could have been right under the City of Talca, the behavior of the Cathedral was actually excellent.

4.5. REFERENCES

AASHTO (2006), Standard Specification for Plain and Laminated Elastomeric Bridge Bearings, AASHTO Designation: M251-06, American Association of State and Highway Transportation Officials, Washington, D.C.

ACI (2005), Building code requirements for masonry structures (ACI-530-05/ASCE 5-05), American Concrete Instittue, Farmington Hills, MI, USA

ACI (2008), Building Code Requirements for Structural Concrete (ACI 318-08) and Commentary, American Concrete Institute, Farmington Hills, MI, USA.

AONBENFIELD (2010), “Event recap report: 02/27/10 Chile earthquake,” Impact Forecasting LLC, Chicago, IL, http://aon.com/, web accessed on Nov 30, 2010.

Buckle, I., Friedland, I., Mander, J., Martin, G., Nutt, R. and Power, M. (2006), “Seismic Retrofitting Manual for Highway Structures: Part 1-Bridges,” MCEER-06-SP10, Multidisciplinary Center for Earthquake Engineering Research.

Chen Y. H. (2003), Seismic evaluation of RC buildings infilled with brick walls, Ph.D. thesis, Tainan (Taiwan) National Cheng-Kung University (in Chinese).

Cimellaro, G., Reinhorn, A., Ambrisi, A., and Stefano, M. (2009), “Fragility Analysis and Seismic Record Selection,” Accepted September 30, 2009, to Journal of Structural Engineering.

Cornell, C. A., Jalayer, F., Hamburger, R. O., and Foutch, D. A. (2002), “Probabilistic Basis for 2000 SAC Federal Emergency Management Agency Steel Moment Frame Guidelines,” Journal of Structural Engineering, 128:526-533.

EERI (2010), “Learning from Earthquakes: The M_w 8.8 Chile earthquake of February 27, 2010,” EERI Special Earthquake Report, Earthquake Engineering Research Institute, http://www.eeri.org/, web accessed on Nov 30, 2010.

Elnashai, A. S. and L. Di Sarno (2008), Fundamentals of Earthquake Engineering, Wiley, Chichester, U.K.

Elnashai, A., Papanikolaou, V. and Lee, D. (2010), ZEUS NL – A system for inelastic analysis of structures, User’s Manual, Mid-America Earthquake (MAE) Center, Department of Civil and Environmental Engineering, University of Illinois at Urbana-Champaign, Urbana, IL.

FEMA (2003), Multi-Hazard Loss Estimation Methodology, Earthquake Model: HAZUS-MH MRI, Technical and User's Manual, Federal Emergency Management Agency, Washington, D.C., USA.

FEMA (1999), Evaluation of earthquake damaged concrete and masonry wall buildings, Basic procedures manual FEMA 306, Washington (DC), Federal Emergency Management Agency.

Filiatrault, A., H. Isoda, et al. (2003), Hysteretic Damping of Wood Framed Buildings. Engineering Structures, 25(4), 461-471.

Hancock, J., Bommer, J., and Stafford, P. (2008), “Numbers of scaled and matched accelerograms required for inelastic dynamic analyses,” Earthquake Engineering and Structural Dynamics, 37, 1585-1607.

INE (2010), Instituto Nacional de Estadísticas, http://www.ine.cl/, web accessed on August 15, 2010.

Izzuddin, B.A., and Elnashai, A.S. (1993), “Adaptive space frame analysis, Part II: A distributed plasticity approach,” Proceedings of the Institution of Civil Engineers, Structures and Buildings, Vol. 99, 317-326.

Jeong, S.-H. and Elnashai, A. (2007), “Probabilistic Fragility Analysis Parameterized by Fundamental Response Quantities,” Engineering Structures, 29, 1238–1251.

Ji, J., Elnashai, A., and Kuchma, D. (2007), “Seismic Fragility Assessment for Reinforced Concrete High-Rise Buildings,” MAE Center Report 07-14.

Kawashima, K., Unjoh, S., Hoshikuma, J. and Kosa, K. (2010), “Damage of transportation facility due to 2010 Chile earthquake,” Bridge Team Dispached by Japan Society of Civil Engineers, Presentation File, http://peer.berkeley.edu/, web accessed on Nov 30, 2010.

Kwon, O., and Elnashai, A. (2006), “The effect of material and ground motion uncertainty on the seismic vulnerability curves of RC structure,” Engineering Structures, 28, 289-303.

Kwon, O. and Kim, E. (2010), Case study: Analytical investigation on the failure of a two-story RC building damaged during the 2007 Pisco-Chincha earthquake, Engineering Structures, Volume 32, Issue 7.

Luo, Y. H. and Durrani, A. J. (1995a), “Equivalent beam model for flat-slab buildings. Part I: Interior connection,” ACI Structural Journal, 92(1), 115–124.

Luo, Y. H. and Durrani, A. J. (1995b), “Equivalent beam model for flat-slab buildings. Part II: Exterior connection,” ACI Structural Journal, 92(2), 250–257.

Mackie, K., Wong, J. and Stojadinovic, B. (2007), “Integrated Probabilistic Performance-Based Evaluation of Benchmark Reinforced Concrete Bridges,” PEER Report 2007/09.

Madan, A., Reinhorn, A. M., Mander, J. B., and Valles, R. E. (1997), Modeling of masonry infill panels for structural analysis, Journal of Structural Engineering, ASCE, 123(10), 1295-1302.

Mander, J. B., Priestley, M. J. N. and Park, R. (1988), “Theoretical Stress-Strain Model for Confined Concrete,” Journal of Structural Engineering, 114(8), 1804-1826.

Martínez-Rueda, J. E. and Elnashai, A. S. (1997), “Confined Concrete Model under Cyclic Load,” Materials and Structures, 30(3), 139-147.

Moroni, M. O., Astroza, M. and Acevedo, C. (2004), Performance and Seismic Vulnerability of Masonry Housing Types Used in Chile, Journal of Performance of Constructed Facilities, 18, 173, DOI:10.1061/(ASCE)0887-3828(2004)18:3(173).

Mostafaei, H. and Kabeyasawa, T. (2004), Effect of infill masonry walls on the seismic response of reinforced concrete buildings subjected to the Bam earthquake strong motion: A case study of Bam telephone center, Earthquake Research Institute, University of Tokyo.

Mukherjee, S. and Gupta, V. K. (2002), “Wavelet-based Generation of Spectrum-compatible Time-histories,” Soil Dynamics and Earthquake Engineering, 22(9-12), 799-804.

NCh 2123 (2003), Confined masonry – Requirements for structural design (NCh 2123.Of1997 Modified 2003), Albañilería Confinada – Requisitos de diseño y calculo (in Spanish).

Nielson, B. (2005), “Analytical Fragility Curves for Highway Bridges in Moderate Seismic Zones,” PhD Thesis, Georgia Institute of Technology.

Nielson, B. and DesRoches, R. (2007), “Analytical Seismic Fragility Curves for Typical Bridges in the Central and Southeastern United States,” Earthquake Spectra, 23 (3), 615-633.

Padgett, J. and DesRoches, R. (2007), “Sensitivity of Seismic Response and Fragility to Parameter Uncertainty,” Journal of Structural Engineering, Vol. 133, No. 12.

Paulay, T. and Priestley, M. J. N. (1992), Seismic design of reinforced concrete and masonry buildings, John Wiley&Sons, Inc.

PEER NGA Database, http://peer.berkeley.edu/nga/index.html

PEER Strong Motion Database, http://peer.berkeley.edu/smcat/index.html

Priestley, M. J. N., Seible, F. and Calvi, G. M. (1996). Seismic design and retrofit of bridges, Wiley, New York.

Ramanathan, K., DesRoches, R. and Padgett, J. (2010), "Analytical Fragility Curves for Seismically and Non-Seismically Designed Multi-Span Continuous Concrete Girder Bridges in Moderate Seismic Zones," Proceedings of the 9th U.S. National/10th Canadian Conference on Earthquake Engineering, Toronto, CA, July 25-29, 2010.

Wen, Y., Ellingwood, B., Veneziano, D. and Bracci, J. (2003), "Uncertainty Modeling in Earthquake Engineering," MAE Center Project FD-2 Report.

Yashinsky, M., Oviedo, R., Ashfod, S., Fargier-Gabaldon, L. and Hube, M. (2010), "Performance of Highway and Railway Structures during the February 27, 2010 Maule Chile Earthquake," Presentation file, http://peer.berkeley.edu/, web-accessed on Aug 15, 2010.

5 TRANSPORTATION NETWORKS, ROADS AND EMBANKMENTS

5.1. INTRODUCTION

The Maule earthquake significantly affected a 500 km zone along the Chilean coastline from the Araucanía region in the south to Valparaíso in the central region as seen in Figure 2.9. The details on the damaging effects of the earthquake are provided in Section 1.2.

Figure 5.1 La Madera road and Itata highway networks surveyed

Although guidelines on assessing the pavement condition are available for normal vehicle loading and climate effects, limited data, research studies, and technical guidance is published on the pavement network's structural and functional condition following a major earthquake. The impact of an earthquake on road network and other transportation facilities can be detrimental as it affects the supply of emergency and medical assistance, food, and water for the people in the damaged areas. In addition, the roadway damage may affect the transportation of commercial goods and services, which are needed to maintain the local economies during the re-building process. An example of the criticality of the transportation infrastructure tragically unfolded after the January 2010 Haiti earthquake (Wikipedia, 2010; Rathje et al., 2010). The damage to the transportation system affected the supplies for people's basic needs as well as the ability to repair the roads.

The MAE Center field reconnaissance mission (transportation and structures groups) inspected several road networks to assess the extent of damage on pavement surfaces, bridge approaches, embankments, and fill areas. The two road networks surveyed and discussed in this report were within 100 km of the city of Concepción. The data presented in this report includes findings from the site visits to these routes: Itata Highway and La Madera road, both shown in Figure 5.1. The damage information summarizes the pavement condition in terms of cracking, embankment failures, International Roughness Index (IRI), as well as general damage observations. The Chilean standards for constructing embankments will also be presented since much of the observed pavement damage was related to embankment movements.

5.2. OVERVIEW OF CHILEAN TRANSPORTATION INFRASTRUCTURE DAMAGE

The Chilean Ministry of Public Works, MOP (Wikipedia, 2010) has developed a transportation infrastructure database that contains a summary of the location and type of earthquake damage in the affected regions. This database is being used for prioritizing and managing the major emergency repair and rebuilding process, which is currently estimated to take four years. The information in this database is being collected at the network level. Hence, it does not necessarily include detailed project-level information on all distress' extent and severity.

The Ministry has classified the damage into two main categories: public and private-operated civil infrastructure. For the public civil infrastructure investment, a total of 1,695 significant failures were registered, of which 717 are roadway damage (Table 5.1). For the private (concession-operated facilities) infrastructure investment, a total of 642 failures were reported with 113 directly related to the roadway (Table 5.2).

The MOP information and pavement condition assessment survey of the two roadway network both observed that the main damage was caused by embankment and bridge approach fill instability. The second major transportation infrastructure damage affected road and pedestrian bridges.

Table 5.1 Number of major earthquake damage/failures reported on public transportation infrastructure by region

Structure Types	Chilean Region							
	Valparaíso	Metropolitana de Santiago	Libertador Gral. Bernardo OHiggins	Maule	Biobío	La Aracanía	Los Ríos	Total
Roads*	40	50	84	74	92	51	2	393
Bridges and Approach Fill**	14	15	27	88	41	24	2	211
Road Access*	2	2	23	13	29	19	0	88
Overpass-Crossing	1	0	2	10	3	0	0	16
Pedastrian Bridges	0	0	1	1	2	0	0	4
Guardrails	0	0	1	0	0	0	0	1
Others	0	0	4	0	0	0	0	4
Total	**57**	**67**	**142**	**186**	**167**	**94**	**4**	**717**

Table 5.2 Number of major earthquake damage/failures on private concession-operated transportation infrastructure by region

Structure Types	Chilean Region							
	Valparaíso	Metropolitana de Santiago	Libertador Gral. Bernardo OHiggins	Maule	Biobío	La Aracanía	Los Ríos	Total
Roads*	3	2	5	0	18	1	0	29
Bridges and Approach Fill**	0	3	5	1	6	0	1	16
Access Roads*	0	1	1	0	3	3	0	8
Overpass-Crossing	3	12	8	6	1	4	0	34
Pedastrian Bridges	2	12	1	0	5	5	1	26
Total	**8**	**30**	**20**	**7**	**33**	**13**	**2**	**113**

*Mainly roads embankments (including small and large embankments)
** All bridges suffered damage at fill access

As of July 2010, the cost of the transportation infrastructure emergency repair is approximated at $317 million while the reconstruction cost is estimated at $378 million (Ministry of Public Works of Chile, 2010b) for the public (non-private concessions)

network. This is considered a significant investment for Chile given that the 2008 national gross domestic product (GDP) was $169 billion. The reconstruction costs will likely be higher since more projects need to be re-designed and upgraded to meet new earthquake standards.

Chilean performance specifications for public and privately operated roads have become more demanding in the past 15 years; however, the construction specifications have not evolved accordingly. The following performance criteria are the requirements for private concession roadways (Ministry of Public Works of Chile, 2010a) and new public construction in Chile:

- Maximum IRI = 3.5 m/km
- Maximun rut depth = 15 mm
- Maximun surface fatigue cracking percentage = 10 percent
- Potholes and localized distress = Zero
- Surface friction coefficient = 0.40 to 0.55

Since many road failures and pavement damages were associated with the structural performance of the embankment, the design and construction specification were reviewed. The standard for the embankment material and construction is defined in the Chilean Road Manual (Ministry of Public Works of Chile, 2000). The current standard requires the material to meet the following specifications:

- California Bearing Ratio (CBR) > 10
- Minimum density = 90 percent (maximum dry density, modified proctor)
- Maximum material size = 150 mm
- Top 300 mm of embankment should be CBR > 20 and the maximum aggregate size = 100 mm

The Chilean standards (Ministry of Public Works of Chile, 2000) also define three types of structural fills: structural fill for under drains, permeable structural fill (for bridge approaches), and light structural fill for bridges in order to reduce settlement and horizontal forces. For permeable structural fill for bridge approaches, the standard requires that the material be comprised of inorganic nonplastic soil and 100 percent shall pass the 80 mm sieve, 35 to 100 percent pass the 5 mm sieve, and 0 to 4 percent pass the 0.075 mm sieve. The fill should also have a 20 percent minimum sand equivalency and compaction shall be in 200 mm layers maximum with a minimum of 95 percent maximum dry density (modified proctor).

5.3. ROAD NETWORK OBSERVATIONS AND EVALUATION

The observations and performance after the earthquake of two private-concession highway projects, shown in Figure 5.1, will now be reviewed. Both highways (La Madera road and Itata highway) are located near the earthquake epicenter. The Concepción

area is the southern hemisphere's most important forestry producer. La Madera road is a 108.7 km two lane route from Concepción to Nacimiento. This road primarily connects Concepción to Los Angeles as well as many local towns in between. In addition to regular traffic, the road is used for wood transport from the forest to local ports as well as by wood pulp manufacturers, and timber suppliers. Hence, the pavement supports heavy commercial truck traffic.

The 75km Itata highway from Concepción to Chillán is a four-lane highway facility, which connects the main north-south interstate in Chile with the 2nd largest city, Concepción, Figure 5.1. This highway also serves the forest industry and enables the bi-directional flow of commercial goods transportation from and to the ports and central region markets.

5.3.1. La Madera Road

La Madera road has three main sections as seen in Table 5.3. Section 1 is hot-mix asphalt (HMA) overlay of jointed concrete, section 2 is HMA over foamed asphalt recycled layer, and section 3 is conventional flexible pavement with HMA surfacing. Post-earthquake data from La Madera concession identified 59 damaged areas. The total linear length of the roadway that experienced earthquake damage was 5.08 km or approximately 5 percent of the total length. More specifically, the percentage of pavement damage was 4.48 km or 4.2 percent. The other 0.6 km (0.8 percent) damage was one bridge damage, one bridge collapse, and 0.288 km of shoulder distress.

Based on the visual inspection of this road network, the most severe pavement distresses were associated with embankment and fill locations; further discussion of the geotechnical causes of damage is provided in Chapter 3 of this report. Overall, the typical pavement damages were a result of bridge approach embankment/fill settlement, sag vertical curve embankment failures, under-drain fill settlement, and embankment slope stability failures or lateral spreading.

Table 5.3 La Madera pavement sections

Kilometer		Thickness by layer and Type (cm)				
Initial	Final	Subase	RFA*	Base	Concrete	Asphalt
0.000	12.000	15	-	-	18	12.7
12.000	20.000	15	15	-	-	5
20.000	45.487	10	15	-	-	5
45.487	48.139	26	-	25	-	7.4
48.139	52.8	26	-	25	-	7.3
52.800	68.000	26	-	25	-	7.3
68.00	78.873	26	-	25	-	7.2
78.873	101.100	20	-	20	-	13
101.100	107.250	21.5	-	21.7	-	12.7
107.250	108.104	26	-	25	-	7.1

* Recycled Foam Asphalt layer

** Jointed Plain Concrete Pavement

5.3.2. Itata Highway Pavement Failures

The Itata highway is a 75 km flexible pavement structure consisting of a 20 cm granular subbase, 20 cm granular base layer, and 13 cm of HMA. Visual assessment of the Itata highway after the earthquake identified 69 locations of roadway damage corresponding to 119 individual distresses. Table 4 summarizes the distress types observed on the roadway surface, embankment, and shoulder areas and their respective percent occurrence. The most prevalent distress observed was transverse cracks. Most cracks (transverse, longitudinal, and surface) resulted from embankment lateral displacement or local settlement. In addition, some roadway settlement resulted from settlement or collapse of drainage pipes under the road. Of the 69 damage locations, 60 percent of them were associated with some sort of embankment failure with the remaining, 33 and 7 percent, pavement surface and shoulder damage, respectively.

Table 5.4 Road network distress type and level on the Itata Highway (0 to 75 km)

Distress Type	Number of Observations	Percent of Occurrence (%)
Transverse crack	24	34.8
Lateral displacement of embankment	21	30.4
Shoulder-Curb separation	19	27.5
Roadway settlement	14	20.3
Longitudinal crack	10	14.5
Pavement surface crack	9	13.0
Shoulder settlement	7	10.1
Road upheaval/bump	3	4.3
Drainage and shoulder collapse	2	2.9
Shoulder crack	2	2.9
Total	119	100%

5.4. ROADWAY DAMAGE ASSESSMENT: VISUAL INSPECTION

Based on the visual inspections of the two roadways, the following typical damages and distresses were observed: sag vertical curve embankment failures, fill settlement near bridge approaches, under-drain fill settlement, and lateral spreading of embankments. Figure 5.2 demonstrates two typical failures of a bridge approach fill settlement and subsequent elevation difference between the road and the bridge. This type of failure slowed traffic flow across bridges. Most bridges on these two networks did not experience severe structural damage and hence, were able to maintain service.

Another common damage observed on La Madera road was embankment failure at the bottom of sag vertical curves as seen in Figure 5.3. Poor soil condition surrounding the embankment yielded the worst damage results. However, less damage was observed when trees or other confining structures exist near the embankment. In some locations, drainage pipes and culverts crossing underneath the roadway settled or collapsed resulting in severe surface distress as seen in Figure 5.4.

Figure 5.2 Typical bridge approach embankment-fill settlement

Figure 5.3 Sag vertical curve pavement failures

Figure 5.4 *Left:* under-drain fill settlement at the roadway surface; *Right:* collapsed drainage pipe

Pavement surface damage was also noticed on roads built on embankments that experienced slope stability distress and lateral spreading. The embankment failures resulted in longitudinal, transverse and diagonal cracks in the road as shown in Figure

5.5. In this case, the resultant pavement distress caused serviceability problems and safety hazards. It was observed that when no lateral confinement was present at the toe of the slope (e.g., trees, retaining walls, etc.) the pavement damage was more severe. This type of failure was also commonly noted by another team that surveyed Chile's infrastructure performance after the earthquake (Vargas, 2010) as well as in Haiti earthquake (Rathje et al., 2010).

Figure 5.5 Pavement damage due to embankment slope stability and lateral spreading

5.5. ROADWAY DAMAGE ASSESSMENT: STRUCTURAL AND FUNCTIONAL EVALUATION

Structural and functional pavement evaluation data were gathered after the earthquake. For Highway La Madera, falling weight deflectometer (FWD) data before and after the earthquake was obtained while IRI measurements for Itata highway were available before and after the earthquake. The purpose of analyzing this data was to determine the change in pavement condition after the earthquake so that future prediction and planning for the effect of an earthquake on the structural and functional condition of a given roadway would be better known.

5.5.1. Falling Weight Deflectometer – La Madera Road

FWD testing was conducted on La Madera road in November 2006 and after the earthquake in April 2010 (Vargas and Bellolio, 2006; Vargas, 2010). The purpose of the FWD analysis was to determine the extent of the pavement structural damage due to the earthquake. Only the section that has foamed asphalt/recycled materials that was constructed in early 2006, from kilometer 12 to 45.5, was analyzed. Figure 5.6 (Top) and Figure 5.7 (Top) are plots of the normalized deflection under a 40 kN plate load (D_0) at 20°C for 2006 and 2010, respectively, while Figure 5.6 (Bottom) and Figure 5.7 (Bottom) are the normalized deflections collected at D_8 sensor located at 1.524 m from the plate load center for the 2006 and 2010 measurements, respectively. The mean

normalized deflection in 2010 decreased by 28 percent from that measured values in 2006 for segment 1 but only 9 percent for segment 2 as seen in Table 5.5. Segment 1 is from 12.0 km to 20.0 km, while segment 2 is from 20.0 km to 45.5km.

It was clear that an increase in total structural capacity of the pavement occurred from 2006 to 2010. The 2010 FWD measurements were conducted in the dry season while the measurements conducted in 2006 were performed near the end of the wet season. However, the decrease in the maximum deflection over time is collectively attributed to the aging of the HMA surface, the curing of the foamed asphalt base layer, and possibly a change in the granular material stiffness. The deflections at the D8 sensor in Table 5.5 indicates that the subgrade modulus has been maintained over time with less than 10 percent change from 2006 to 2010. In addition, the back-calculated subgrade modulus averaged 100 MPa for both 2006 and 2010, which signifies a good subgrade soil modulus.

The location of the pavement failures immediately after the earthquake are noted on the deflection plot in Figure 5.6 and Figure 5.7 (vertical lines) to determine if there were specific correlations between the deflections in 2006 and failures in 2010. No clear correlation exists between the pavement structural capacity (including subgrade modulus) and the locations of 2010 failure locations based on the deflection basin or maximum surface deflections. During the visual survey after the earthquake, it was empirically noted that the La Madera sections that have binder-rich foamed asphalt performed relatively better. In general, the FWD test data suggested that the earthquake did not cause unforeseen network level damage to the pavement structure except for the obvious local damage areas reported during the visual surveys. No quantifiable trends were seen in the FWD data as a result of the earthquake. Additional FWD data is needed over time to verify if changes in the material or structural capacity may show up after the first rainy season.

Table 5.5 Normalized Maximum (D0) and 1.524 m Offset Deflection (D8) in Segment 1 (12 km to 20 km) and Segment 2 (20 km to 45.5 km)

	Year	Centre Plate Deflections (microns)		1.524m offset Deflections (microns)	
		Segment 1 12 to 20 km	Segment 2 20 to 45.5 km	Segment 1 12 to 20 km	Segment 2 20 to 45.5 km
Lane 1	2006	647.2 (120.7*)	493.1 (116.9)	67.4 (19.5)	61.3 (19.8)
	2010	465.1 (105.9)	393.3 (116.8)	61.7 (20.8)	64.7 (24.1)
	Difference	182.1	99.8	5.7	-3.4
Lane 2	2006	725.4 (136.9)	465 (117.4)	78.9 (28.5)	64.7 (17.2)
	2010	456.2 (92.4)	426.0 (120.3)	62.7 (20.5)	69.5 (20.4)
	Difference	269.2	39.0	16.2	-4.8

* Standard deviation

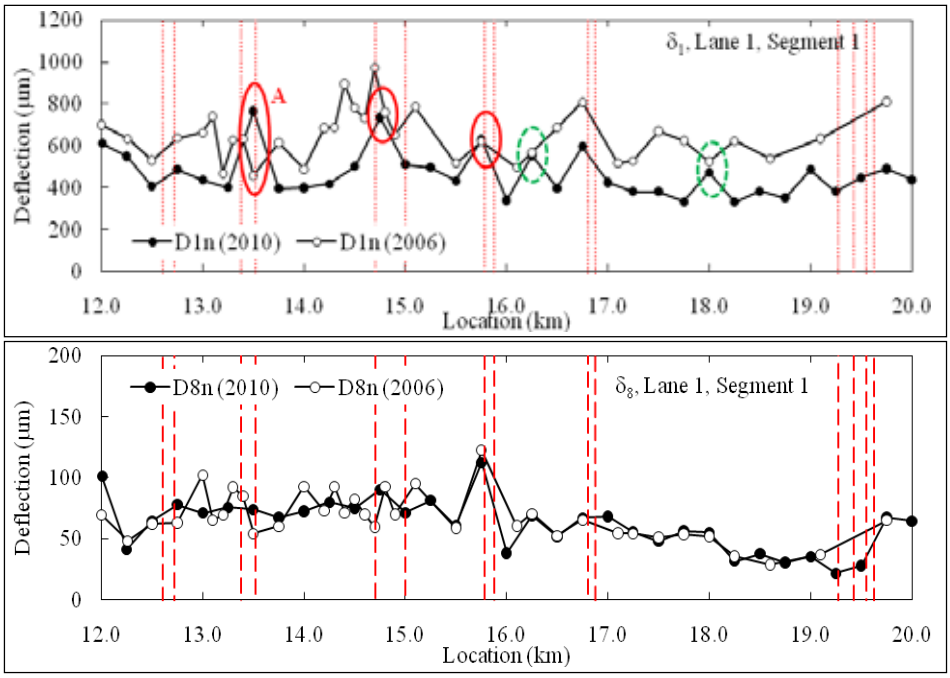

Figure 5.6 *Top*: maximum center loading plate deflection; *Bottom:* deflection at sensor offset of 1.524 m on lane 1 of segment 1 (normalized to 40 kN and 20 °C).

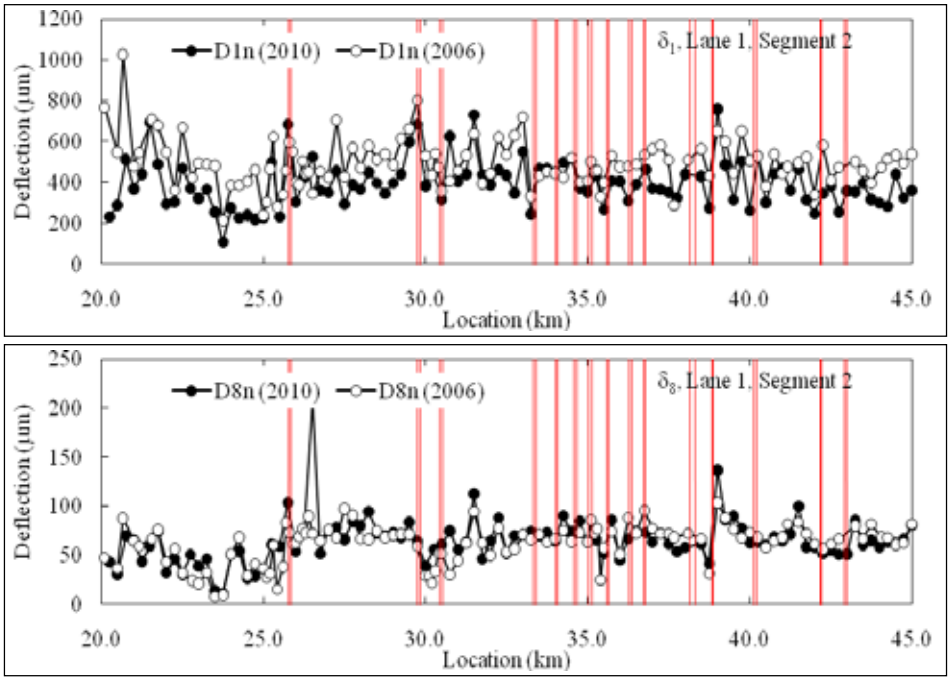

Figure 5.7 *Top*: maximum center loading plate deflection; *Bottom:* deflection at sensor offset of 1.524 m on lane 1 of segment 2 (normalized to 40 kN and 20 °C).

5.5.2. IRI Measurements: Itata Highway

It was expected that the roughness of the road would increase after this major seismic event. IRI data was collected by the Itata highway concession as required by its operating contract. The IRI measurements for lane 4 (driving lane) on the Itata highway are shown in Figure 5.8 for August 2009 and April 2010 (ASPA, 2009; ASPA, 2010) as an example. The IRI in 2010 was measured after some of the earthquake-damaged areas were repaired or patched. Mean IRI values for the four lanes are presented in Table 5.6. The IRI for this pavement increased 3.6 percent in the passing lanes and 8.35 percent in the driving lanes over the seven-month period. This increase in IRI is significantly higher than a well-maintained roadway and is attributed to the effect of the earthquake, especially in the driving lane to local settlement and emergency patching. Despite the effects of this earthquake, the IRI of the roadway still meets the maximum specification requirements of 3.5 m/km.

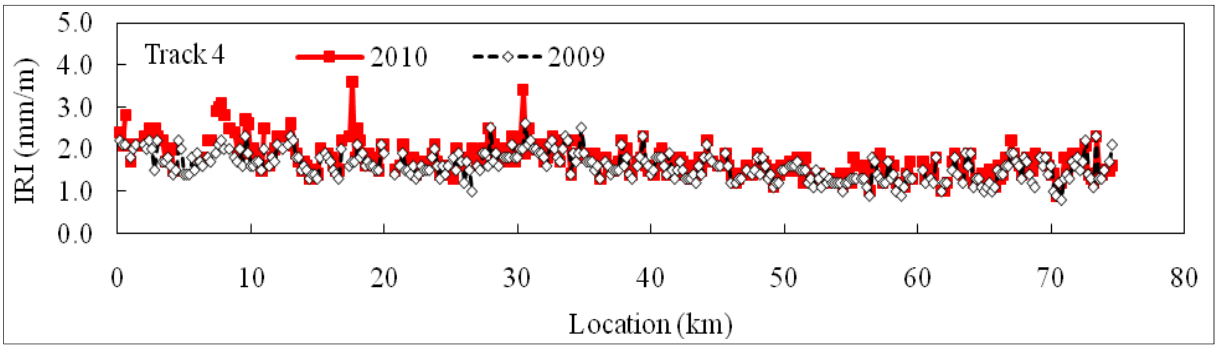

Figure 5.8 Longitudinal variations in IRI from 2009 to 2010 for Lane 4 of Itata highway

Table 5.6 Average IRI in 2009 and 2010 for Itata Highway

Year	IRI (m/km)			
	Lane 1-Passing	Lane 2-Passing	Lane 3-Driving	Lane 4-Driving
2009	1.37	1.41	1.70	1.60
2010	1.42	1.46	1.84	1.73
Change (%)	+3.4	+3.8	+8.4	+8.3

5.6. DISCUSSION

In general, a significant number of the pavement damage was related to embankment movements. A large number of the embankments that structurally failed were constructed with material that just met the minimum specification requirements. It appears that the present Chilean specifications for embankments were not adequate to withstand an earthquake of the magnitude experienced in 2010. In addition, embankment settlement and slope stability analyses may need to be conducted to better understand the causes of the catastrophic slope failures and settlements.

A large number of earth-stabilized bridge approaches had major failures or collapses, while the remaining suffered minor damage. Bridge approaches where mechanically stabilized earth was utilized had excellent performance with no visual distresses observed. This suggests that the fill construction and/or material selection and compaction played an important role in the bridge approach failures and may suggest that this construction specification is inadequate to withstand such an earthquake.

The Maule earthquake occurred at the end of the Chilean summer but if the earthquake would have occurred during the winter rainy season, the damage could have been more severe. The Concepción region usually has more than 1,000 mm of rain during winter, which results in saturated soil condition. Therefore, it can be concluded that total pavement damage could have been significantly worse if the earthquake happened during winter.

5.7. CONCLUSIONS

The Maule earthquake caused considerable damage to transportation networks. Several pavement networks were surveyed for characteristic damage after the earthquake. The main failures on the pavement surface were a result of fill material settlement at bridge approaches, under-drain settlement, embankment slope failures, and lateral spreading of the embankment. The surveys indicated that mechanically-stabilized fills used at bridge approaches performed better than earth-stabilized bridge approaches during the earthquake. Most of the failed fill areas meet the current specification requirements suggesting an evaluation of current fill standards is necessary. Traditional pavement visual assessment guidelines were found to be unsuitable for evaluating earthquake damage on roadways since the distress mechanisms are different. The field surveys concluded the need for developing a standardized condition assessment tool with guidelines to evaluate pavement damage after an earthquake.

Falling weight deflectometer data was collected and analyzed to determine the effects the earthquake had on the pavement structural capacity from 2006 to 2010. In general, surface deflections showed little change in the pavement structure as a result of the earthquake and the changing in surface deflections were primarily related to the aging of the asphalt layer. This means the pavement network showing no surface distress should be expected to perform as originally anticipated. Surface roughness data was collected and International Roughness Index (IRI) was calculated to determine the effects the earthquake had on the pavement functional performance. The roughness measurements were performed five months before the earthquake and immediately after the emergency repairs. The average IRI changed 3.6 to 8.4 percent, in the passing and driving lanes, respectively. The IRI changes were a combination of both local settlement of the roadway and emergency repair construction quality.

5.8. REFERENCES

APSA S.A. (2009), Functional evaluation of international roughness index (IRI) by laser profilometer for Itata highway from 0.000 to 75.000 km, Interim Report, APSA, Santiago, Chile, (in Spanish).

APSA S.A. (2010), Functional evaluation of international roughness index (IRI) by laser profilometer for Itata highway from 0.000 to 75.000 km, Interim Report, APSA, Santiago, Chile, (in Spanish).

Ministry of Public Works of Chile (2000), Road Manuals, Vol. 5, Section 5.205. Ministry of Public Works, Chile (in Spanish).

Ministry of Public Works of Chile. (2000), Road Manuals, Vol. 5, Section 5.206. Ministry of Public Works, Chile (in Spanish).

Ministry of Public Works of Chile (2010a), "Chile: Opportunities in infrastructure 2009-2010," www.mop.cl, Accessed July 30, 2010.

Ministry of Public Works of Chile (2010b), General Internal Statistics, email correspondence.

Rathje, E, Bachhuber, J., Cox, B., French, J., Green, R., Olson, S., Rix, G., Wells, D. and Suncar, O. (2010), "Geotechnical Engineering Reconnaissance of the 2010 Haiti Earthquake," Report of the National Science Foundation-Sponsored Geoengineering Extreme Events Reconnaissance (GEER) Team, Version 1, February 22, 2010

http://www.geerassociation.org/GEER_Post%20EQ%20Reports/Haiti_2010/Cover_Haiti10.html.

Ruegg, J. C., Rudloff, A., Vigny, C., Madariaga, R., de Chabalier, J. B., Campos, J., Kausel, E., Barrientos, S., and Dimitrov, D. (2009), "Interseismic strain accumulation measured by GPS in the seismic gap between Constitución and Concepción in Chile," Physics of the Earth and Planetary Interiors, Vol. 175, Issue 1-2, pp. 78 – 85.

USGS (2010), "U.S. Geologica Survey (USGS) shake map: offshore Maule, Chile," http://earthquake.usgs.gov/earthquakes/shakemap/global/shake/2010tfan/ , Accessed July 30, 2010.

Vargas, J. and Bellolio, J. P., (2006), Pavement structural evaluation at Camino, Madera from 12.000 to 45.000 km, Report APSA 06-160-01, APSA, Santiago, Chile (in Chilean).

Vargas, J. (2010), Pavement structural evaluation with FWD deflection at Camino, Madera from 12.000 to 45.000 km, Report APSA 10-033-01, APSA, Santiago, Chile (in Spanish).

Wikipedia. (2010), "Damage to infrastructure in the 2010 Haiti earthquake," http://en.wikipedia.org/wiki/Damage_to_infrastructure_in_the_2010_Haiti_earthquake, Accessed July 30, 2010.

6 SOCIO-ECONOMIC FEATURES AND IMPACT ON COMMUNICATIONS

6.1. INTRODUCTION

Chile has a history of frequent and high intensity earthquakes on record (Volk, 2010). Closely following the Haiti earthquake of January 12 where a 7.0 magnitude earthquake caused hundreds of thousands of deaths, estimates range from 230,000 to 300,000 according to (Vorbe, 2010), to many more homeless (over 1 million people) and tremendous material and economic damage, Chile's earthquake inescapably and originally was covered in international news in relation to Haiti. For instance, On March 1, 2010, the front page headline in the New York Times was "Headline: Chile Mobilizes Soldiers to Aid after Quake", with a sub-headline of "Millions Are Displaced as Death Toll Climbs". The article displayed both the tendency to overestimate damage as well as comparisons to Haiti. Chile's much stronger earthquake sparked a tsunami that swept away entire villages and reconfigured the coastal topography in the affected region. The natural disaster resulted in 521 deaths. Damage estimates range from 30 billion dollars in damage from national authorities, 18 percent of Chile's GNP (Volk, 2010) to a much lower private estimate of 10 billion dollars, 6 percent of GNP (Navia, 2010). Although the location and effects differed drastically from that of Haiti, originally news coverage linked the two as do continuing academic debates that compare the two (Latin American Studies Association: Forum, XLI: 3, 2010). To understand the relatively minor damage incurred in Chile in relation to Haiti, a more detailed study of Chile will illuminate the situation.

The country of Chile is a thriving and dynamic political entity with a successful economy by global standards[2]. Ranked #44 in 2009 in the United Nations (UN) Human development Index, it is situated atop the "High Human Development, HHD (developing countries)" category. It is the highest ranked Latin American country in this index, ahead of Argentina, Uruguay, Cuba, Mexico, and Costa Rica, other countries in this same HHD category. According to Volk (2010) Chile has pursued joining the "developed" category for years, and the current President Piñera reassures his people that this will be achieved by 2018. According to the latest UN data, Chile's 17 million people are overwhelmingly urban (88+ percent), literate (98.65 percent), with high life expectancy (81.6/75.5, women/men), and low fertility rates (1.9 live births per women). Literacy rates vary according to reporting agency between 96.5 (UNDP, 2009 – web reference) to 98.65 percent (UNICEF, 2010 – web reference). In terms of the Latin American region, Chile has a relatively peaceful democratic past, with the notable exception of seventeen years of military rule under General Pinochet (1973-1990) who deposed a democratically elected President Allende. In sum, these statistical and social indicators

[2] While beyond the scope of this chapter, issues of aggregate data such as GDP and GNP do not reveal uneven wealth distribution across people and regions.

document Chile's placement high atop the developing countries index, at the border of the "developed" category.

6.2. GEOGRAPHY AND TOPOGRAPHY

One very influential element in Chile's development and its social, cultural, political, economic, and communications situation is its geography. Chile is a very long country (4,270 km of contiguous territory plus a long archipelago terminating in Antarctica), with a narrow width (averaging 177 km east to west). This width is deceptively large as the presence of the Andes mountains to the east, to the west the Pacific Ocean borders the nation with rugged coastal territory. Together with the mountains an oceanside take up much of the possible livable or traversable space. Moreover, and perhaps as a result of its topography, Chile is a sparsely populated country. Its density index is 192nd in the world compared to Haiti's 31st. This translates into 22.6 as compared to 361.5 inhabitants per square kilometer (Navia, 2010).

In particular, the transportation and communications implications of geography and topography and population density are great since, as communications scholars have documented, communications and transportation are nearly symbiotic until the development of electronic and digital media. To wit, communications lines historically have been erected alongside transportation lines. In fact, as Guback and Bettig (1987) have noted, in the German language of the nineteenth century there was only one word for both communications and transportation. The history of communications technology documents that transportation routes which often privilege commerce and military operations over interpersonal travel, provide the framework for communications. For example, telegraph poles run parallel to railroad lines, as the original semaphoric system of telegraphy was connected to railway stations. As well, communication lines follow imperial paths rather than domestic needs (Smith, 1980). This means that in most countries with a colonial history—as is the case with Chile-- transportation, and thus communications networks, flow from the internal areas of the country out to a port that connects via waterways with the mother colony. In Chile this means that major ports such as Iquique in the north, Valparaíso in the central region, and Talcahuano in the south served as a departure point for exportation of raw materials and arrival point of colonial settlers, expert knowledge, and capitalized goods. Given its long and narrow terrain, Chile has traditionally depended and continues to depend on these three major ports for international commerce. Until the twentieth century, sea-lanes accounted for most of the transportation, especially in regards to commerce, from north to south as well as for communications from east to west [3]. Even in contemporary times, transportation of goods, especially major agricultural exports such as fruit, seafood, lumber, and wine, is still carried out partly through sea lanes. Communication with

[3] Most notably the British controlled underwater cables that transported communications. This was a major part of the reason that the US invested so heavily in telegraph and radio technology.

seafaring modes of transportation remains of essential importance. The most reliable form of sea to shore communication is radio.

Finally, another item of relevance to the study of transportation and communications is the reliance on the one north-south road, previously known as the Panamerican Highway[4] and now as Highway 5 (Route 5). It is imperative that in such a long country, this highway serve as the major avenue of material delivery and human transportation within the country. Food, people, and newspapers—all of those that travel on land--rely on this highway to reach markets and people. In the case of crisis, or political turmoil, any disruption of this highway can have disastrous effects in terms of scarcities and isolation. For instance, one of the destabilizing tactics used by those seeking to topple the Allende government in the early seventies (1970-1973), was to pay off the truck drivers to strike and thus create immediate food shortages throughout Chile, especially in the highly populated central region that not only relies on food from other regions but also is the seat of most of the political power in the country. With that knowledge in mind, the north-south transportation corridor is of great strategic importance to the country. A disruption caused by a natural disaster, such as a major earthquake, inevitably will lead to destabilization and food shortages.

There is also research on disaster communications drawn primarily from the sub-fields of disaster medicine and information technology deployment. Scholars in these areas note that “during a disaster communications may be congested or misused” (Garshnek and Burkle, 1999). Success or failure of a disaster response is often determined by timely access to communication and reliable information (Ibid., p. 213). Establishing efficient, rapid, and reliable telecommunication pathways to facilitate sharing of transportation and information reduces mortality and morbidity. Whereas in some cases (such as Haiti) the communications system was “inadequate or nonexistent,” in others (such as Chile) the “disaster itself is responsible for immobilizing the existing communications infrastructure” (Garshnek, Sinchi, and Burkle, 1998, p. 223).

6.3. REGIONAL DISPARITIES

Another background element of relevance to this report is the regional distribution of population, media, and power in Chile. Although a rather recent historical trend, by 2010 88 percent of the 17 million Chilean population is urban. This nearly reverses the distribution of population in just four decades. Furthermore, the bulk of the urban population resides in the greater Santiago metropolitan area with 40 percent or 6.8 million people concentrated in that city and another 2 million in Valparaíso. The uneven distribution of population generates an uneven concentration of political and financial clout that in turn negatively affects those regions beyond the greater metropolitan area of Santiago in terms of distribution of resources. The implications for a natural disaster

[4] This highway theoretically runs the length of The Americas south of the US border. However, in some parts the Panamerican Highway is more of a metaphor that a real road.

is that resources will first be deployed in the central metropolitan area, regardless of need or intensity, and will slowly, if ever, trickle down to the area closer to the epicenter that falls outside the metropolitan region. This concentration of population, power, and resources inevitably includes interpersonal and mass media as a means of communications. For example, landline telephony is more widely available in the Santiago metropolitan region than anywhere else in the country, and even there landline accessibility is not total. This concentration of land lines means that until recently much of the population had to rely on public telephony, or even more recently, mobile telephony. The same applies to television—with original deployment first limited to downtown Santiago. Radio remains a much more widely available medium.

6.4. POLITICAL TRANSITION

The earthquake on February 27, 2010 came at a time of political transition for Chile, thirteen days ahead of the scheduled transfer of power from Michelle Bachelet, a left of center president of the coalition Concertacion that had ruled the country since 1990 when President/General Augusto Pinochet had stepped down after seventeen years in power. The incoming President Sebastian Piñera represents a right of center coalition. Thus, part of the contributing factors to the post-earthquake confusion was a power vacuum and struggle and difficult communication between the outgoing president Bachelet and the incoming president Piñera. The ministerial and bureaucratic government staff, many of whom are politically appointed, were also in a state of disarray. Bachelet's staff was moving out, and Piñera's staff was either moving in or yet to be appointed. While the original response to the earthquake was voiced by President Bachelet, much of the resources devoted to earthquake recovery were in fact decided by the incoming president who, in turn, was forced to abandon, or at least background, most of his proposed campaign promises in the wake of the urgent needs following the disaster.

6.5. SEASONAL AND OTHER TIMING ELEMENTS

The February earthquake occurred at the end of Chile's summer vacation season. In fact, schools were to begin their fall instruction the Monday after the earthquake. As well, the earthquake happened on a Friday night, the beginning of a weekend in the last weekend of the summer season. All of these elements are relevant in terms of where people were at the time of the earthquake. To begin with, many in the middle class were either still away on vacation or making their way back to the major metropolitan areas. Many young people were still up partying at 3:34 a.m. local time. Not many people were on the road or in public places at that time of the night.

There are positive and negative outcomes of the timing of the earthquake. To be sure, the lack of people concentrated in schools, roads, or major shopping centers prevented possible chaos and casualties. The vacation time meant both that many people were away from the urban areas but also that many of the people who would

manage the crisis were not at work or even around the cities at the time. The late night hour meant that workers, say in emergency alert posts, were also not at work. Reconnecting people, either in person or via forms of communication, was a major challenge after the earthquake—a challenge that in the case of coastal communities, cost life and material damage.

Given its rather developed status and high literacy rates, Chile has a thriving media system. Prior to the military coup Chile had a vibrant newspaper culture that has begun to recover since 1990. As well, Chile's radio and television development and deployment followed traditional lines of expansion, from the major cities first to the provinces later. Radio networks traditionally lay in the hands of powerful economic sectors—for example, Radio Minería belonged to the powerful copper mines. Like in many countries, Chile's television network was first operated by large universities and was not commercial, and only since the eighties has it transitioned into private sector ownership and prominence with a minimum presence of public broadcasting. As with other highly networked countries, Chile has exhibited, over the past decade, a growth and reduction in absolute and proportional numbers of internet connectivity trough dial-up and then growth through other connectivity forms such as digital subscriber line (DSL) and wireless means. Similarly Chileans have adopted mobile telephone technology, especially as landlines were difficult (if not impossible) and very expensive to get in many locations.

Whereas scholars find that "land lines provide the links between nodes in telecommunications networks and offer point-to-point transmission along a wire or fiber-optic cable medium … The disadvantages related to disaster management are that land lines cannot attach to anything mobile, cannot reach remote locations economically, cannot broadcast a signal simultaneously to all parts of a continent, and the system may be damaged during a disaster." (Garshnek, Sinchi, and Burkle, 1998, p. 224). All of these factors took place in Chile following the earthquake. Given that most of the damage was suffered by remote locations, the limits of reliance on landline telephony and integrated digital networks were clearly exposed.

Transnational flows of population and capital result in external communications networks. Communications research shows, much like with internal national networks, that international communications networks are developed to facilitate transfer of information about capital and military. Nonetheless, there is also a need for people-to-people communication. While cosmopolitan and upper middle class professionals who experience high degrees of mobility make use of these networks, recent development of digital technology also facilitates their use by other groups such as seasonal, undocumented, or working class migrants. Local telephone centers, cheap telephone cards, and now—internet telephony such as Skype—enable those with limited resources to stay connected to their homelands. One need not own a personal computer with home internet access as internet centers allow low-income people to

access social networks such as Facebook as well as to make Skype calls and check e-mail.

While Chile does not match the level and magnitude of migration as countries like Mexico, it has experienced waves of outward migration due to political changes. Thus, there are far flung Chilean communities dating back to 1970 and 1973. Additionally waves of German and Italian migrations to Chile result in transnational flows to and from those two countries. Moreover, the level of education and development of the country means that professionals also have transnational careers and that businesses send Chileans abroad as well as non-Chileans to Chile. Thus given its national development as a globally integrated economy, news about Chile and its earthquake were likely to be covered in countries with whom it shared strong migration flows and economic ties.

Finally, Chile serves as a regional node of immigration for countries whose economies are not as strong. Immigrants from Bolivia, Peru, and Argentina currently expand the transnational mix that becomes more noticeable when communications traffic increases due to a natural disaster. Therefore, due to regional proximity and citizen presence, news coverage of earthquake will increase in neighboring countries as a way to inform national population about welfare of citizens.

6.6. COMMUNICATIONS EFFECTS

A major earthquake, as this one, inevitably, was bound to cause major disruptions. While the disruptions were much smaller than the worst-case scenario due to the frequent occurrence of and therefore knowledge about earthquakes in the zone and the resulting degree of preparedness enabled by a relatively wealthy economy, the disruptions were great nonetheless. Electricity, gas, sewage, and water infrastructures were immediately disrupted with different rates of reinstatement. In particular, in terms of communications, there were some expected and some unexpected outcomes.

Government itself suffered from an immediate inability to communicate with its own agencies and military. In the case of Concepción the military was deployed by Monday 29 (two days after the earthquake) in order to gain control of the situation amidst feared looting and chaos (Volk, 2010). A curfew from dusk till dawn was instituted and enforced. In these affected areas, communication and transportation were so severely disrupted that emergency vehicles such as ambulances and fire trucks could not receive accurate information nor communicate with each other as to location of people and situations.

The magnitude and duration of the earthquake resulted in short-, middle-, and long-term disruptions. The short-term effects were felt during and immediately after the earthquake. Middle range effects comprise the effort to resume transportation and communications flow and services in the aftermath. Long-term effects refer to the reconceptualization of networks, some of which may have been damaged and others, which remain to be deployed, as the information is gathered post-earthquake. Nearly all

communications crashed immediately after the earthquake. Different elements began to be restored from within a few hours to nearly two weeks, depending on the mode and location. In the long term the entire network needs to be reassessed, especially reliance on electric and electronic telecommunications and the relative lack of attention paid to radio.

Following the initial shock of the earthquake people attempted to move to a safe place and to contact relatives and friends in the immediate vicinity and farther away. While Chilean people are used to mid-level tremors and know where to seek shelter (e.g. doorframes, outdoors, etc.), the earthquake was so strong that people could not move while it lasted. Many people did not take the beginning of the earthquake seriously—after all, they are used to strong tremors (called earthquakes elsewhere). By the time people realized that this was one of the “big ones”, it was too strong to move. This was repeatedly reported. Although everyone knew what to do and where to go during an earthquake, in the middle of this one nobody could move. Additionally, strong aftershocks occurred for weeks after the earthquake, and certainly immediately following it. The immediate aftermath of the quake resulted in total electrical outage in the affected areas. People in Santiago, Valparaíso and Viña del Mar, Concepción and Talcahuano, Chillán, Talca, Rancagua, etc. survived the earthquake only to surface in total darkness with sirens of all kinds blaring (building, automobile, and emergency vehicles and warning systems). In this setting people attempted to move and communicate. Needless to say, roads, especially in urban areas such as Santiago, Valparaíso, Viña del Mar, and Concepción became immediately congested. Without streetlights, it was difficult to see if there were transportation network failures.

People immediately attempted to make phone calls, as it was evident that there was an electrical power outage and therefore internet, television, and electric radio were not usable. Those with battery-operated radios originally could not find an operating radio station. In the affected area, Radio Bío Bío was able to transmit within an hour through its emergency generators. Those with landlines were sometimes able to make a phone call, but more often, this network crashed or functioned intermittently. Those with mobile telephone—nearly everyone with a mobile telephone—attempted to make phone calls.

In the short-term, with nearly everyone who had a mobile phone attempting to place a phone call immediately after the earthquake, the system crashed. Cell phone users tried other strategies such as sending out text and twitter messages with the reasoning that these would be somehow kept in the system and sent and received at a time when the system came back to work. In fact, this was not an unsuccessful approach as the system occasionally functioned and some of these messages were sent and received. In the middle term range, cell phones would become discharged and without electricity, there was nowhere to charge them. Cell phone companies began to send mobile recharging units to certain cities and neighborhoods. These would generate long lines of people. Electric companies also began to deploy mobile units for recharging not just mobile telephones, but that was certainly one of the uses of this effort. In the long-range

cell phone companies and digital communications industry need to expand their capacity to account for the possibility that more than 10 percent of users will make demands on the system. Given Chile's propensity for large earthquakes, this is not a remote possibility in the near future.

Nearly all disaster communications research and conventions begin with the necessity for and integrated and operable communications system. While some research stresses the importance of satellite and internet technology, in a disaster case when electricity is out of order, we return to the global mass medium, transistor radio. The keystone element of a crisis system is of communications is radio. As Manoj et al. (2007, p. 51) note "lack of radio interoperability" severely hampers disaster relief and information sharing efforts. Moreover, radio operations have to be integrated at the city, regional, and national level, across people, communities, and layers of government and other institutions that become relevant in such a situation.

In Chile, immediately in the aftermath of the earthquake radio communication was interrupted. However, radio station emergency generators were activated by some radio stations and they became a primary and, in many cases, the sole source of mass media information for people and governments in the affected regions, especially those farther away from Santiago wherein communications and transportation were more quickly restored.

Ham radio operators had legal agreements with the government with legal clauses written specifically for the case of earthquakes (Title VIII, Article 53—which states "In exceptional cases such as earthquakes …. This network will be activated as the emergency network."). Immediately following the earthquake, the emergency network determined that there was a "dead zone" of transmission between Rancagua to the north of the epicenter and Valdivia to the south, a 761 km swath. Within 10 minutes of the earthquake the ham radio network was activated and in operation. By 4:10 a.m. there was an alert distributed about the tsunami. However despite the thousands of messages sent, and the fact that access to this network was free and continuous within the network, the lack of organized interaction with authorities rendered its efficacy less than useful and in some cases altogether negligible.

Newspapers as well suffered a break in production. In Concepción two days passed before local newspapers, El Sur and El Diario de Concepción, could begin to distribute, in much shorter versions dedicated totally to the earthquake aftermath. Since distribution channels were also disrupted, newspapers were sold on street corners by people yelling out the name of the newspapers, like in the nineteenth century, and quickly sold out whenever available. This traditional form of media was in high demand, especially against the backdrop of intermittent electric and electronic media availability.

Interviews with some close to the epicenter revealed that most people suffered at least two days of total lack of infrastructure: water, gas, sewage, electricity, and any form of communications other than interpersonal. As many said: "nos fuimos a la negra" (we lived through a total black out). People tried to reach their families, and for those

who managed to, they stayed in an extended family situation for as long as two weeks. Others who were in far flung places on vacation took many days in returning due to transportation and road issues as well as local restrictions on traveling after dark. Everyone agreed that the main form of communication was interpersonal, word of mouth.

Return to a fully networked communications status took up to two weeks. Within 24-48 hours local newspapers and radio stations were available in most urban and suburban settings. By Monday, those connected to larger organizations (government, corporations, and the military) in the large cities, but especially in Santiago secured access to networked electric and electronic communications. In particular, this institutional connection to networked resources proved crucial in sending and receiving communication to and from abroad for those with transnational connections. More efficient than emailing, those connected to Facebook found that posting a general message such as “La familia Nahuel esta bien—todos” (The Nahuel family is well—all of us) was much more efficient and economical than trying to individually call or email single individuals. Transnational triangulation was also possible. For example, someone living in the U.S. with a cousin in Germany could try to find out via that German connection if they had heard from common relatives and friends in Chile. This networked set of connections were accessed by people of all socioeconomic status, from migrant laborers to highly paid professionals, as a way of finding out and distributing information about particular individuals and families.

Whereas those connected manage to get news of their status out to others, those in the region without these connections might remain more or less unconnected for a week or more; in most households there was a week gap in electric power. Even up to the time of the MAE Center trip in April there was still little knowledge about communities to the south of Bíobío. Most of the recovery and assessment effort began in Santiago, though it was not the most affected region. Efforts flowed, not very evenly nor rapidly, through other cities. Remote villages and populations fell beyond the scope and original impulse of the communications and recovery effort.

6.7. COMMUNICATION FAILURE

Despite the infrastructural disruptions and damage mentioned in the previous section, there was relatively little material damage and human loss of life in relation to the magnitude and length of the earthquake. However, the total failure in communications meant that populations could not be warned about the impending tsunamis that hit the coastal areas following the earthquakes. Whatever warning systems were in place on paper did not function at the time. Whether this was completely due to the failure of telecommunications systems or if there was also an interpersonal communications element to it, remains to be further investigated. Some of those interviewed suggested that there was a social occasion in which many of the emergency warning personnel were participating. The MAE Center team also

interviewed a couple of dockworkers in Talcahuano, the port city near Concepción, and they claimed that they called the Coast Guard to find out if there was danger of tsunamis and they were told “no.” These particular workers nonetheless sent people home and took high ground that is why they lived to tell the tale as their workplace was thoroughly damaged, if not destroyed, by the waves. In fact, coastal populations headed to the hills because of previous earthquake readiness training thus mitigating more extensive loss of life.

Given the character of Chile’s topography, there are clusters of populations throughout the length of the coast. Public warning systems in the networked age (Botterell and Addams-Morring, 2007) have to be tailored to the local conditions. In the case of most coastal communities in Chile, one can assume electrical power in the best of times, but in the disruption of communications that occurred immediately after the earthquake, semaphoric, sound signal, and radio messages would have been most helpful to coastal residents.

Despite not being in the epicenter zone, Santiago suffered some disruption and damage. Beginning with the airport as a zone of entry into the country, minor damage and necessary mandatory inspections caused it to close for two days following the earthquake and to operate below full capacity for another week. Cities and regions most affected took longer, still in process as per the conversation of the MAE Center team with the mayor of Talca and according to Volk (2010). The regional tendency to spend more resources on the capital city bore itself out in this case. Despite or perhaps due to its being less affected, repairs in Santiago were addressed first.

6.8. CONCLUSIONS

Major international media are deployed according to geopolitical reasons. Similarly, coverage of international news is as much about geopolitical interests of the covering country as it is about “objective” facts. Therefore, countries that matter to major global powers are more likely to have media coverage and correspondents than those whose participation in geopolitics is more marginal. In addition, media coverage centers on major cities. This is the case in the U.S. as much as in any other country. For instance, the San Francisco earthquake of 1989 (known as the Loma Prieta earthquake) was originally covered by local broadcasters and reporters because that city is not considered major enough to have major international correspondents. Thus if an earthquake occurs in any other city, coverage will be filtered through the location of the major city. In the case of the *New York Times* coverage, the stories by-lined by Mark Lacey were filed from Lima, Peru.

In the case of Chile, due to its status as a node of economic productivity and bilateral trade agreements with the U.S. as well as extensive trading with European and Asian countries, there were quite a few international correspondents in Santiago. Original coverage came from Santiago and foregrounded the damage and disruption in Santiago. There was less coverage about Valparaíso and Concepción, and much less

coverage about the areas closer to the epicenter and thus most damaged such as Talca and Constitución. Somehow the *New York Times* early reports included photographs from Talca and Constitución (Figure 6.1), though CNN reports pictured mostly the damage in Santiago (Figure 6.2).


Major Quake Jolts Chile, Setting Off Pacific Tsu

The quake in Chile on Saturday caused severe damage, including in Talca, above. The epicenter was about 70 miles from Concepción, Chile's second-largest city, but Santiago, the capital, also shook for nearly 90 seconds. More photos are at nytimes.com.

Figure 6.1 Front page New York Times article and photo on February 28, 2010—the day after the earthquake. While the photograph is of Talca, most of the article focused on the damage in Santiago and Concepción

Figure 6.2 Photograph from cnn.com on February 27, 2010, Santiago damage

In the aftermath of the earthquake, international news covered some of the major elements of damage, such as the building Alto Río in Concepción (Figure 4.19, see Section 4.2), and some of the more spectacular—especially visually—photographs about the destruction after the tsunami, especially in Talcahuano as this city is easily accessible from, indeed connected to, Concepción. In accordance with the patterns of international coverage, news of the earthquake were quickly replaced with other international news as the middle and long range effects became more pronounced and the immediate aftermath was no longer news. Middle and long term effects are often not considered "news" as these are much more difficult to discuss and difficult to visualize. In the United States, little about the earthquake was even mentioned after mid-March, except in Latina/o media where it continued to be a news item, even if not in the front page. In the popular Univisión show "Sábado Gigante" Don Francisco, its Chilean host, occasionally focuses attention on the victims of the quake and raising funds to send to Chile.

While the epicenter of the earthquake was closest to a city called Constitución, the closest big city is Concepción. Needless to say, there was little media presence in Constitución which is 234 km from Concepción. As well, Constitución cannot be reached directly by the Pan-American Highway (Route 5) but by far less traveled Highway 126 and a combination of other coastal roads that also suffered much more damage from the earthquake than Route 5. Not only were media not able to reach that city and other coastal communities easily but neither were warnings and emergency help. Had the city not engaged in recent earthquake preparedness, which included possible post-earthquake tsunami drills, more citizens might have perished. Scholarship on disaster communications shows that "Success or failure of a disaster response is often determined by timely access to communication and reliable information… Establishing efficient, rapid, and reliable telecommunication pathways to facilitate sharing of transportation and information will reduce mortality and morbidity" (Garshnek and Burkle, 1999, p. 213). This lack of communication and reliable information had disastrous consequences in Constitución. As significant portion of the total casualties from the earthquake were from Constitución due to the tsunami. National and international media, however, have reported little directly from this most affected city and region as it is both difficult to reach via roads and it is also, for the same reasons, not a hub of media production or coverage.

New media, such as digitally delivered internet access for personal and business/institutional uses has been singled out in recent research as a key component of emergency help delivery post disaster. For example, Garshnek et al. (1998) single out satellite communications as a reliable technology. Sun Oh (2003), Meissner, et al. (2002), and Botterell and Addams-Morring (2007) also include satellite, digital, and electricity intensive telecommunications systems as part of their strategy for managing communications during a disaster. However, as Manoj and Hubenko Baker (2007) note: "Above all, the emergency communication tools for the general public must be affordable, available, and applicable during their day-to-day life in order to ensure that

they will be used during a crisis" (p. 52). Affordability and availability in relation to new technologies is something that is very much interrelates to socio-economic resources. The presence of business and government institutions in the big cities, especially in the capital city of Santiago, meant both that not only those institutionally networked systems but also that a swath of the population is able to afford to be networked at home. Concepción (ca. 900,000 people), though much smaller than Santiago (ca. 6 million people), also has some big businesses, government, and educational institutions that provided workers with access at the office and with the salaries to afford access at home.

While the earthquake resulted in near total blackout up through the Santiago metropolitan area for at least 24 hours, by Monday morning many of those whose jobs included digital connectivity could draw on those resources to communicate regionally, nationally, and internationally. Some reported that they were able to Skype from work to loved ones in the more affected region. Landlines were among the first to work sporadically so Skype to landline was an early tactic. Internet social network postings such as Facebook were also quite useful as were individual emails. However, these options were only open to those with access to institutions whose power supplies were privileged over individual households. In turn, the few connected could reach a regional, national, and transnational circle of connections with an emphasis on the latter as the two former were likely to be disrupted.

Communications and transportations systems need to be accessible and reliable, especially during times of crisis and disaster. The two remain symbiotic, even in the contemporary digital era. What this means in the case of Chile or any other country is that access to roads and the ability to share information is likely to be disrupted after crisis and/or disaster at the precise moment when that access is most urgently important. Whereas much of contemporary research on disaster communication and crisis warning singles out satellite and digital technology as a crucial component of a strategy of recovery, the preliminary accounts from the ground in the Chilean situation suggest that we need to reconsider and re-foreground traditional media. Both government agencies and individuals were hampered in their efforts by their reliance on the new communications technologies. The total electric black out immediately after the earthquake and the less than organized alternative communication network response meant that the warning of impending tsunamis did not reach its target audience, the coastal population near the epicenter. Most of the loss of life was due to this failure in communications. While, the material damage, although large in absolute numbers but small in relation to the magnitude of the earthquake, was mostly inevitable—that is, the country was not prepared for 2 meter waves and earthquake based damage was to be expected in many settings because of a complex set of variables (e.g. the mostly adobe structures in the historic downtown of Talca dated back to an age where seismic construction was not part of the equation), the loss of life in the coastal regions was more or less easily preventable.

Foremost from the perspective of communications systems, there is a need for individuals and institutions to keep a backup system of communications. The most reliable and affordable such system is a network of battery powered radio receiver and/or ham radio equipment. This network does not rely on electricity and can cover large distances, especially in the coastal area[5]. This means that local and national governments, as well as the military, have to create and support such a network. In turn, this network needs to be integrated so that inter-agency communication can occur in disaster times when access to information is so crucial. National and regional governments need to keep information, and possibly support, a network of generator powered ham radio operators to provide back up when electric and electronic networks fail. Of course digital and satellite supported communications networks are not irrelevant, but we cannot rely on these since they are highly susceptible to failure in times of natural disaster, especially in world regions where the network may not be as strong or as broad as necessary. For instance, many people still are not internet connected and thus disconnected from broader network that internet allows. This network particularly needs to be strengthened in coastal region. A skeletal emergency network needs to be maintained 24/7.

As a complementary network, digital mobile telephony providers need to expand network capacity so it can better sustain the high demands of another potential occurrence of earthquake or other natural disasters. While one of the two national mobile telephony networks bounced back a bit sooner, the fact remains that neither was able to function under maximum demand.

Another element in the communications outlook is that in times of crisis people revert to traditional networks of familial and interpersonal communications. In this sense, transportation networks are crucial as in the modern world, including in Chile, families do not live in the same household or compound. This meant that the immediate reflex of most Chileans was to travel “home.” This caused major congestion in dark roads, some of which were damaged. A public service media campaign instructing residents on evacuation and also on the feasibility and timing of traveling “home” is in order.

As noted by communications scholars, transportation and communications networks are inextricably entwined especially in times of crisis. Much touted de-centralization promises of electronic network did not come into effect during time of crisis. Traditional media served information needs for the population. A better integrated ham radio network would also help government and military needs. This is not a call for great infrastructural investment but for a return to the mass media which has proven to be more reliable in this setting and under similar circumstances.

[5] Radio transmission in mountainous regions is a bit more prone to interference, but even there it remains the most reliable in times of natural disaster.

6.9. REFERENCES

Botterell, A. and Addams-Morring, R. (2007), Public Warning in the Networked Age: Open Standards to the Rescue?, Communications of the ACM, 50: 3, 59-60.

Dupuy, A. (2010), After the Earthquake: Recovery and Sovereignty in Haiti. Latin American Studies Association: Forum, XLI: 3, 13-15.

Garshnek, V., Sinchi, K. and Burkle, F. M. (1998), Disaster assessment and satellite communication: on the threshold of a new era, Space Policy, 14: 4, 223-227.

Garshnek, V. and Burkle, F. M. (1999), Telecommunications Systems in Support of Disaster Medicine: Applications of Basic Information Pathways, Annals of Emergency Medicine, 34: 2, 213-218.

Guback, T. and Bettig, R. V. (1987), Translating the Manifesto into English, Journal of Communication Inquiry, 11(2), 3–16.

Han, C. (2010), Earthquake in Chile: Poverty and Social Diagnoses, Latin American Studies Association: Forum, XLI: 3, 9-12.

Lerner, D. (1958), The Passing of Traditional Society, Modernizing the Middle East, Free Press: Glencoe, IL.

Manigat, L. F. (2010), Opportunity Amidst the Wreckage: Rebuilding Haiti's University System, Latin American Studies Association: Forum, XLI: 3, 19-21.

Manoj, B. S. and Hubenko Baker, A. (2007), Communication Challenges in Emergency Response, Communications of the ACM, 50: 3, 51-53.

Meissner, A., T. Luckenbach, T. Risse, T. Kirste, and Kirchner, H. (2002), Design Challenges for an Integrated Disaster Management Communication and Information System, The First IEEE Workshop on Disaster Recovery Networks (DIREN), New York City, co-located with IEEE INFOCOM.

Navia, P. (2010), Small Earthquake in Chile: Not May Dead, Latin American Studies Association: Forum, XLI:3, 6-8.

Smith, A. (1980), The geopolitics of information: How Western Culture Dominates the World, New York: Oxford University Press.

Sun Oh, E. (2003), Information and communication technology in the service of disaster mitigation and humanitarian relief, Communications, 2: 730-733.

Volk, S. S. (2010), The Chilean Earthquake of 2010: Three Perspectives on One disaster, Latin American Studies Association: Forum, XLI:3, 3-5.

Vorbe, C. (2010), Earthquake, Humanitarianism, and Intervention in Haiti, Latin American Studies Association: Forum, XLI:3, 16-18.

6.9.1. Web references

United Nations Children's Fund (UNICEF)

Nation Master

a. Regions
b. Media
c. Internet
d. Energy

Organization for Economic Co-Operation and Development (OECD)

a. Publications

Instituto Nacional de Estadisticas (INE) de Chile

a. XLS files

Fast Company (social media after quake)

United Nations Educational, Scientific and Cultural Organization (UNESCO)

a. Public Reports

Nick Burcher (Facebook)

Sysomos

Inside Facebook

United Nations Development Programme (UNDP)

7 SUMMARY AND CONCLUSIONS

On February 27, 2010 at 03:34 am local time, a major earthquake of magnitude 8.8 struck central Chile. The earthquake nucleated in the subduction region between the oceanic Nazca plate and the continental South American plate. The epicenter of the earthquake was approximately 8 km off the Chilean coast (35.909° S, 72.733° W) and the hypocenter was located at a depth of 35 km. The fault rupture zone covered a region of approximately 100,000 square kilometers, causing major disruption and losses. The earthquake magnitude, its source and mechanism of rupture are expected. There have been over 25 major earthquakes with magnitude greater or equal 8.0 in the past 500 years.

Whereas over a million people were affected by the earthquake, the total damage due to ground shaking and the tsunami that followed is relatively limited. Less than 2.5% of the engineered building stock was damaged, while a total of about one third of a million buildings, mostly non-engineered suffered varying degrees of damage. About 530 people died, including about 200 who were killed by the consequential tsunami. There are different estimates of direct economic loss; Chilean sources indicate a direct economic impact bill of $30 billion. Whereas the death toll was much lower than the large magnitude would have implied, the earthquake was highly disruptive to the life and livelihood of a large proportion of the population. One of the most devastating effects of the earthquake was the impact on land, sea and air transportation, and telecommunications, as detailed below.

Few records from the earthquake were made publicly available; of those the CCSP station recorded peak accelerations in the three directions (0.61g, 0.58g and 0.61g in NS, EW and UD) are quite high and of approximately the same value. The duration of this record, assessed from the plot of energy versus time, is approximately 70 seconds, which is consistent with the magnitude. The bracketed duration, with a threshold of 0.05g, is much longer, yielding 100-120 seconds of strong ground shaking for the CCSP record. It is imprudent to draw general conclusions from such a small number of recordings, especially that most of them were only available in picture form, hence cannot be processed and interrogated. It is however observed from the available spectra that the shaking amplification exceeded substantially the Chilean code requirements in the period range from 0.2 to 0.7 seconds. The Chilean code seems to envelope the recorded motion spectra very well for longer and shorted periods.

The restrictions that were imposed on the measured earthquake records that have not been available until the time of publication of this report has adversely affected the quality of the investigations undertaken. It is strongly recommended that the issue of public release of earthquake records immediately after the earthquake be addressed and arrangements made to ensure the wide dissemination of records for use by the engineering and seismology communities.

The earthquake has resulted in failures in a number of geotechnical systems including embankments, port structures, bridge and building foundations and was in many cases consistent with observations from prior earthquakes. Numerous highway and roadway embankments failed due to either liquefaction of underlying soils or due to what appears to be insufficient compaction of the embankment structure itself. Liquefaction and lateral spreading damaged a number of ports and bridges including approach abutments as well as bridge piers. Site amplification due to presence of soft soils is likely responsible for observed damage at a number of bridge overpasses in Santiago. On the other hand, retaining walls and underground structures including tunnels appear to have performed very well despite the long duration of shaking. It was also reported that areas where ground improvement was performed, liquefaction was prevented and building foundations performed well.

Three of the 15 administrative divisions, Santiago, Bíobío and Maule, were severely affected from the earthquake due their proximity to the fault. Santiago is the capital and largest city in Chile. PGAs in the range of 0.2 g to 0.5 g were observed. Buildings in general performed very well. A limited number of RC buildings suffered significant damage due to structural deficiencies such as soft stories, horizontal and vertical irregularities, and short-column effects. Several other buildings were damaged due to the failure of RC walls since proper confinement in walls were not required until recently in the Chilean Building Code.

The Bíobío region is located at the south half of the rupture area. Main damage to the region was in the coastal towns, which were severely damaged due to the tsunami that followed the earthquake. In Concepción, capital of Bíobío region and second largest city in Chile, several buildings collapsed and several 15 to 20 story buildings were severely damaged and will have to be demolished. In terms of transportation networks, most of the highways and streets suffered only minor damage but a few bridges were damaged or suffered collapse. While the number of failed bridges is small, they constituted critical links in the regional transportation network and led to significant impact on the area. At the time of the field investigation around one and half months after the earthquake, only 30 percent of industries were operating in the region due to the damage to structures, lack of power, or difficulty in accessing the facility. There were also failures in critical lifeline networks, such as gas, electricity, water, and wastewater.

The epicenter of the earthquake was located offshore the Maule Region. Talca is the capital of the Maule region with a population of 230,000 and a building stock of 75,000 houses. The city suffered the heaviest damage from the earthquake due to its proximity to the rupture area. In addition, there was a large number of adobe houses in Talca built without seismic provisions, thus compounding the damage. Approximately one fifth of the buildings were severely damaged. After the earthquake, the city suffered damage of critical lifeline network including gas, water, and electricity. All lifeline networks were recovered in seven-to-ten days. Downtown areas took longer to recover from damage as networks were relatively dense and therefore difficult to repair. In

general, the central valley area of the Bíobío region, was not largely affected by the earthquake except for damage to a few highway bridges and slopes. The area, however, suffered failures in water irrigation system.

Considering the large magnitude and large rupture area of the earthquake, the damage to bridge structures was relatively not significant. The majority of highways are constructed and maintained by private sectors. These highway networks are as long as 2,200 km in length and have around 2,000 bridges with spans longer than 10 m. Among these bridges, only 1 percent (8 highway and 12 pedestrian bridges) collapsed due to the earthquake. Approximately 100 bridges (50 highway and 50 pedestrian) were damaged requiring repairs.

The MAE Center team conducted case study analysis of a building and two highway bridges to investigate the failures noted during the field mission. The structures are modeled using fiber-based finite element analysis software and inelastic dynamic time history analyses are conducted. For the building structure, the analysis results indicated that during the earthquake the increased shear demand (due to presence of masonry infill walls) at the columns might have exceeded the capacity resulting in the shear failures observed during the field mission. The case studies on the bridge structures studied the role of the seismic restrainers (commonly observed in bridges in Chile) and shear keys on the bridge response. It is concluded that seismic restrainers do not have the adequate strength to limit the movement of the bridge superstructure; however, they increase the energy dissipation by increasing the friction between the superstructure and the elastomeric bearings. It is also inferred from the analyses that the strength of the shear keys is critical for the performance of the bridge. Premature failure of a shear key causes uneven and excessive displacements at the ends of the superstructure. Then the girder ends slip off from the bearing supports and result in torsion of the superstructure being accumulated unidirectionally.

Several churches were heavily damaged in the earthquake. However, relatively modern churches, such as the Cathedral of Talca, fared very well, with significant non-structural damage and minor structural distress.

There is limited data and guidelines for the evaluation of earthquake-damaged roadways. The condition of two road networks, Itata highway and La Madera road, were visually evaluated shortly after the earthquake to document typical pavement failure patterns. These two road networks were also selected because structural and functional data before and after the earthquake were available. Overall, pavements built on embankments experienced significantly more damage than other pavement sections built on grade. In general, the main distresses encountered were lateral displacement of embankment, pavement cracking due to embankment or subgrade displacement, under-drain fill settlement, and shoulder-curb separation. Embankment-related distresses appeared to be more pronounced in sag vertical curves and bridge approaches. Most of the failed fill areas met the current specification requirements suggesting a revision of current fill standards is warranted. Falling weight deflectometer

data was analyzed before and after the earthquake on one of the road networks. It was concluded that no measureable damage had occurred to the pavement structure that was not otherwise observed during the visual survey. Surface roughness data was also collected and International Roughness Index (IRI) was calculated to determine the effects the earthquake had on the pavement functional performance. As a result of the earthquake and subsequent patching, the average IRI changed 3.6 to 8.4 percent, in the passing and driving lanes, respectively. The roadway case studies highlighted and reinforced the need for developing a standardized condition assessment tool and guidelines that can be used to evaluate pavements after an earthquake.

The February earthquake occurred at the end of Chile's summer vacation season. In fact, schools were to begin their fall instruction the Monday after the earthquake. There are positive and negative outcomes of the timing of the earthquake. The lack of people concentrated in schools, roads, or major shopping centers prevented possible chaos and casualties. The vacation time meant both that many people were away from the urban areas but also that many of the people who would manage the crisis were not at work or even around the cities at the time. The late night hour meant that workers, say in emergency alert posts, were also not at work.

The earthquake on February 27, 2010 came at a time of political transition in Chile. The ministerial and bureaucratic government staff, many of whom are politically appointed, were also in a state of disarray. It is also observed that the uneven distribution of population generated an uneven concentration of political and financial clout that in turn negatively affected those regions beyond the greater metropolitan area of Santiago in terms of distribution of resources. The implications for the earthquake is that resources were first deployed in the central metropolitan areas, regardless of need or intensity, and will slowly trickle down to the area closer to the epicenter that falls outside the metropolitan region.

Communication networks were greatly affected from the earthquake, resulting in unexpected outcomes. Government itself suffered from an immediate inability to communicate with its own agencies and military. In the affected areas, communication and transportation were so severely disrupted that emergency vehicles such as ambulances and fire trucks could not receive accurate information nor communicate with each other as to location of people and situations. The total failure in communications meant that populations could not be warned about the impending tsunamis that hit the coastal areas following the earthquakes. Whatever warning systems were in place on paper did not function at the time. Return to a fully networked communications status took up to two weeks. Whereas those connected managed to get news of their status out to others, those in the region without these connections might have remained more or less unconnected for a week or more; in most households there was a week gap in electric power. Even up to the time of the MAE Center trip in April there was still little knowledge about communities to the south of Bíobío.

The MAE Center field reconnaissance team considers that Chile responded very well to the massive earthquake; an earthquake that would have totally devastated a less prepared community with a lower level of rigorous design and well-controlled construction industry. Contrasting the impact of the Maule earthquake on Chile with the impact of recent earthquakes of lesser magnitudes around the world confirms that Chilean engineering is of a very high standard and that apart from severe logistical disruption and economic loss to industry and commerce, Chile is in a reasonable state of earthquake response preparedness.

APPENDIX A – FIELD MISSION DETAILS

A.1. FIELD MISSION MEMBERS AND SPECIALIZATION

Table A.1 The Mid-America Earthquake Center team and specializations

Name	Affiliation	Expertise	Technical Role
Amr Elnashai	University of Illinois	Earthquake engineering	Team Leader
Imad Al Qadi	University of Illinois	Transportation and pavement	Focus on pavement failures
Youssef Hashash	University of Illinois	Geotechnical earthquake engineering	Focus on geotechnical failures
Jefferey Roesler	University of Illinois	Transportation	Focus on transportation systems and pavement failures
Angharad Valdivia	University of Illinois	Media and communication	Focus on the role of media
Bora Gencturk	University of Illinois	Earthquake engineering	Documentation and reporting coordinator, focus on building failures
Oh Sung Kwon	Missouri University of Science and Technology	Earthquake engineering	Focus on soil structure interaction and bridge failures
Sung Jig Kim	University of Connecticut	Earthquake engineering	Focus on building failures, ground motion processing
Jazalyn Dukes	Georgia Institute of Technology	Earthquake engineering	Focus on building failures
Seong Hoon Jeong	Inha University	Earthquake engineering	Focus on bridge failures

A.2. CHILEAN HOST ORGANIZATIONS

1. Catholic University of Chile
2. University of Concepción
3. University of Chile
4. Municipality of Talca
5. Roadway Concession Itata
6. Roadway Concession Talca

A.3. FIELD MISSION ITINERARY

Table A.2 Field mission itinerary

Date		Description
April 12	AM	Arrive in Santiago
	PM	Meetings at the Catholic University of Chile
April 13	AM	Pick-up rental cars Visit to damage sites in Santiago (Ciudad Empresarial)
	PM	Drive to Concepción (stop at bride and pavement failures along Route 5 including the case study 3)
April 14	AM	Meetings at the University of Concepción Visit the damaged buildings of the University of Concepción (including the case study 1: the Odontology Building)
	PM	Visit to damage sites in Concepción, Talcahuano and Coronel
April 15	AM	Meetings at the Roadway Concession of Itata Visit to a damaged bridge managed by the Roadway Concession of Itata (case study 2)
	PM	Drive to Talca Meetings with the Roadway Concession of Talca
April 16	AM	Meeting with city officials in Talca Visit damage sites in Talca (including the case study 4: the Cathedral of Talca)
	PM	Transfer back to Santiago and return rental cars
April 17	AM	Meetings at the University of Chile
	PM	Team leaves Chile

A.4. ROUTE AND VISITED SITES

The locations of the sites/organizations categorized under: building, bridge, historical and underground structures, ports, embankments, landslides, foundation failures, and hosting organizations; and separated by regions: Santiago, Santiago to Curicó along Route 5, Curicó-Talca-Mataquito, Talca, Talca-Chillán along Route 5, Chillán-Concepción-Talcahuano-Coronel-Lota-Arauco, Concepción, and ports of Talcahuano and St. Vicente; visited by the MAE Center team are summarized in Table A.3 through Table A.11, and shown on maps in Figure A.1 through Figure A.8.

Table A.3 Information on building structures visited by the MAE Center team

Icon	Name/Description	Latitude	Longitude
B1	Ciudad Empresarial Hotel	33°23'23.20"S	70°37'8.93"W
B2	University of Concepción - Chemistry Building	36°49'46.25"S	73° 2'13.42"W
B3	University of Concepción - Gymnasium	36°49'35.47"S	73° 2'12.10"W
B4	Case Study 1: University of Concepción - Odontology Building	36°49'32.78"S	73° 2'11.35"W
B5	Damaged Highrise in Concepción	36°49'45.02"S	73° 2'43.00"W
B6	O'Higgins Tower in Concepción	36°49'44.35"S	73° 3'16.70"W
B7	Alto Río Condominium in Concepción	36°49'41.82"S	73° 3'42.07"W
B8	Building close to Talcahuano Port	36°43'9.76"S	73° 6'29.63"W
B9	Building at the Talcahuano shorefront	36°43'6.13"S	73° 6'29.94"W
B10	Building at the Talcahuano Port	36°42'58.19"S	73° 6'28.06"W
B11	Typical adobe failures in Talca	35°25'32.82"S	71°39'2.74"W
B12	Edificio Aranjuez	35°25'40.75"S	71°39'57.46"W
B13	Tribunales de Justicia de Talca	35°25'16.65"S	71°40'3.83"W
B14	Building at the Ciudad Empresarial Business Complex	33°23'16.99"S	70°37'2.57"W

Table A.4 Information on ports visited by the MAE Center team

Icon	Name/Description	Latitude	Longitude
P1	Shipwreck at the Talcahuano Port	36°42'46.84"S	73° 6'35.15"W
P2	Port of Talcahuano	36°42'52.21"S	73° 6'30.22"W
P3	Port of Coronel	37° 1'43.95"S	73° 8'59.16"W
P4	Port Lota	37° 5'50.26"S	73° 9'33.59"W
P5	Port St. Vicente	36°43'31.86"S	73° 7'56.60"W

Table A.5 Locations of the hosting organizations

Icon	Name/Description	Latitude	Longitude
H1	Catholic University of Chile	33°29'56.48"S	70°36'48.69"W
H2	University of Concepción	36°49'45.97"S	73° 2'13.35"W
H3	Roadway Concession of Itata	36°43'47.60"S	72°51'38.39"W

Table A.6 Information on bridge structures visited by the MAE Center team

Icon	Name/Description	Latitude	Longitude
R1	Las Mercedes Bridge	34° 4'19.41"S	70°45'45.18"W
R2	Route 5 overpass near Chillán	36°35'4.79"S	72° 6'29.62"W
R3	Perquilauquén Bridge	36°15'15.04"S	71°48'49.84"W
R4	Paso Cladio Arrau	36°39'32.32"S	72°19'29.96"W
R5	Puente Mataquito	35° 3'2.56"S	72° 9'44.13"W
R6	Miraflores Bridge	33°23'39.37"S	70°46'9.85"W
R7	Lo Echevers Bridge	33°22'34.17"S	70°44'51.87"W

Table A.7 Information on historical structures visited by the MAE Center team

Icon	Name/Description	Latitude	Longitude
I1	Edificio Intendencia Maule in Talca	35°25'34.79"S	71°39'55.43"W
I2	Liceo de Niñas Marta Donoso	35°25'22.76"S	71°39'28.55"W
I3	Iglesia Los Salesianos	35°25'43.68"S	71°39'36.64"W
I4	Cathedral of Talca	35°25'33.25"S	71°40'0.93"W

Table A.8 Information on embankments visited by the MAE Center team (in addition to those mentioned in Chapter 5)

Icon	Name/Description	Latitude	Longitude
E1	Route 5 overpass embankment, to Retiro at Tucapel Mill	36° 3'4.35"S	71°46'4.82"W
E2	Roadway embankment - 5 km south of Parral	36°11'8.42"S	71°49'31.49"W

Table A.9 Information on underground structures visited by the MAE Center team

Icon	Name/Description	Latitude	Longitude
U1	Highway tunnel on Route 5	33°54'46.32"S	70°43'31.92"W
U2	Highway box structure	33°32'29.30"S	70°37'20.72"W

Table A.10 Information on landslides visited by the MAE Center team

Icon	Name/Description	Latitude	Longitude
L1	Aracua Landslides	37°14'31.97"S	73°25'16.35"W

Table A.11 Information on foundation failures visited by the MAE Center team

Icon	Name/Description	Latitude	Longitude
F1	Green building	36°42'51.36"S	73° 6'58.92"W

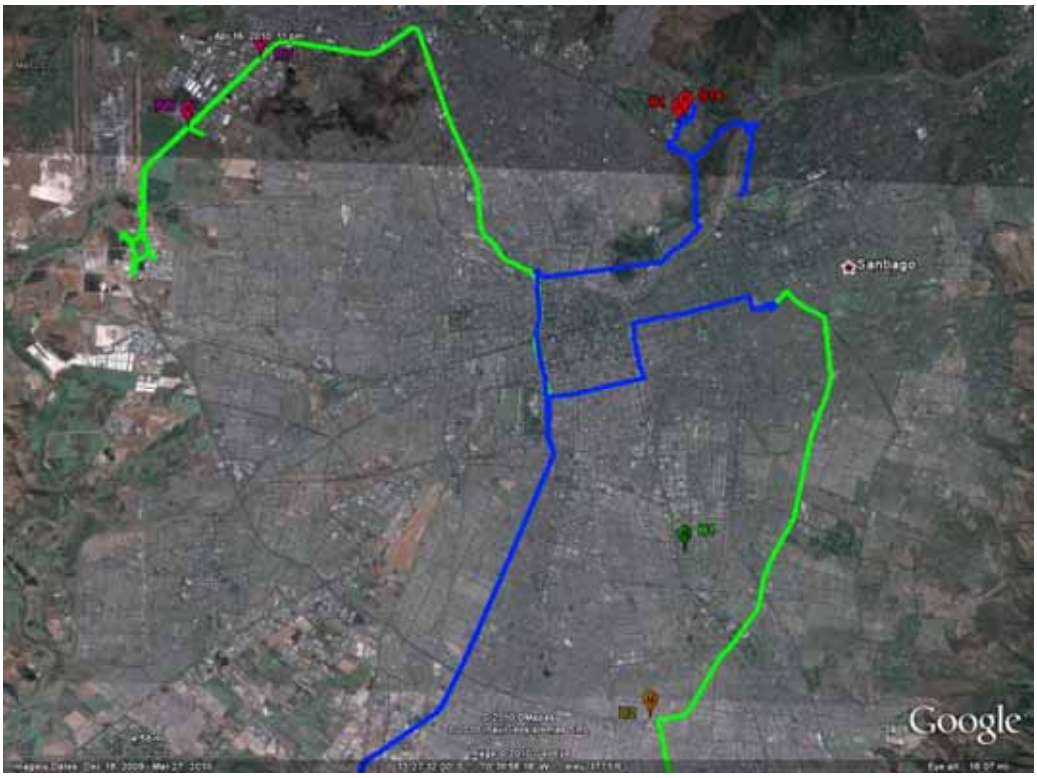

Figure A.1 Santiago region

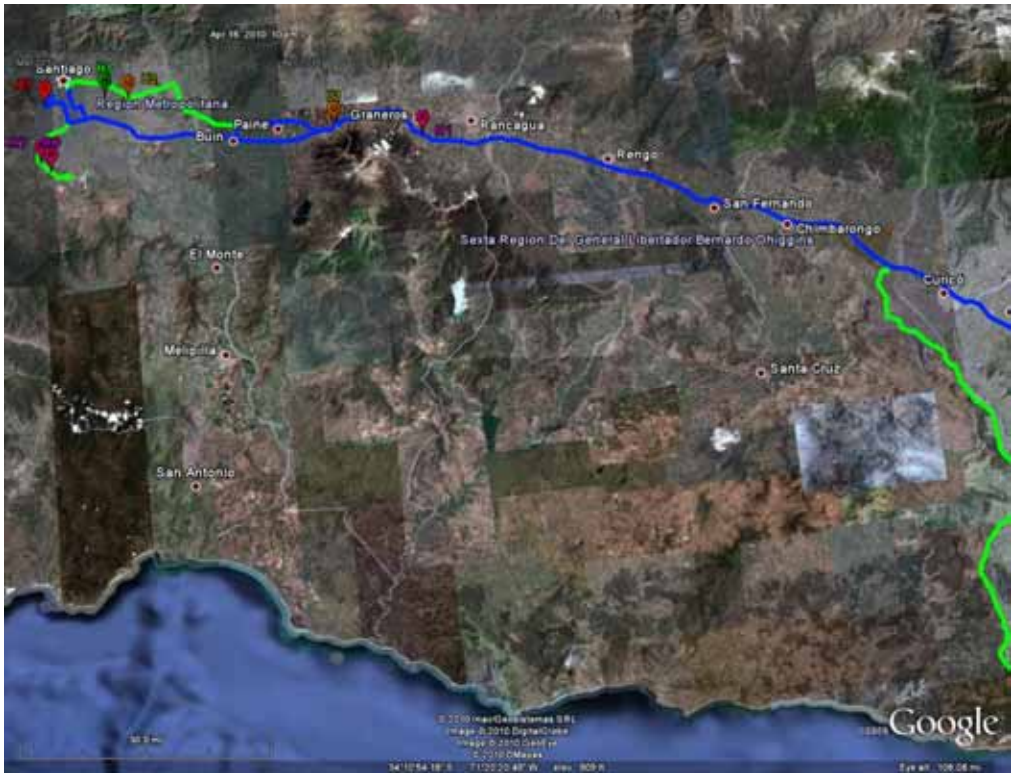

Figure A.2 Santiago to Curicó along Route 5

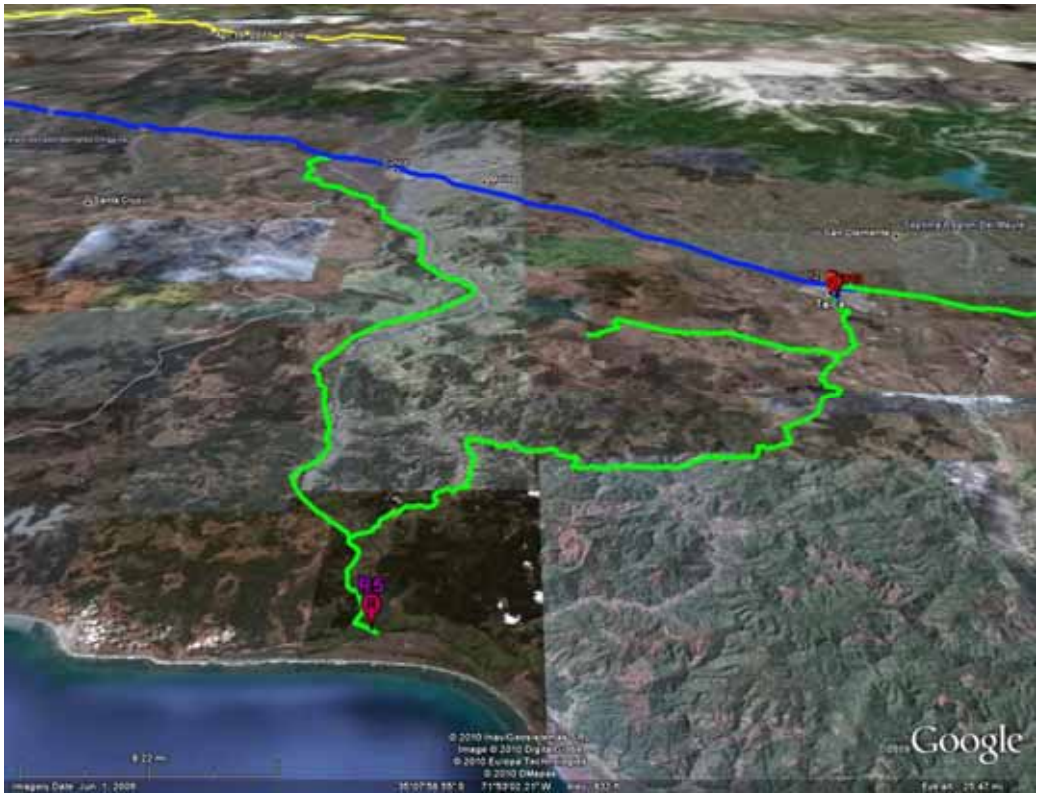

Figure A.3 Curicó-Talca-Mataquito

Figure A.4 Talca region

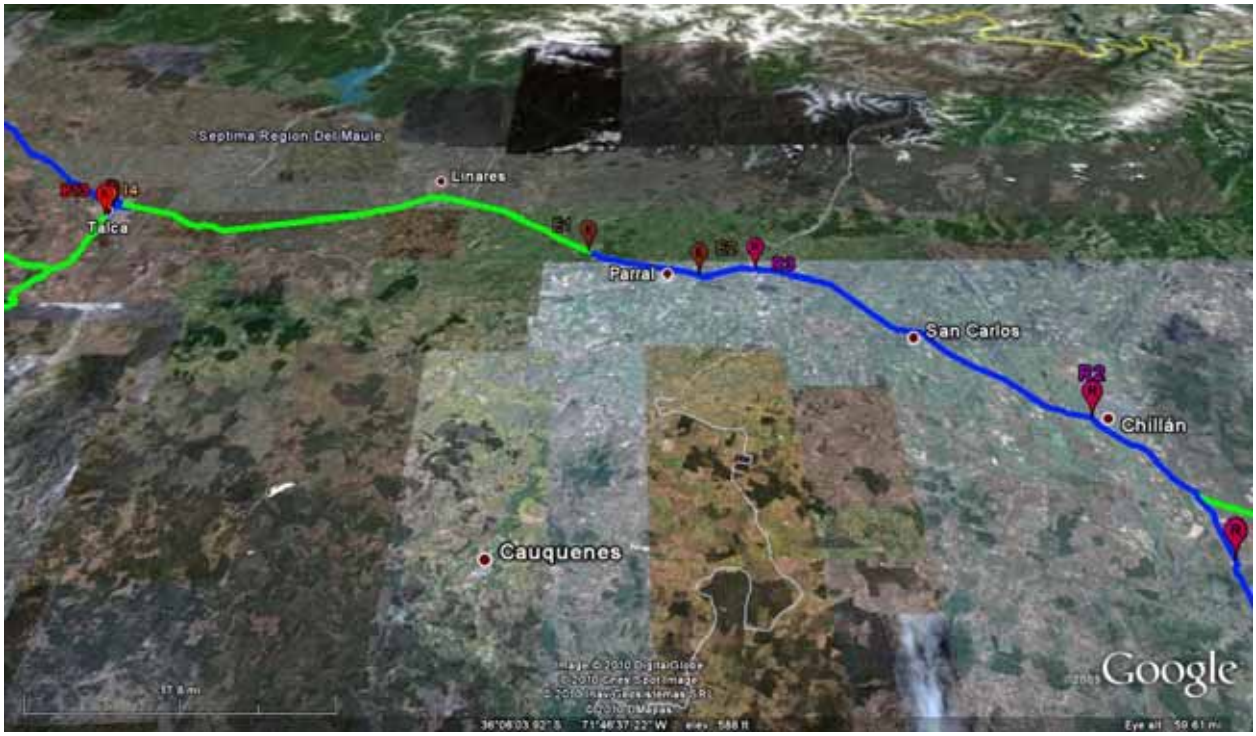

Figure A.5 Talca-Chillán along Route 5

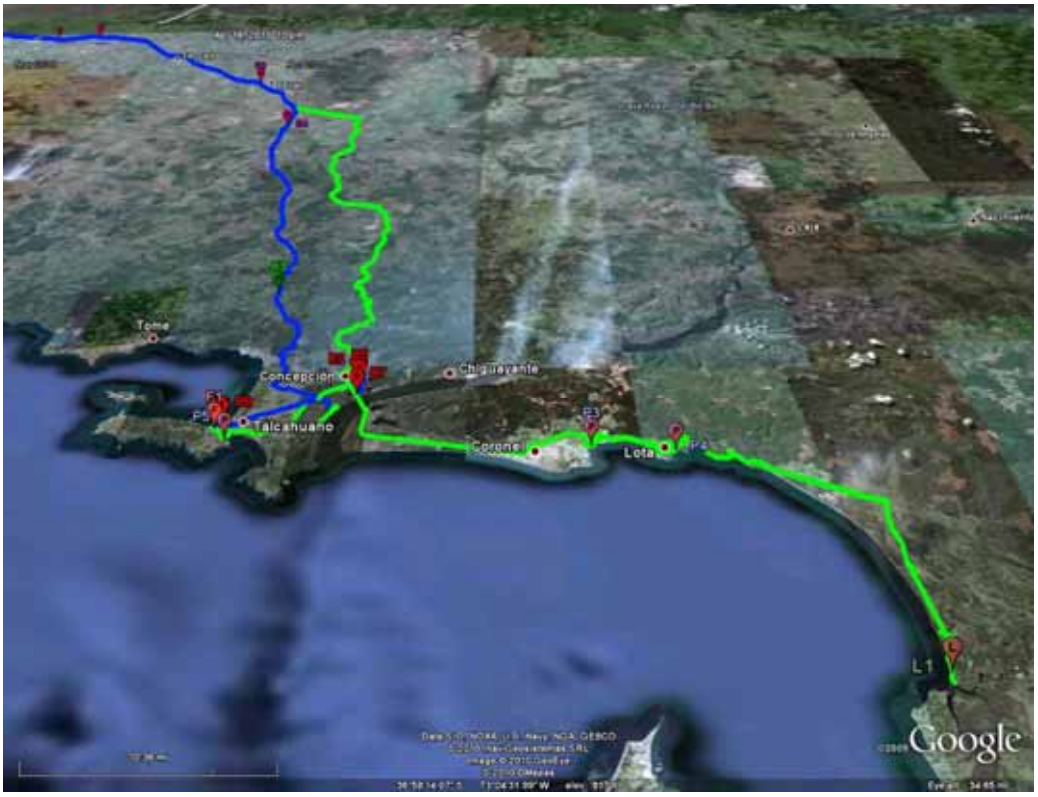

Figure A.6 Chillán-Concepción-Talcahuano-Coronel-Lota-Arauco

Figure A.7 Concepción region

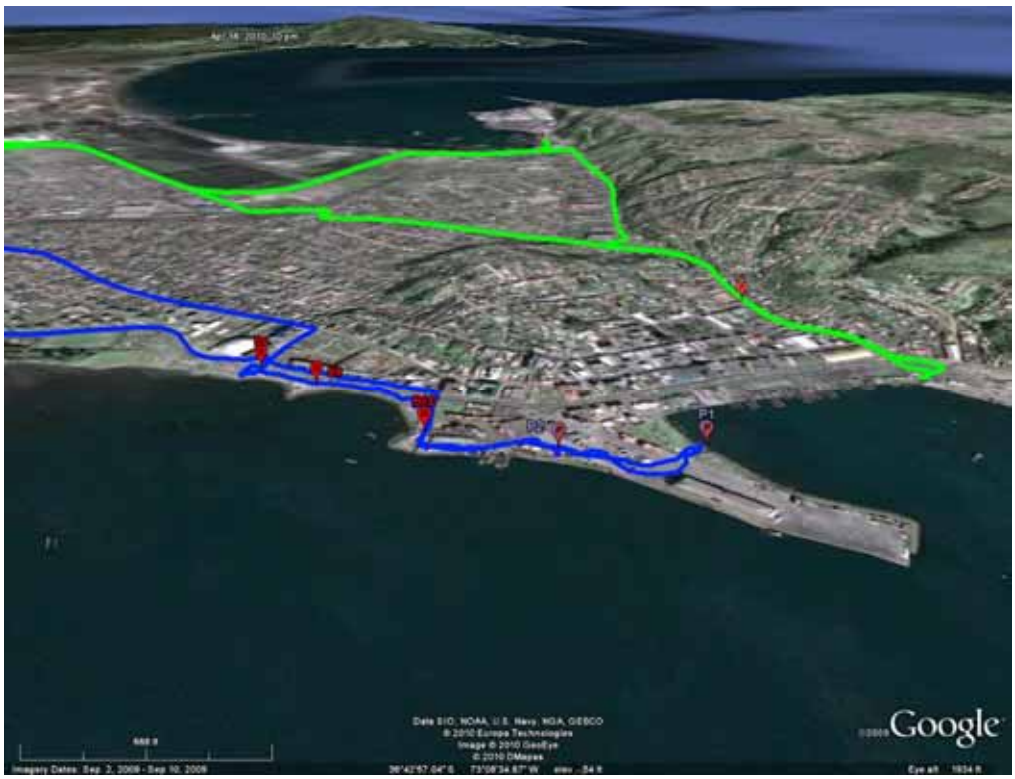

Figure A.8 Ports of Talcahuano and St. Vicente

APPENDIX B – STRONG GROUND MOTION

The information provided here is complementary to Section 2.4. For full references see Section 2.5.

B.1. PGA AND RESPONSE SPECTRA ATTENUATION RELATIONSHIPS

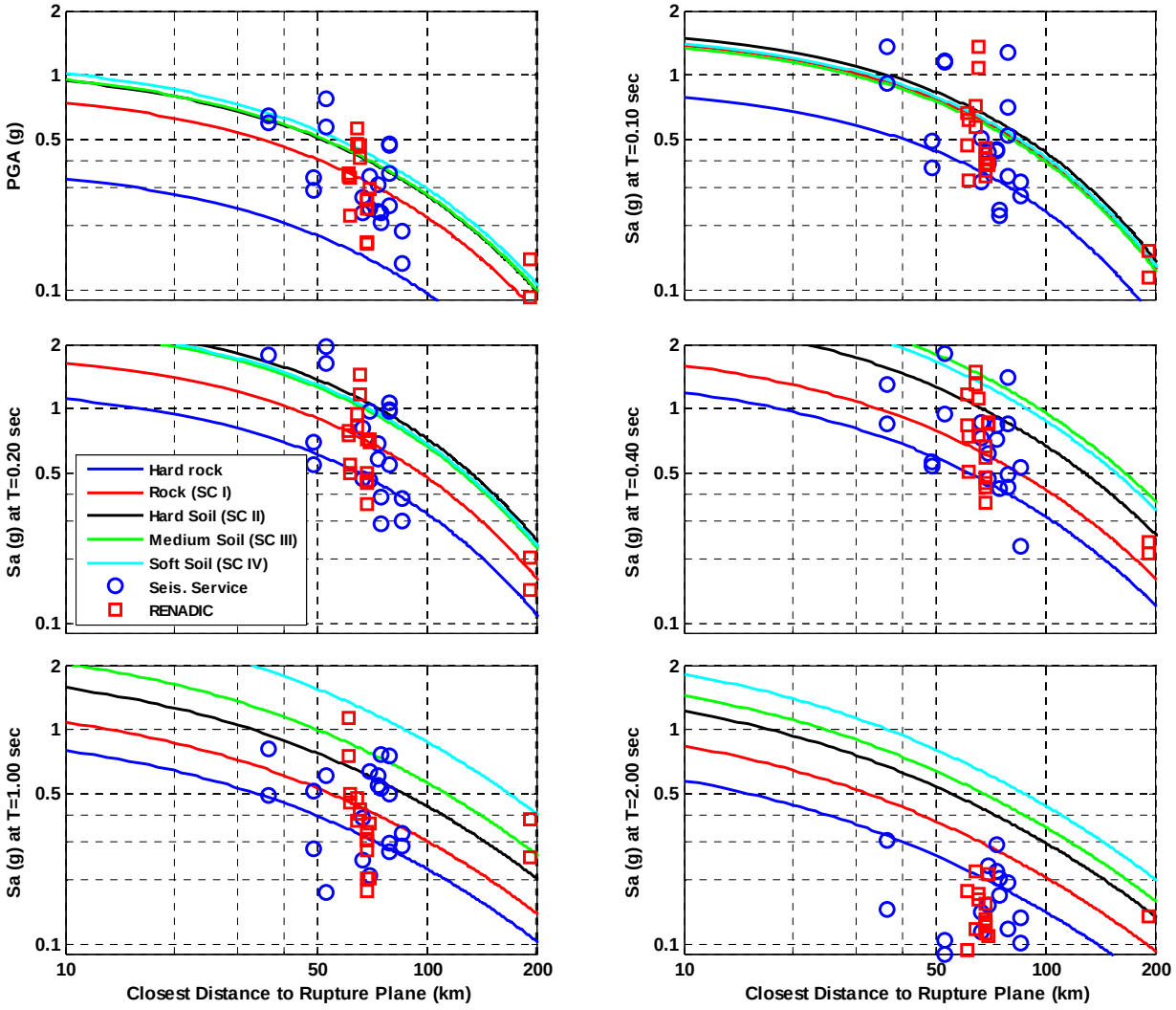

Figure B.1 PGA and response spectra attenuation relationships by Zhao et al. (2006)

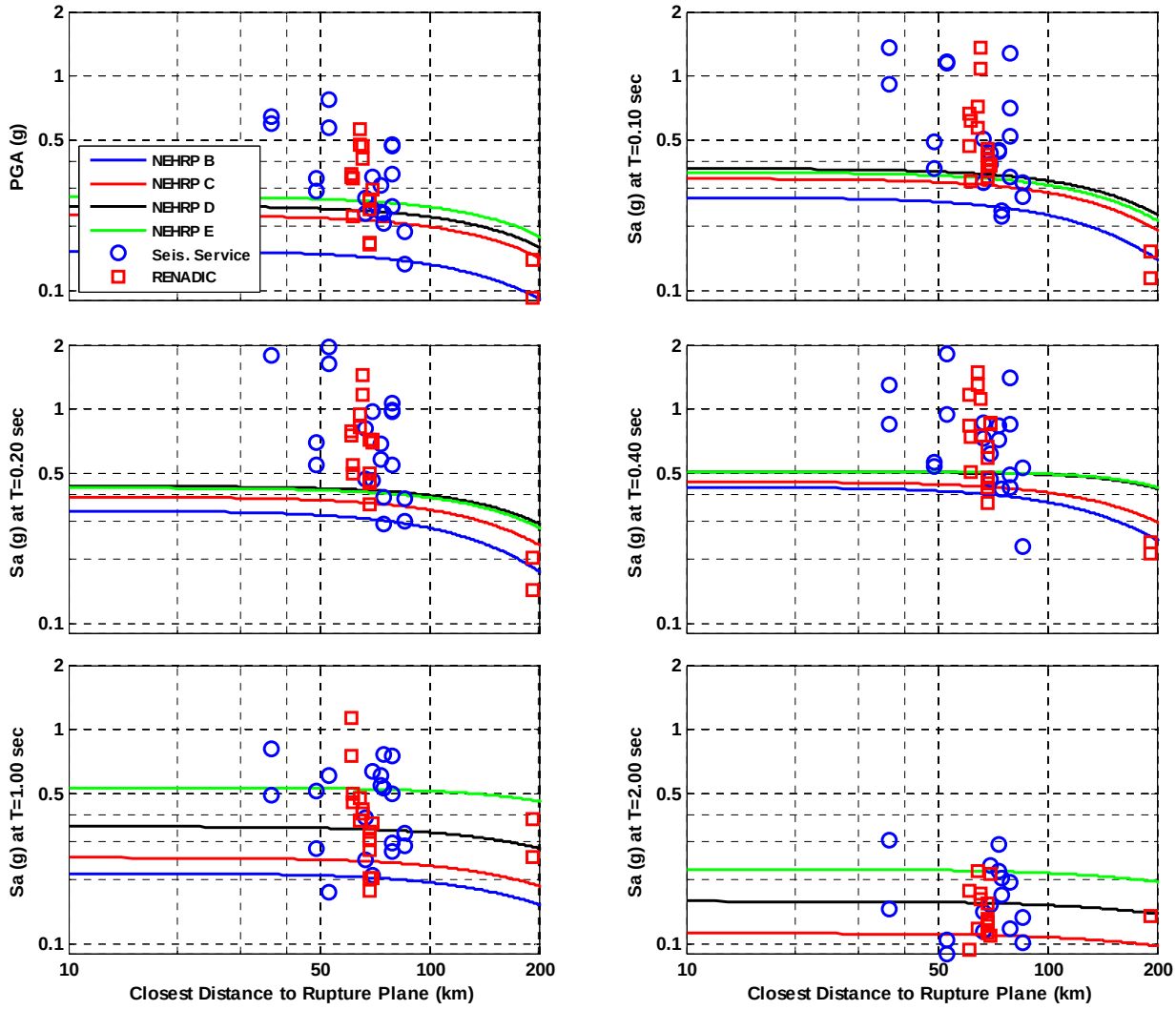

Figure B.2 PGA and response spectra attenuation relationships by Atkinson and Boore (2003)

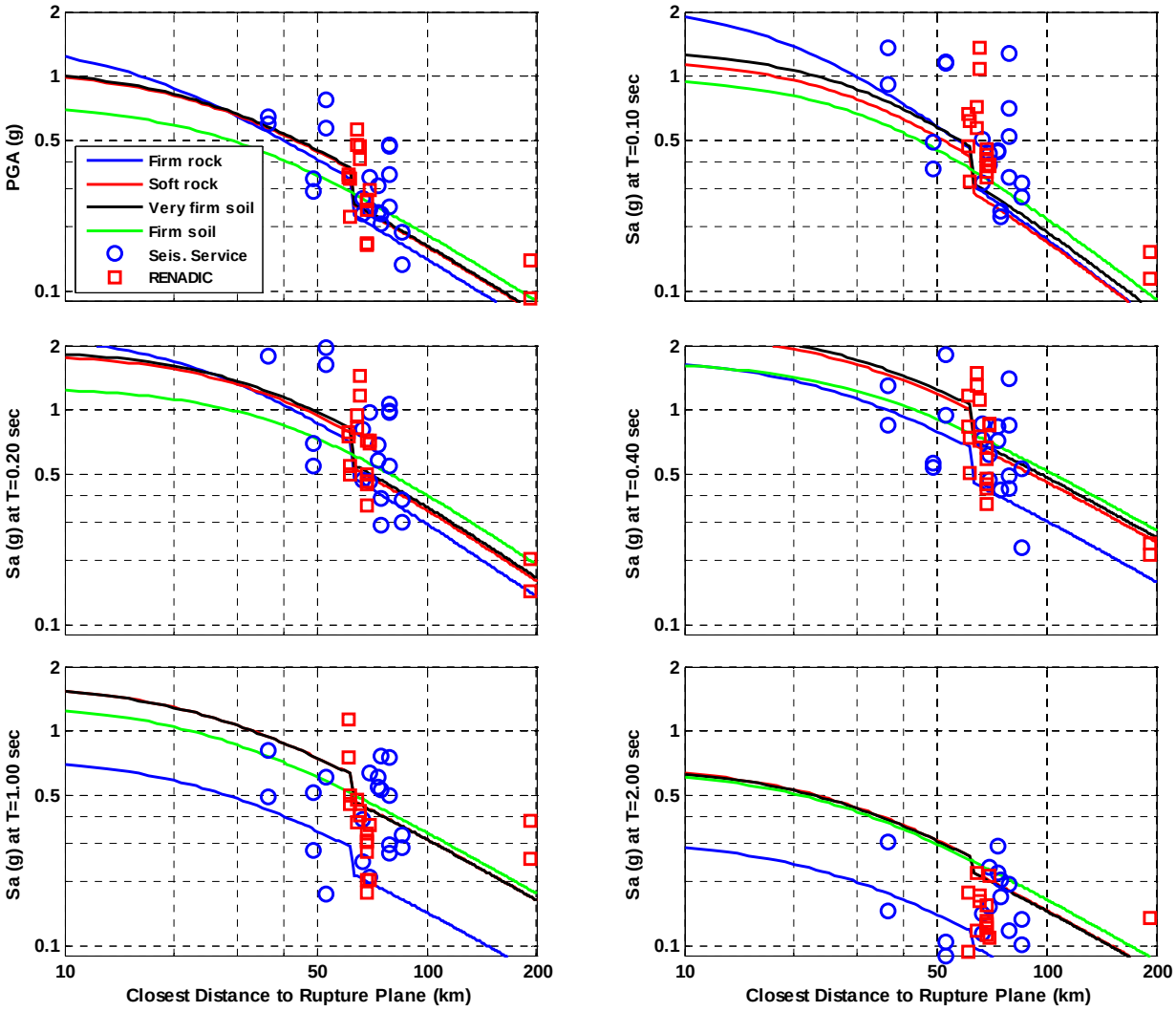

Figure B.3 PGA and response spectra attenuation relationships by Campbell and Bozorgnia (2003)

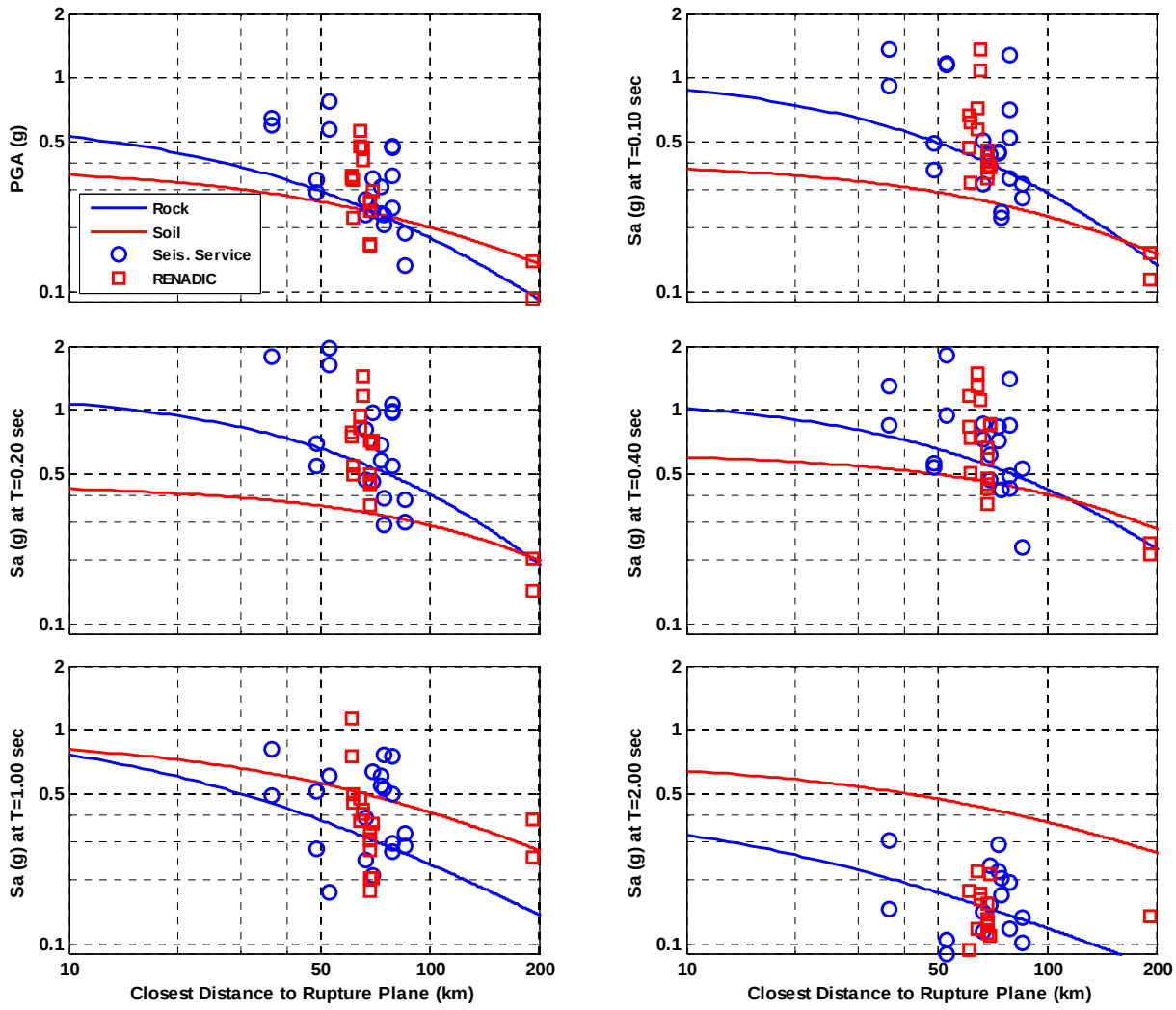

Figure B.4 PGA and response spectra attenuation relationships by Gregor et al. (2002)

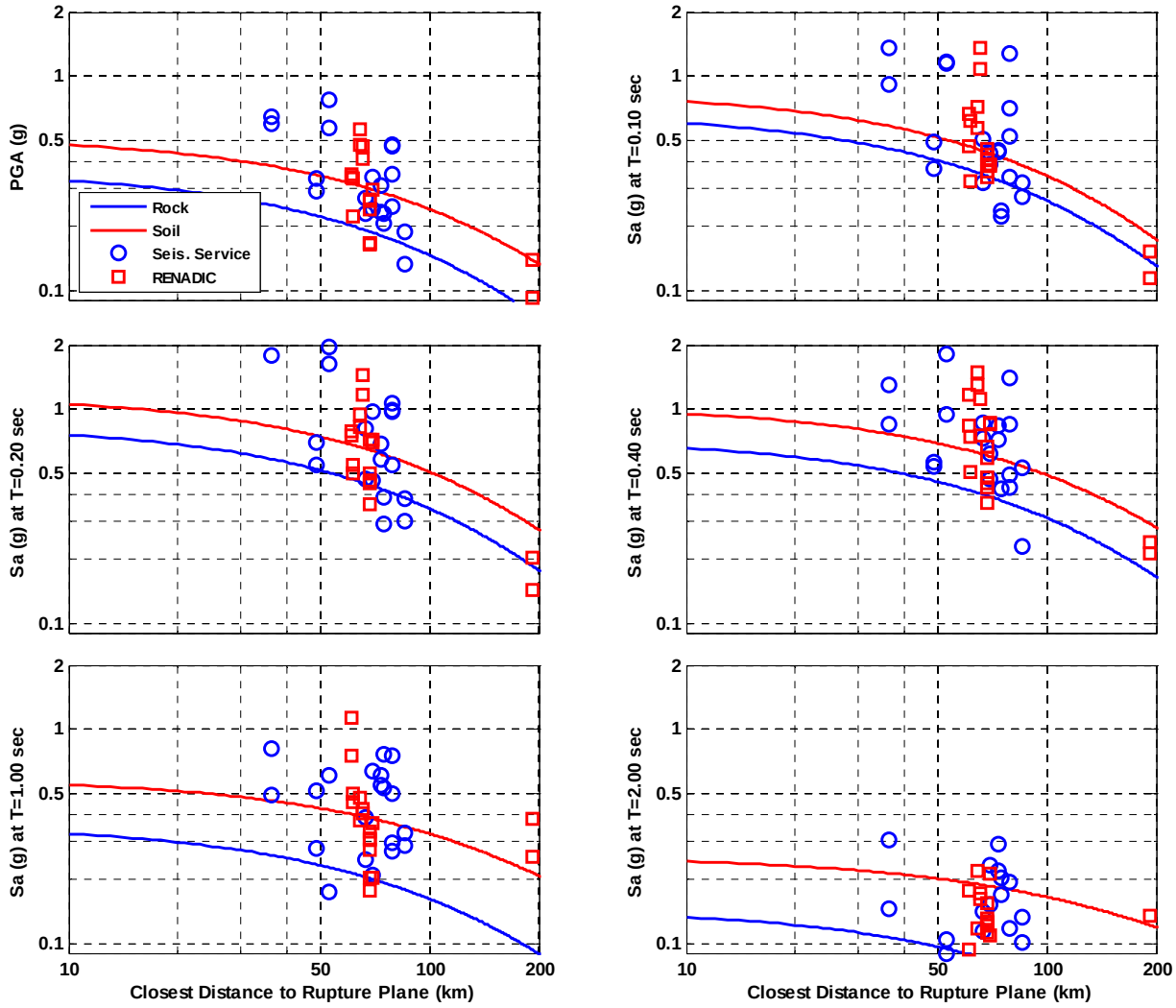

Figure B.5 PGA and response spectra attenuation relationships by Youngs et al. (1997)

APPENDIX C – CONSTRUCTION SPECIFICATIONS FOR THE CATHEDRAL OF TALCA

Work components referred to: these specifications and basis for calculation refer to the construction of the foundation, walls, pillars, and floor and roof beams contained in the plans of the consulting engineers (Alberto Covarrubbias P. and Carlos Infante C.) in accordance with the project architect (Ramon Venegas C.).

Levels: the main level corresponds to the first finished floor at 0.65 m on the level of the sill.

Installation tasks: Includes land clearing, temporary facilities, layout and replanting permits and municipal taxes in force on that date.

Excavation and earth moving: Will be the depth and width indicated in the details of the foundation.

Reinforced concrete, basis for calculations: Concrete has been calculated in accordance with the rules for calculation and construction of reinforced concrete works established by decree #1726 of July 10, 1933 and under the following conditions:

- Floor live loads – 500 kg/m^2
- Stair live loads – 500 kg/m^2
- Weight of floor and stucco – 100 kg/m^2
- The pillars have been calculated to withstand all loads simultaneously
- Maximum pressure on the ground – 1.5 kg/cm^2
- Seismic coefficient – 1/10 g

The execution of the work must be done in all its parts according to the construction and Chilean standards of 1933 for the execution of reinforced concrete works.

Mat reinforcement details: will be made by the consulting engineers who will deliver early enough to properly conduct the work. In all of the reinforcement in the long direction, these details will be made in accordance with the quantities of reinforcement listed in the plans and drawings of the beams/girders/joists.

Reinforcement in the slabs at the supports: when the main truss/reinforcement of the slab is parallel to the support, use a higher reinforcement, not less than half that of the other supports, nor less than 1/4 diameter at 20 (no units). This reinforcement will aim to resist the fixed end moments. In the main beams this longitudinal reinforcement equal to 5 times the thickness of the fiber and will not be less than 3/8 at 20.

Cement: foreign cement is employed which complies with the rules governing the acceptance and use of this material in public works. In each batch of cement that is ordered by the consulting engineers or their representatives, strength testing will be done in the shop.

Sand: river sand of good quality, thick, clean and varying well in size of 7-35mm.

Coarse Aggregate: gravel or crushed stone, clean and variable in size.

Reinforcement: will be of mild steel with circular cross-section of premium quality and made in Chile. Fabricated by Siemens-Martin.

Proportions: in works for reinforced concrete in general, 1:2:4 or 8 bags of cement per cubic meter of concrete made. The consulting engineers and their representatives reserve the right to modify the proportions between sand and gravel keeping the quantities of cement per cubic meter constant.

Preparation and Placement of Concrete: the concrete will be made by machine with as little water proportioned as possible; it is absolutely unacceptable if the water rises to the surface in appreciable quantities. Concrete placement may not commence while the reinforcement mats have not been reviewed and accepted by the consulting engineers or representatives. Special precautions were taken so that the reinforcement is maintained in its proper place during the pour. Resuming the work of the placement of the concrete, must scrape and place the cement grout before the concrete sets.

Forms and Scaffolds: scaffolds will be made solid enough to not deform or fall with loads that they need to support. The beams and slab molds will be made with camber necessary so that after removal of forms, beams and slabs will have flat faces and corresponding levels. Reinforcement must be accepted by the consulting engineers or representatives prior to placement in the forms. Plumb defects that occur in the concrete work resulting from error of lack of ties in the mold, and which go beyond 2 cm, must be repaired by the contractor at their own cost.

Traffic on the forms: once the trusses are placed, avoid any traffic on the molds/forms and make the concrete settle on the boards and planks.

Breakdown and removal of forms: everything will be done by written consent of the engineers or consultants who they represent.

Watering of the concrete: the concrete must be protected for the first 7 days, from abrupt changes in temperature, and from the direct solar rays, taking care to keep the proper permanent moisture state.

Tests: the contractor will be required to provide workers sandbags and other items necessary to conduct stability testing of the work. These tests will effect up to 10 percent of the floors. Tests may also be ordered to measure the execution of the construction of test blocks or beams. The concrete used for these tests must be made at the same time and place.

Reinforcing Dimensions: the plans indicate the reinforcement at the center should be considered to be placed in three templates, two bent bars and a straight bar. The bent bars penetrate the adjacent extremes around 0.2 of the length of the section. The reinforcement of the beams are listed in a special box – the bent bars of a section

should be considered continuous and extending into the next section to account for the negative moments.

Masonry: Masonry Bricks to be used should be top quality, well cooked and placed completely submerged in water. The mortar will be a mix of cement and sand at a 1:6 ratio. The masonry walls are erected prior to casting the pillars embedded in them that are especially packed/compressed to ensure a good interlocking between the two.

Structure of iron steeple: The top of the pyramid-shaped tower of iron is anchored at the bottom with reinforced concrete.

Roofing slabs: Will be oak with sections indicated in the detailed plans

Covering of tile: Is of plain/flat tile.

Tinsmith: Channels and flashings will be zinc. Water outputs will be cast iron. Gutters/downspouts will be galvanized iron.

Pavements:

- The two outdoor terraces and crypt are green stone from Maule
- Reconstituted marble for the aisles
- Marble in the center part

Tower Ladder: Made of iron

Terraces: The entries will be tiered green stone steps from Maule, along with the stairway to the crypt. All other interior steps will be marble.

Choir stairs: Choir stairs will be concrete covered with wood (Rauli wood).

Stucco: Both interior and exterior will be white cement and speculum

Doors: All of the doors of the cathedral are wood according to detail drawings.

Windows: The windows are iron.

Glass: All of the windows will have stained glass

On February 27, 2010 at 03:34 am local time, a powerful earthquake of magnitude 8.8 struck central Chile. The epicenter of the earthquake was approximately 8 km off the central region of the Chilean coast. With an inclined rupture area of more than 80,000 square km that extends onshore, the region of Maule was subjected to a direct hit, with intense shaking of duration of at least 100 seconds, and peak horizontal and vertical ground acceleration of over 0.6 g. The earthquake caused the death of 521 persons, with almost half of the fatalities caused by the consequential tsunami. Over 800,000 individuals were directly affected through death, injury and displacement. More than a third of a million buildings were damaged to varying degrees, including several cases of total collapse of major structures. The transportation system was dealt a crippling blow, with 830 failures registered with the Ministry of Public Works on roads in both the public and private transportation networks. Disruption of commerce as well as the rescue and response effort resulted from the damage to roads, embankments and bridges. On the whole, the performance of engineered structures was reasonable, taking into account the magnitude and proximity of the earthquake. The latter conclusion is supported by the observations from several back-analyses presented in this report. Damage to non-engineered construction is as expected in major earthquakes. Most reinforced concrete bridges behaved well.

The role of social networking tools in enabling the affected population to communicate was a most interesting feature in the response to this earthquake. Due to the failure of the power grid, and the congestion of the cellphone network, the population resorted to short message service and web social media. Ham radio networks were activated to fill gaps due to the failure of the radio network in places. The failure in ham radio broadcast in coastal regions might have increased the fatalities because tsunami warning did not reach all hazardous locations.

The MAE Center field reconnaissance team members consider that Chilean engineering was proven to be robust and that seismic design provisions and construction practices are of high standard. The extensive damage from this M_w = 8.8 earthquake is expected and within the 'life safety' performance target of seismic design codes.

The Mid-America Earthquake Center is a graduated National Science Foundation Engineering Research Center, which was funded under cooperative agreement reference EEC 97-01785.